EFFECT OF TEMPERATURE AND CURING ON THE EARLY HYDRATION OF CEMENTITIOUS MATERIALS

by

MD SARWAR SIDDIQUI

B.S., Bangladesh University of Engineering and Technology, Dhaka, 2007

A THESIS

submitted in partial fulfillment of the requirements for the degree

MASTER OF SCIENCE

Department of Civil Engineering
College of Engineering

KANSAS STATE UNIVERSITY
Manhattan, Kansas

2010

Approved by:

Major Professor
Dr. Kyle Riding

Copyright

Abstract

Concrete is the most widely used construction material. Concrete strength and durability develop from a series of exothermic reactions involving water called hydration. Long-term durability and performance of concrete is very much dependent on the early hydration behavior of cementitious materials. This study examined the effects of curing temperature and access to moisture on the early age reaction rate of cementitious materials, and methods for quantifying these effects.

Apparent activation energy (E_a) relates the effects of temperature on the cement hydration reaction. There are various methods and calculation techniques for estimating E_a that result in greatly varying values. Cement paste and mortar are often used to calculate E_a and used later for concrete. E_a values were calculated using cement mortar and paste by isothermal calorimetry and showed excellent correlation. This validates the use of E_a based on cement paste in modeling concrete behavior. E_a values were also calculated by chemical shrinkage and it showed potential for use in calculating E_a.

Cementitious materials need free water to be available for hydration to continue. Curing with either waxy curing compounds or ponded water are common practices. The thickness of distilled water, lime-saturated water, and cement pore water used as a curing method affects the rate of hydration. Water-cementitious material ratio (w/cm) and sample depth affect the performance of water curing, with low w/cm being the most significant. Partial replacement of sand by fine lightweight aggregate also improves the hydration of cementitious material much more than conventional water ponding. Curing compounds showed improvements in cement hydration compared to uncured samples.

Table of Contents

List of Figures

List of Tables

Acknowledgements

I would like to express my deepest gratitude to my major professor Dr. Kyle Riding for his continuous support and guidance throughout the research. I would also like to acknowledge Dr. Mustaque Hossain and Dr. Hayder Rasheed for their help as my committee members and also for the extraordinary level of education I received from them.

I want to thank Mr. David Suhling and Mr. Ryan Benteman of Kansas State University for their help in the laboratory. I am grateful to my fellow graduate students Shahidul Islam and Sharmin Sultana for their help and encouragement. Finally, I want to thank my family and friends for their affection, love and encouragement toward my study at Kansas State University.

Dedication

To my parents, for their unconditional love and support.

CHAPTER 1 - INTRODUCTION

1.1 Introduction

Concrete is the most widely used construction material in the world. Cement, water and aggregate are the basic ingredients of concrete. Concrete gains strength by a series of chemical reactions of portland cement with water called hydration. Supplementary cementitious materials (SCMs) are used as a partial replacement of portland cement to increase strength, durability, and to decrease costs.

Hydration reactions are exothermic. Rate of reaction of cementitious materials are dependent on curing temperature like all other exothermic reactions. The effect of curing temperature on the rate of reaction of cementitious materials is related to the strength development of cementitious materials, and is also very important for concrete transportation, concrete finishing and formwork removal. The Apparent activation energy (E_a) of cementitious material has been used to quantify the effects of curing temperature on hydration. E_a represents the combined effects of time and temperature on the hydration of cementitious materials.

There are different methods and calculation techniques to estimate E_a. Mortar strength [1], heat of hydration [2, 3], and setting time [4, 5] are common properties used to calculate E_a. ASTM C 1074 [1] is the most widely used method for apparent activation energy calculations. Three different calculation techniques based on mortar strength developments at different isothermal temperatures are described in the standard. Other calculation techniques for E_a have also been described by other researchers [2-8]. This research has been conducted to quantify the variability of E_a values calculated from different methods and calculation techniques. Often, E_a values are determined for cement paste and mortar and later used for concrete. To find out the suitability of this practice E_a was calculated for cement paste and mortar made with the same

cementitious materials and w/cm, and was compared to see whether there is any effect of aggregate on the E_a values. This study compared the differences in activation energy calculated using different methods from mortar strength results, time of set, isothermal heat of hydration, and chemical shrinkage experiments. Both cement paste and mortar were used to determine the chemical shrinkage for apparent activation energy calculation.

Concrete curing is the process of improving the hydration characteristics of cementitious materials by adding extra water to the concrete surface after setting, preventing water loss to the atmosphere, or controlling the concrete temperature [9]. Water ponding, water spraying, fogging, plastic film, wet burlap, and liquid membranes are some of the conventional methods used for curing. Internal curing is another method that has been proven to be effective, particularly for low water-cementitious material ratio (w/cm). Low w/cm is commonly used for high-strength and high-performance concrete. At low w/cm there is a higher propensity for autogenous shrinkage or bulk volume decrease of concrete [10]. Internal curing is accomplished by adding presoaked highly absorbent materials to the concrete mixture. These materials release water to the concrete after set when it is most needed. This not only improves the hydration of the cementitious materials but also reduces the autogenous shrinkage, and subsequently improves cracking performance. Conventional curing methods improve the quality of near surface concrete; however internal curing is not limited to the top surface as presoaked highly absorbent materials are uniformly distributed. In this study, the effects of curing on different w/cm and sample depths were studied to identify more efficient ways of curing. Different heights of curing water with different ionic compositions were used to find out the effect of curing water height. Finally, the effectiveness of lightweight aggregate to improve the hydration of mortar was studied.

1.2 Research Objectives

The research objectives of this study are as follows:

1. To quantify the influence of methods and calculation techniques on the apparent activation energy of cementitious materials;
2. To examine the suitability of chemical shrinkage data as a viable source of data for calculating the of apparent activation energy;
3. To determine the variation of apparent activation energy from cement paste to mortar;
4. To determine the effects of water curing amount and ionic concentration on the hydration of cementitious materials;
5. To determine the effect of curing compound on the early hydration of cementitious materials in dry and sealed environment; and
6. To determine the effects of internal curing on the improvement of hydration of cementitious materials.

1.3 Organization of the Thesis

This thesis has been divided into five chapters. Chapter 1 is the introduction. Chapter 2 discusses the current state of the art, including the basic hydration process of cementitious materials, effects of curing on hydration, description of some of the more common supplementary cementitious materials, and different methods and calculation techniques for apparent activation energy calculation. Chapter 3 discusses the effects of methods and calculation techniques on the apparent activation energy of cementitious materials. The apparent activation energy values were calculated using different methods and calculation techniques, with possible correlations. This chapter also includes apparent activation energy values calculated from cement paste and mortar. Chapter 4 discusses the effects of curing on the initial

hydration of cementitious materials. This chapter includes the effect of water curing, lime-saturated water curing and curing compounds on different w/cm and sample thickness of cement paste. This chapter also presents the advantage of internal curing in low w/cm. Finally, Chapter 5 presents the study conclusions and recommendations for future research.

References

1. ASTM C 1074, “Standard Practice for Estimating Concrete Strength by the Maturity Method,” American Society for Testing and Materials, Pennsylvania, 2009.
2. Kada-Benamer, H., Wirquin, E., and Duthoit, B., "Determination of Apparent Activation Energy of Concrete by Isothermal Calorimetry," Cement and Concrete Research, V. 30, 2000, pp. 301-305.
3. Wang, J., Yan, P., and Hongfa, Y., "Apparent Activation Energy of Concrete in Early Age Determined by Adiabatic Test," Journal of Wuhan University of Technology-Mater. Sci. Ed., September, 2007, pp. 537-541.
4. Pinto, R. C. A., and Hover, K. C., "Application of Maturity Approach to Setting Time," ACI Material Journal,V. 96, No. 6, 1999, pp. 686-691.
5. Garcia, L., Castro-Fresno, D., and Polanco, J., "Maturity Approach Applied to Concrete by Means of Vicat Tests." ACI Material Journal, V. 105, No, 5, 2008, pp. 445-450.
6. Ma, W., Sample, D. , Martin, R., and Brown, W. P., "Calorimetric Study of Cement Blends Cotaining Fly Ash, Silica Fume, and Slage at Elevated Temperature," V. 16, Cement, Concret, and Aggregates, 1994, pp. 93-99.
7. Poole, J. L., Riding, K. A. , Folliard, K. J., Juenger, M. C. G., and Schindler, A. K., "Methods for Calculating Activation Energy for Portland Cement," ACI Materials Journal, V. 104, No. 1, 2007, pp. 303-311.
8. Tank, R. C., and Carino, N. J., "Rate Constant Functions for Strength Development of Concrete," ACI Materials Journal, V. 88, No. 1, 1991, pp. 74-83.
9. Lura, P., “Autogenous Deformation and Internal Curing of Concrete,” Ph.D. Dissertation, Technical University of Delft, Netherland, 2003.

10. Kovler, K., and Jensen, M., "Novel Technique for Concret Curing," Concrete International, V. 27, 2005, pp. 39-42.

CHAPTER 2 - LITERATURE REVIEW

2.1 Introduction

Concrete is a heterogeneous material consisting of rock, sand, portland cement and water. When water is added to portland cement, a chemical reaction begins which is called hydration. The cement hydration products bind the concrete components together and are responsible for the strength development, porosity, permeability, and dimensional stability.

The activation energy of a chemical reaction represents the relationship of the chemical reaction rate to the reaction temperature. In the case of cement hydration however, several chemical reactions happen simultaneously. The term apparent activation energy (E_a) is used to represent the average temperature dependence of the multiple chemical reactions that occur during hydration. Various measurable properties such as the cement heat of hydration evolution, amount of chemically bound water, chemical shrinkage, amount of calcium hydroxide ($Ca(OH)_2$) and strength are dependent on the percent of cement reacted, and can, therefore, be used to calculate E_a. Different methods and calculation techniques are used to determine E_a, which could influence the calculated value.

This chapter contains a literature review which serves to provide the necessary background in concrete technology, chemical composition and hydration process of different cementitious systems, and the effect of curing on the hydration of cementitious materials. It also includes a description of various supplementary cementitious materials and chemical admixtures used in this study. A brief discussion on chemical shrinkage and factors that influence chemical shrinkage is also presented here. As several methods are currently used to determine E_a, a summary of different methods and calculation techniques used to quantify E_a is also included.

2.2 Cement

2.2.1 Cement Composition

Limestone, clay, and shale are fired in a kiln at 1400 - 1650 °C to produce clinker. The clinker is then cooled and ground with 3-5 percent gypsum to make portland cement. The gypsum is added to control the rate of set of the cement, giving the material a pot life which allows for transportation, placement, and finishing of the concrete.

Clinker normally contains four major phases; alite, belite, tricalcium aluminate, and tetracalcium aluminoferrite. Alite is the most abundant component of modern portland cement (PC) clinkers, accounting for 50-70% of the total mass of clinker. Alite is tricalcium silicate modified in composition and crystalline structure by incorporation of foreign ions, especially Mg^{2+}, Al^{3+} and Fe^{3+} [1]. Alite is mostly responsible for the early strength gain of cement. Belite constitutes 15- 30% of modern PC clinkers and is an impure version of dicalcium silicate. It reacts slowly with water and contributes little to the early strength gain; but is primarily responsible for the concrete's long-term strength development. Tricalcium aluminate, sometimes called aluminate, normally comprises 0-12% of portland cement. It can react rapidly with water and cause undesirable rapid setting, called flash set, unless a set-controlling agent like gypsum is added. The PC clinker usually consists of 0-15% by weight of tetracalcium aluminoferrite, also called ferrite. The rate of reaction of ferrite with water is variable and dependent on the composition [1].Commonly used shorthand notations in cement chemistry are CaO=C, SiO_2=S, Al_2O_3=A, Fe_2O_3=F, MgO=M, K_2O=K, Na_2O=N, SO_3=$\overline{S}$, H_2O=H, TiO_2=T, P_2O_5=P, and CO_2=$\overline{C}$ [1, 2] and will be used in the remainder of this thesis. The compounds typically found in cement and their shorthand notations are presented in Table 2.1.

Table 2.1: Typical Compound Composition of Portland Cement [3].

Chemical Name	Chemical Formula	Shorthand Notation
Tricalcium silicate	$3CaO.SiO_2$	C_3S
Dicalcium silicate Tricalcium aluminate	$2CaO.SiO_2$	C_2S
Tricalcium aluminate	$3CaO.Al_2O_3$	C_3A
Tetracalcium Aluminoferrite	$4CaO.Al_2O_3.Fe_2O_3$	C_4AF
Calcium sulfate dihydrate (Gypsum)	$CaSO_4.2H_2O$	$C\overline{S}H_2$

2.2.2 Cement Types

There are different types of cement in use, some of which have special purposes and uses. Specifications for the cement types are in general based on chemical composition or physical properties, such as, specific surface area or aluminate content, and partly on performance tests, such as, setting time and compressive strength development under standard conditions. According to ASTM C150 [4] there are five standard types of cement, shown in Table 2.2. Blended cements are also widely used in construction. Blended cement is the mix of portland cement and supplementary cementitious materials (SCMs), such as, fly ash or ground granulated blast-furnace slag. These pozzolanic materials are added to the portland cement during manufacturing. Six types of blended cements are specified in ASTM C 595 [5], shown in Table 2.3. In the U.S., it is much more common for the supplementary cementitious materials to be added separately to the concrete during batching.

Table 2.2: Portland Cement Classification [4].

Material	Description
Type I	Normal
Type II	Moderate sulfate resistance
Type III	High early strength
Type IV	Low heat of hydration
Type V	High sulfate resistance

Table 2.3: Blended Cement Classification [5].

Material	Description
Type IS	Portland–blast furnace slag cement
Type 1P	Portland-pozzolan cement
Type P	Portland-pozzolan cement (slow strength gain)
Type I(PM)	Pozzolan-modified portland cement
Type S	Slag cement
Type I(SM)	Slag-modified portland cement

2.2.3 Hydration of Cement

When water is added to cement, various components of cement dissolve at a different rate. When the ions in solution reach supersaturation for a given type of cement phase, precipitation occurs causing nucleation and growth of hydration products. These reactions are exothermic, which means that heat is liberated during the reaction. Due to the reaction between various dissolved ions in the pore water, new compounds are produced. These hydrates give hydrated cement paste its strength, rigidity, durability and toughness.

The six most important and common chemical reactions in portland cement hydration are shown in Reactions 2.1 to 2.6:

$C_3S + 5.3H \rightarrow C_{1.7}SH_4 + 1.3CH$ **Reaction 2.1**

$C_2S + 4.3H \rightarrow C_{1.7}SH_4 + 0.3CH$ **Reaction 2.2**

$C_3A + 3C\overline{S}\,H_2 + 26H \rightarrow C_6A\overline{S}_3H_{32}$ **Reaction 2.3**

$C_3A + C_6A\overline{S}_3H_{32} + 4H \rightarrow 3C_4A\overline{S}\,H_{12}$ **Reaction 2.4**

$C_3A + 6H \rightarrow$ C-A-H **Reaction 2.5**

$3C_4AF + 33C\overline{S}\,H_2 + 42H \rightarrow 3C_4A\overline{S}\,H_{12} + 3CH + 3FH_3$ **Reaction 2.6**

Calcium silicate hydrates (C-S-H) form with the addition of water to either tricalcium silicate or dicalcium silicate. About 50 to 60% of the total volume of the portland cement

reaction products are C-S-H, which is responsible for the majority of the strength gain of hydrated concrete [6]. During Reactions 2.1 and 2.2, calcium hydroxide is formed as a byproduct, which does not significantly contribute to the concrete strength gain or durability, and may become unstable when exposed to acids [6].

The second series of reactions involves the aluminate compounds in cement, as shown in Reactions 2.3 to 2.5. Gypsum ($C\overline{S}\,H_2$), is added to the cement to control the setting of the hydrated portland cement. As water is added, ettringite ($C_6A\overline{S}_3H_{32}$) forms until the excess calcium sulfate is consumed. Monosulfoaluminate ($C_4A\overline{S}\,H_{12}$) will then begin to form from the reaction between C_3A and ettringite, as shown in Reaction 2.4. If there is any unused C_3A remaining after all of the ettringite has converted to monosulfoaluminate, the C_3A will hydrate as shown in Reaction 2.5, to form a calcium aluminate hydrate, C-A-H. The third series of reactions is the hydration process of tetracalcium aluminoferrite, C_4AF, as shown in Reaction 2.6.

2.3 Effect of Curing on Hydration

Curing is the process of preventing water loss from the concrete, potentially providing excess water for the cementitious material to react further, or controlling the concrete temperature. Curing water is available for the hydration of the cement after setting, but does not contribute to the increase in cement particle spacing as mixing water does. Curing is critical to allow the cement to more fully hydrate and provide for strong, durable, and long lasting concrete. Cementitious materials with a higher degree of hydration will have a stronger bond with the aggregates, smaller pores, and less interconnection between pores [7-10]. Strength difference between moist-cured and air-cured Type I cement can be as high as 58% after 6 months [11]. The effect of curing is even more important at early ages for the development of durable concrete, especially when blended cements are used [12, 13]. Curing also improves the shrinkage

characteristics [14] of cementitious materials which is one of the major causes of concrete cracking and subsequent deterioration. Autogenous shrinkage becomes more predominant at lower w/cm [15]. Autogenous shrinkage is the bulk volume reduction in concrete from the self desiccation of the concrete that occurs from the net chemical shrinkage of concrete, or the absolute volume reduction from the hydration reaction products occupying less volume than the reactants.

Theoretically complete hydration is possible when w/c is greater than 0.42 [16]. Use of low w/cm is common practice to obtain high strength and high performance concrete, making curing even more important for these concrete mixtures because not enough mixing water is available for complete hydration. Conventional curing methods like water ponding, water spraying, fogging, plastic film, wet burlap, and liquid membrane only cure the near surface layer. To cure the whole mass of the concrete uniformly and effectively the concept of internal curing was developed [17-19]. Internal curing is done by adding presoaked highly absorbent materials to the concrete like saturated lightweight aggregate [15, 19-22], and super-absorbent polymers [15, 23, 24].

2.4 Supplementary Cementitious Material

Most supplementary cementitious materials are pozzolans that are capable of reacting in cementitious systems, and contributing to strength gain and durability. Pozzolans are siliceous or alumino-siliceous materials that form calcium silicate hydrates or calcium alumino-silicate hydrates upon reaction with calcium hydroxide. Additional hydration products can form depending on the composition of SCM. SCMs are used to improve the concrete workability, durability, and cracking risk. SCMs have a reduced heat of hydration and slow down the rate of strength gain, but can have a higher ultimate strength [25]. Volcanic tuff and pumice, volcanic

glasses, diatomite, calcined clays and shales, rice husk ash, and high-reactivity metakaolin are common natural pozzolans. Ground granulated blast furnace slag (GGBFS), fly ash, silica fume are the most common SCMs used and are industrial byproducts, keeping these materials out of landfills while improving the concrete.

2.4.1 Ground Granulated Blastfurnace Slag

Blastfurnace slag is a byproduct of iron manufacturing. It is formed as a liquid at 1350-1550^{o}C. The molten slag can be cooled rapidly with water to form small glassy granules which can then be ground and used as an SCM. For a wide range of steel producing countries, the composition range of GGBFS is: MgO, 0- 21%; Al2O3, 5- 33%; SiO2, 27- 42%; and CaO, 30-50% [27]. In the United States, GGBFS is specified according to ASTM C 989 [28], which classifies GGBFS into three grades based on the strength development of a 50% replacement of portland cement by GGBFS. The relative proportion of slag and cement used in construction varies widely. Mass concrete projects have used GGBFS to replace up to 80% of the portland cement [29], however dosages in the 35-50% range are more typical [30, 31]. The slag reaction is considerably slower than the alite reaction which leads to lower early-age strengths. In one concrete mixture, a replacement of 65% of the portland cement by GGBFS resulted in 50% lower compressive strength at two days, but an increase in compressive strength by about 12% at 91 days [27]. GGBFS can increase the workability and finishability of concrete and decrease both the rate and total amount of heat released during hydration.

2.4.2 Fly Ash

Fly ash is captured from the flue gas of coal burning power stations and is composed principally of very fine, glassy, spherical particles due to the rapid cooling process. The chemical composition of the fly ash depends on the type of coal burned and the coal burning conditions during production. Anthracitic or bituminous coal gives ash high in SiO_2, Al_2O_3 and Fe_2O_3 and low in CaO, whereas sub-bituminous or lignite coals give ash higher in CaO and lower in SiO_2, Al_2O_3 and Fe_2O_3. Small percentages of crystalline materials can also be found in the fly ash such as quartz, mullite, hematite, or magnetite. These materials are however largely inert [32]. Fly ash is classified according to ASTM C 618 [26], where Class F and Class C fly ash must have a minimum (SiO_2+Al_2O_3+Fe_2O_3) content above 70% and 50%, respectively. Table 2.4 presents a typical range of chemical composition for the two classes of fly ash.

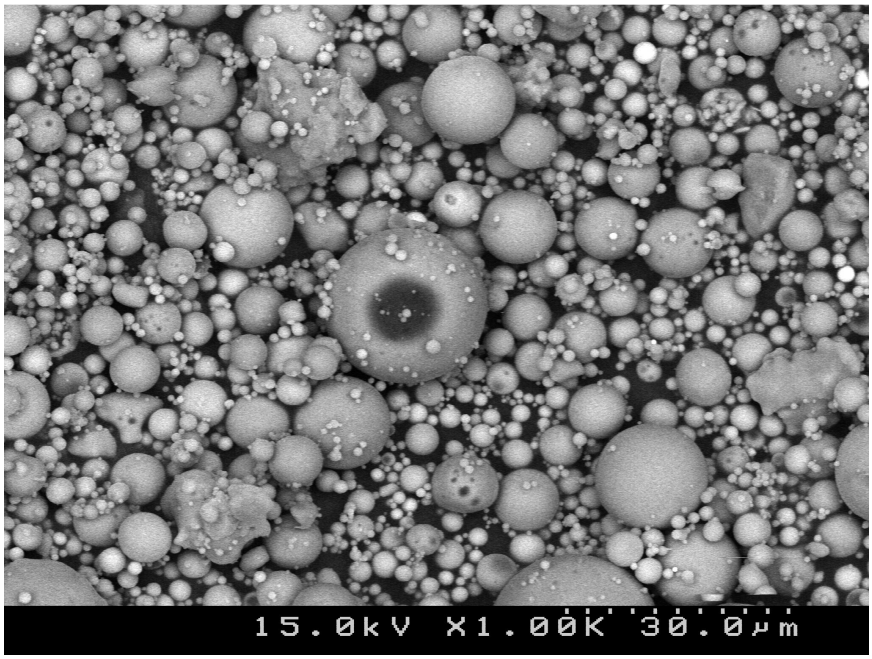

Figure 2.1: Scanning Electron Micrograph of Fly Ash Particles. Note the Characteristic Spherical Shape that Helps Improve Workability (personal communication, Kyle Riding).

Table 2.4: Typical Range of Chemical Composition of Fly Ash [33].

Oxide	Range of Chemical Composition (% by Weight)	
	Class F Fly Ash	**Class C Fly Ash**
SiO_2	38-65	33-61
Al_2O_3	11-63	8.0-26
Fe_2O_3	3.0-31	4.0-10
CaO	0.6-13	14-37
MgO	0.0-5.0	1.0-7.0
Na_2O	0.0-3.1	0.4-6.4
K_2O	0.7-5.6	0.3-2.0
SO_3	0.0-4.0	0.5-7.3

2.4.3 Silica Fume

Silica fume is a byproduct of the production of silicon or silicon alloys. Some silica is lost as a vapor in the manufacturing process which when cooled, gives very fine, solid particles. The particles are generally spherical, have an average diameter of around 100 nm, and are made up principally of amorphous SiO_2. Most of the silica fume used in concrete has been derived from the production of alloys with at least 75% ferrosilicon, which yields SiO_2 content in the silica fume of 84% or higher [34]. ASTM C 1240 [35] specifies a minimum SiO_2 content of 85% for silica fume in concrete mixtures. Typically, the specific surface area of silica fume as measured using BET nitrogen adsorption is 20,000 m^2/kg, which is much finer than that of cement or most other SCMs [34]. Silica fume density is above 2000 kg/m^3, however the bulk density of the undensified powder varies from 130 to 430 kg/m^3 [36]. Table 2.5 presents a typical range of chemical compositions for silica fume. High strength concrete will often include silica fume. The concrete permeability decreases when silica fume is used through consumption of CH and division of the pores to a finer pore size distribution. This is a principle reason for the

increased use of silica fume for making high performance and high durability concrete. Silica fume also decreases the bleeding, workability, and pumpability of the concrete [37].

Table 2.5: Chemical Compositions of Silica Fume from the Production of Elementary Silicon and 75% Ferrosilicon Alloy [38].

Compounds	Si	75% Fe-Si
SiO_2	94-98	86-90
Al_2O_3	0.1-0.4	0.2-0.6
Fe_2O_3	0.02-0.15	0.3-1.0
MgO	0.3-0.9	1.0-3.5
CaO	0.08-0.3	0.2-0.6
K_2O	0.2-0.7	1.5-3.5
Na_2O	0.1-0.4	0.8-1.8
C	0.2-1.3	0.8-2.3
S	0.1-0.3	0.2-0.4
Loss on ignition	0.8-1.5	2.0-4.0

2.4.4 Metakaolin

Metakaolin is obtained by calcination of pure kaolin clay at moderate temperatures, usually 600-800^{o}C. Clay minerals lose most of their absorbed water at 100-200^{o}C. At 500-600^{o}C, kaolin clay loses water by dehydroxilization. After calcining, the metakaolin is ground for use in concrete. As a reactive alumino-silicate material, metakaolin will react with the calcium hydroxide and is capable of producing high strength and low permeability concrete.

2.5 Chemical Admixtures

Chemical admixtures are ingredients that are added to the concrete during mixing to achieve certain properties or performance. Air entrainers, water reducers, and set control agents are the most common admixtures used in the concrete industry. ASTM C 494 [39] includes seven types of admixtures used to control set and reduce the concrete water demand.

2.5.1 Water Reducing Admixtures

ASTM C 494 [39] defines water reducing admixtures (WRA) as admixture chemical which reduces the amount of water required to produce concrete of a desirable consistency. ASTM C 494 [39] describes two basic types of WRA, low-range and high-range water reducing admixtures. Type A and D are low-range water reducing admixtures. Both these admixtures provide at least 5% of water redaction when used in concrete, while the type D admixture also retards initial setting from 1 to 3.5 hours [39]. Types F and G are high-range water reducing admixtures. High-range water reducers provide at least 12% water reduction. Type G water reducers also retard the initial setting time by 1 to 3.5 hours [39]. Low-range water reducing admixtures are commonly derived from natural organic materials, such as, sugars and lignins. Two types of high-range water reducers have been used, sulfonated melamine or naphthalene-formaldehyde condensates and polycarboxylates. Water-reducing admixtures help disperse cementitious materials by making the cement particles hydrophilic as shown in Figure 2.2 [37, 40]. Doses of water reducing admixtures can be adjusted to obtain desired range of water reduction and setting time, however care is needed as the retardation response is not linear with dosage.

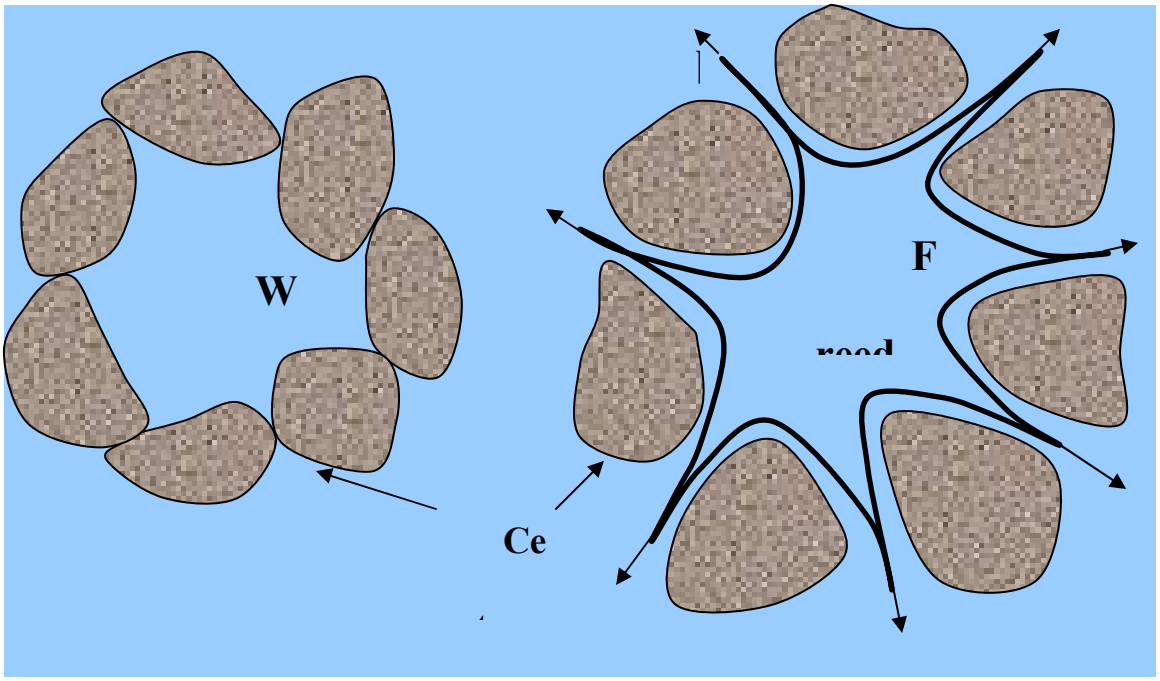

Figure 2.2: Dispersion Mechanism of Water Reducing Admixture; (a) Charged Cement Particles Trapping Water, (b) Cement Grains are Separated by Water Reducers, Releasing the Water to be Available for Better Flow Hydration. After [37]

2.6 Chemical Shrinkage

When cementitious materials hydrate, the absolute volume of the reaction products (e.g. C-S-H gel and CH) is smaller than the volume of the reactants (C_3S and water). This volume reduction is called chemical shrinkage and is proportional to the degree of hydration [41,42]. Autogenous shrinkage is the bulk material shrinkage that is triggered by chemical shrinkage and is equal to the chemical shrinkage until a self-supporting C-S-H skeleton is strong enough to resist the contracting force (i.e. Set time) [41]. The chemical shrinkage is the total absolute volume change of the cement paste, whereas the autogenous shrinkage is the bulk volume change.

2.6.1 Factors Influence Chemical Shrinkage

The cement composition, supplementary cementing materials, curing temperature, and water-cement ratio all influence the chemical shrinkage of cementitious materials. The chemical shrinkage of mixtures with supplementary cementitious materials varies depending on the type of admixtures used. Silica fume has been shown to accelerate the chemical shrinkage while slag reduces the shrinkage rate [43]. As the temperature increases, both the hydration and the chemical shrinkage rate increase [44]. The effect of water-cementitious materials ratio (w/cm) and sample size on chemical shrinkage varies. At early ages, the chemical shrinkage is independent of the water-cementitious material ratio and sample size [44], but with time a lower water-cementitious material ratio gives a lower total chemical shrinkage because of the lower degree of hydration [45].

2.7 Apparent Activation Energy

The apparent activation energy (E_a) of concrete characterizes the sensitivity of concrete property development to temperature [46]. This relationship was developed to describe the reaction rate of individual salts in solution at different temperatures [46]. For portland cement however, several reactions occur simultaneously. The term apparent activation energy is used to represent the temperature dependence of the overall sum of reactions that take place during hydration [47]. The apparent activation energy of the concrete can be determined by either mechanical, calorimetric means, or any other method that measures the degree of cementitious material hydration [48]. The mechanical method is based on mortar cube strength at six ages cured at three different temperatures [49]. To get a more accurate method for calculation of apparent activation energy, Ma et al. [50] developed a method based on isothermal calorimetry. Variations of this method have been tried on both isothermal and adiabatic experiments, although

the isothermal condition has proven more effective [51]. In 1999 Zhang [52] proposed another microwave based technique which was shown to be effective for apparent activation energy calculations. Despite the accuracy and effectiveness of both the isothermal calorimetry and microwave technique, they both require sophisticated or expensive technology.

The Arrhenius equation is commonly used to characterize the temperature sensitivity of the hydration of cementitious materials, which allows for the calculation of E_a [53]. Arrhenius showed that variation of specific rate of reaction with temperature can be expressed as follows

$$k = A.e^{-\frac{E_a}{RT}} \qquad \textbf{Eq. 2.1}$$

where

R = universal gas constant (8.314 J/mol/K),

T = temperature (K) at which the reaction occurs,

k = the rate of heat evolution (W),

A = the proportionality constant (same units as k), and

E_a = activation energy (J/mol).

2.7.1 Measurement Techniques for Apparent Activation Energy

There are various methods that have been used to calculate E_a. These methods vary in the physical property measured, applicability, and ease of use. Sections 2.7.1.1 to 2.7.1.3 document several of the more common methods that have been used to calculate the apparent activation energy of cementitious materials.

2.7.1.1 Mortar Strength

ASTM C 1074 [1] describes how to calculate the activation energy of a mortar from compressive strength tests. In this method, the mortar strength is measured on 50 mm (2 in) mortar cubes at

three different temperatures. Compressive strength of a mortar cube at a particular time and temperature is considered to be the average of the compressive strength of three cubes. The activation energy is then calculated from the measured strength values.

2.7.1.2 Time of Set

Calculation of E_a from the setting time was first proposed by Pinto and Hover in 1998 [54]. Initial and final setting is measured at different temperatures to calculate E_a. This method was further validated by Garcia et al. [55] using a simpler technique. The assumption used is that the initial and final set times are reached after a certain level of microstructure develops for any cement mixture, or after a certain degree of hydration for a particular w/cm is achieved. This method follows the same conventional maturity technique that is described in ASTM C1074 where the initial and final set depend on the time and curing temperature [54].

2.7.1.3 Heat of Hydration

This method for calculating the hydration reaction activation energy was first proposed by Ma et al. [50] and further developed by Kada et al [47]. This method is based on the measurement of heat released due to the hydration of cement at several isothermal temperatures. As cement hydration is an exothermal reaction, energy is released during the reaction in the form of heat. As the rate of heat released is a function of the rate of hydration, a measure of the cement degree of hydration can be calculated at any time t by measuring the total amount of heat generated up to that time. The amount of energy released is measured using a heat flux sensor (usually a peltier sensor) to measure the cooling required to keep the sample at a constant temperature. In this method, the amount of heat generated by cement hydration is measured at different isothermal temperatures.

2.7.2 Calculation Techniques

Several different calculation techniques have been proposed for the different experimental methods used for determining a cement or mortar activation energy. This section discusses some of the more common calculation methods used.

2.7.2.1 Single Linear Approximation

This method is discussed by Ma et al [50]. This method depends on a first-order approximation of the reaction rate. The reaction rate is calculated using a linear fit to the positive slope portion or acceleration region of the isothermal calorimetry plot, shown in Figure 2.3 (a), which is similar to a first-order differential rate equation [56]. An Arrhenius plot is then created by plotting the inverse of temperature in Kelvin ($1/T$) as the abscissa and $\ln(k)$ as the ordinate, as shown in Figure 2.3 (b). E_a is calculated by multiplying the slope of the best fit straight line by the Universal gas constant, R.

Despite the simplicity of this method, it has some serious drawback which limits the use of this method. The determination of the linear acceleration phase region is subjective because the selection of the linear portion of the acceleration part of the heat evolution rate is usually done manually. At low temperatures it is very difficult to identify the beginning of the acceleration period. Moreover, this method is only used for the change in the acceleration portion of the curve and neglects what occurs in the later hydration rate evolution [53].

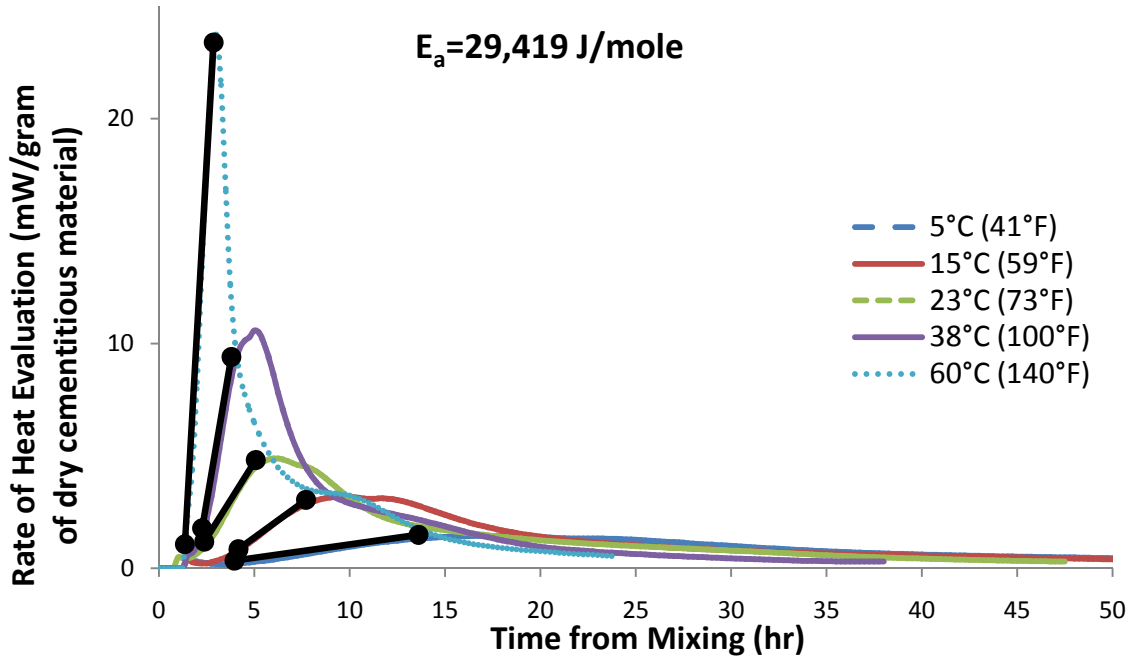

(a)

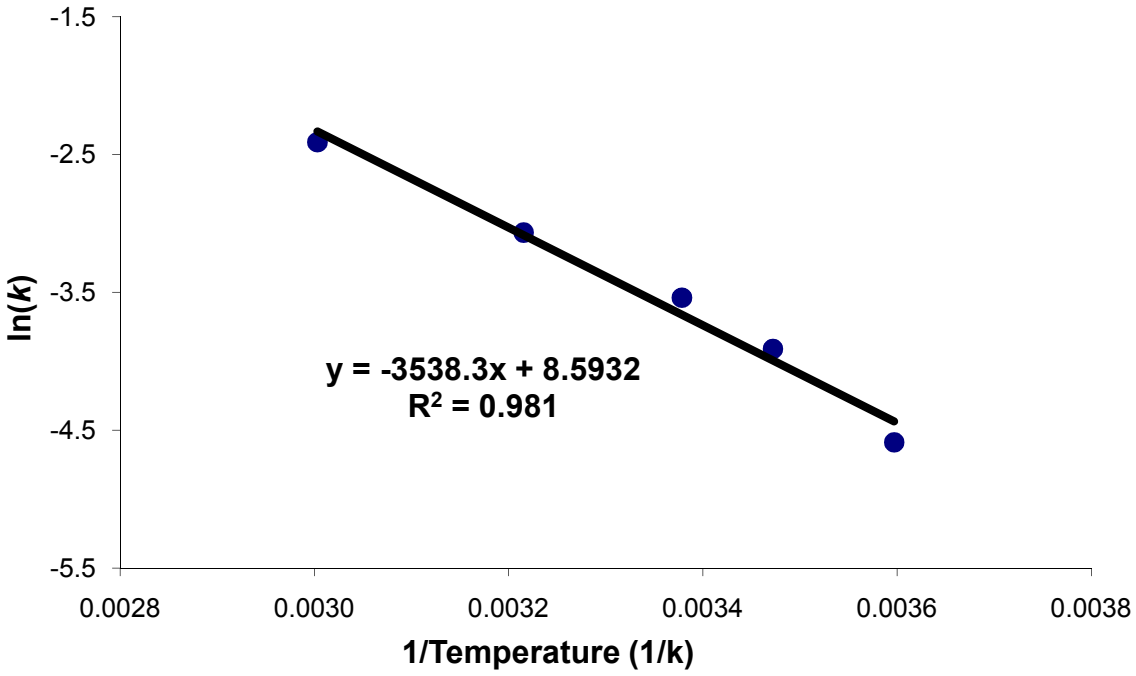

(b)

Figure 2.3: Calculation of E_a by Single Linear Approximation Method; (a) Determination of k from the Linear Portion of the Acceleration Period; (b) E_a from Arrhenius Plot.

2.7.2.2 Incremental Calculation

Some researchers have argued that E_a of portland cement should be dependent on degree of hydration [46, 47]. An E_a value that changes with the degree of hydration is problematic for practical use in temperature, creep, or strength calculations and is really contrary to the intent of the activation energy. The cementitious system degree of hydration α at any time t can be defined as the total amount of heat evolved at time t divided by the total amount of heat available to be released based on the cementitious material composition, as shown in the Eq. 2.2 [46-47, 57-59].

$$\alpha = \frac{H(t)}{H_u} \qquad \textbf{Eq. 2.2}$$

where,

α = the degree of hydration at time t,

$H(t)$ = cumulative heat of hydration from time 0 to time t (J/gram), and

H_u = total heat available for reaction (J/gram).

The value of degree of hydration varies from 0 to 1, where 0 means no hydration and 1 means complete hydration of the cementitious material.

The value H_u is a function of cement composition and amount and type of supplementary cementing materials and may be calculated as follows [60]:

$$H_u = H_{cem} \cdot P_{cem} + 461 \cdot P_{slag} + 1800 \cdot PFA - CaO \cdot PFA \qquad \textbf{Eq. 2.3}$$

where,

P_{slag} = slag to total cementitious content mass ratio,

PFA = fly ash to total cementitious content mass ratio,

PFA-CaO = fly ash CaO to total fly ash content mass ratio,

P_{cem} = cement to total cementitious content mass ratio, and

H_{cem} =available heat of hydration of the cement (J/gram).

The value H_{cem} can be calculated as shown in Eq. 2.4 [60]:

$$H_{cem} = 500 \cdot P_{C_3S} + 260 \cdot P_{C_2S} + 866 \cdot P_{C_3A} + 420 \cdot P_{C_4AF} + 624 \cdot P_{SO_3} + 1186 \cdot P_{Free\,Ca} + 850 \cdot P_{MgO} \quad \textbf{Eq. 2.4}$$

where,

H_{cem} = the total heat of hydration of portland cement (J/gram) at α = 1.0,

P_i = the mass of *i*-th component to total cement content ratio, and

$i = P_{C_3S}, P_{C_2S}, P_{C_3A}, P_{C_4AF}, P_{SO_3}, P_{Free\,Ca}$ and P_{MgO}

It is generally agreed upon that the activation energy of cement remains constant between $\alpha = 0.1$ to $\alpha = 0.5$ [47]. After that, there is some debate as to whether or not the activation energy should change. At early ages the hydration is controlled by nucleation and growth mechanisms and later on is controlled by diffusion through hydrated layer [46, 47]. The incremental calculation method is used to attempt to describe how E_a changes as the reaction becomes dominated by other mechanisms such as diffusion, water availability, or space for products to form [53]. The following section will show the mathematical process how E_a is calculated by this method.

A commonly used relationship is a three-parameter model defined in Eq. 2.5 [60, 61].

$$\alpha(t_e) = \alpha_u \cdot e^{-\left[\frac{\tau}{t_e}\right]^{\beta}} \quad \textbf{Eq. 2.5}$$

where,

$\alpha(t_e)$ = the degree of hydration at equivalent age t_e,

τ = the hydration time parameter (hours),

β = the hydration shape parameter, and

α_u = the ultimate degree of hydration.

The equivalent age t_e can be calculated from the Eq. 2.6 shown below

$$t_e(T_r) = \sum_0^t e^{-\frac{E_a}{R}\left(\frac{1}{T_C}-\frac{1}{T_r}\right)} \cdot \Delta t \qquad \textbf{Eq. 2.6}$$

where,

$t_e(T_r)$ = equivalent age at reference temperature T_r, and

T_c = temperature of the concrete; E_a and R are as defined previously.

E_a can be determined at any age if the reaction rate at a different temperature $k(T)$ can be computed at a constant α. If $P(t)$ is the power required to maintain the isothermal condition, then Eq. 2.7 represent the relation between α, $k(T)$ [47].

$$k(T) \cdot f(\alpha) = \left(\frac{d\alpha}{dt}\right)_T \qquad \textbf{Eq. 2.7}$$

where,

$k(T)$ = the reaction rate J/s,

$f(\alpha)$ = the function depending on degree of hydration,

α = the degree of hydration as in Eq. 2.2, and

$\frac{d\alpha}{dt}$ = the rate of change of degree of hydration.

If H_u is the total amount of heat available for the reaction of a mixture, the rate of change of α can be expressed as shown in the Eq. 2.8 [47].

$$\frac{d\alpha}{dt} = \frac{1}{H_u} \cdot \left(\frac{dH(t)}{dt}\right) = \frac{P(t)}{H_u} \qquad \textbf{Eq. 2.8}$$

where,

H_u and $H(t)$ have been defined previously.

If calibration of the calorimeter is good, then the reaction rate can be calculated by the power released as shown in Eq. 2.9 [47].

$$k(T) = \frac{1}{H_u} \cdot \left[\frac{P(t)}{f(\alpha)} \right]_T = P(\alpha, T) \qquad \textbf{Eq. 2.9}$$

where,

$P(\alpha, T)$ = the power measured for a given α, T.

E_a values over a range of α can be calculated by this method. By using a best-fit line, E_a can be calculated for any number of temperatures. Eq. 2.10 can be used to compute E_a as a continuous function of α. [46, 47]

$$E_a(\alpha) = \frac{n\sum_1^n \frac{1}{T_n} \cdot \ln(P(\alpha, T_n)) - \sum_1^n \frac{1}{T_n} \cdot \sum_1^n \frac{1}{\ln(P(\alpha, T_n))}}{n\sum_1^n \left(\frac{1}{T_n}\right)^2 - \left(\sum_1^n \frac{1}{T_n}\right)^2} \cdot R \qquad \textbf{Eq. 2.10}$$

where,

T_n = Isothermal test temperature (different for each test n).

There are several serious limitations of this method. This method is very sensitive to errors in measurement and calculation. Measurement precision and bias also affect the quality of the result, especially at low temperatures [53]. The incremental method also produces a variable E_a, which is not easily quantifiable or implementable in temperature prediction or maturity models [53].

2.7.2.3 ASTM C 1074

ASTM specifies that the mortar strength measured at different ages and at three different isothermal temperatures be used to calculate E_a. There are three different calculation procedures proposed by ASTM C 1074 to calculate E_a from the mortar strength results [49]. These processes vary only by the technique used to determine the *k*-value, which is the rate constant then used to construct the Arrhenius plot.

2.7.2.3.1 Linear Fit

Determination of the final setting time is required for this method. A graph is created by plotting the reciprocal of age beyond the final setting as the abscissa and the reciprocal of strength (MPa) as the ordinate. The *k*-value is determined for each temperature by dividing the intercept of each line by the slope of each line, shown in Figure 2.4 (a).

2.7.2.3.2 Hyperbolic Function

This method does not use the final setting time, but instead fits the k-value following Eq. 2.11.

$$S = S_u \frac{k(t - t_o)}{1 + k(t - t_o)} \qquad \textbf{Eq. 2.11}$$

where:

S = average cube compressive strengthen at the age t,

t = test age,

S_u = limiting strength,

t_o = age when strength development is assumed to begin, and

k = the rate constant.

The S_u, t_o, and k valus are determined from best fit curves by a least squared method. Figure 2.4 (b) shows the best fit curve using Eq. 2.11 by a least squares fitting technique.

2.7.2.3.3 Two Steps Method

In this method a plot of the reciprocal of the strength (Y-axis) versus reciprocal of age (X-axis) is made using strength values from the last four test ages. The limiting strength S_u is calculated as the inverse of the Y-axis intercept. Figure 2.4 (c) shows the process used to

determine S_u. The value of S_u for each of the three temperatures is used to compute the value of A for the first four compressive strength points as shown in Eq. 2.12

$$A = \frac{S}{(S_u - S)} \qquad \textbf{Eq. 2.12}$$

where, S and S_u are defined earlier.

A plot of A versus age is then made for each curing temperature, where the slope of the best-fit straight line for each curing temperature is the k-value for that temperature, shown in Figure 2.4 (d).

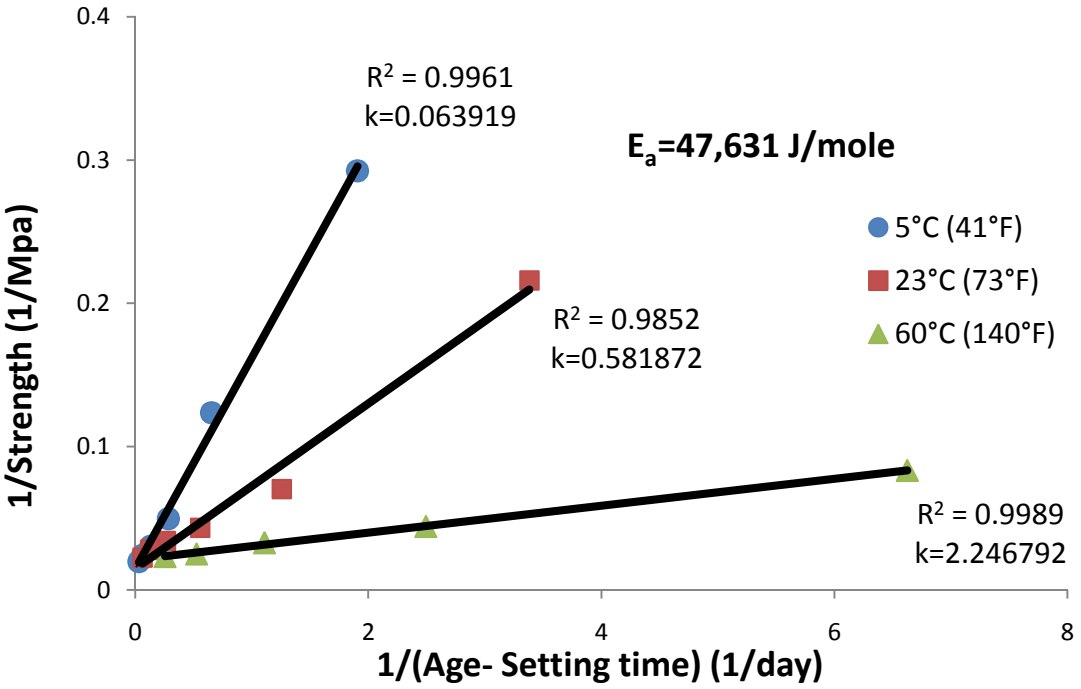

(a)

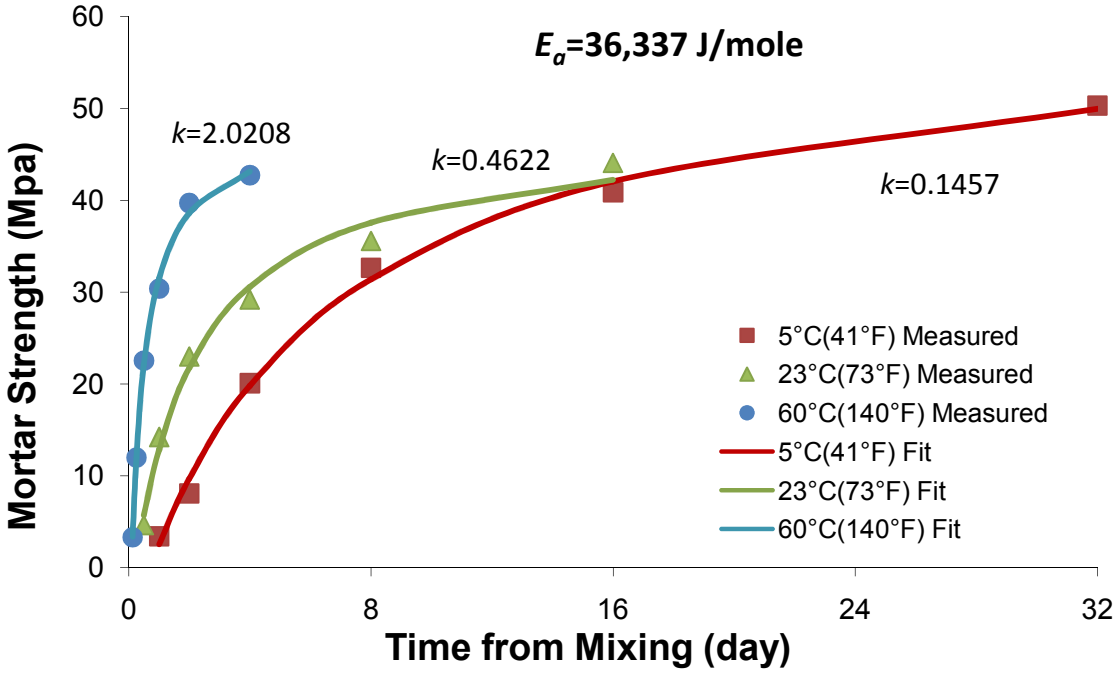
E_a=36,337 J/mole
k=2.0208
k=0.4622
k=0.1457
Mortar Strength (Mpa)
Time from Mixing (day)
5°C(41°F) Measured
23°C(73°F) Measured
60°C(140°F) Measured
5°C(41°F) Fit
23°C(73°F) Fit
60°C(140°F) Fit
0
10
20
30
40
50
60
0
8
16
24
32

(b)

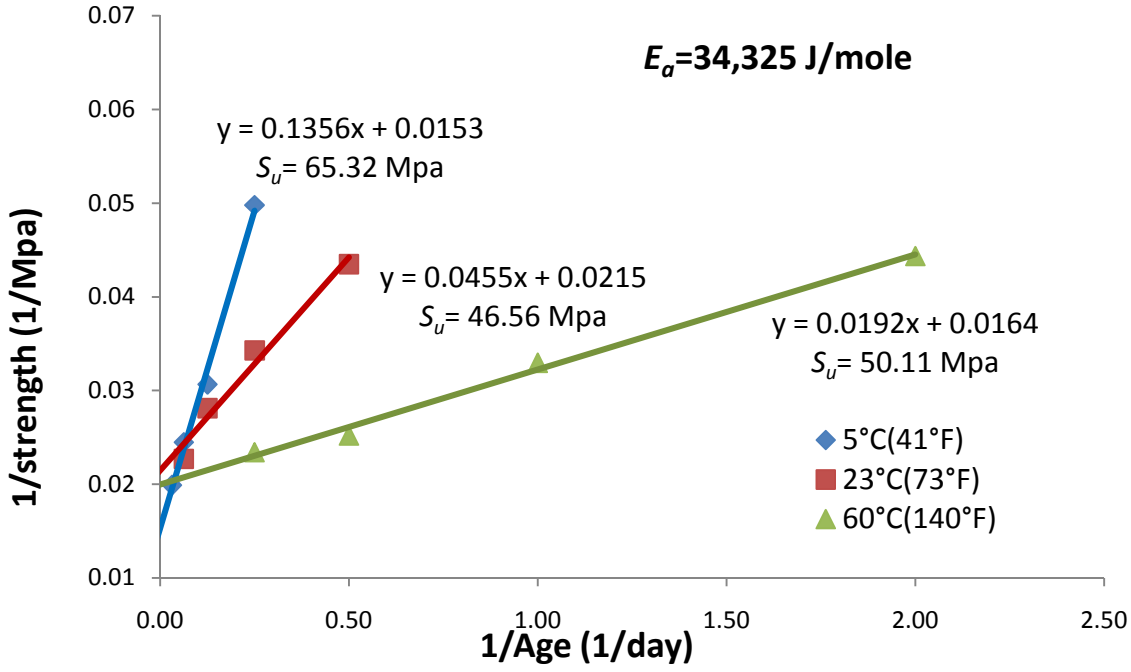
E_a=34,325 J/mole
y = 0.1356x + 0.0153
S_u= 65.32 Mpa
y = 0.0455x + 0.0215
S_u= 46.56 Mpa
y = 0.0192x + 0.0164
S_u= 50.11 Mpa
5°C(41°F)
23°C(73°F)
60°C(140°F)
1/strength (1/Mpa)
1/Age (1/day)
0.01
0.02
0.03
0.04
0.05
0.06
0.07
0.00
0.50
1.00
1.50
2.00
2.50

(c)

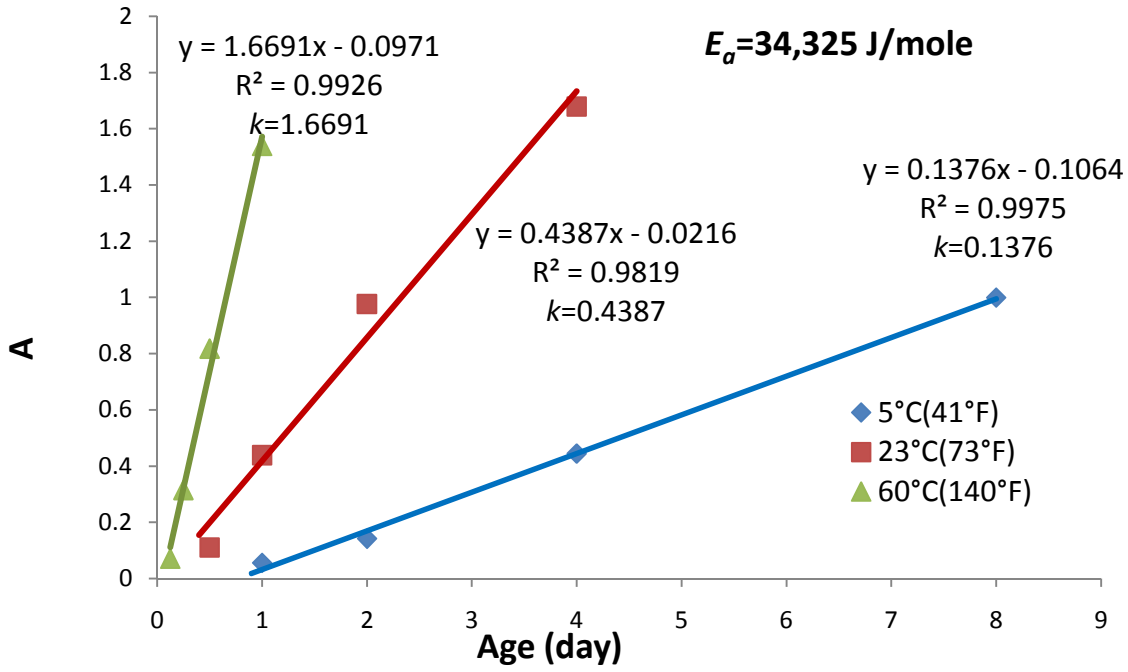

(d)

Figure 2.4: Determination of *k* by ASTM C 1074 Method; (a) Linear Fit, (b) Hyperbolic Function and (c and d) Two Steps Method.

After calculating the *k*-value using any of the methods discussed earlier, E_a is calculated by multiplying the negative of the slope of the best-fit straight line of the Arrhenius plot by the Universal gas constant *R*.

2.7.2.4 Exponential Method

This calculation method modifies the ASTM C 1074 method and was developed to calculate E_a from isothermal calorimetry data [48, 53, 62]. This method is very similar to the ASTM C 1074 method with Eq. 2.5 used to fit the experimental data instead of Eq. 2.12. This method overcomes a weakness with the ASTM C 1074 method, in that the ASTM C 1074 method considers the strength or hydration development before the time of set to be zero [53].

The relationship between τ at the reference temperature and test temperature to t and t_e, is shown in Eq. 2.13 [62].

$$\frac{t_e}{t} = f(T_c) = \frac{k(T_c)}{k(T_r)} = \frac{\tau_c}{\tau_r} \quad \textbf{Eq. 2.13}$$

where,

τ = chronological age,

τ_e = the equivalent age by Eq. 2.5,

$f(T_c)$ = the age conversion factor,

$k(T_c)$ = the reaction rate at concrete temperature T_c,

$k(T_r)$ = the reaction rate at reference temperature T_r,

τ_c = the hydration time parameter at concrete temperature T_c, and

τ_r = the hydration time parameter at reference temperature T_r.

E_a can be calculated from Eq. 2.14, which is derived from Eq. 2.1 and 2.13 [62].

$$E_a = -\frac{\ln\left(\frac{\tau_r}{\tau_c}\right)}{\left(\frac{1}{T_r} - \frac{1}{T_c}\right)} \cdot R \quad \textbf{Eq. 2.14}$$

where E_a, t, T_r, T_c, and R are as defined previously.

In this method τ, α_u, and β are determined from a least squares fit of the experimental data, shown in Figure 2.5. E_a is then calculated from the Arrhenius plot with the τ term used as the rate constant as shown in Eq. 2.15:

$$\ln[k(T)] = -\ln(\tau) \quad \textbf{Eq. 2.15}$$

where, k and τ are defined earlier.

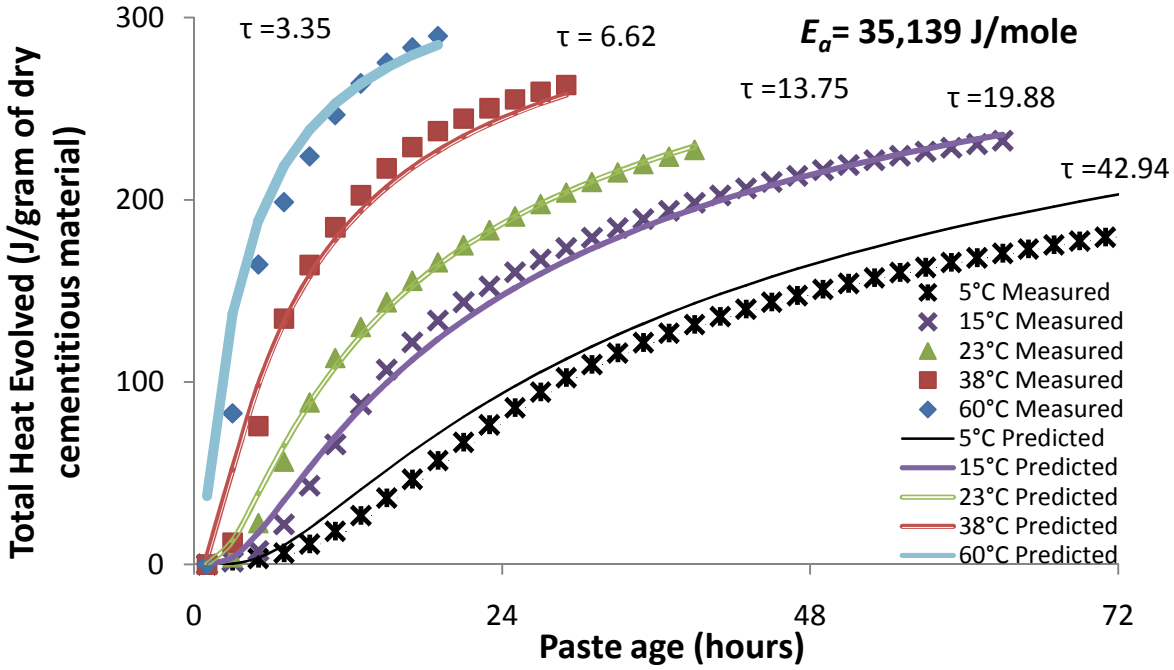

Figure 2.5: Determination of τ from Least Squares Best Fit Curve.

2.7.2.5 Setting Time

This calculation technique for calculating E_a from setting times was first described by Pinto and Hover [54]. In this method, inverse of setting time was used as the rate constant in the Arrhenius plot. Figure 2.6 shows an example of the Arrhenius plot for setting time.

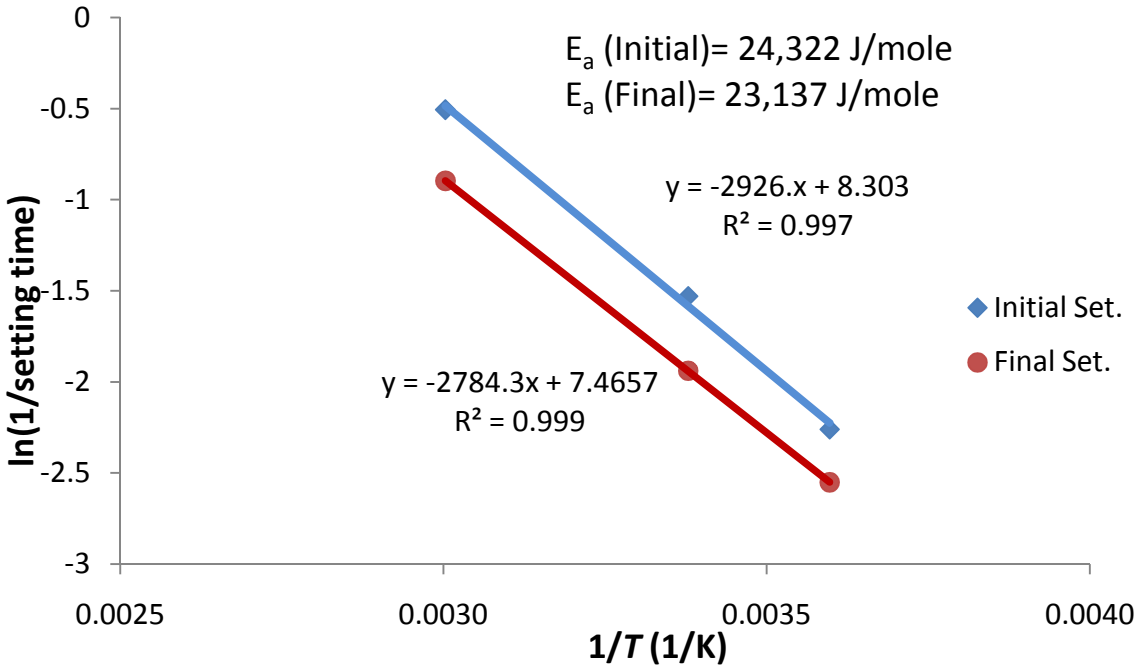

Figure 2.6: Determination of E_a by setting time method.

References

1. Taylor, H. F. W., “Cement Chemestry,” Academic Press Limited, San Diego, CA, , 1990.
2. Mindess, S., and, Young, J. F., “Concrete,” Prentice-Hall Inc., New Jersey, 1981.
3. Bogue, R. H., “The Chemistry of Portland Cement,” Reinhold Publishing Corporation, New York, 1947, pp. 572.
4. ASTM C 150, “Standard Specification for Portland Cement,” American Society for Testing and Materials, Pennsylvania, 2009.
5. ASTM C 595, “Standard Specification for Blended Hydraulic Cements,” American Society for Testing and Materials, Pennsylvania, 2009.
6. Schindler, A. K., "Concrete Hydration, Temperature Development, and Setting at Early-Ages," Doctoral Dissertation, The University of Texas at Austin, Austin, TX, 2002.
7. Neville, A. M., “Property of concrete,” Longman Singapore Publishers, Singapore, 1984.
8. ACI Committee 201, “Guide to durable concrete.” Journal fo the American Concree Institute, 1991, pp. 544-574.
9. Al-Gahtani, R. A. S., and Al-Assdoun S. S., “ Influence of construction practices on concrete durability,” ACI Material Journal, V. 86, No. 6, 1989, pp. 566-576.
10. Singh, G.; and Singh, J.,”Material of Construction,” Standard Book Service, Delhi, 1979, pp. 203.
11. Price, W. H. "Factors influencing concrete strength." ACI Journal, V. 47, No. 2, 1951, pp. 417-432.
12. Ramezanianpour, A. A. and Malhotra, V. M., "Effect of Curing on the Compressive Strength, Resistance to Chloride-Ion Penetration and Porosity of Concretes Incorporating

Slag, Fly Ash or Silica Fume," Cement and Concrete Composites, V. 17, No. 2, 1995, pp. 125-133.

13. Zain, M. F. M., Safiuddin, M. and Yusof, K. M., "Influence of Different Curing Conditions on the Strength and Durability of High Performance Concrete," In the Proceedings of the Fourth ACI International Conference on Repair, Rehabilitation and Maintenance, ACI SP-193, American Concrete Institute, Farmington Hills, Michigan, USA., 2000, pp. 275-292.
14. Aitcin, P. C., "High-Performance Concrete," London, E&FN Spon, 1998.
15. Kovler, K.; and Jensen, M., "Novel Techniques for Concrete Curing." Concrete international, V. 27, 2005, pp. 39-42.
16. Meeks, K. W., and Carino, N. J., "Curing of High-Performance Concrete: Report of the State-of-the-Art," NISTIR6295, U.S. Department of Commerce, 1999.
17. Bentz, D., Lura, P., and Roberto, J. W., "Mixture Proportioning for Internal Curing," Concrete International, V. 27, N0. 2, 2005, pp. 35-40.
18. Mather, B., "Self-Curing Concrete, Why Not?," Concrete International, V. 223, 2001, pp. 46-47.
19. Weber, S., and Reinhardt, H. W. "A New Generation of High-Performance Concrete: Concrete with Autogenous Curing," Advanced Cement-Based Materials, V. 6, 1997, pp. 59-68.
20. Hoff. G., and Elimov, R., "Concrete Production for the Hibernia Platform," Second CANMET/ACI International Symposium on Advances in Concrete Technology, supplementary papers. Las Vegas, 1995, pp. 717-739.

21. Kovler, K., Bentur, A., Lange, D. A., Bentz, D., Van Breugel, K., Lura, P., Zhutovsky, S., and Souslikov, A., "Autogenous Curing of High-Strength Cementitious Materials by Fine Uniformly Distributed LightLightweight," Research Report to U.S.-Israel Binational Science Foundation, Technion, Haifa, 2004.
22. Villarreal, V. H., "Building Better Pavements Through Internal Hydration—A Work in Progress," Proceedings of the R. Villarreal International Symposium on Durability of Concrete, Monterrey, México, 2005, pp. 13.
23. Jensen, O. M., and Hansen, P. F., "Water-Entrained Cement-Based Materials: Principles and Theoretical Background," Cement and Concrete Research, V. 31, 2001, pp. 647-654.
24. Jensen, O. M., and Hansen, P. F., "Water-Entrained Cement-Based Materials: II-Experimental Obsurvations," Cement and Concrete Research, V. 32, 2002, pp. 973-978.
25. Warner, J., "Practical Handbook of Grouting - Soil, Rock and Structures," John Wiley & Sons., Hoboken, NJ, 2004.
26. ASTM C 618, “Standard Specification for Coal Fly Ash and Raw or Calcined Natural Pozzolan for Use in Concrete,” American Society for Testing and Materials, Pennsylvania, 2009.
27. Smolczyk, H. G., “Slag Structure and Identification of Slag,” 7th International Congress on the Chemistry of Cement, V. 1. Paris, France, p. III- 1/3 ,1980.
28. ASTM C 989, “Standard Specification for Slag Cement for Use in Concrete and Mortars, “American Society for Testing and Materials, Pennsylvania, 2009.
29. Bognacki, C., "Innovative Uses of Slag Cement at the Port Authority of New York and New Jersey." Presentation at ACI Spring 2005 Convention, April 20, 2005.

30. Lim, S. N., and Wee, T. H., "Autogenous Shrinkage of Ground-Granulated Blast-Furnace Slag Concrete," ACI Materials Journal, V. 97, No. 5, 2000, pp. 587-593.
31. Sanjayan, J. G., and Sioulas, B., "Strength of Slag Cement Concrete Cured in Place and in Other Conditions," ACI Materials Journal, V. 97, No. 5, 2000, pp. 603-611.
32. Chancey, R. T., "Characterization of crystalline and amorphous phases and respective reactivates in a Class F fly ash," Doctoral Dissertation, The University of Texas at Austin, Austin, TX, 2008.
33. Roy, D. M., Luke, K., and Diamond, S., "Characterization of Fly Ash and Its Reactions in Concrete, " Fly Ash and Coal Conversion By-Products: Characterization, Utilization, 528 and Disposal I, Materials Research Society Symposia Proceedings, 1989, pp. 3-20.
34. ACI 234, "Silica Fume in Concrete," American Concrete Institute, Farmington Hills, Michigan, 1996.
35. ASTM C 1240, "Standard Specification for Silica Fume Used in Cementitious Mixtures," American Society for Testing and Materials, Pennsylvania, 2009.
36. Chandra, S., "Waste Materials Used in Concrete Manufacturing," William Andrew Publishing /Noyes, New York, 1997, pp. 556.
37. Taylor, P. C., Kosmatka, S. H., Voigt, G. F., et al., "Integrated Materials and Construction Practices for Concrete Pavement: A State-of-the-Practice Manual", Center for Transportation Research and Education, Iowa State University, December, 2006.
38. Hjorth, L., "Microsilica in concrete," Nordic Concrete Research, V. 1, Dec. 1982, pp. 72-81.
39. ASTM C 494, "Standard specification for Chemical Admixtures for Concrete," American Society for Testing and Materials, Pennsylvania, 2009.

40. Edmeades, R. M., and Hewlett, P. C., “Cement Admixtures, Lea’s Chemistry of Cement and Concrete," 4th ed., Arnold Publishers, New York, 1998, pp. 837-901.
41. Tazawa, E., and Miyazawa, S., “Chemical Shrinkage and Autogenous Shrinkage of Hydrating Cement Paste”, Cement and Concrete Research, V. 25, No. 2, 1995, pp. 288-292.
42. Gonzalez, A., “An evalution of the ASTM standard method for measuring chemical shrinkage of hydraulic cementitious pastes”, M.A.Sc. Thesis, University of Toronto, Canada, 2007.
43. Justnes, H., “Autogenous Shrinkage of Cementitious Paste-State-of-the-Art”, ACI 7th International Symposium on Recent Advances in Concrete Technology, ACI, 2004, pp 199-213.
44. Baroghel-Bouny, V., Mounanga, P., Loukili, A. and Khelidj, A., “From Chemical and Microstructural Evaluation of Cement Pastes to the Development of Autogenous Deformations”, ACI International SP-220 Autogenous Deformation of Concrete, 2003, pp 1-22.
45. Geiker, M., “Studies of Portland Cement Hydration”, Doctoral thesis, Institute of Mineral Industry, The Technical University of Denmark, Lyngby, Denmark, 1983.
46. D’Aloia, L., and Chanvillard, G., “Determining the ‘Apparent’ Activation Energy of Concrete; E_a-Numerical simulations of the Heat of Hydration of Cement,” Cement and Concrete Research, V. 32, 2002, pp. 1277-1289.
47. Kada-Benameur, H., Wirquin, E., and Duthoit, B., “Determination of Apparent Activation Energy of Concrete by Isothermal Calorimetry,” Cement and Concrete Research, V. 30, 2000, pp. 301-305.

48. Wirquin, E., Broda, M., and Duthoit, B., "Determination of the Apparent Activation Energy of One Concrete by Calorimetric and Mechanical Means; Influence of Super-Plasticizer," Cement and Concrete Research, V. 32, 2002, pp. 1207-1213.
49. ASTM C 1074, "Standard practice for estimating concrete strength by the maturity method," American Society for Testing and Materials, Pennsylvania, 2009.
50. Ma, W., Sample, D., Martin, R., and Brown, P. W., "Calorimetric Study of Cement Blends Containing Fly Ash, Silica Fume, and Slag at Elevated Temperatures," Cement, Concrete, and Aggregates, V. 16, 1994, pp. 93-99.
51. Kada-Benameur, H., Duthoit, B., and Lejeune, G., "Dispositif d'étude de la cinétique d'hydratation des bétons par calorimétrie isotherme," Bulletin de liaison des Laboratories des Ponts et Chaussées, 1997, pp. 31-40.
52. Zhang, X., Yang, Y., and Ong, C. K., "A Novel Way of Estimation of the Apparent Activation Energy of Cement Hydration Using Microwave Technique," Journal of Material Science, V. 34, No. 13, 1990, pp. 3143-3147.
53. Poole, J. L., Riding, K. A., Folliard, K. J., Juenger, M. C. G., and Schindler, A. K., "Methods for Calculating Activation Energy for Portland Cement," ACI Materials Journal, V. 104, No. 1, 2007, pp. 303-311.
54. Pinto, R. C. A., and Hover, K. C., "Application of Maturity Approach to Setting Times," ACI Materials Journal, V. 96, No. 6, 1999, pp. 686-691.
55. García, L., Castro-Fresno, D., and Polanco, J., "Maturity Approach Applied to Concrete by Means of Vicat Tests," ACI Materials Journal, V. 105, No, 5, 2008, pp. 445-450.

56. Glasstone, S., Laidler, K. J., and Eyring, H., "The Theory of Rate Processes: The Kinetics of Chemical Reactions," Viscosity, Diffusion, and Electrochemical Phenomena. McGraw-Hill Book Company, Inc. New York, 1941, pp. 611.
57. Van Breugel, K., "Prediction of Temperature Development in Hardening Concrete," Prevention of Thermal Cracking in Concrete at Early Ages, RILEM Report 15, E&FN Spon, London, 1998, pp. 51-75.
58. Copeland, L. E., Kantro, D. L., Verbeck, G., "Part IV-3 Chemistry of Hydration of Portland Cement," 4th International Symposium of the Chemistry of Cement, Washington, D.C., 1960, pp. 429-465.
59. De Schutter, G., and Taerwe, L., "Degree of Hydration-Based Description of Mechanical Properties of Early-Age Concrete," Materials and Structures, V. 29, No. 6, 1996, pp. 335-344.
60. Schindler, A. K., and Folliard, K. J., "Heat of Hydration Models for Cementitious Materials," ACI Materials Journal, V. 102, No. 1, 2005, pp. 24-33.
61. Pane, I., and Hansen, W., "Concrete Hydration and Mechanical Properties under Nonisothermal Conditions," ACI Materials Journal, V. 99, No. 06, 2002, pp. 534-542.
62. Schindler, A. K., "Effect of Temperature on Hydration of Cementitious Materials," ACI Materials Journal, V. 101, No. 1, 2004, pp. 72-81.

CHAPTER 3 - EFFECT OF METHODS AND CALCULATION TECHNIQUES ON APPARENT ACTIVATION ENERGY OF CEMENTITIOUS MATERIAL

3.1 Introduction

Many chemical reaction rates can show sensitivity to the reaction temperature. An explanation of the physical process responsible for this temperature dependence was first proposed by Swedish scientist Svante Arrhenius in 1889. Under the classic definition, the activation energy is the minimum energy required for a reaction to occur for a single reaction. The higher the temperature is, the higher the number of molecules with a kinetic energy high enough for the reaction to occur. In cement hydration however, multiple reactions take place simultaneously, all of which are affected by temperature. The term apparent activation energy (E_a) is used to represent the average effect of temperature on the combined reactions [1]. Whether for a single reaction with the activation energy, or multiple reactions, the activation energy is determined empirically. The apparent activation energy is commonly used for strength prediction for formwork removal or load application according to the maturity method as specified in ASTM C 1074 [2], cement degree of hydration (DOH) or creep calculations. The accuracy of the concrete strength predicted under realistic temperatures depends on the accuracy of E_a.

Researchers have developed various methods and calculation techniques to determine the apparent activation energy of cementitious materials [2-9]. These methods are based on different physical property measurements of cementitious materials that develop with the progress of hydration. The strength development [2], heat of hydration [3, 4], and time of set [5, 6] have

been used to determine the activation energy for concrete. The wide variety of measurement and calculation methods can result in different E_a values, warranting further study.

This study is an effort to present the variability of apparent activation energy of cementitious materials for different methods and calculation techniques. Both cement mortar and paste were studied, as activation energies are often quantified using paste samples and then used to predict the properties of concrete. The E_a was calculated from mortar cube strengths, time of set using vicat and mortar penetrometer, isothermal heat of hydration, and chemical shrinkage measurements and were measured for a wide variety of cementitious systems in this study. The calculation techniques described in ASTM C 1074 [2] (using hyperbolic function, linear fit and two steps method), a three parameter exponential model [8, 10, 11], and single linear approximation methods were used to calculate the kinetic rate constant used in the Arrhenius plot to calculate the apparent activation energy. A comparison of E_a values from the different measurement and calculation techniques is made. Finally, the effect of aggregates on E_a was evaluated by comparing the values obtained from cement paste and mortar at the same water-cementitious material ratio (w/cm).

3.2 Materials

A Type I cement was used in all mixtures studied. Two fly ashes – one Class C and one Class F, one silica fume, one slag, and metakaolin from two different sources were used in this study. Table 3.1 shows the chemical composition of the materials used in this study. Table 3.2 shows the cement phases calculated by the Bogue method and Rietveld refinement of x-ray diffraction measurements [12, 13]. A sand-cementitious material ratio of 2.75 by weight was used for the mortar experiments. Table 3.3 shows the material proportions used for the cement paste mixtures tested using isothermal calorimeter, vicat needle, and chemical shrinkage.

Table 3.4 shows the material proportions for the mortar mixtures tested using isothermal calorimeter, penetrometer, and mortar cube strength. Ten mixtures of cement paste for isothermal calorimetry were also prepared with the same cementitious materials and w/cm used in the mortar experiments to compare the E_a values obtained from cement paste and mortar in isothermal calorimetry. Chemical shrinkage and time of set experiments at the higher w/cm with paste were not attempted because of excessive bleeding at the higher w/cm, making these measurements difficult.

Table 3.1: Physical and Chemical Properties of Cementitious Materials.

Properties	Type I Cement	Class C Fly Ash	Class F Fly Ash	Metakaolin-1	Metakaolin-2	Slag
Specific Gravity	3.15	2.78	2.35	2.2	2.7	2.5
SiO_2, %	21.34	31.88	55.57	50.68	52.02	33.83
$Al2O_3$, %	4.74	17.83	23.98	43.62	44.39	11.45
Fe_2O_3, %	3.29	5.54	4.18	0.49	0.68	0.49
Si + Al + Fe, %	29.37	55.25	83.73	94.79	97.09	45.77
CaO, %	62.94	27.98	8.06	0.12	0.19	38.52
MgO, %	1.69	7.65	2.06	0.08	0.09	11.63
SO_3, %	2.68	2.86	0.5	0.09	0.09	2.55
Na_2O, %	0.14	2.15	0.66	0.28	0.25	0.28
K_2O, %	0.53	0.34	1.11	0.2	0.18	0.38
Total Alkalis as Na_2O	0.48	2.37	1.39	0.41	0.36	0.53
Blaine fineness (m^2/kg)	360.1	-	-	-	-	-

Table 3.2: Composition of Type I Portland Cement.

Properties	C_3S (%)	C_2S (%)	C_3A (%)	C_4AF (%)	Gypsum (%)	Hemihydrate (%)	Arcanite (%)
Type I Cement	66.96	16.49	2.92	9.29	2.31	1.68	0.23

Table 3.3: Cement Paste Material Proportions

Mixes	Description
Ty I	100% Type I cement; w/cm=0.35
25% C	75% Type I cement + 25% Class C fly ash; w/cm=0.35
25% F	75% Type I cement + 25% Class F fly ash; w/cm=0.35
15% M-1	85% Type I cement + 15% Metakaolin-1; w/cm=0.35
15% M-2	85% Type I cement + 15% Metakaolin-2; w/cm=0.35
6% SF	94% Type I cement + 6% Silica Fume; w/cm=0.35
25% S	75% Type I cement + 25% Slag; w/cm=0.35
WRA	100% Type I cement with water reducing admixture; w/cm=0.35
5% C 20% F	75% Type I cement + 5% Class C +20 % Class F fly ash; w/cm=0.35
20% C 5% F	75% Type I cement + 20% Class C +5 % Class F fly ash; w/cm=0.35

Table 3.4: Mortar Material Proportions

Mixes	Description
TyI-0.5	100% Type I cement; w/cm=0.5
TyI-0.45	100% Type I cement; w/cm=0.45
25% C	75% Type I cement + 25% Class C fly ash; w/cm=0.45
25% F	75% Type I cement + 25% Class F fly ash; w/cm=0.45
10% M-1	90% Type I cement + 10% Metakaolin-1; w/cm=0.45
5% SF	95% Type I cement + 5% Silica Fume; w/cm=0.45
25% S	75% Type I cement + 25% Slag; w/cm=0.45
WRA	100% Type I cement with water reducing admixture; w/cm=0.4
5% C 20% F	75% Type I cement + 5% Class C +20 % Class F fly ash; w/cm=0.45
20% C 5% F	75% Type I cement + 20% Class C +5 % Class F fly ash; w/cm=0.45

The fine aggregate used in this study met ASTM C 33 [14] requirements and had a fineness modulus of 3.3, bulk specific gravity of 2.5 and absorption of 0.42%.

3.3 Experimental Methods

3.3.1 Mixing Procedure

Materials for all mixtures were mixed at room temperature. Cement and other supplementary cementing materials (SCM) were preblended for one minute before mixing. For the mixtures used in the chemical shrinkage and isothermal calorimetry experiments, a small vertical laboratory mixer was used. In this procedure, water was added to the dry materials and allowed to rest for 15 seconds so that the cementitious material could absorb the water. The cementitious materials and water was mixed at 500 rpm (revolution per minute) for two minutes for cement paste. For mortar samples, the fine aggregates were slowly added to the mix over the first two minutes. The mix was then allowed to rest for another two minutes and mix again for another three minutes at 2000 rpm. For the larger paste and mortar samples required for mortar strength and time of set testing, mixing was performed according to ASTM C305 [15].

3.3.2 Mortar Strength

ASTM C 1074 [2] specifies the use of mortar cube compressive strength for the determination of E_a of cementitious materials. Mortar cubes were prepared and strengths were measured as per ASTM C 109 [16] specification. Three 50 mm x 50 mm mortar cubes were made and tested for compressive strength for each of the six different ages tested. The cubes were cured in saturated lime water at three different temperatures: 5^{o}C (41^{o}F), 23^{o}C (73^{o}F), and 60^{o}C (140^{o}F). The average of each set of three cubes tested at a particular age was considered to be one data point in the analysis. For cubes cured at 5^{o}C (41^{o}F), strength tests were performed at 1, 2, 4, 8, 16, and 32 days. For cubes cured at 23^{o}C (73^{o}F), strength tests were performed at 12hr,

1, 2, 4, 8, and 16 days. Finally, for cubes cured at 60°C (140°F), strength tests were performed at 6 hr, 12 hr, 1, 2, 4, and 8 days to capture the faster rate of reaction.

3.3.3 Time of Set

The concept of using the setting time as a measure of degree of hydration was first proposed by Pinto and Hover [5] and inspired from earlier research by Freiesleben-Hansen, and Pedersen [17]. In this study, Vicat needle testing according to ASTM C 191 [18] was used for cement pastes while the penetration resistance according to ASTM C 403 [19] was used for mortars to measure the time of set. Although the vicat needle testing was not done with a cement paste of normal consistency, the vicat needle test method has been used before on cementitious materials of various w/cm [20]. The cement paste and mortar setting time was measured at three different temperature at 5°C (41°F), 23°C (73°F), and 60°C (140°F).

3.3.4 Heat of Hydration

Cementitious materials gain strength from the exothermic reaction between cement and water. This generated heat can be used as a measurement of the cementitious system degree of hydration. The isothermal conduction calorimeter measures at a constant temperature the heat flow rate from the cement sample to a heat sink using a peltier sensor [21, 22]. In this study, the heat of hydration was measured using an eight-channel isothermal calorimeter (W.R. Grace Adiacal TC) at five different temperatures: 5°C (41°F), 15°C (59°F), 23°C (73°F), 38°C (100°F), and 60°C (140°F). The total heat of hydration was calculated by integrating the heat of hydration rate with time. E_a was calculated using the Arrhenius equation as shown in Eq. 3.1.

$$k = A.e^{-\frac{E_a}{RT}} \qquad \textbf{Eq. 3.1}$$

Where,

R = Universal gas constant (8.314 J/mol/K),

T = temperature (K) at which the reaction occurs,

k = the rate of heat evolution (W),

A = the proportionality constant (same units as k), and

E_a = activation energy (J/mol).

3.3.5 Chemical Shrinkage

As discussed earlier, chemical shrinkage can be a measure of the cement degree of hydration and therefore, can be used to calculate E_a. Chemical shrinkage can be measured by measuring the change in volume (first developed by Geiker [23] and then adopted as ASTM C 1608 [24]) or by the change in bouyancy in a cement paste [23, 25, 26]. In this study, the volumetric chemical measurement technique has been adopted as shown in Figure 3.1.

Plastic vials were used as the sample containers. A cement paste sample was placed in the bottom of the sample container, with distilled water carefully placed above the sample to avoid mixing. A rubber stopper with a glass pipette inserted through a hole in center of the stopper was then placed in the top of the vial. After the rubber stopper was inserted at the top of the sample container, the pipette was filled with water followed by a small amount of colored petrol with a lower density than water. A temperature controlled water bath was used to maintain a constant curing temperature. A webcam was used to take pictures of the water level in the pipette by monitoring the bottom of the colored petrol level. Automatic image analysis of the pipette water level was performed using the LMC Shrinkage Suite developed by Bishnoi in 2008. Figure 3.2 shows a sample picture taken by the webcam. The chemical shrinkage for each mixture was

taken as the average of four samples. Both cement paste and mortar mixes were used for chemical shrinkage determination.

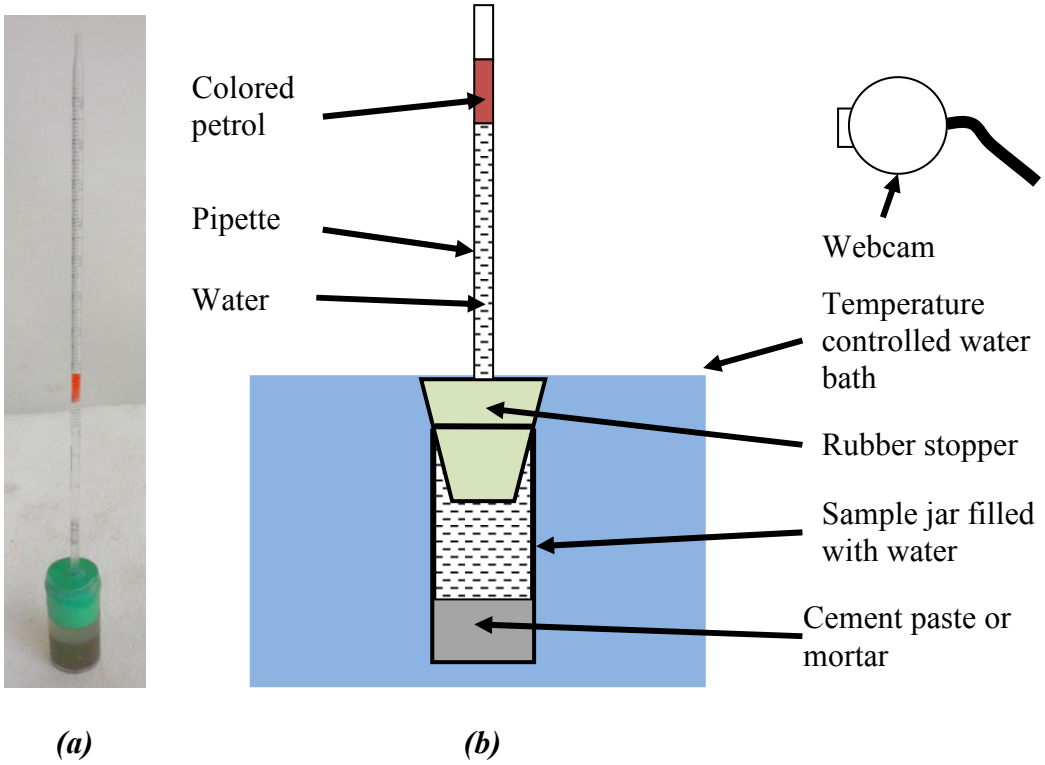

Figure 3.1: Chemical Shrinkage Setup; (a) Chemical Shrinkage Sample; and (b) Schematic Diagram of Chemical Shrinkage Bath.

Figure 3.2: Webcam Image of Pipette Water Level.

The effect of vial size and sample depth on the chemical shrinkage was also checked. To measure the chemical shrinkage correctly it is very important to choose a proper sample thickness. The effect of sample thickness on the chemical shrinkage is shown in Figure 3.3. If the sample is too thick, there will be a significant delay before the water can diffuse to the bottom of the sample to take the place of the space left vacant from chemical shrinkage. At higher temperatures when the rate of hydration is much higher, the critical sample thickness may be smaller. The water level drop in the chemical shrinkage test was measured at different depths at 23°C (73°F), and 38°C (100°F) to determine the optimum sample thickness. The thinner 5 mm sample tends to show higher chemical shrinkage in both experiments. It is suspected that it was a practical problem of not being able to gently place water on top of the thin sample without mixing that contributed to the higher shrinkage measured [27]. If it were a problem of the water having difficulty diffusing to the sample bottom in thicker samples, then the chemical shrinkage

measured would decrease with sample thickness which was not seen with the 10 and 15 mm samples.

The effects of the sample diameter were also tested using 26 mm and 30 mm inner diameter samples, as shown in Figure 3.4. Two sample depths of 10 mm and 15 mm were used for each sample diameter. The results showed that there is no significant effect of sample diameter as would be expected. For the remainder of the study, paste samples with a depth of 10 to 15 mm and a diameter of 26 mm corresponding to samples with a mass of 12 to 18 g were used. The same thickness of cement paste and mortar samples were used. Chemical shrinkage was measured for both cement paste and mortar at three different temperatures: 5°C (41°F), 23°C (73°F), and 38°C (100°F).

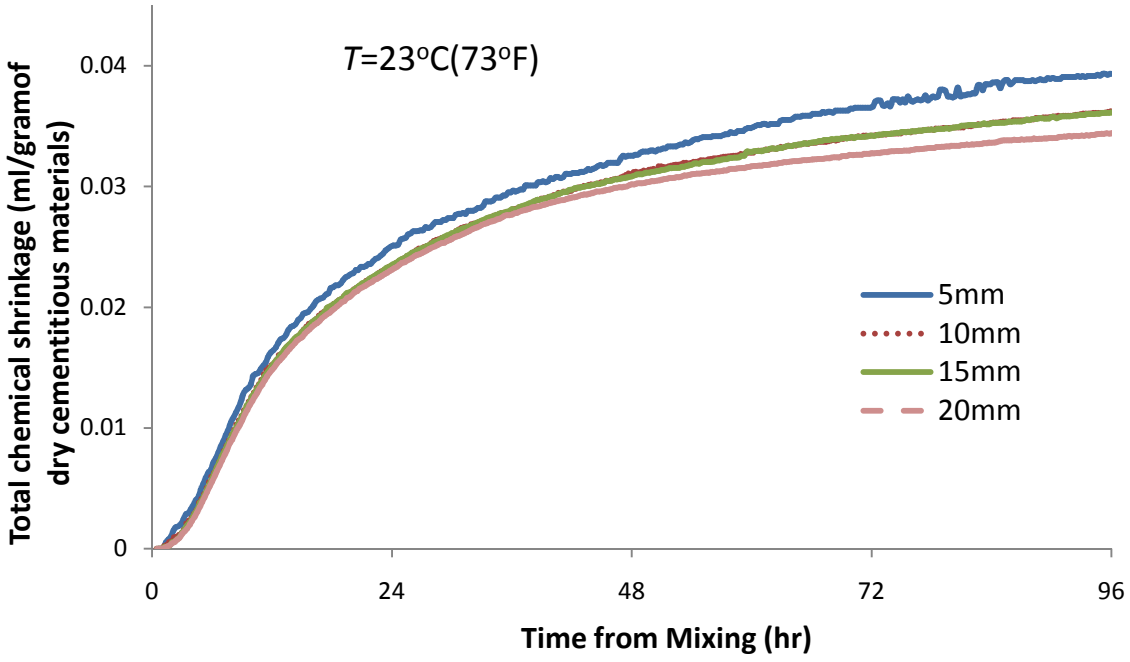

(a)

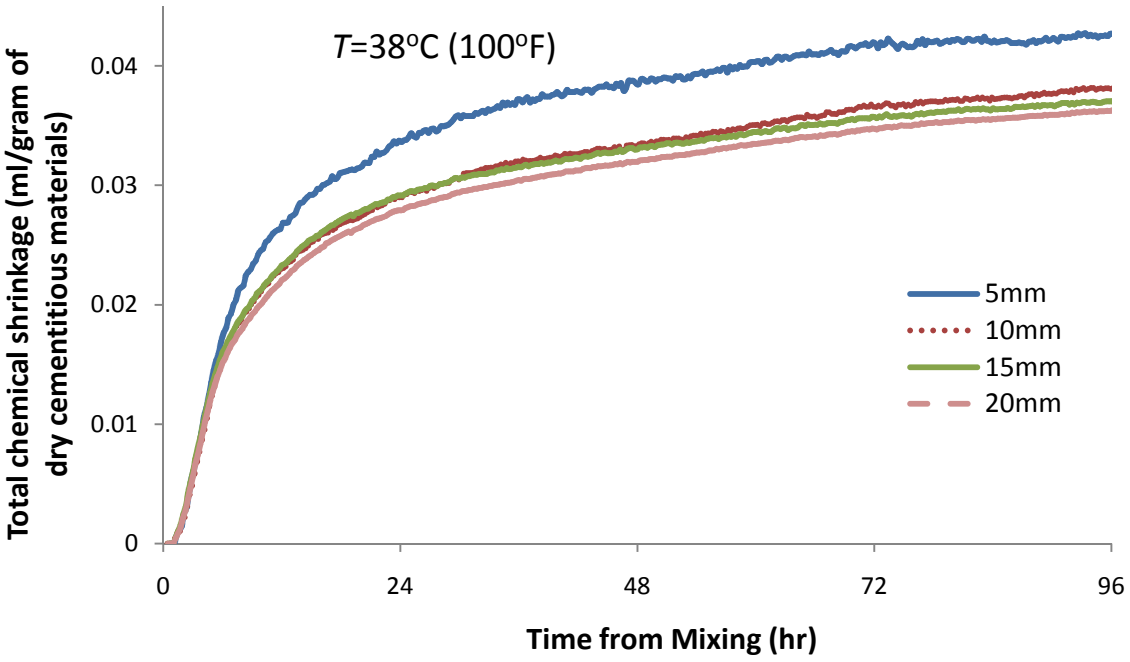

(b)

Figure 3.3: Effect of Sample High on Chemical Shrinkage; (a) 23 °C (73 °F); and (b) 38 °C (100 °F).

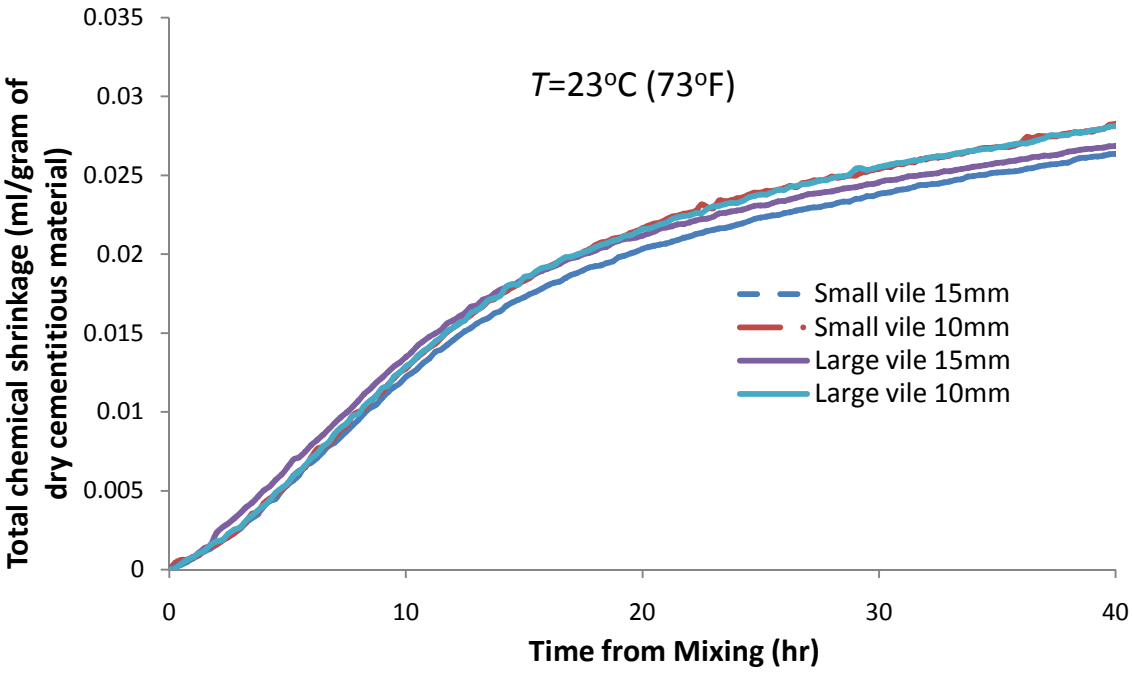

Figure 3.4: Effect of Vial Size on Chemical Shrinkage.

3.4 Calculation Techniques

The exponential method and ASTM C 1074 hyperbolic function were used for calculating E_a from the isothermal calorimetry and chemical shrinkage data. Additionally the single linear approximation technique was used to calculate E_a from the isothermal calorimetry data. The ASTM C 1074 linear fit, hyperbolic function and two step methods were used to calculate E_a from the mortar cube strength. E_a was calculated from setting time data by the method proposed by Pinto and Hover [5].

3.4.1 Single linear approximation

The single linear approximate method is the simplest method for calculating E_a from isothermal calorimetry or chemical shrinkage data [7]. The slope of the linear part of the acceleration phase of the cement hydration was used to calculate the rate constant k [7]. E_a can be calculated as the universal gas constant R (= 8.314 $Jmole^{-1}k^{-1}$) multiplied by the slope of a line fit to the $\ln(k)$ versus $1/T$, which known as the Arrhenius plot.

3.4.2 ASTM C 1074

ASTM C 1074 specifies three methods for determination of E_a from mortar cube strength [2]. These techniques vary only by the calculation method used to obtain the rate constant k.

3.4.2.1 Linear Fit

The k-value for different temperatures was determined from the graph by plotting the reciprocal of age beyond the final setting as the abscissa and reciprocal of strength as the ordinate. The intercept of each best fit line is divided by the slope to obtain the rate constant k for each temperature. This technique was only used for the mortar cube strength method.

3.4.2.2 Hyperbolic Function

This method uses a hyperbolic equation for rate constant *k* determination, Eq. 3.2.

$$S = S_u \frac{k(t - t_o)}{1 + k(t - t_o)} \quad \textbf{Eq. 3.2}$$

where,

S = Cumulative heat of hydration/ chemical shrinkage/ average cube compressive strengthen at the age t,

t = test age,

S_u = Ultimate cumulative heat of hydration/ ultimate chemical shrinkage/limiting strength,

t_o = age when heat of hydration/ chemical shrinkage/ strength development is assumed to begin, and

k = the rate constant.

In the conventional method outlined in ASTM C 1074, S_u, t_o, k are determined by regression analysis for each temperature individually. This method will be referred to as the hyperbolic-U method. For determination of the E_a from the total heat of hydration and chemical shrinkage, the S_u, t_o, and k at 23°C (73°F) were first determined. Then t_o and k for the other temperatures were determined while the S_u value was kept equal to the value determined at 23°C (73°F). This technique will be referred to as hyperbolic-E in this paper for simplicity.

3.4.2.3 Two Steps Method

This method determines the *k*-value from mortar strength values in two steps. First, a plot of the reciprocal of strength (ordinate) versus the reciprocal of age (abscissa) was made using the strength values from the last four sample ages. The reciprocal of the interception of the Y-axis is the limiting strength S_u. The value of S_u for each of the three temperatures tested was determined.

The values of A using the first four test ages were calculated according to Eq. 3.3 for each temperature:

$$A = \frac{S}{(S_u - S)} \qquad \textbf{Eq. 3.3}$$

where, S and S_u were defined earlier.

A plot of A versus age was then made for each curing temperature, where the slope of a best-fit straight line for each curing temperatures was the k-value for that temperature. This method was used for mortar compressive strength only. E_a was then calculated from the Arrhenius plot discussed earlier.

3.4.3 Exponential Method

To calculate E_a from isothermal calorimetry and chemical shrinkage, a three-parameter exponential hydration function shown in Eq. 3.4 was used [8, 10, 11]. The three-parameter exponential function was advantageous in that the values before setting are non-zero [8].

$$H(t_e) = H_{ult} \cdot e^{-\left[\frac{\tau}{t_e}\right]^{\beta}} \qquad \textbf{Eq. 3.4}$$

where,

$H(t_e)$ = Total heat evolved/ total chemical shrinkage/ strength at equivalent time t_e,

H_{ult} = Total ultimate heat/ chemical shrinkage/ strength,

τ = the hydration time parameter (hours),

β = the hydration shape parameter, and

α_u = the ultimate degree of hydration.

In this study Eq. 3.4 was used with H_{ult}, τ and β first determined for the 23°C temperature through a least squares fit. The H_{ult} and β value for the cementitious system at the other temperatures were set equal to the value found at 23°C. The τ for a temperature was then

fit to the experimental data at that temperature using a least squares fit. The different τ values for each of the temperatures were then used as the rate constants in the Arrhenius plot. For chemical shrinkage tests, E_a was also calculated by fitting H_{ult}, β and τ individually for each temperature, with the τ values still used as the rate constants. This was done as the ultimate chemical shrinkage may be dependent on the curing temperature. The first method will be referred to as exponential-E and the later one as exponential-U for simplicity.

3.4.4 Time of Set

It has been shown that the E_a of cementitious materials can be calculated from the initial or final setting time at different temperatures [5]. The inverse of the setting time is used as the rate constant in this method. For both cement paste and mortar, initial and final setting times were used to calculate E_a values using this method.

3.5 Results and Discussions

The heat of hydration rate and cumulative heat of hydration data for all of the mixtures are presented in Appendix A. The isothermal calorimetry showed that metakaolin results in an increase in the heat of hydration rate and especially the aluminate reaction peak, as found by other researchers [28]. Fly ash and water reducing admixtures showed a delay in the onset of hydration. E_a was calculated by the Single Linear Approximation method, exponential-E, hyperbolic-U and hyperbolic-E method and presented in Appendix B.

3.5.1 Mortar Strength

A total of 540 mortar cubes were made to determine the mortar cube strength at 5 °C (41 °F), 23 °C (73 °F), and 60 °C (140 °F) and are found in Appendix C. The three methods

described by ASTM C 1074 were used to calculate E_a. Appendix D shows the rate constants and calculated E_a for the compressive strength experiments.

3.5.2 Time of Set

Both initial and final setting time was measured for the cement paste and mortar at 5 °C (41 °F), 23 °C (73 °F), and 60 °C (140 °F) and are shown along with the calculated E_a in Appendix E. The E_a values found are lower than values documented in earlier studies [5, 6]. Pinto and Hover also mixed their specimens at room temperature, and found much higher activation energies, whereas the activation energies calculated by Garcia et al. were much closer to those measured in this study. Both studies used the internal temperature of the concrete for E_a calculation which considers the effect of temperature rise of the concrete due to the heat of hydration. However, the curing temperature was used for E_a calculation in this study, potentially accounting for the difference in calculated E_a values.

3.5.3 Chemical shrinkage

For both cement paste mixtures at a 0.35 w/cm and mortar, E_a was calculated from chemical shrinkage experiments. The chemical shrinkage development for all cement paste and mortar experiments are shown in Apendix F. Exponential-E, expponential-U, hyperbolic-U, and hyperbolic-E calculation techniques were used for E_a calculations from chemical shrinkage. Calculated E_a values are presented in Appendix G.

3.5.4 Comparison between different methods

Setting time vs total heat of hydration for both cement paste and mortar are presented in Figures 3.5(a) and 3.5(b). For both the cement paste and mortar, E_a values calculated from setting time (both initial and final setting time) measurements give much lower values than those

from the isothermal total heat of hydration for the two calculation techniques. E_a values calculated from mortar strength using ASTM C 1074 linear fit from mortar strength give relatively higher values than the total heat of hydration for both the exponential and hyperbolic-E, shown in Figure 3.6. However, E_a values from mortar strength using the ASTM C 1074 hyperbolic function result in relatively lower values than the total heat of hydration for both exponential-E and hyperbolic-E. The ASTM C 1074 two step method results in lower E_a values than the exponential-E and hyperbolic-E calculated values from the total heat of hydration.

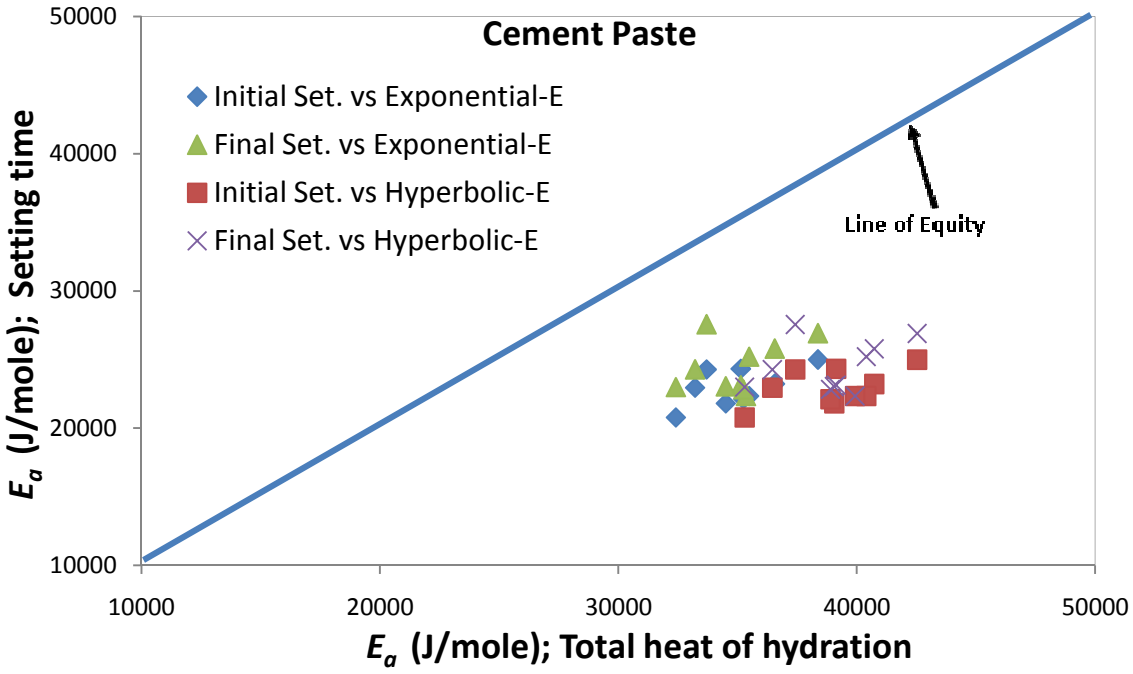

(a)

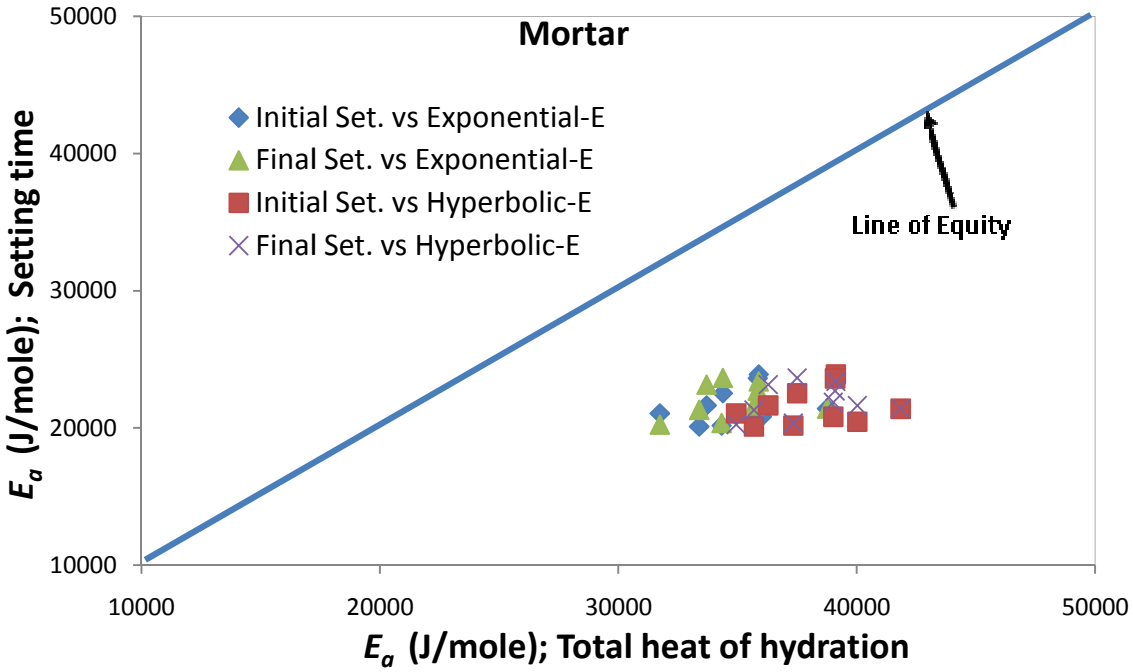

(b)

Figure 3.5: Comparison of E_a value; setting time vs total heat of hydration; (a) cement paste and (b) mortar.

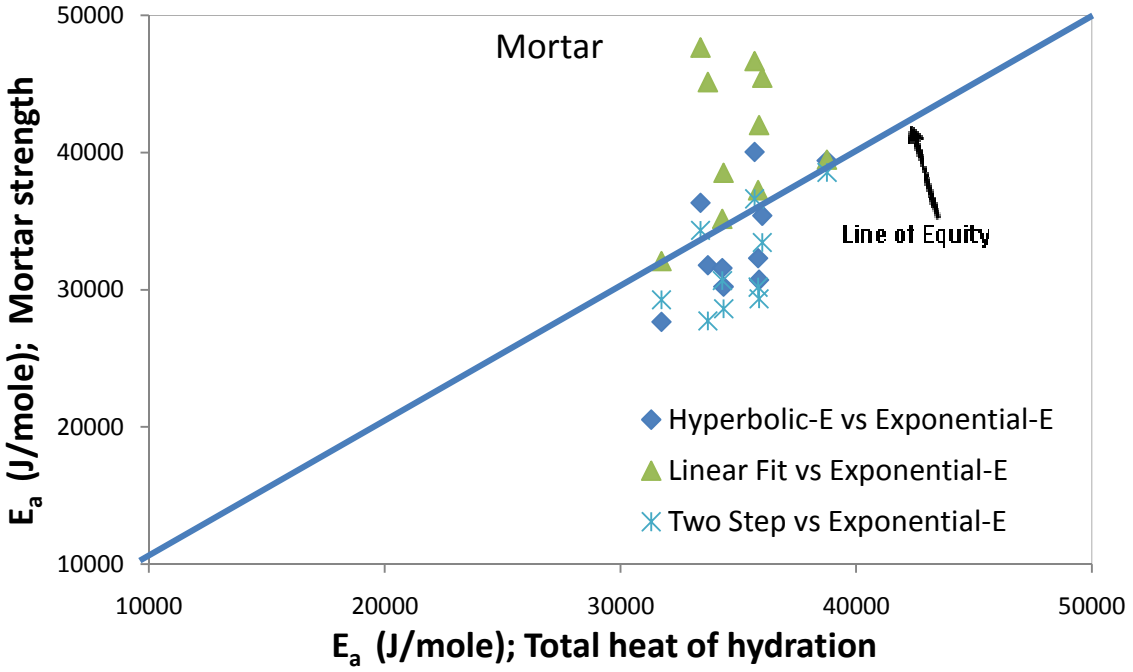

(a)

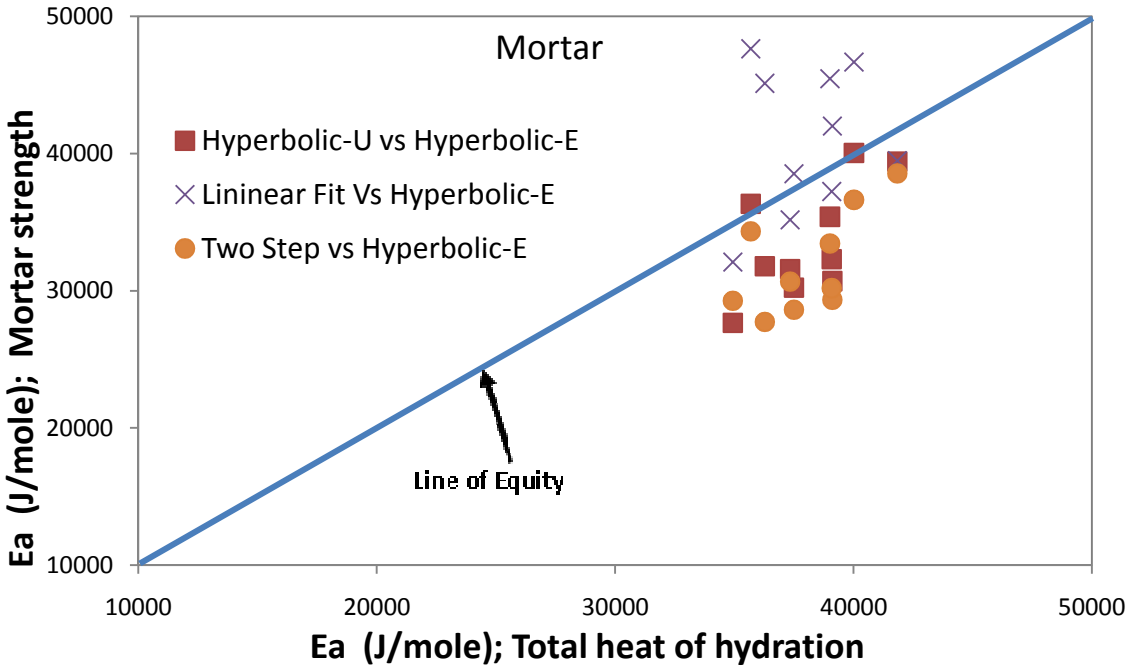

(b)

Figure 3.6: Comparison of E_a Values for Mortar Strength vs Total Heat of Hydration.

E_a values calculated from the final setting time gives slightly higher values than E_a values calculated from the initial setting time, shown in Figure 3.7. The relationship between initial and final setting time E_a values calculated from mortar (R^2=0.5648) shows better aggrement than E_a values calculated from cement paste (R^2=0.4494). E_a value, nonetheless, can be calculated by using either of the setting time values with little difference.

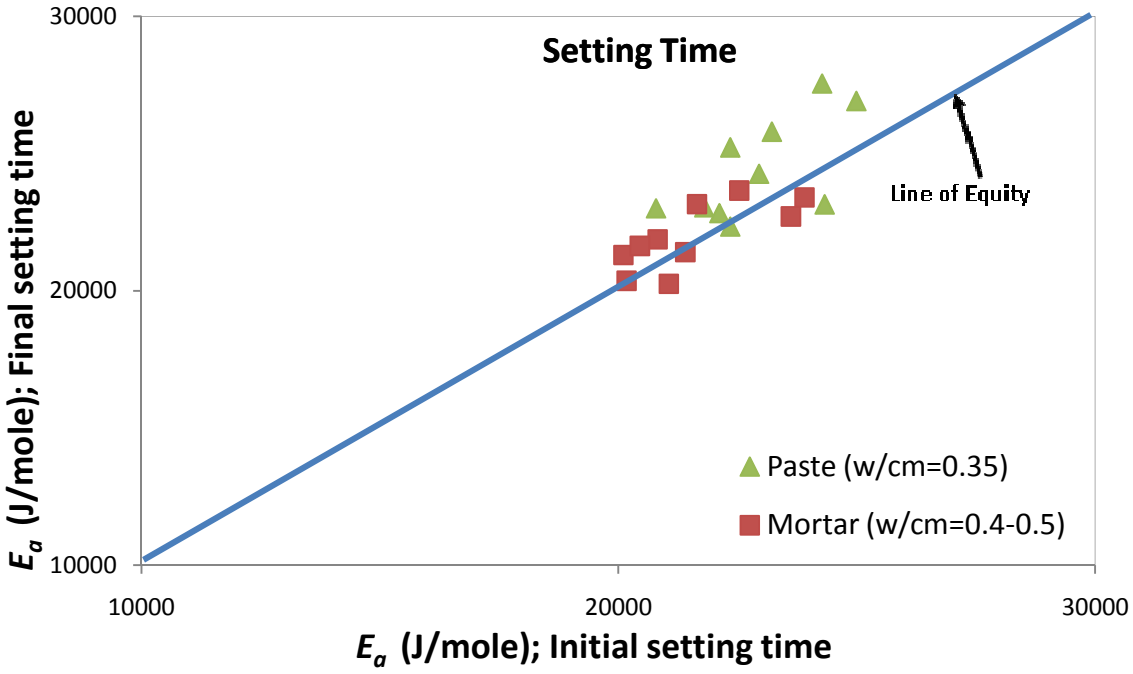

Figure 3.7: Comparison of Calculation Techniques for Setting Time.

Comparison between different calculation techniques for total heat of hydration is presented in Figure 3.8. The hyperbolic-E method gives slightly higher E_a values than the exponential-E method, but in a predictable manner (R^2=0.9082) as shown in Figure 3.8(a). The hyperbolic function does not model the hydration before setting time, whereas S-curves, such as, the three parameter function used does not have that limitation. The good correlation between these two methods shows how well both equations fit the total heat of hydration and represent their temperature sensitivity. Other calculation techniques for the total heat of hydration do not show any significant relation.

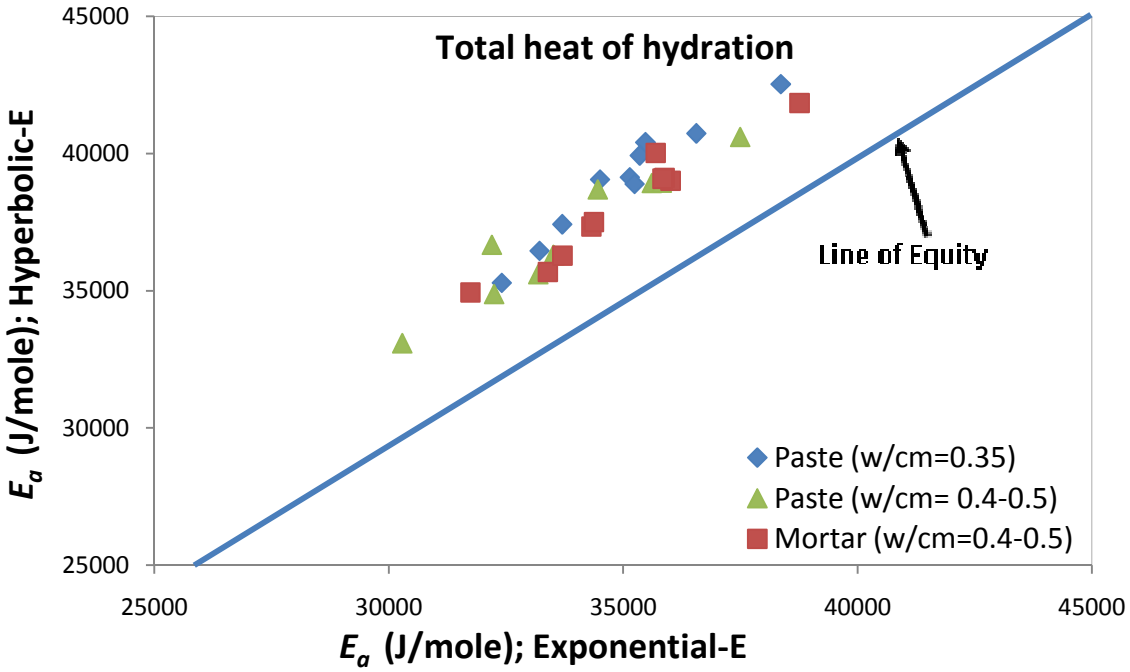
Total heat of hydration
Line of Equity
Paste (w/cm=0.35)
Paste (w/cm= 0.4-0.5)
Mortar (w/cm=0.4-0.5)
45000
40000
35000
30000
25000
25000
30000
35000
40000
45000
E_a (J/mole); Hyperbolic-E
E_a (J/mole); Exponential-E

(a)

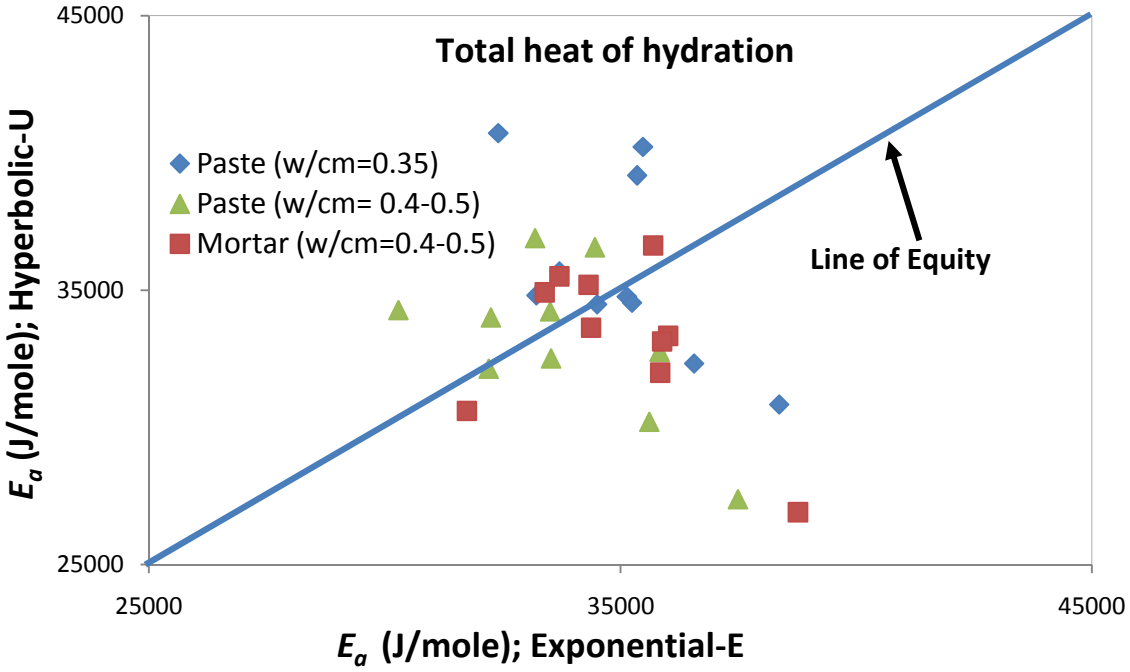
Total heat of hydration
Line of Equity
Paste (w/cm=0.35)
Paste (w/cm= 0.4-0.5)
Mortar (w/cm=0.4-0.5)
45000
35000
25000
25000
35000
45000
E_a (J/mole); Hyperbolic-U
E_a (J/mole); Exponential-E

(b)

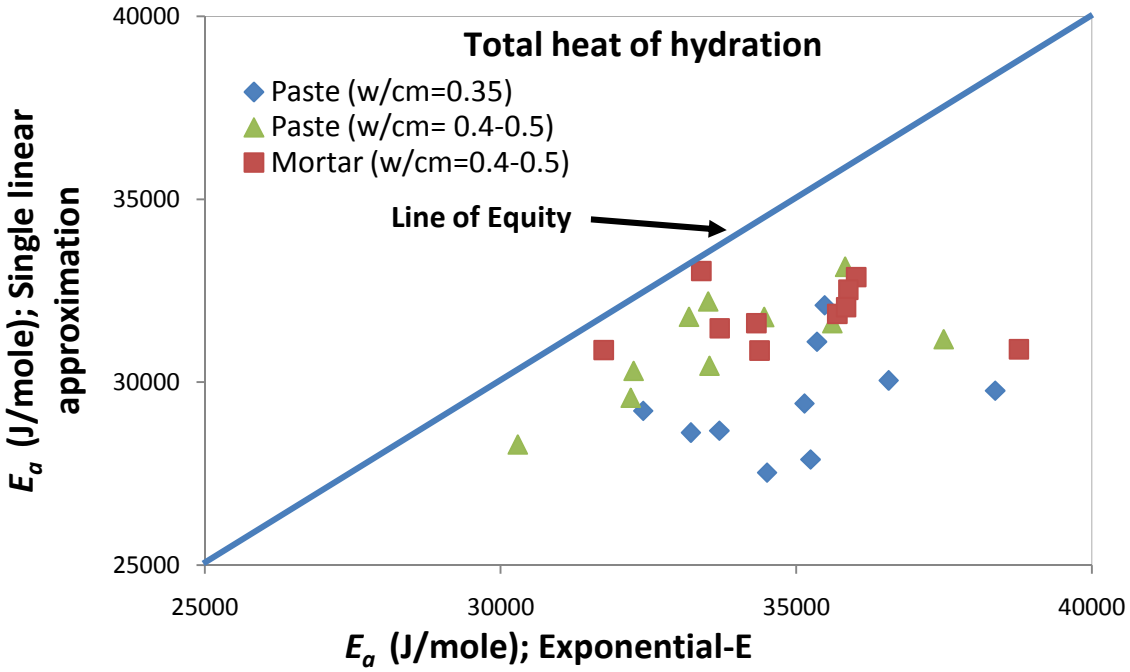

(c)

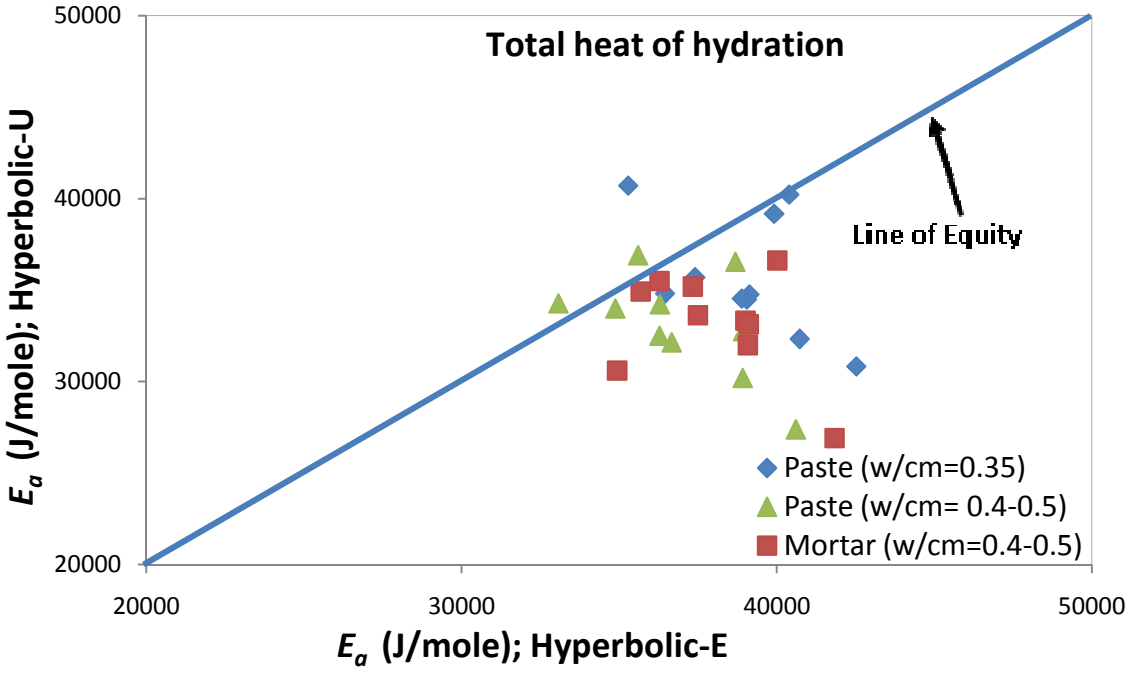

(d)

Figure 3.8: Comparison of Different Calculation Techniques for Total Heat of Hydration; (a) ASTM C 1074 Hyperbolic-E vs Exponential-E; (b) ASTM C 1074 Hyperbolic-U vs Exponential-E; (c) Single Linear Approximation vs Exponential-E; and (d) ASTM C 1074 Hyperbolic-U vs ASTM C 1074 Hyperbolic-E.

For mortar strength from ASTM C 1074, linear fit E_a values do not show any significant relation with the ASTM C 1074 hyperbolic function E_a, shown in Figure 3.9(a). These methods have two different approaches for finding k values. The hyperbolic function considers k from curve fitting and is more influenced by the later-age strength development. The linear fit is more oriented to the measured values and the early-age behavior of strength development. The ASTM C 1074 two step method gives slightly lower values than ASTM C 1074 hyperbolic function but showed good correlation with each other (R^2=0.8596), shown in Figure 3.9(b). This may be due to the fact that both these methods are more dependent on predicted values than on the measured values.

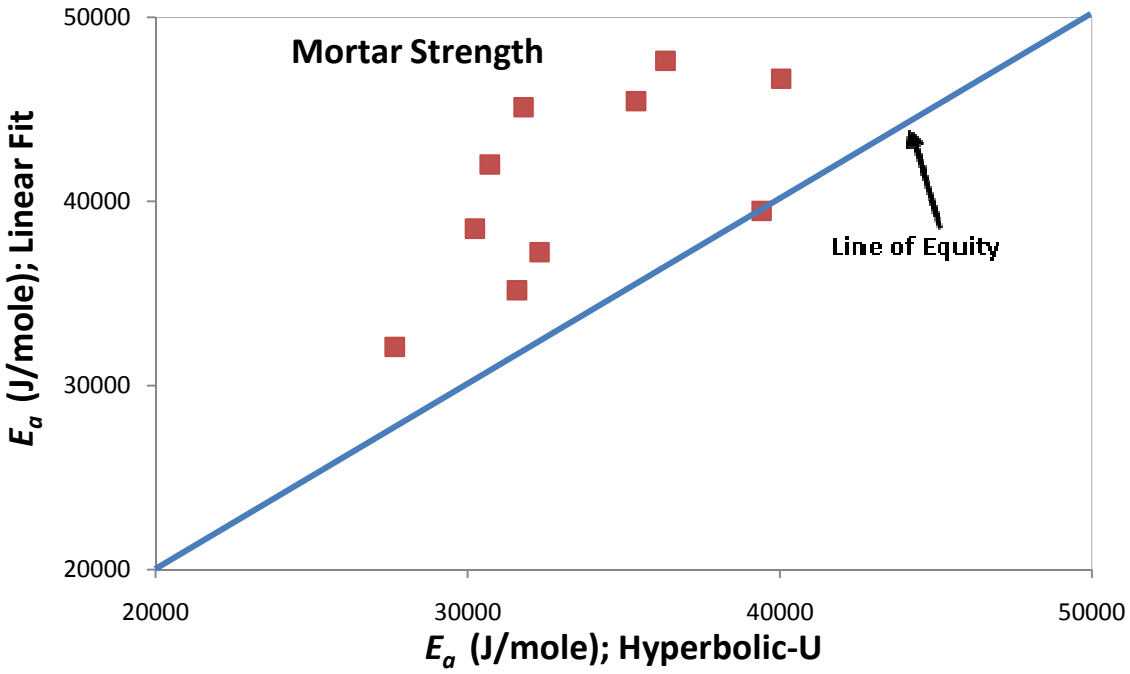

(a)

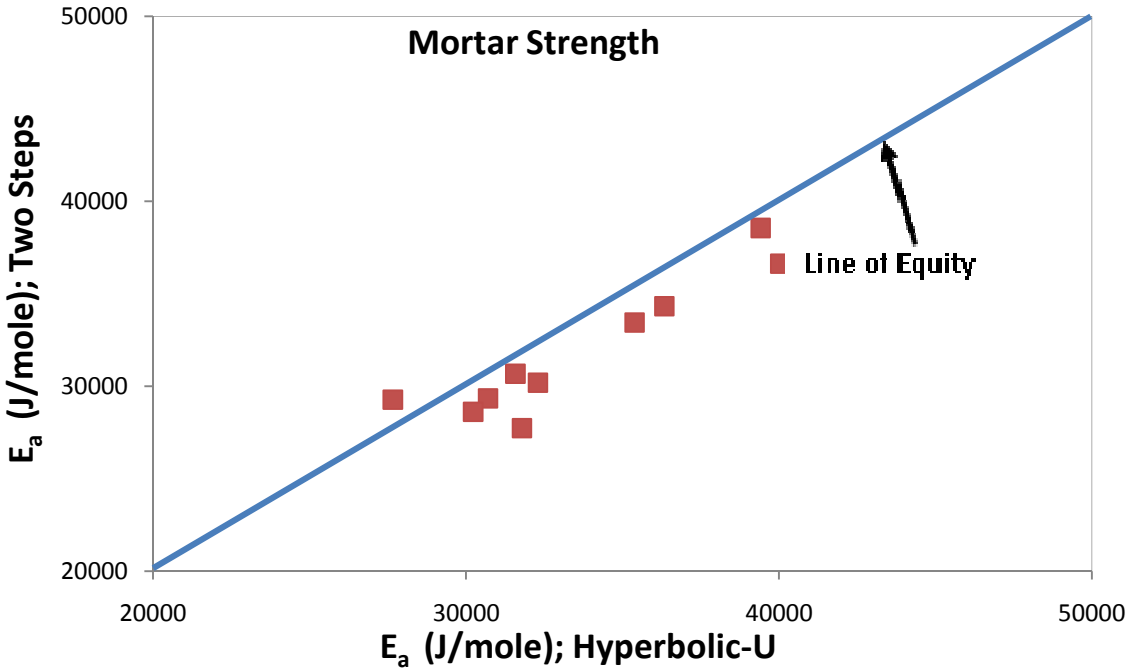

(b)

Figure 3.9: Comparison of Calculation Techniques for Mortar Strength; (a) ASTM C 1074 Linear Fit vs ASTM C 1074 Hyperbolic-U, and (b) ASTM C 1074 Two Steps Method vs ASTM C 1074 Hyperbolic-U.

ASTM C 1074 hyperbolic-E and exponential-E method E_a values, calculated from chemical shrinkage data, correlate well as shown in Figure 3.10(a). Thus, both equations fit well with the chemical shrinkage development curve. Mortar $E_{a,}$ calculated by ASTM C 1074 hyperbolic-E, gives lower values, and cement paste sample (R^2=0.7087) shows better correlation than mortar samples (R^2=0.5406). However; E_a values calculated using the ASTM C 1074 hyperbolic function and exponential method, unequal H_{ult} do not show any significant relationship, which is shown in Figure 3.10(b).

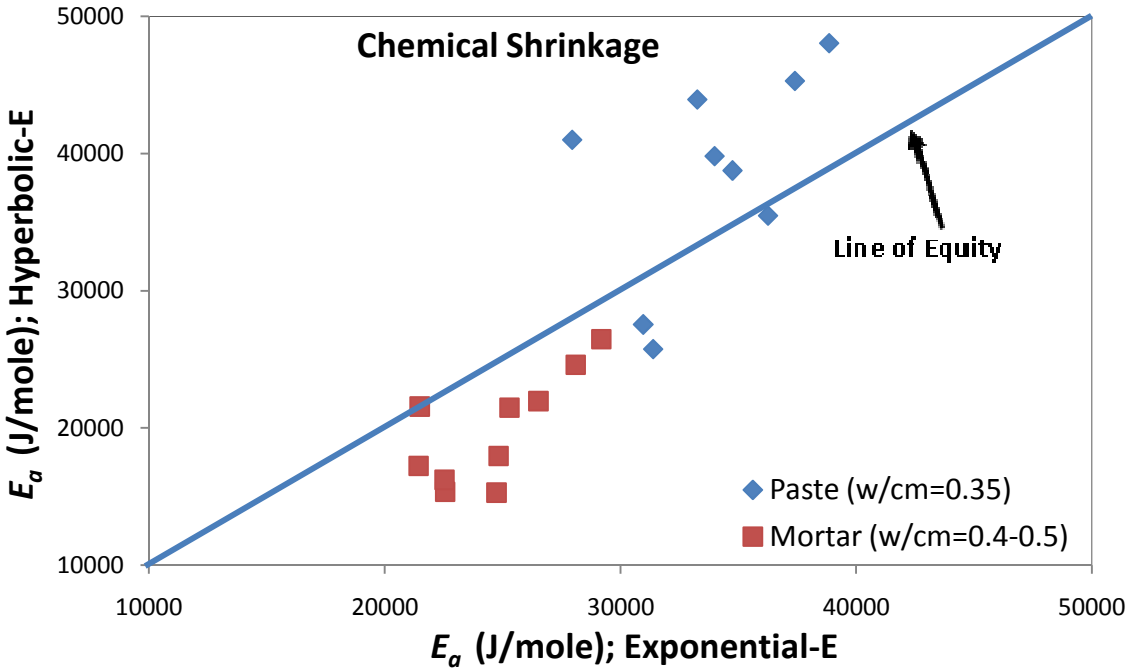

(a)

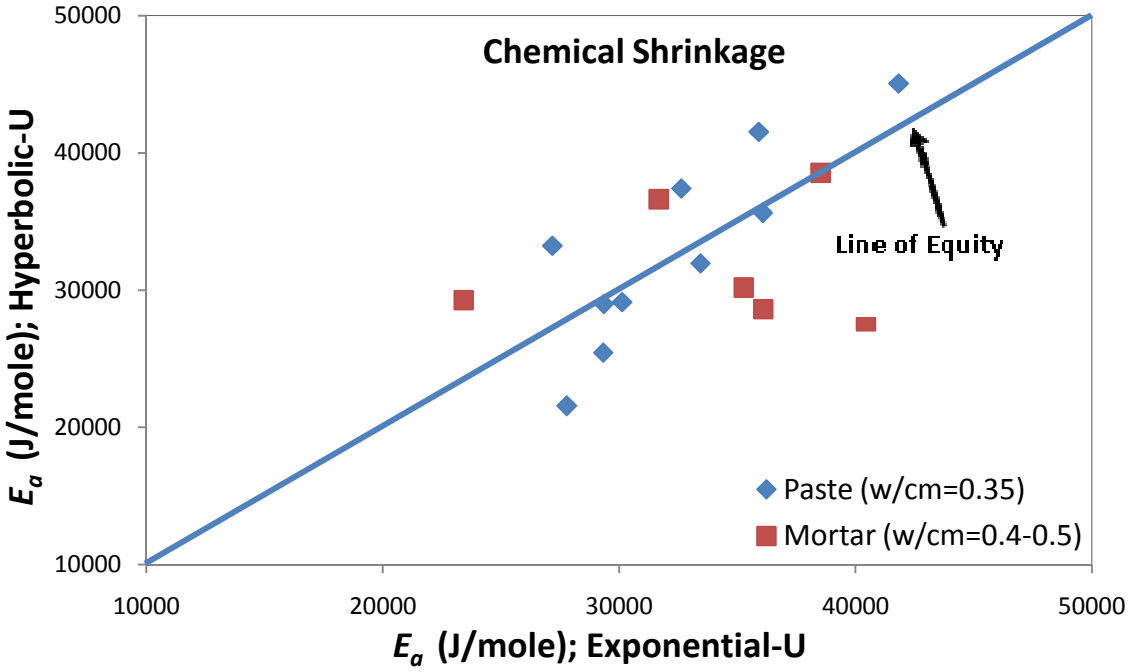

(b)

Figure 3.10: Comparison of Different Calculation Techniques for Chemical Shrinkage; (a) ASTM C 1074 Hyperbolic-E vs Exponential-E; (b) Hyperbolic-U vs Exponential-U.

3.5.5 Mortar vs Cement Paste

Both cement paste and mortar results show very similar E_a values for three different calculation techniques from the cumulative heat of hydration as shown in Figure 3.11. This means that there is no significant effect of aggregates on the apparent activation energy of cementitious materials for all calculation methods used. Small effects of the aggregates on the hydration do not affect the temperature sensitivity, meaning that apparent activation energies calculated from cement pastes can be applied with confidence to those used in mortar and concrete.

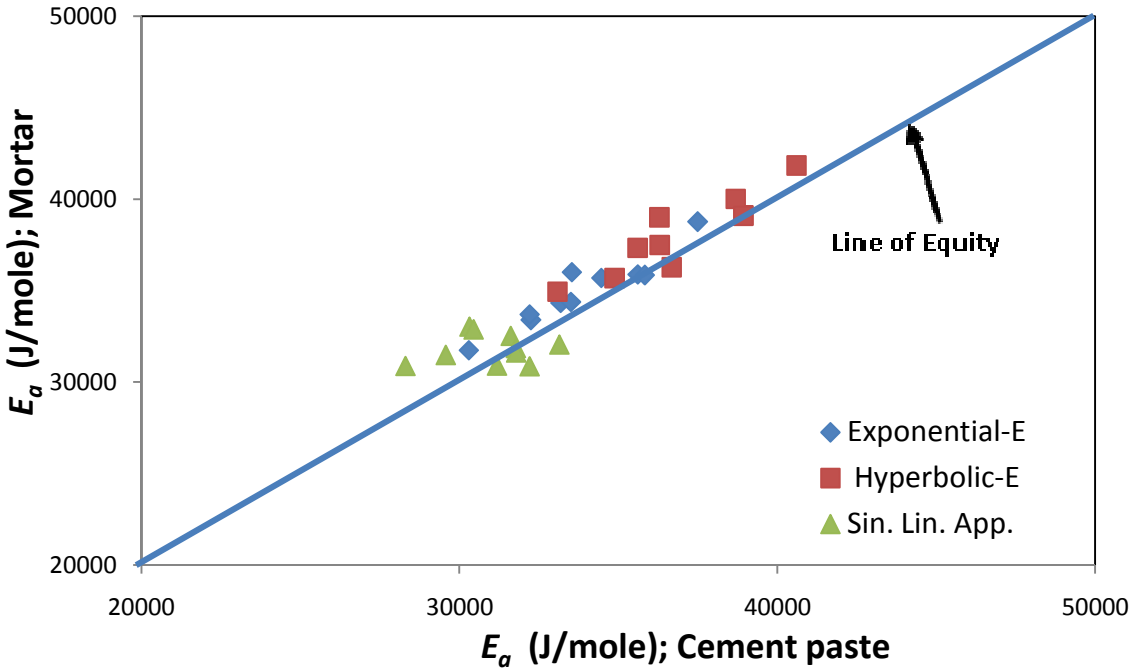

Figure 3.11: Comparison of Mortar vs Cement Paste E_a Values.

3.5.6 Evaluation of Chemical Shrinkage as a Mean of E_a Calculation

Chemical shrinkage has a high potential for E_a calculation. The potential of chemical shrinkage was evaluated by comparing with the E_a values obtained from the total heat of hydration as shown in Figure 3.12. Four different calculation techniques were tried in this study. The exponential-U method gave the best results as compared to that from isothermal calorimetry,

apart from the mixtures containing a water reducing admixture. The water reducing admixture has some air entrainment property. These air bubbles may affect the chemical shrinkage giving erroneous results.

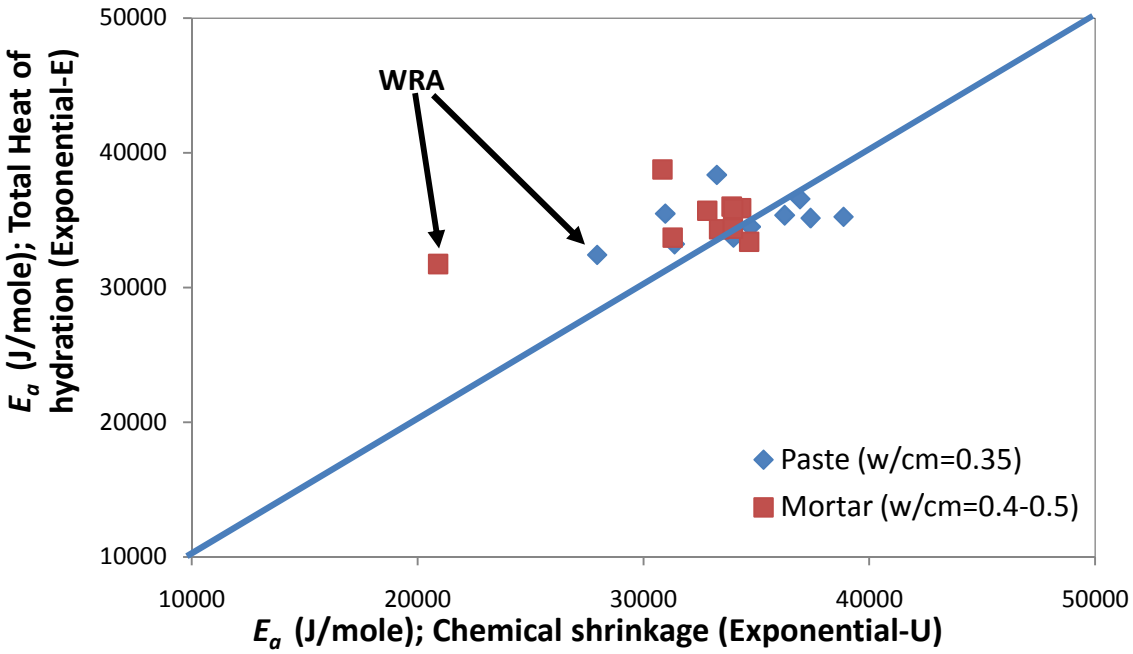

(a)

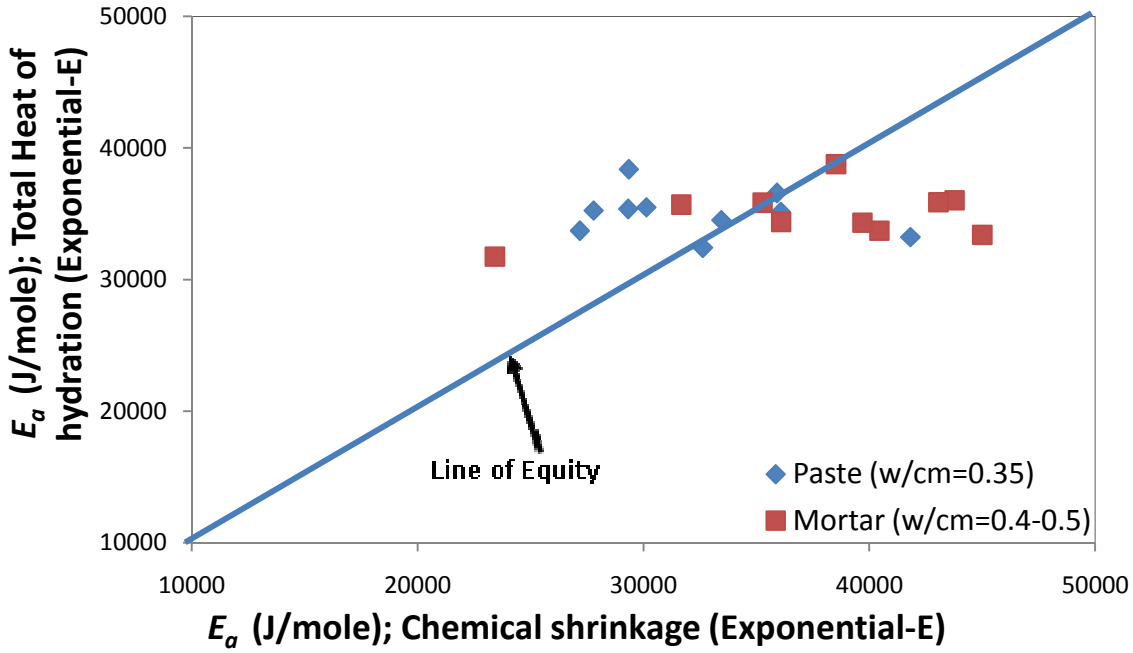

(b)

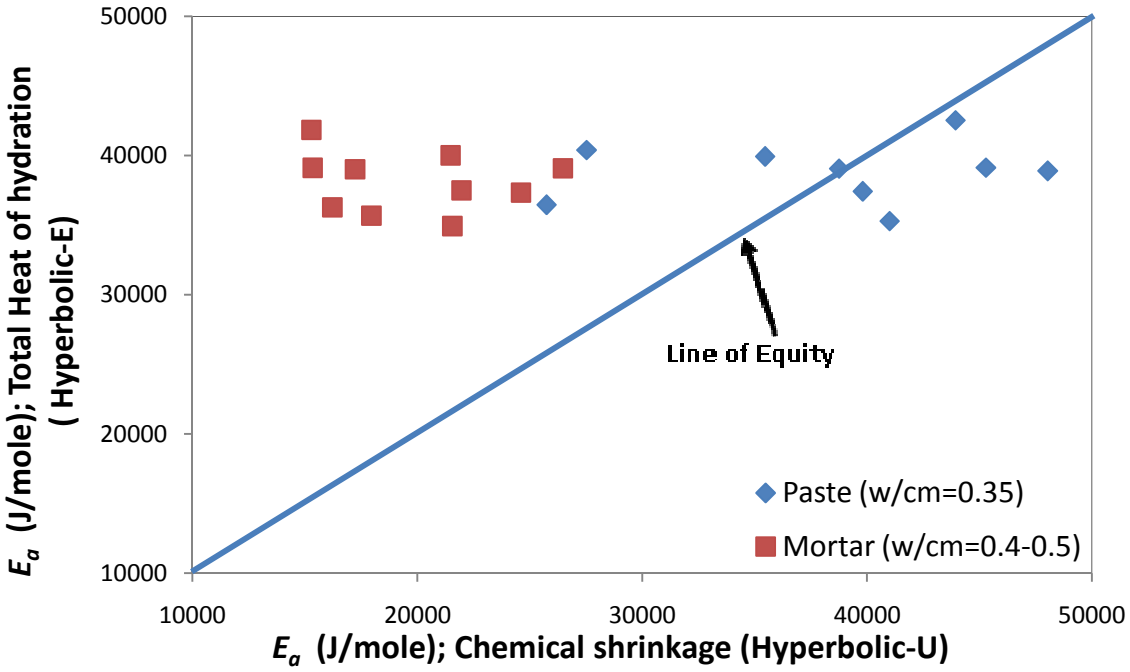

(c)

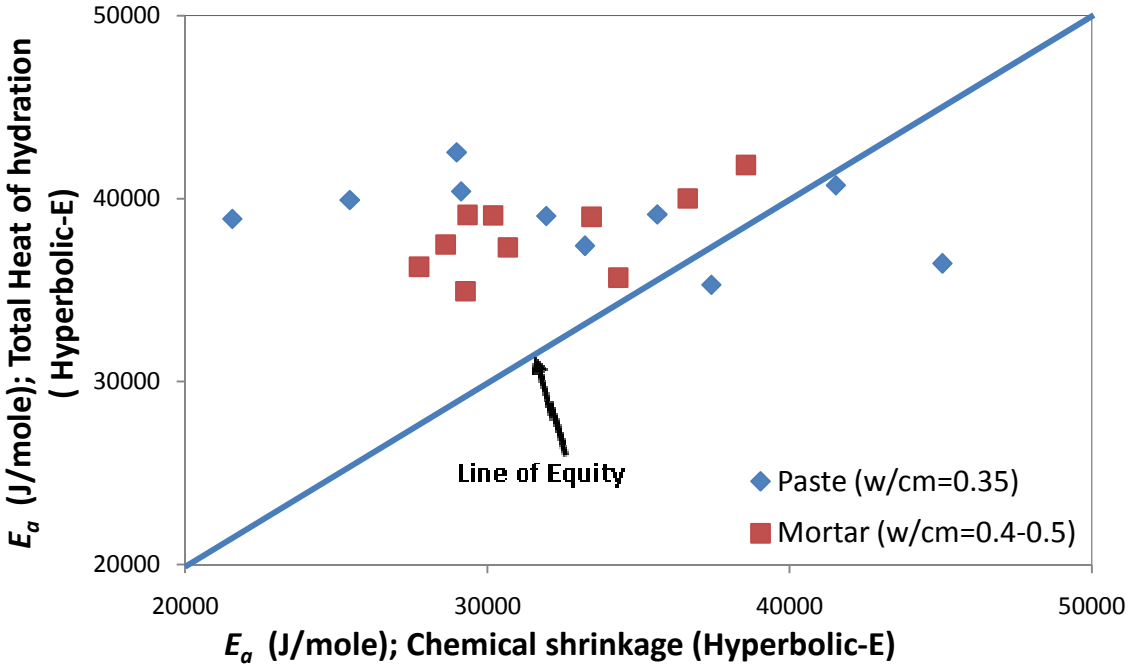

(d)

Figure 3.12: Evaluating Chemical Shrinkage as a Mean of E_a Calculation.

3.6 Conclusions

From the experimental and calculated results, the following conclusion can be drawn:

- There is a significant effect of estimation methods on the E_a values of cementitious materials. The selection of the method used to estimate E_a should be based on the purpose of the maturity function used – whether it is for time of set, strength, or degree of hydration modeling. Physical properties besides just hydration development can affect the results.
- E_a values vary with the calculation techniques. The exponential method and ASTM C 1074 hyperbolic function are in good agreement for total heat of hydration and the ASTM C 1074 two step method correlates with the E_a calculated using the ASTM C 1074 hyperbolic function from mortar strength.
- Both initial and final setting times give similar response for E_a values, indicating that the initial and final setting are influenced equally by temperature.
- Both cement paste and mortar give similar E_a values for the same measurement and calculation method. This means that E_a calculated from cement pastes can be used for concrete mixtures.
- Apart from water reducer or air entrainment admixtures, chemical shrinkage can be used for E_a calculation and exponential-U method gives similar results to exponential-E method for total heat of hydration.

References

1. Taylor, H. F., “Cement Chemistry,” San Diego, CA, Acadumic Press Inc., 1990.
2. ASTM C 1074, “Standard Practice for Estimating Concrete Strength by the Maturity Method,” American Society for Testing and Materials, Pennsylvania, 2009.
3. Kada-Benamer, H., Wirquin, E., and Duthoit, B., "Determination of Apparent Activation Energy of Concrete by Isothermal Calorimetry," Cement and Concrete Research, V. 30, 2000, pp. 301-305.
4. Wang, J., Yan, P., and Hongfa, Y., "Apparent Activation Energy of Concrete in Early Age Determined by Adiabatic Test," Journal of Wuhan University of Technology-Mater. Sci. Ed., V. 22, No. 3, V. 22, No. 3, September, 2007, pp. 537-541.
5. Pinto, R. C. A., and Hover, K. C., "Application of Maturity Approach to Setting Time," ACI Material Journal, V. 96, No. 6, 1999, pp. 686-691.
6. Garcia, L., Castro-Fresno, D., and Polanco, J., "Maturity Approach Applied to Concrete by Means of Vicat Tests." ACI Material Journal, V. 105, No, 5, 2008, pp. 445-450.
7. Ma, W., Sample, D. , Martin, R., and Brown, W. P., "Calorimetric Study of Cement Blends Cotaining Fly Ash, Silica Fume, and Slage at Elevated Temperature," Cement, Concret, and Aggregates, V. 16, 1994, pp. 93-99.
8. Poole, J. L., Riding, K. A. , Folliard, K. J., Juenger, M. C. G., and Schindler, A. K., "Methods for Calculating Activation Energy for Portland Cement," ACI Materials Journal, V. 104, No. 1, 2007, pp. 303-311.
9. Tank, R. C., and Carino, N. J., "Rate Constant Functions for Strength Development of Concrete," ACI Materials Journal, V. 88, No. 1, 1991, pp. 74-83.

10. Schindler, A. K., "Effect of Temperature on Hydration of Cementitious Materials," ACI Materials Journal, V. 101, No. 1, 2004, pp. 72-81.
11. Wirquin, E., Broda, M., and Duthoit, B., "Determination of the Apparent Activation Energy of One Concrete by Calorimetric and Mechanical Means; Influence of a Super-Plasticizer." Cement and Concrete Research, V. 32, 2002, pp. 1207-1213.
12. Rietveld, H. M., "A profile refinement method for nuclear and magnetic structures," Journal of Applied Crystallography, V. 2, 1969, pp. 65–71.
13. ASTM C 150, "Standard Specification for Portland Cement," American Society for Testing and Materials, Pennsylvania, 2009.
14. ASTM C 33, "Standard Specification for Concrete Aggregates," American Society for Testing and Materials, Pennsylvania, 2009.
15. ASTM C 305, "Standard Practice for Mechanical Mixing of Hydraulic Cement Pastes and Mortars of Plastic Consistency," American Society for Testing and Materials, Pennsylvania, 2009.
16. ASTM C 109, "Standard Test Method for Compressive strength of Hydraulic Cement Mortars," American Society for Testing and Materials, Pennsylvania, 2009.
17. Freiesleben-Hansen, P., and Pedersen, E. J., "Maturity Computer for Controlled Curing and Hardening of Concrete," Nordisk Betong, V. 1, No. 19, 1977, pp. 21-25.
18. ASTM C 191, "Standard Test Method for Time of Setting of Hydraulic Cement by Vicat Needle," American Society for Testing and Materials, Pennsylvania, 2009.
19. ASTM C 403, "Standard Test Method for Time of Setting of Concrete Mixtures by Penetration Resistance," American Society for Testing and Materials, Pennsylvania, 2009.

20. Bentz, D. P., Peltz, A. M., and Winpigler, J., "Early-Age Properties of Cement-Based Materials. II: Influence of Water-to-Cement Ratio," Journal of Materials in Civil Engineering, V. 21, No. 9, 2009, pp. 512-517.
21. Broda, M., Wirquin, E., and Duthoit. B., "Conception of an isothermal calorimeter for concrete-Determination of the apparent activation energy," Materials and Structures, V. 35, No. 251, 2002, pp. 389-394.
22. Wadsö, L., "Operational Issues in Isothermal Calorimetry," Cement and Concrete Research, V. 40, No. 7, 2010, pp. 1129-1137.
23. Geiker, M., "Studies of Portland cement hydration: measurements of chemical shrinkage and a systematic evaluation of hydration curves by means of the dispersion model," Ph.D. Dissertation, Copenhagen, Denmark.: Technical University of Denmark, 1983.
24. ASTM C 1608, "Standard Test Method for Chemical Shrinkage of Hydraulic Cement Paste," American Society for Testing and Materials, Pennsylvania, 2009.
25. Sant, G., Lura, P. , and Weiss, J., "Measurement of volume change in cementitious materials at early ages. Review of testing protocols and interpretation of results," Transportation Research Record, 2006, pp. 21-29.
26. Knudsen, T., and Geiker, M., "Obtaining hydration data by measurement of Chemical Shrinkage with an Archimeter," Cement and Concrete Research, V. 15, 1985, pp. 381-382.
27. Zhang, J., Weissinger, E. A., Peethamparan, S., and Scherer, G. W. "Early hydration of setting of oil well cement," Cement and Concrete Research, V. 40, 2010, pp. 1023-1033.

28. Justice, J. M., and Kurtis, K. E., "Influence of Metakaolin Surface Area on Properties of Cement-Based Materials," Journal of Materials in Civil Engineering, ASCE, V. 19, No. 9, 2007, pp. 762-771.

CHAPTER 4 - BENEFITS OF CURING ON THE INITIAL HYDRATION OF CEMENTITIOUS MATERIALS

4.1 Introduction

After mixing it is very important to keep the temperature and moisture content of newly placed concrete in control. Curing is the process of maintaining the desirable temperature and moisture content for concrete. Curing significantly influence the property development of hardened concrete. Curing improves strength, durability, dimensional stability, resistance to surface-wear, and freezing and thawing, and reduces porosity and ion-penetration. For Type I cement curing can increase the strength by more than 58% after 6 months [1]. Studies have shown that once the relative humidity within the capillary drops below 80%, hydration virtually stops [2]. Water-cementitious material ratio (w/cm) greater than 0.42 is theoretically sufficient for complete hydration [3].

Curing also improves the durability of the concrete. Curing with low w/cm concrete mixtures is critical to allow for a more complete cement hydration and a more discontinuous pore network. The use of low w/cm ratios also contribute to the development of autogenous shrinkage of concrete. Kovler and Jensen showed that autogenous shrinkage is small at a w/cm greater than 0.4 but can be significant when w/cm is below that. [4]. Curing procedures have been developed that make it possible to mitigate autogenous shrinkage in high-strength and high-performance concrete [5].

Conventional techniques like water ponding, water spraying, fogging, plastic film, wet burlap, and liquid membranes improve curing by reducing moisture loss and providing an additional supply of water to the near surface layers. This method generally depends on one dimensional movement of water and has a very limited depth of influence. Internal curing has

been developed to help water reach cement grains on the concrete interior where ponded water has not been able to reach [6-9]. Internal curing is a concept of curing the whole concrete mass by storing water inside the concrete by means of highly absorbent material like saturated lightweight aggregate [4, 9-12] or super-absorbent polymers [4, 13, 14]. Water is kept inside of the internal reservoirs during mixing which later slowly releases into the cement matrix. Because of the low diffusivity of water in dense concrete, the water released from the internal water reservoirs can only cure 1 mm to 2 mm of the cement paste around the reservoir [15, 16]. Success of internal curing techniques mostly depends on the size, amount, sorptivity, and distribution of saturated particles.

This study was conducted to determine the effects of different curing methods on the early hydration of cementitious materials. Both cement paste and mortar were studied. Water ponding, curing compounds, and fine lightweight aggregate as internal reservoirs (FLAIR) were evaluated for their curing efficiency. Lime-saturated water and cement pore water (CPW) ponding was also used to investigate the effects of dilution of the ionic concentrations during hydration. The effects of curing on cement paste containing silica fume and ground granulated blast furnace slag (GGBFS) were also examined in this study.

4.2 Materials

The physical and chemical properties of cementitious materials that were used in this study are presented in Table 1. One hundred percent Type I cement (Ty I), 5% silica fume (5%SF), and 35% slag (35%S) were used in this study. Cement pastes with a water-cementitious material ratio (w/cm) of 0.275 to 0.35 and mortars with a w/cm of 0.45 were used in this study. An ASTM C 33 siliceous fine aggregate [17] and a lightweight fine aggregate were used in the mortar mixtures. Lightweight fine aggregates were sieved and recombined in the laboratory to

have the same gradation as the siliceous fine aggregate. The bulk specific gravity (SG) and percent absorption of siliceous fine aggregate were 2.5 and 0.42, respectively. The bulk specific gravity (SG) and percent absorption after 48 hours soaking of lightweight fine aggregate were 1.49 and 16.87, respectively. The mortar fine aggregate-cementitious material ratio was 2.75 by weight for siliceous aggregate. Ten percent, 20%, 30%, 40%, 50%, and 100% of siliceous aggregate was replaced by volume with lightweight aggregate presoaked for 48 hours to determine the effectiveness of internal curing of concrete with FLAIR.

Table 4. 1: Physical and Chemical Properties of Cementitious Materials.

Properties	Type I Cement	Slag
Specific Gravity	-	2.5
SiO_2, %	21.34	33.83
$Al2O_3$, %	4.74	11.45
Fe_2O_3, %	3.29	0.49
Si + Al + Fe, %	29.37	45.77
CaO, %	62.94	38.52
MgO, %	1.69	11.63
SO_3, %	2.68	2.55
Na_2O, %	0.14	0.28
K_2O, %	0.53	0.38
Total Alkalis as Na_2O	0.48	0.53
blaine fineness (m^2/kg)	360.1	-
C_3S (%)	66.96	-
C_2S (%)	16.49	-
C_3A (%)	2.92	-
C_4AF (%)	9.29	-
Gypsum (%)	2.31	-
Hemihydrate (%)	1.68	-
Arcanite (%)	0.23	-

Distilled water was used for mixing and curing in this study. A white water-based curing compound was also used. A mid range water reducing admixture (WRA) (785ml/100kg) was used in mortar (for both siliceous and lightweight fine aggregate) to improve the workability.

4.3 Experimental Methods

4.3.1 Mixing Procedure

In this study, ASTM C 305 [18] mixing procedure was followed for both cement paste and mortar mixing. Cementitious materials as well as fine aggregate were premixed dry for one minute prior to the start of cement paste of mortar mixing. Both the cement paste and mortar were mixed at room temperature and placed in the isothermal calorimeter within 15 minutes from the addition of water to the cementitious materials.

4.3.2 Application of Curing Compound

Distilled water, lime-saturated water, cement paste pore water and curing compound were used for curing. Distilled water, lime-saturated water and cement paste pore water were applied at the top of the cement paste and mortar samples. These curing liquids were gently applied so that liquid does not disturb the cement paste or mortar surface and effect the w/cm. The samples were sealed in their plastic containers after the curing liquid was placed on top of the sample. Cement paste pore water was collected by extracting water from cement paste made with the same cement used in this study and with a w/cm of 1.5. The schematic diagram of the vacuum filtration setup used to extract the pore solution from the cement paste is shown in Figure 4.1 (a). Two layers of curing compound were applied by spraying at the top surface of the some of the cement paste. The effect of curing compound on the hydration of cementitious material was

measured in a sealed and drying environment. A drying environment was created by placing 6 g of drierite above but not touching the samples as shown in Figure 4.1 (b).

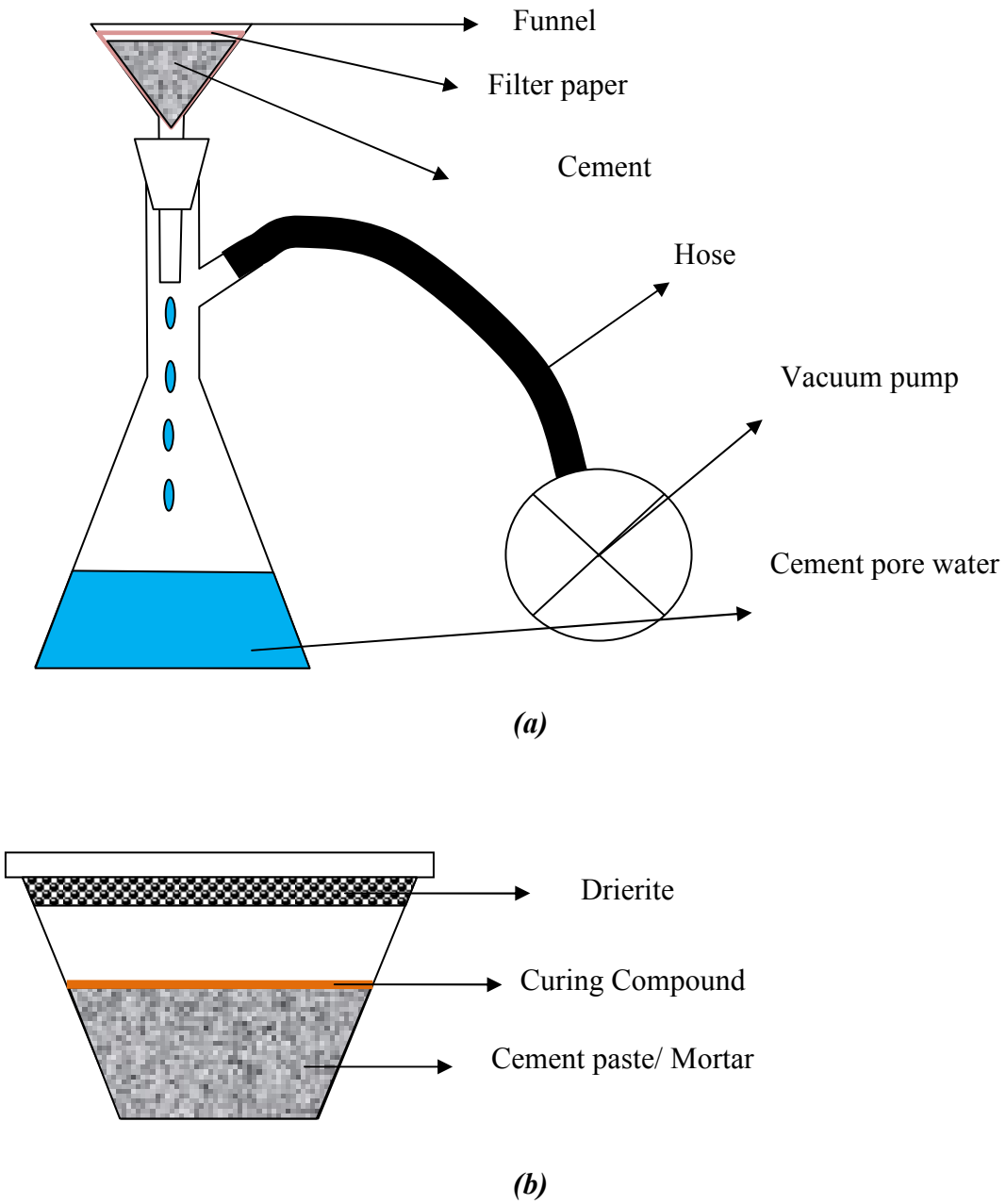

Figure 4.1: (a) Schematic Diagram of Cement Pore Water Collecting Device, and (b) Schematic Diagram of Drierite Placement on the Curing Compound Cured Cement paste/ mortar.

4.3.3 Determination of Degree of Hydration

An eight channel isothermal calorimeter (W.R. Grace Adiacal TC) was used in this study to measure the exothermal heat evolution of the cementitious systems studied. The working principal of an isothermal calorimeter was discussed in earlier studies [19,20]. The degree of hydration (DOH) was then calculated from the cumulative heat of hydration using Eqs. 4.1 through 4.3 [21-25]:

$$\alpha = \frac{H(t)}{H_u} \qquad \textbf{Eq. 4.1}$$

where,

α = the degree of hydration at time *t*,

H(t) = cumulative heat of hydration from time 0 to time *t* (J/gram), and

H_u = total heat available for reaction (J/gram).

H_u is a function of the cement composition, amount and type of supplementary cementitious materials (SCMs), and may be calculated as follows [26].

$$H_u = H_{cem} \cdot P_{cem} + 461 \cdot P_{slag} + 1800 \cdot PFA - CaO \cdot PFA \qquad \textbf{Eq. 4.2}$$

where,

P_{slag} = slag to total cementitious content mass ratio,

PFA = fly ash to total cementitious content mass ratio,

PFA-CaO = fly ash CaO to total fly ash content mass ratio,

P_{cem} = portland cement to total cementitious content mass ratio, and

H_{cem} =available heat of hydration of the cement (J/gram).

The value H_{cem} can be calculated as shown in Eq. 3 [26].

$$H_{cem} = 500 \cdot P_{C_3S} + 260 \cdot P_{C_2S} + 866 \cdot P_{C_3A} + 420 \cdot P_{C_4AF} + 624 \cdot P_{SO_3} + 1186 \cdot P_{Free\,Ca} + 850 \cdot P_{MgO} \qquad \textbf{Eq. 4.3}$$

where,

H_{cem} = the total heat of hydration of portland cement (J/gram) at α = 1.0,

P_i = the mass of *i*-th component to total cement content ratio, and

$i = P_{C_3S}, P_{C_2S}, P_{C_3A}, P_{C_4AF}, P_{SO_3}, P_{Free\,Ca}$ and P_{MgO}.

4.4 Results and Discussions

The effect of sample thickness and amount of curing water available on hydration was examined by using a Type I cement at a w/cm of 0.35 at 23°C (73°F). Distilled water, lime-saturated water and cement pore water were used to study the effects of the ionic concentrations on evolution of hydration. Figures 4.2 and 4.3 show the effect of curing water thickness and sample thickness on the rate of heat evolution of cementitious materials. As the curing water thickness increases, the maximum rate of heat evolution decreases. Increasing sample thickness also decreases the maximum rate of heat evaluation. The third hydration peak also decreases, confirming the decrease in aluminate hydration found by Lura et al [27]. Curing water also triggers a slight acceleration. These effects reduce as the sample thickness increases, potentially because the changes in ionic concentrations in the pore solution are lower for the larger amount of cement paste. The water cured samples show a decrease in the maximum rate of heat evolution, but because of the slight acceleration still have a higher degree of hydration than sealed samples at the time of maximum heat evolution rate. Figure 4.4 represents the effect of lime-saturated curing water height and sample thickness on the rate of heat evolution of cementitious materials. Lime-saturated water showed a larger acceleration than the distilled water, possibly because the sample reached its supersaturation limit for calcium hydroxide precipitation earlier. But sample thickness does not show any significant effect on the acceleration. The lime-saturated water samples also show a decrease in the aluminate peak, just

as the samples cured with distilled water. Increasing sample thickness shows a reduction in the second and third peaks in the heat evolution rate, similar to the samples with distilled water curing. Lime-saturated water curing also gives a higher DOH at the time of the maximum rate of heat evolution. Figures 4.5 and 4.6 show the effect of extracted fresh cement paste pore water thickness as a curing liquid and sample thickness on the rate of heat evaluation of cementitious material. Cement pore water also shows a very slight acceleration of hydration, but nowhere near that of saturated lime water. The effects of cement paste pore water curing decreased with sample thickness much more than that of saturated lime water curing. The effects of cement pore water and sample thickness on the maximum rate of heat evolution is not as significant as distilled water and lime-saturated water, showing that changes in sulfate concentration from curing water can have a significant effect on the cement hydration.

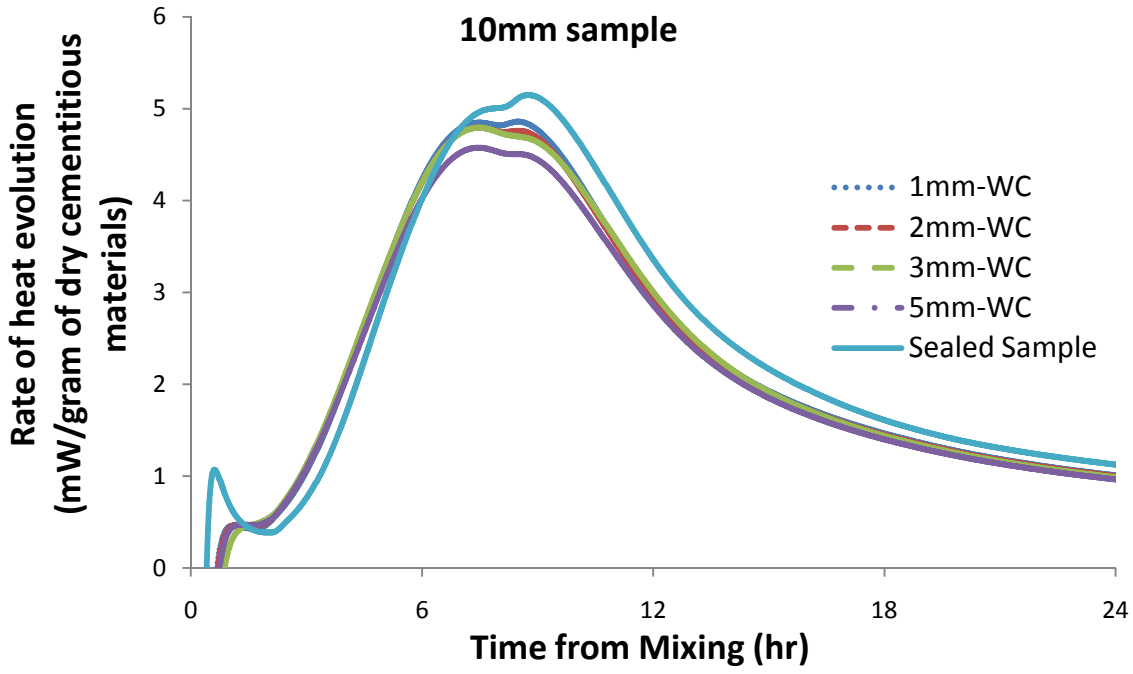

(a)

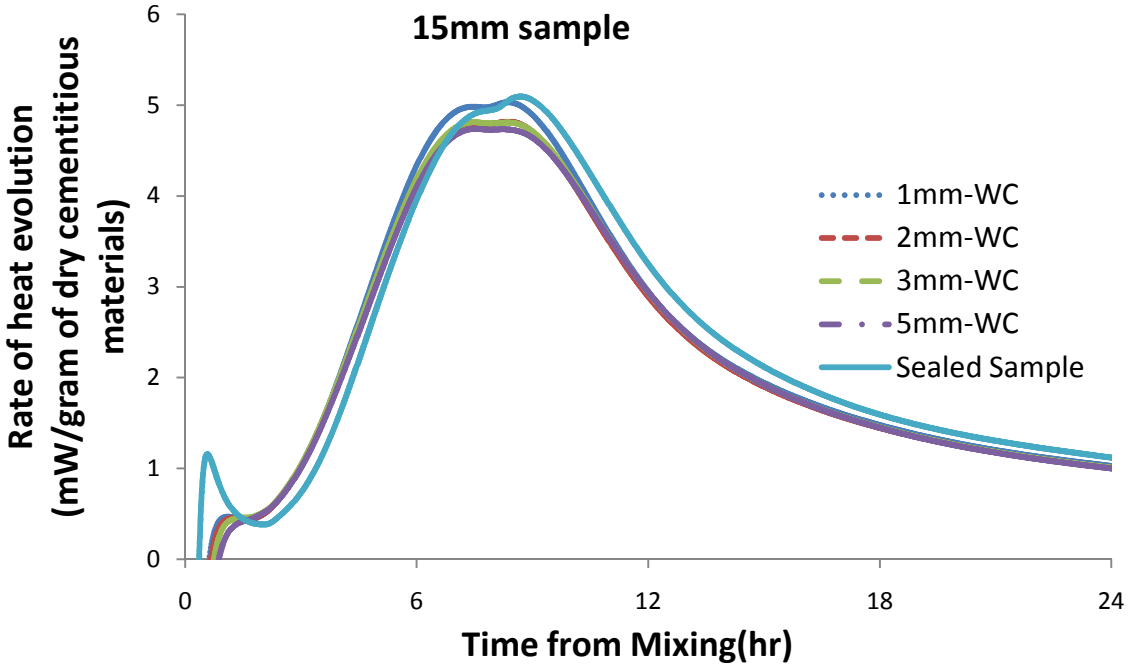
15mm sample
Rate of heat evolution (mW/gram of dry cementitious materials)
Time from Mixing(hr)
1mm-WC
2mm-WC
3mm-WC
5mm-WC
Sealed Sample
0
1
2
3
4
5
6
0
6
12
18
24

(b)

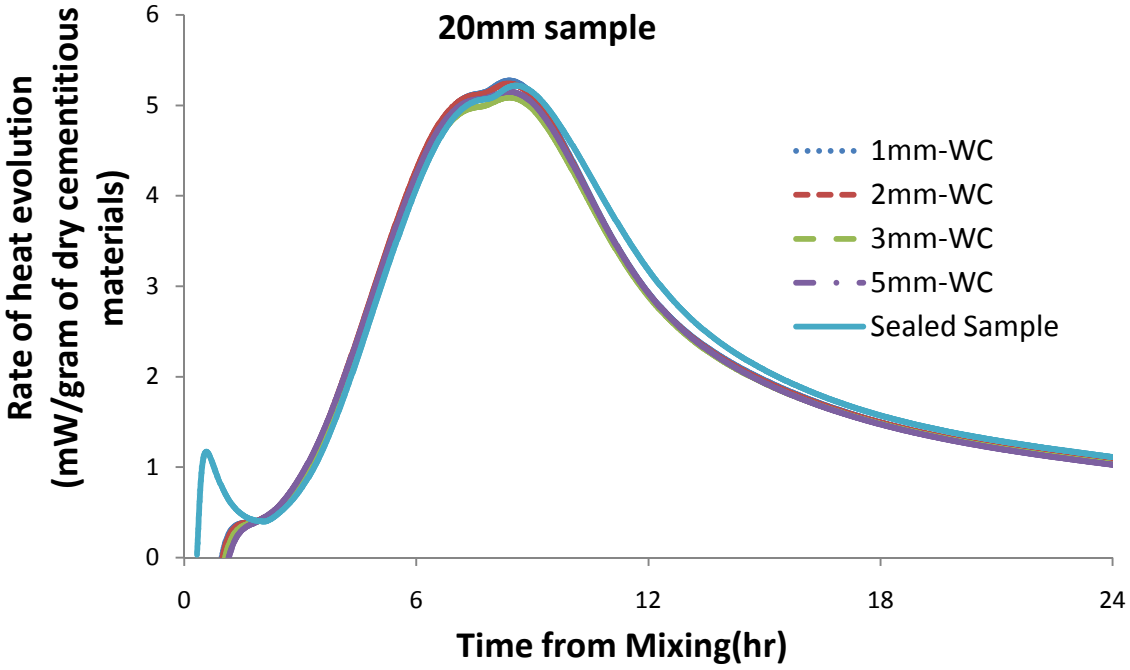
20mm sample
Rate of heat evolution (mW/gram of dry cementitious materials)
Time from Mixing(hr)
1mm-WC
2mm-WC
3mm-WC
5mm-WC
Sealed Sample
0
1
2
3
4
5
6
0
6
12
18
24

(c)

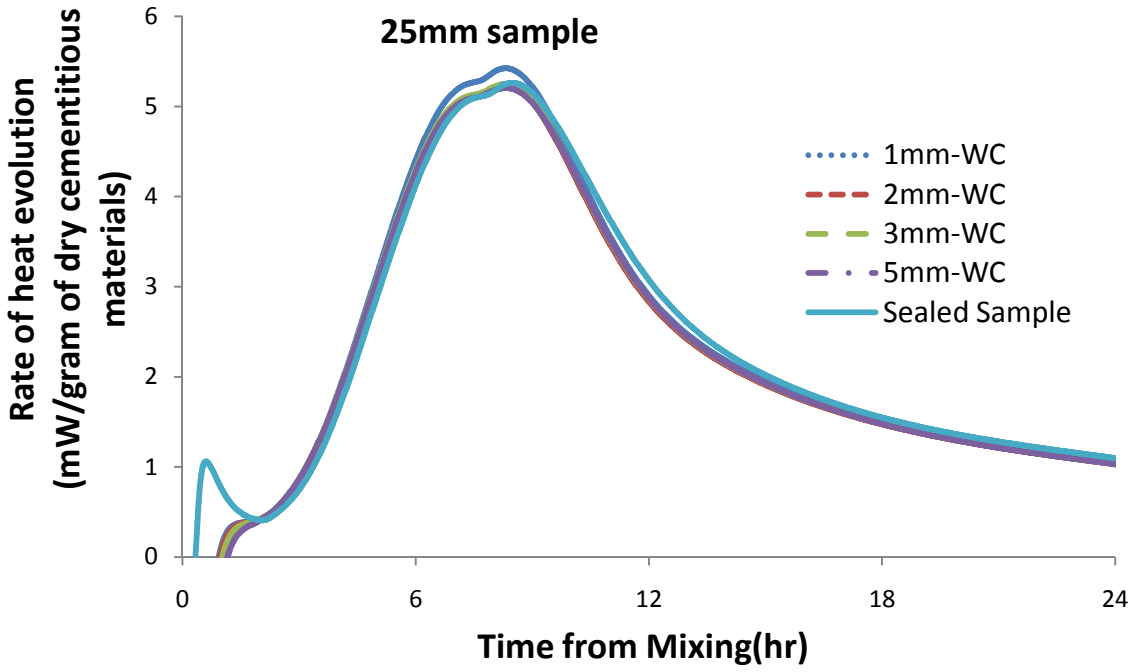

(d)

Figure 4.2 Effect of Curing Water Height on the Rate of Heat Evolution for 100% Type I Cement Paste (w/cm=0.35) at 23°C (73°F); (a) 10 mm Sample Thickness, (b) 15 mm Sample Thickness, (3) 20 mm Sample Thickness, and (d) 25 mm Sample Thickness.

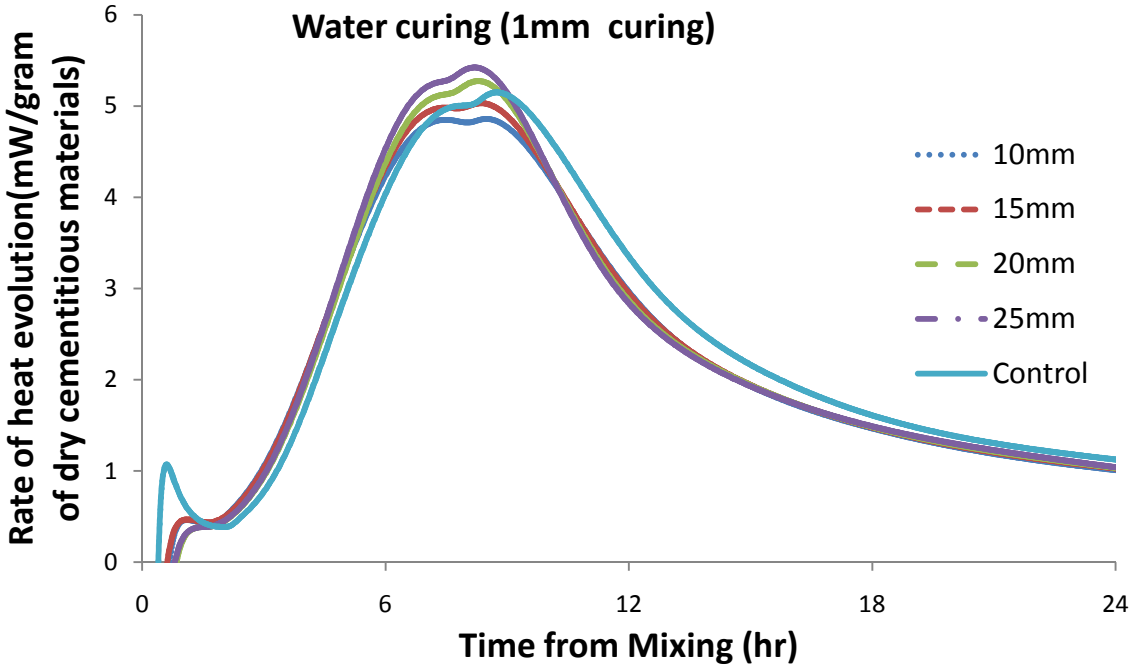

Figure 4.3: Effect of Water Cured Sample Depth on the Rate of Heat Evolution for 100% Type I Cement Paste (w/cm=0.35) at 23°C (73°F).

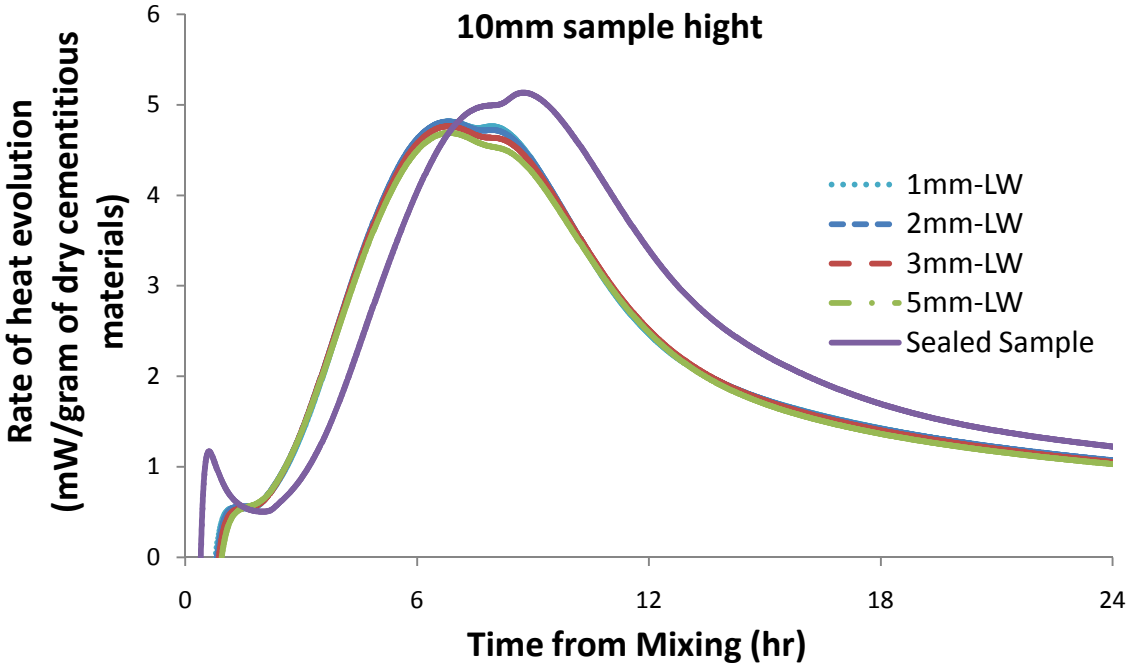

(a)

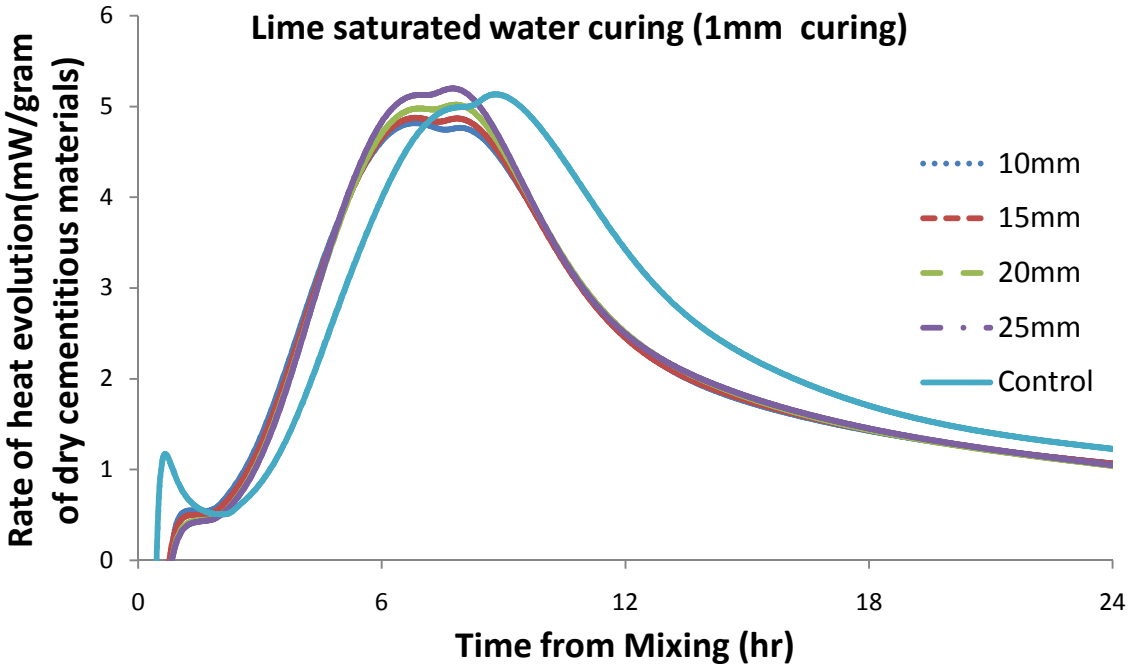

(b)

Figure 4.4: Effect of Lime-Saturated Water Curing on the Rate of Heat Evolution for 100% Type I Cement Paste (w/cm=0.35) at 23°C (73°F); (a) Effect of Curing Height, and (b) Effect of Sample Depth.

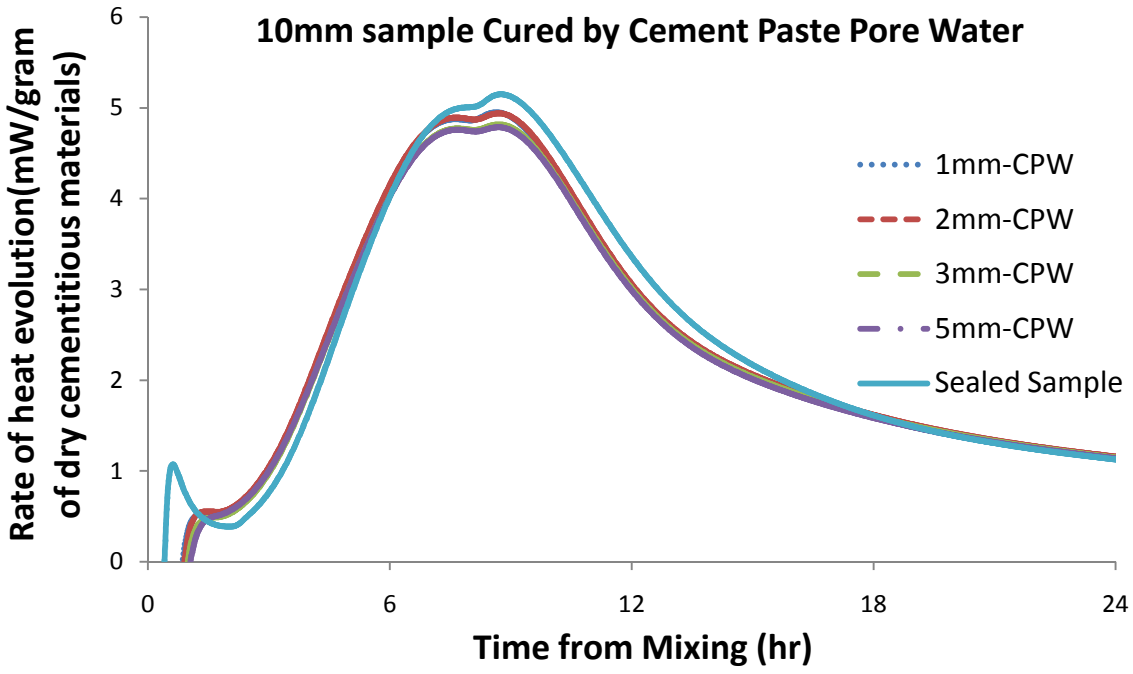
10mm sample Cured by Cement Paste Pore Water
Rate of heat evolution(mW/gram of dry cementitious materials)
Time from Mixing (hr)
1mm-CPW
2mm-CPW
3mm-CPW
5mm-CPW
Sealed Sample
0
1
2
3
4
5
6
0
6
12
18
24

(a)

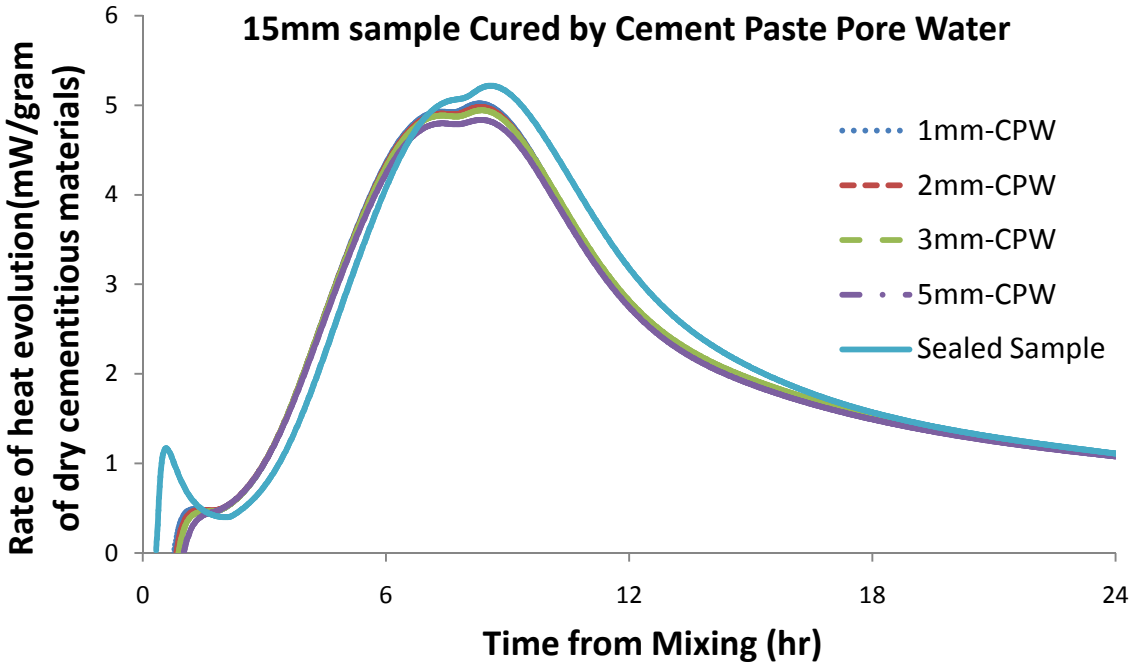
15mm sample Cured by Cement Paste Pore Water
Rate of heat evolution(mW/gram of dry cementitious materials)
Time from Mixing (hr)
1mm-CPW
2mm-CPW
3mm-CPW
5mm-CPW
Sealed Sample
0
1
2
3
4
5
6
0
6
12
18
24

(b)

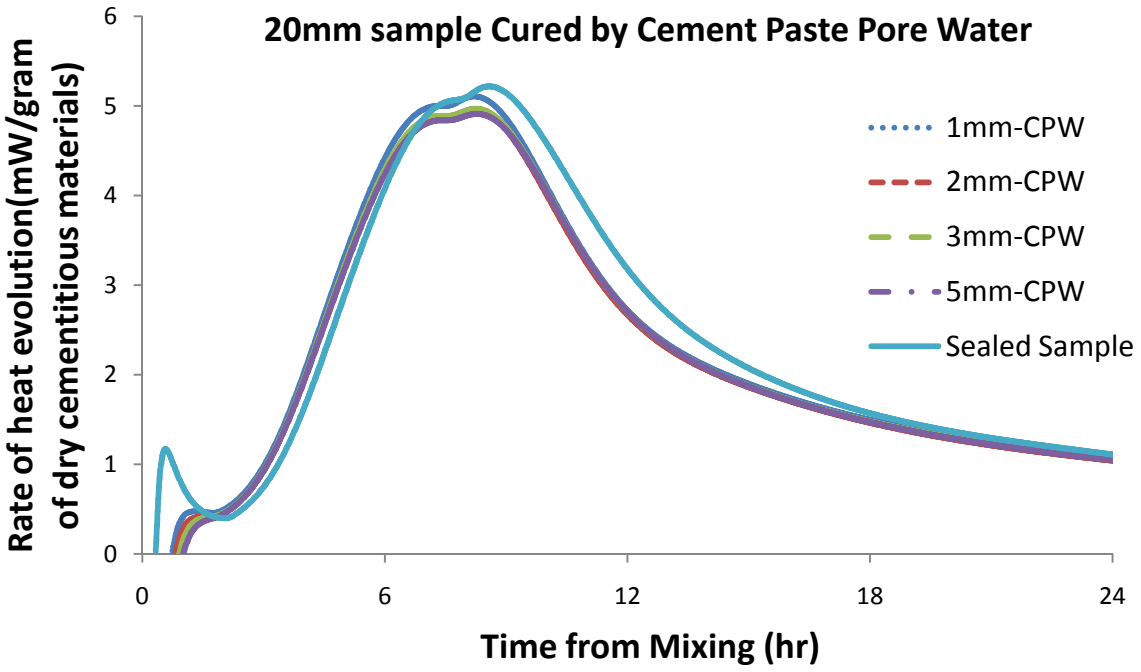

(c)

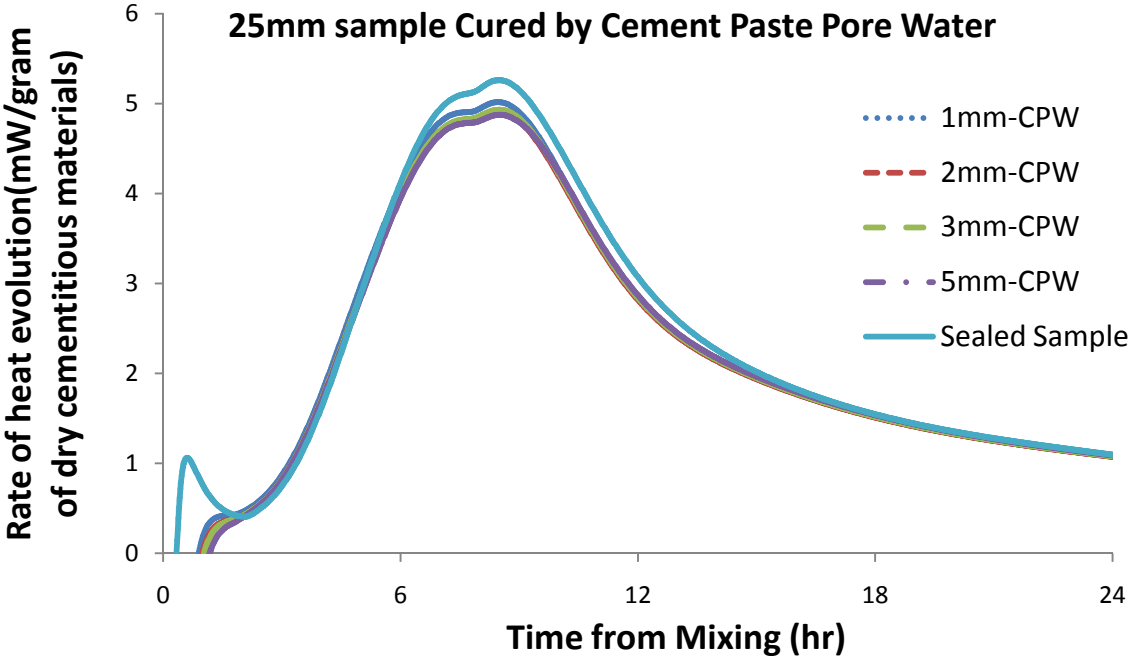

(d)

Figure 4.5: Effect of Cement Pore Water Height on the Rate of Heat Evolution for 100% Type I Cement Paste (w/cm=0.35) at 23°C (73°F); (a) 10 mm Sample Thickness, (b) 15 mm Sample Thickness, (3) 20 mm Sample Thickness, and (d) 25 mm Sample Thickness.

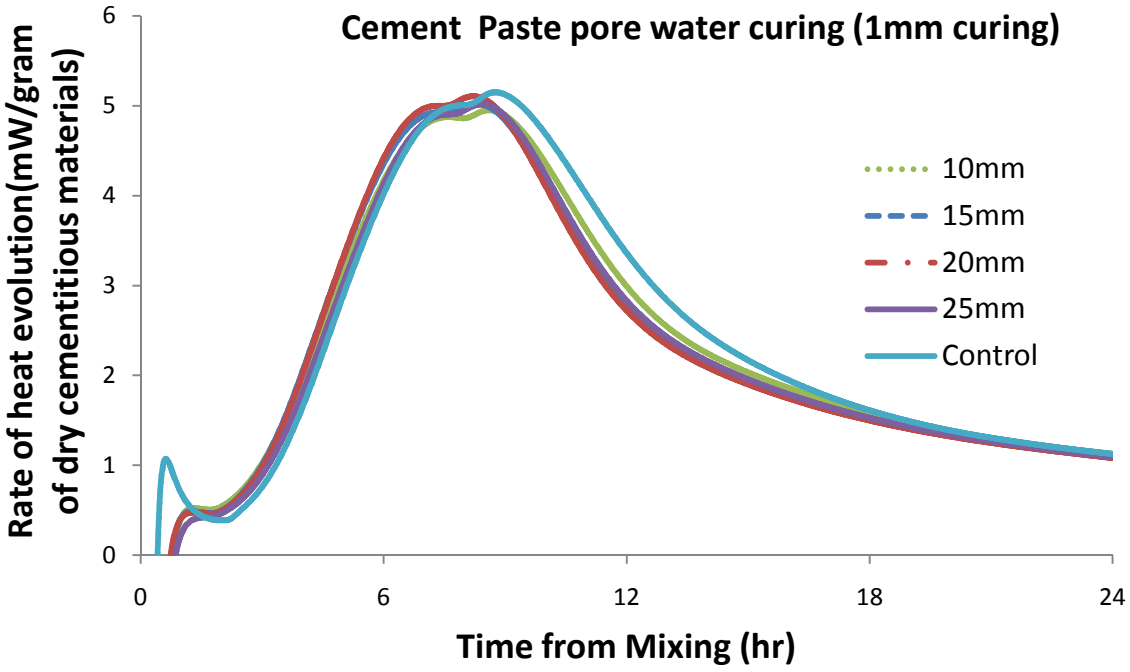

Figure 4.6: Effect of Sample Depth of Cement Pore Water Cured Sample on the Rate of Heat Evolution for 100% Type I Cement Paste (w/cm=0.35) at 23°C (73°F).

To quantify the effects of water ponding on the degree of hydration of cementitious materials, various depths of cement paste and mortar samples with various w/cm was studied at two different temperatures (23°C and 38°C). Calorimetry was performed on samples with a w/cm of 0.275, 0.3, 0.325, and 0.35 at 23°C (73°F) and a w/cm 0.275 and 0.35 at 38°C (100°F). For cement pastes, sample depths of 10, 20, and 30 mm were used at 23°C (73°F), whereas sample depths of 10, 15, and 20 mm were used at 38°C (100°F) to determine the effect of curing on the sample thickness. The smaller sample heights at 38°C (100°F) were used because of measurement sensitivity limits of the calorimeter. Three ml of curing water was applied at the top of the paste samples to provide a thin film of curing water. Figures 4.7 and 4.8 show the cumulative heat of hydration of cement pastes at 23°C (73°F) and 38°C (100°F), respectively. Figures 4.9 and 4.10 show an increase in DOH for cement paste at 23°C (73°F) and 38°C

(100^{o}F), respectively, for different w/cm and different sample depths. Water cured cement paste samples showed a higher cumulative heat of hydration than sealed cement paste samples after seven days. Both the sealed and water-cured samples generate an equal cumulative heat of hydration up to a certain period of time. Self desiccation then starts, after which the water-cured samples and sealed samples cumulative heat of hydration start to diverge. The point of divergence is the point where the cumulative heat of hydration curves starts to diverge. Figure 4.11 shows the DOH and uncombined water available per gram of cementitious material at the point of divergence for different w/cm. DOH at the point of divergence increases with the increase of w/cm. For the w/cm of 0.275 to 0.325 the DOH at the point of divergence increases linearly with the increase of w/cm but then showed a larger increase in DOH at w/cm from 0.325 to 0.35. Uncombined water available shows an increasing relationship with w/cm at the point of divergence between the cured and sealed specimens. For the w/cm of 0.275 to 0.325, the uncombined water increases linearly with the increase of w/cm. It is yet unclear as to this small difference between 0.325 and 0.35 w/cm, although possible causes are experimental error, difference in pore size distributions, change in the availability of water. Average DOH of different sample thickness for water-cured and sealed samples after seven days at 23^{o}C (73^{o}F) are presented in Figure 4.12. DOH for the sealed samples increase almost linearly with the increase in w/cm. Water-cured samples however show a nonlinear decrease in DOH with a decreasing w/cm, probably because of more limited space at the lower w/cm. Figure 4.13 shows the effect of sample depth and w/cm on the increase of DOH, compared with the sealed sample of equal thickness after seven days at the two different temperatures tested. For w/cm of 0.325 and 0.35, sample thickness does not have any noticeable effect on increase in DOH, indicating that the water is able to penetrate the full sample depth.

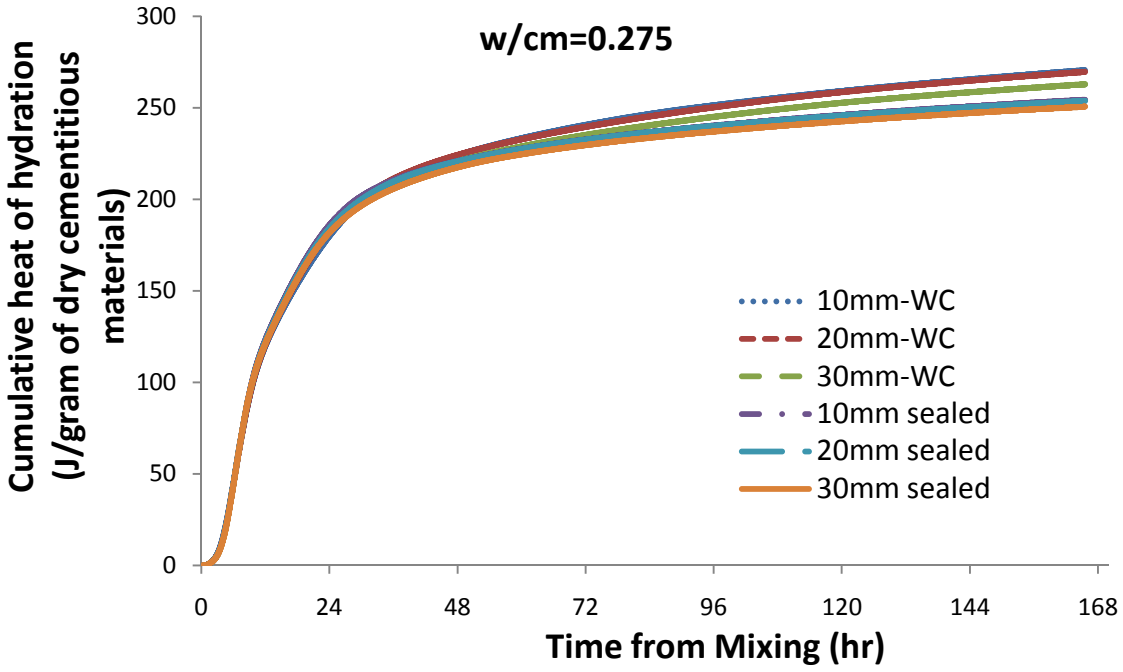

(a)

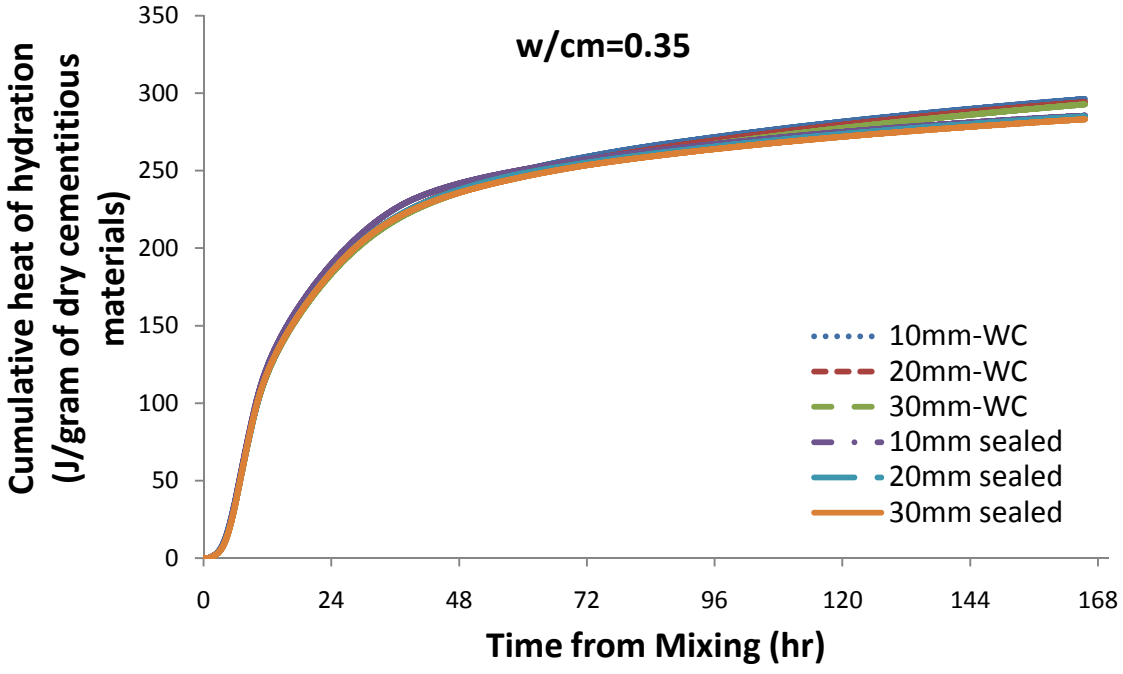

(b)

Figure 4.7: Effect of Water Curing on the Degree of Hydration of Type I Cement at 23°C (73°F); (a) w/cm= 0.275 and (b) w/cm= 0.35.

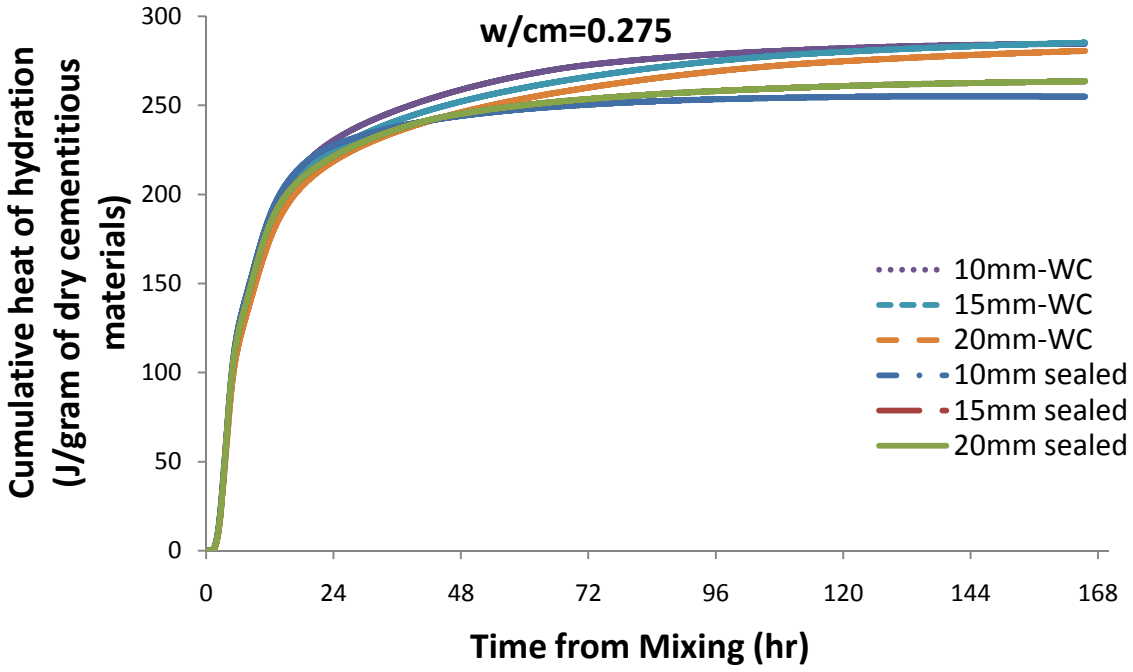

(a)

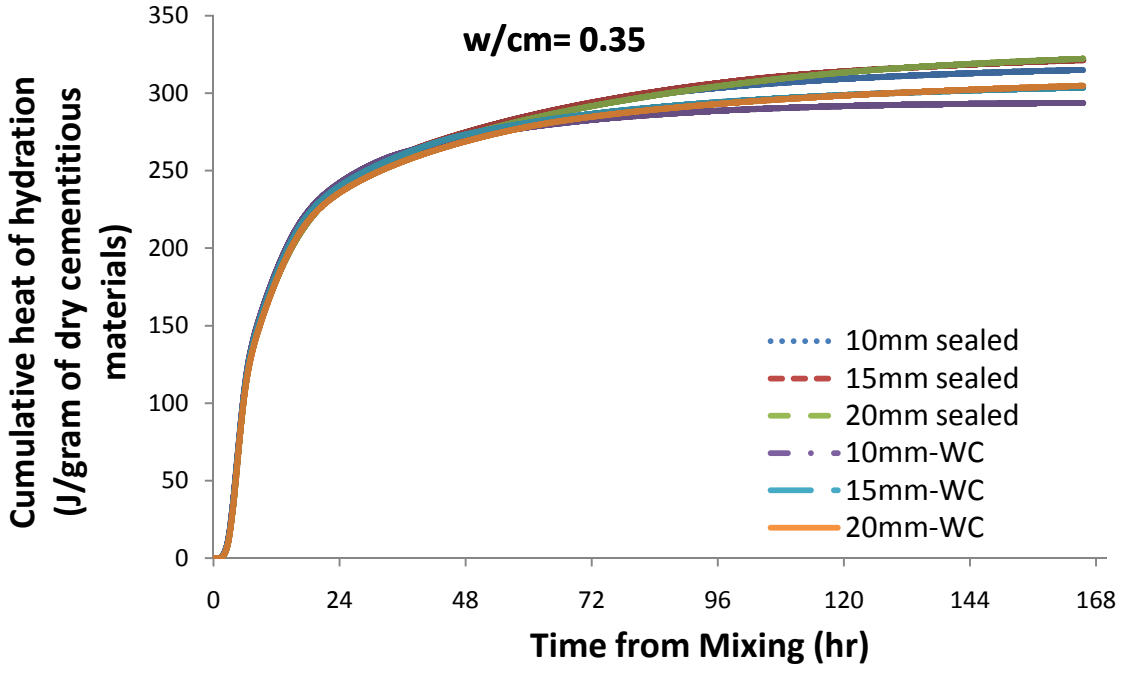

(b)

Figure 4.8: Effect of Water Curing on the Degree of Hydration of Type I cement at 38°C (100°F); (a) w/cm= 0.275 and (b) w/cm= 0.35.

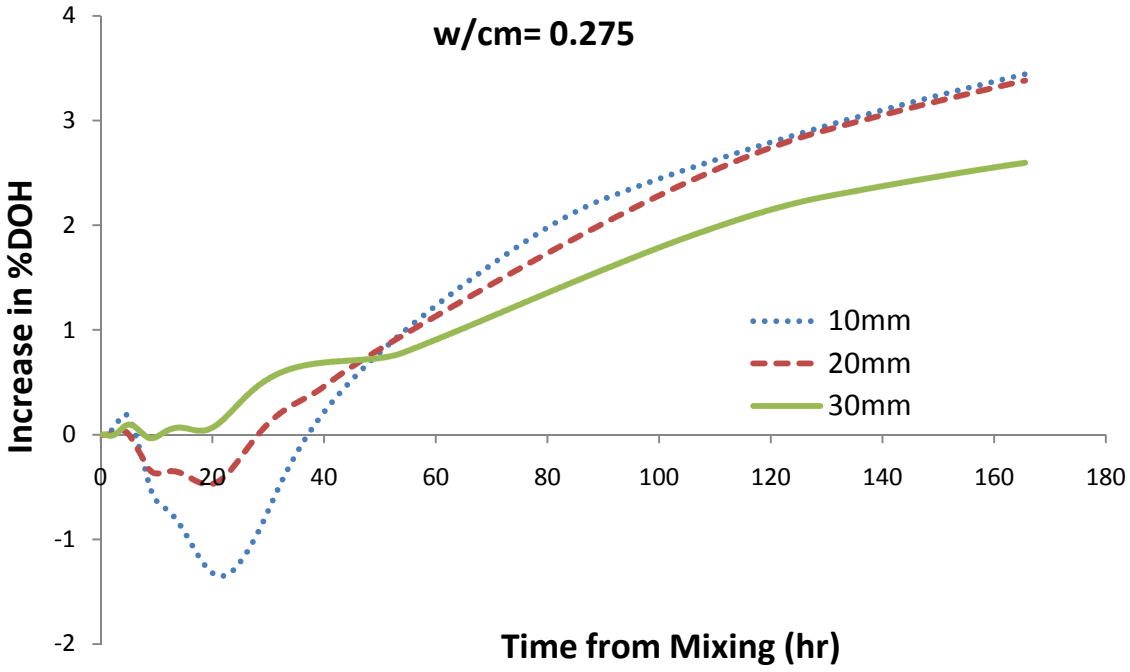
w/cm= 0.275
Increase in %DOH
Time from Mixing (hr)
10mm
20mm
30mm
4
3
2
1
0
-1
-2
0
20
40
60
80
100
120
140
160
180

(a)

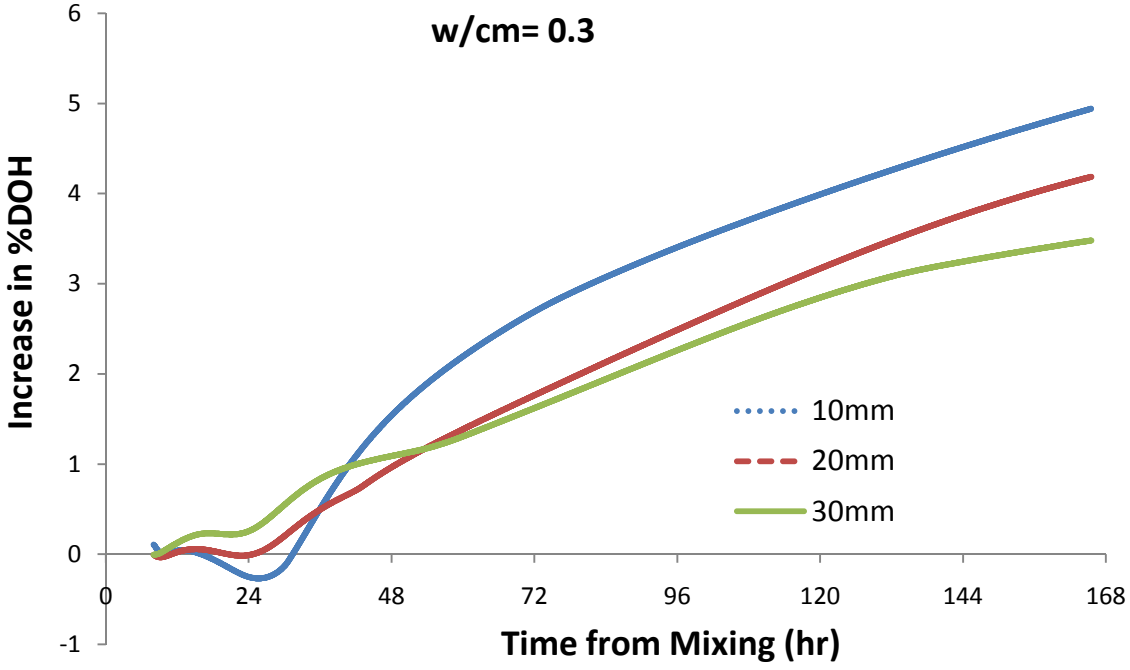
w/cm= 0.3
Increase in %DOH
Time from Mixing (hr)
10mm
20mm
30mm
6
5
4
3
2
1
0
-1
0
24
48
72
96
120
144
168

(b)

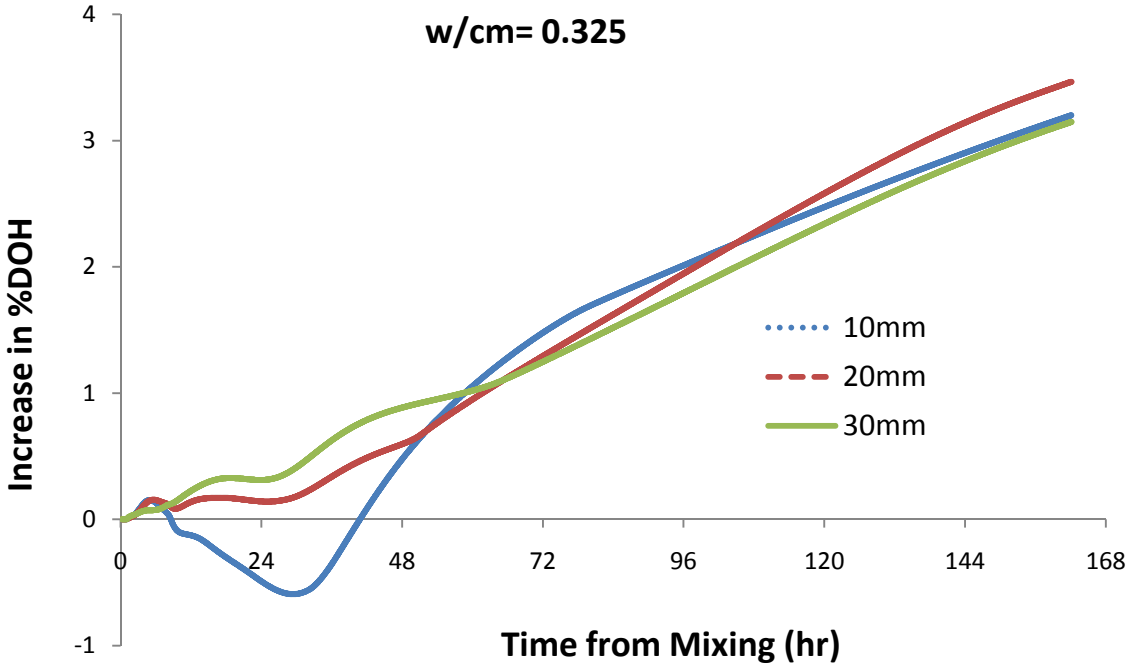

(c)

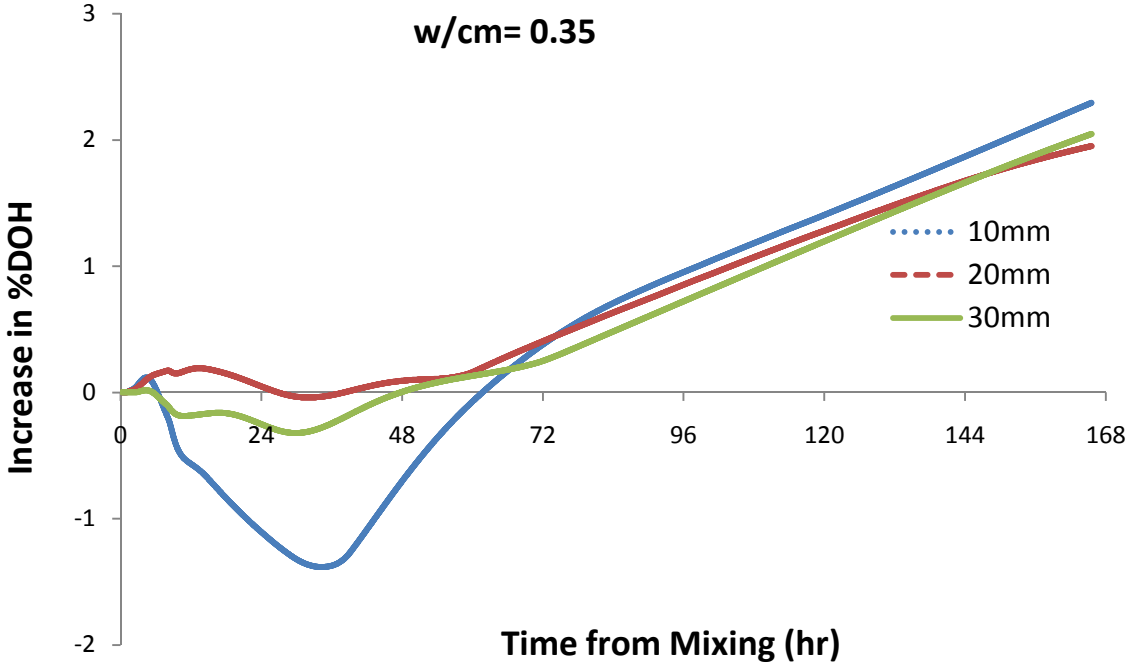

(d)

Figure 4.9: Increase in % Degree of Hydration of Type I Cement at 23°C (73°F); (a) w/cm= 0.275, (b) w/cm= 0.3, (c) w/cm= 0.325 and (d) w/cm= 0.35.

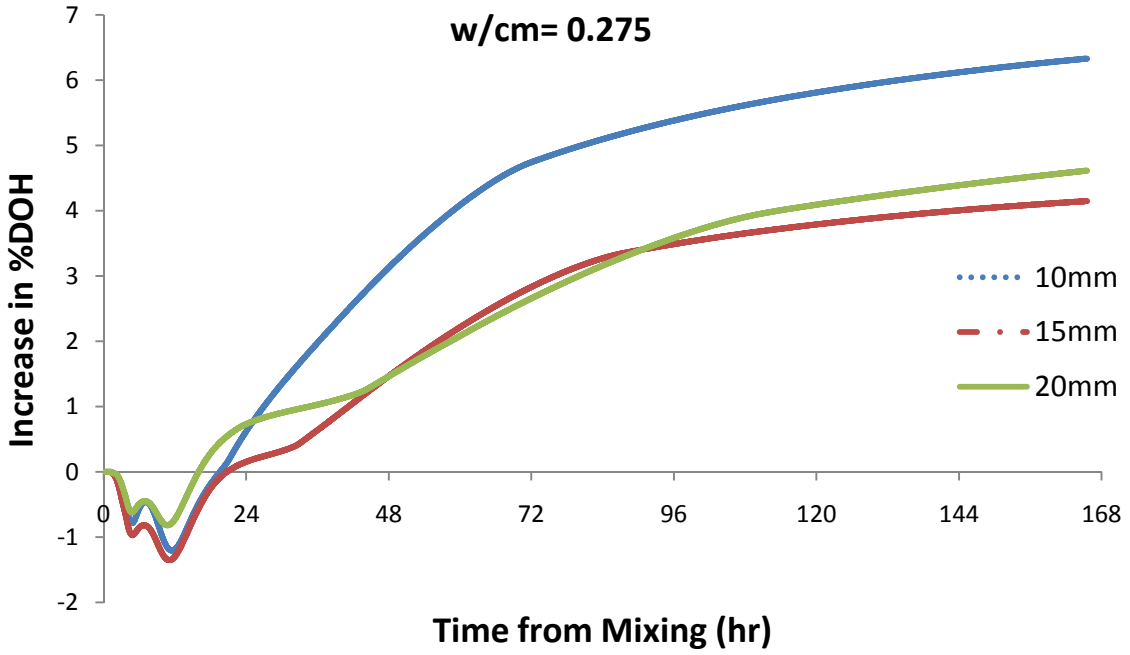

(a)

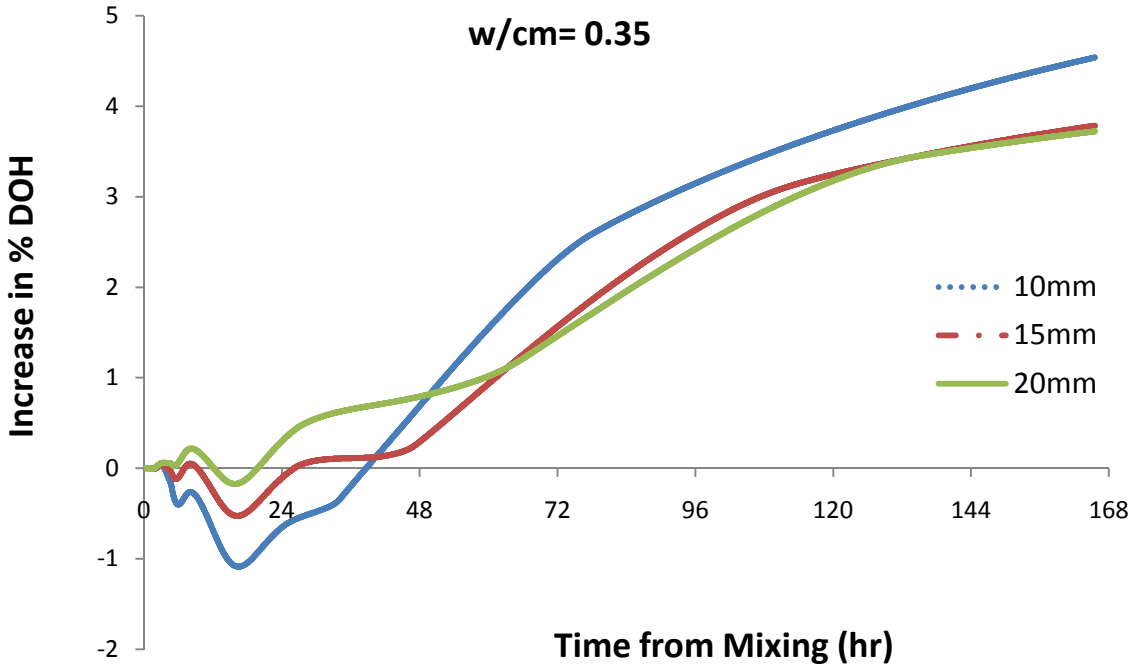

(b)

Figure 4.10: Increase in % Degree of Hydration of Type I Cement at 38°C (100°F); (a) w/cm= 0.275, and (b) w/cm= 0.35.

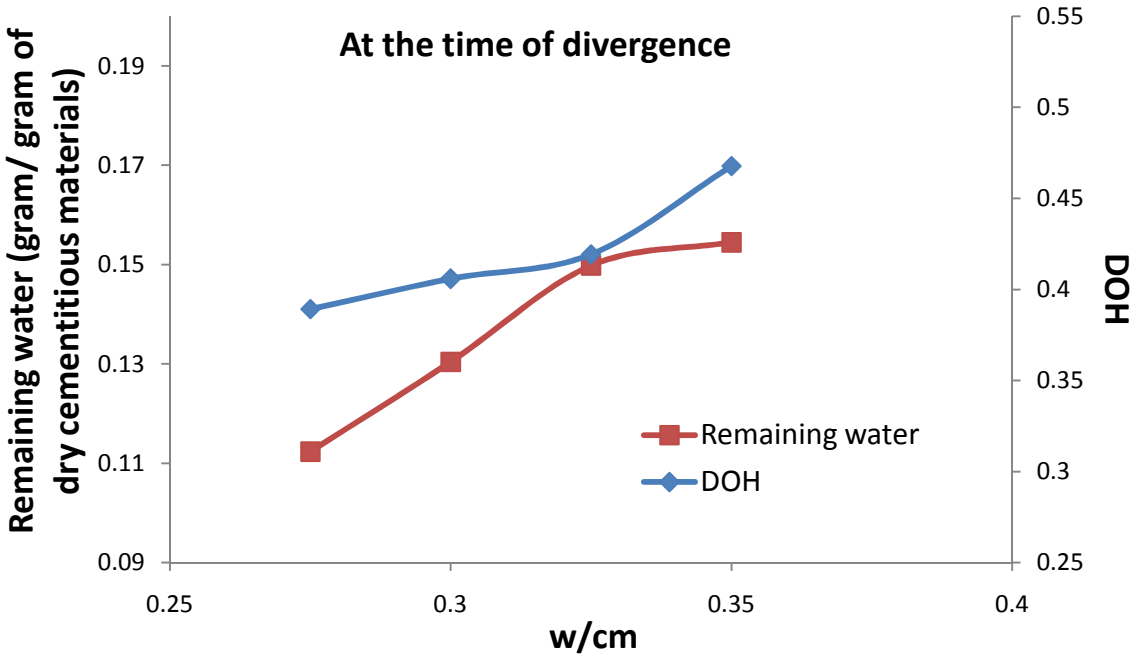

Figure 4.11: Remaining Uncombined Water for 1gram of Cementitious Materials and DOH at the Time of Divergence at 23°C (73°F) for 100% Type I cement paste.

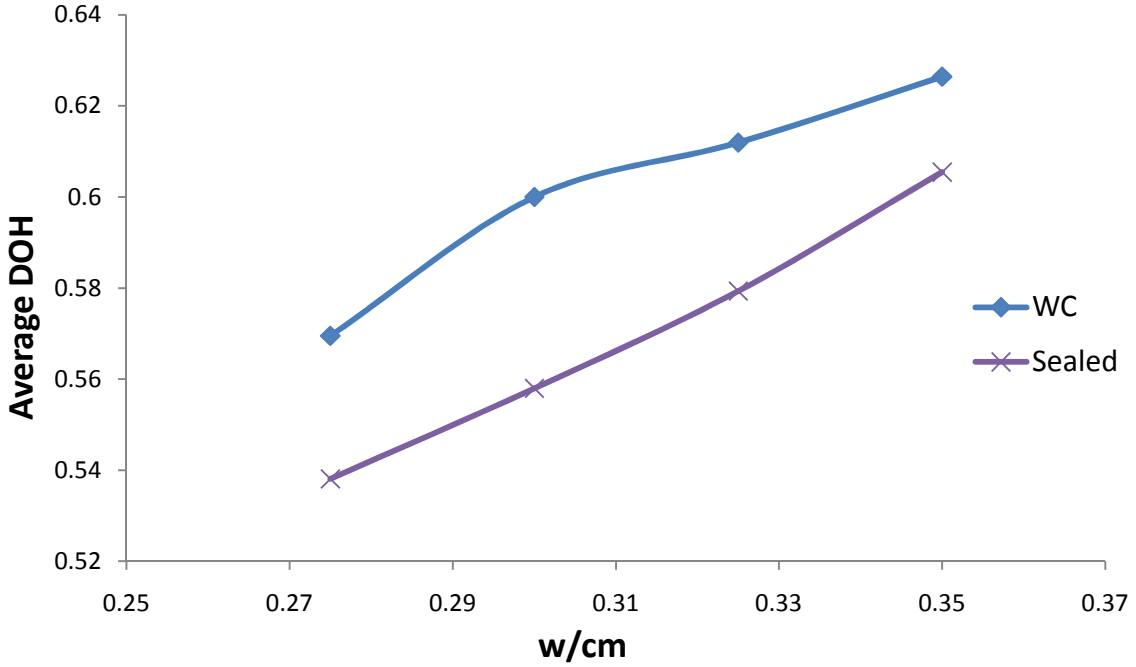

Figure 4.12: Effect of w/cm on the Average DOH of Water Cured and Sealed Samples for 100% Type I Cement Paste at 23°C (73°F) After 7days.

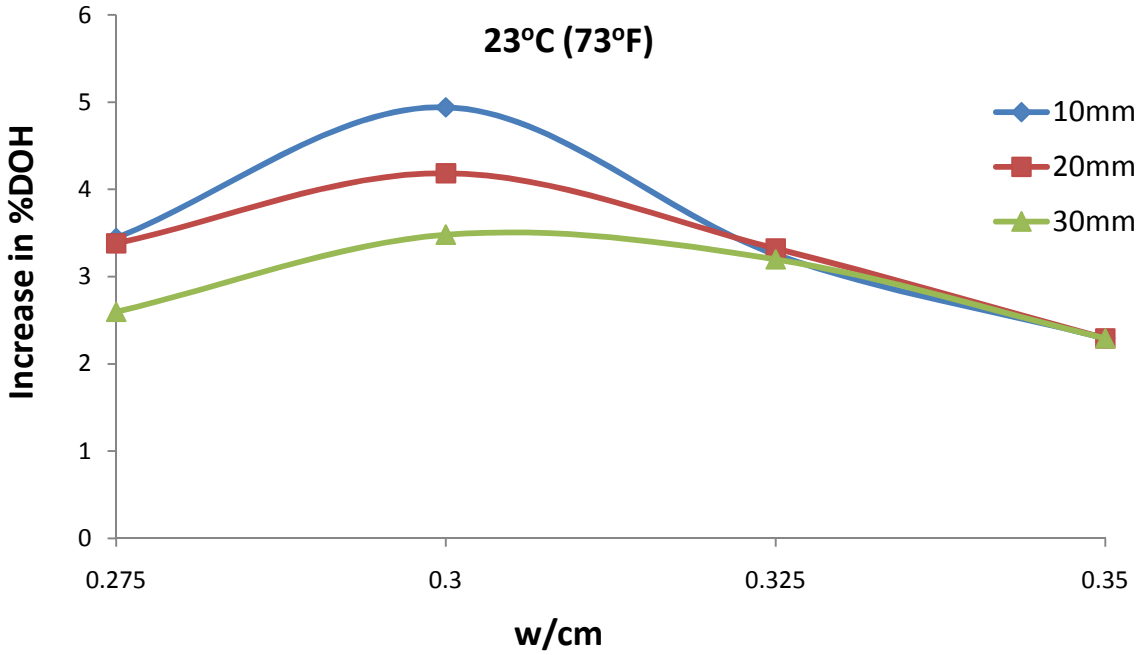

(a)

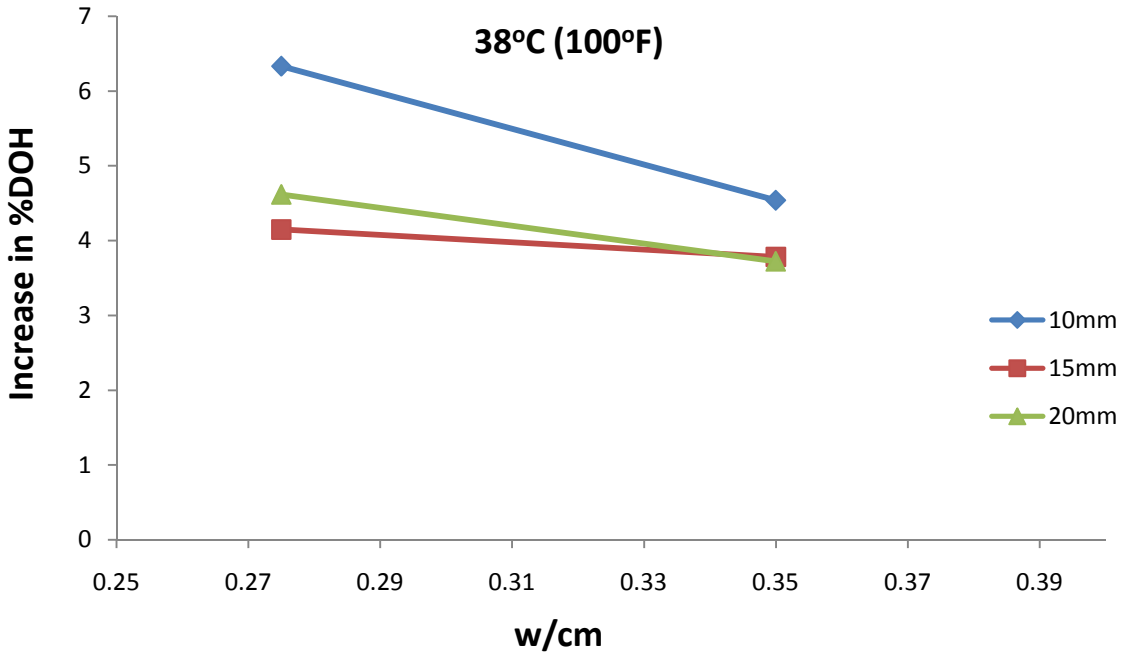

(b)

Figure 4.13: Effect of Sample Depth and w/cm on increase in DOH than the Sealed Sample of Equal Thickness after 7 days for 100% Type I Cement Paste; (a) 23°C (73°F) and (b) 38°C (100°F)

The effect of curing on cement paste hydration with supplementary cementitious materials (SCMs) was also studied. Pastes with cement replaced by 5% silica fume (5%SF) or 35% slag (35%S) were studied at 23°C (73°F). A w/cm of 0.275 was used for the samples with SCMs at sample thicknesses of 10 mm and 30 mm in isothermal calorimetry. Figure 4.14 shows the effect of water curing on 5%SF and 35%S compared to 100% Type I (Ty I) cement. Slag showed a higher increase in DOH than silica fume for the 10 mm sample, while both of the SCM samples showed a higher increase in DOH from water curing than the ordinary portland cement sample at the same w/cm and with 10 mm sample thickness. At the higher sample thickness of 30 mm the 30%S. 5%SF and 100% Ty I mixtures give similar increases in DOH. As both silica fume and slag reduce the porosity of cementitious materials, it becomes very difficult for the water to penetrate and reach the unhydrated cementitious particles.

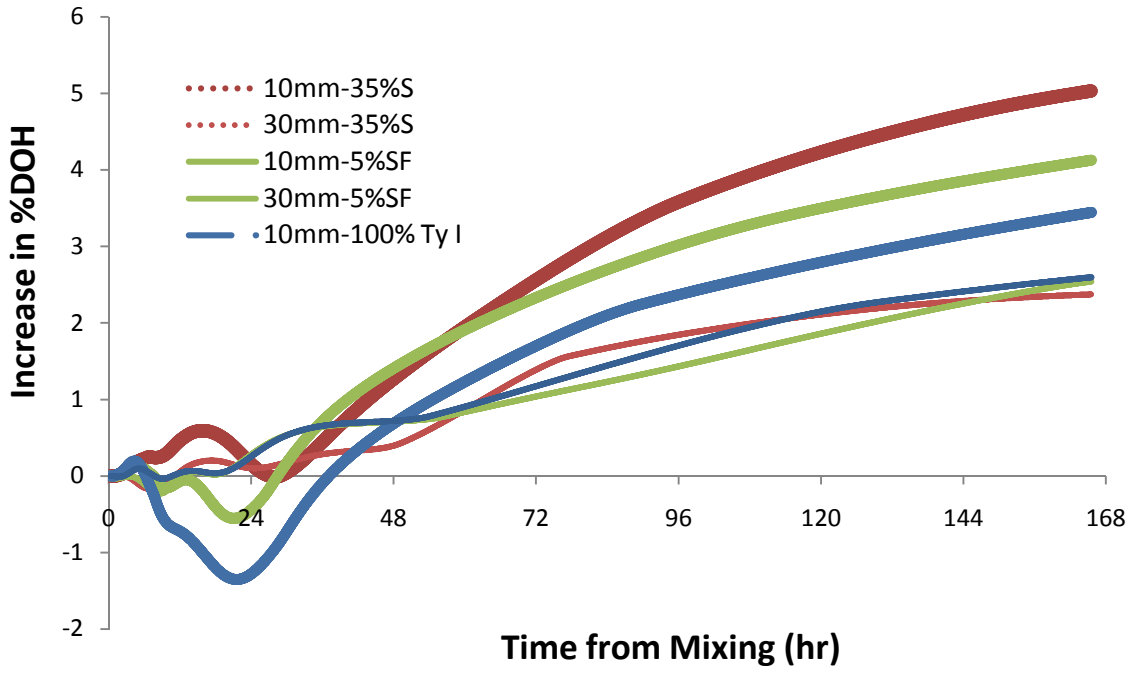

(a)

Figure 4.14: Effect of Water Curing on the early Property Development of 35%S and 5%SF at 23°C (73°F).

Figure 4.15 represents the effect of water curing on Type I cement mortar at 0.45 w/cm. Very little difference in cumulative heat of hydration is seen from the use of water curing, as would be expected at w/cm greater than 0.42. Figure 4.16 shows the effect of presoaked lightweight fine aggregate to improve the hydration of cementitious materials. Even at a w/cm of 0.45, the use of FLAIR improves the DOH of mortar, much more than external water curing. An increase in the amount of flair provided increased the hydration of cement, although with diminishing returns. This implies that complete replacement of sand by FLAIR is not necessary to increase the amount of cement hydration products. Figure 4.17 illustrates the how the FLAIR percentage used increases the amount of cement paste cured with a diminishing return.

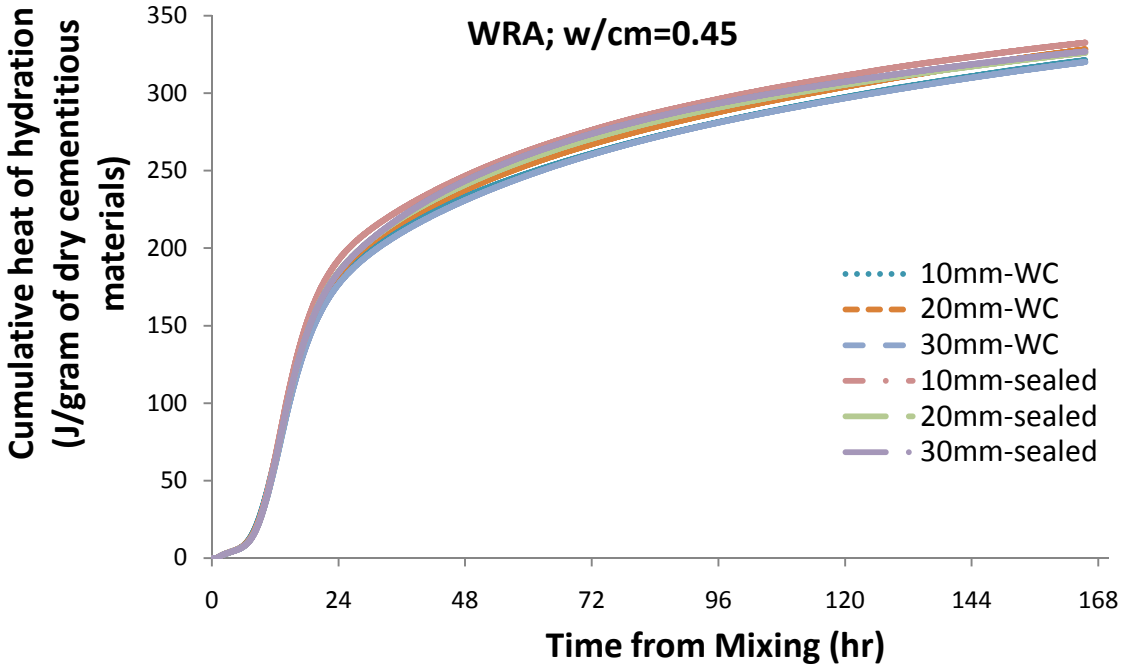

Figure 4.15: Effect of Water Curing on the Degree of Hydration of 100% Siliceous Aggregate, 100% Type I Portland Cement Mortar (w/cm=0.45) at 23°C (73°F).

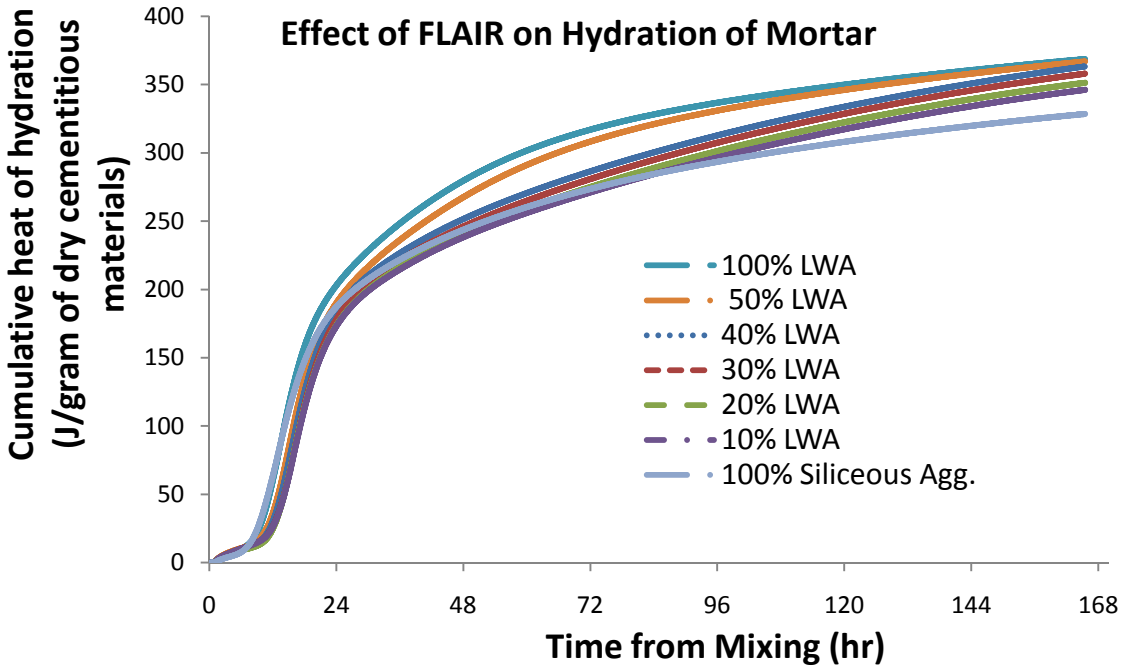
Effect of FLAIR on Hydration of Mortar
Cumulative heat of hydration (J/gram of dry cementitious materials)
400
350
300
250
200
150
100
50
0
0
24
48
72
96
120
144
168
Time from Mixing (hr)
100% LWA
50% LWA
40% LWA
30% LWA
20% LWA
10% LWA
100% Siliceous Agg.

(a)

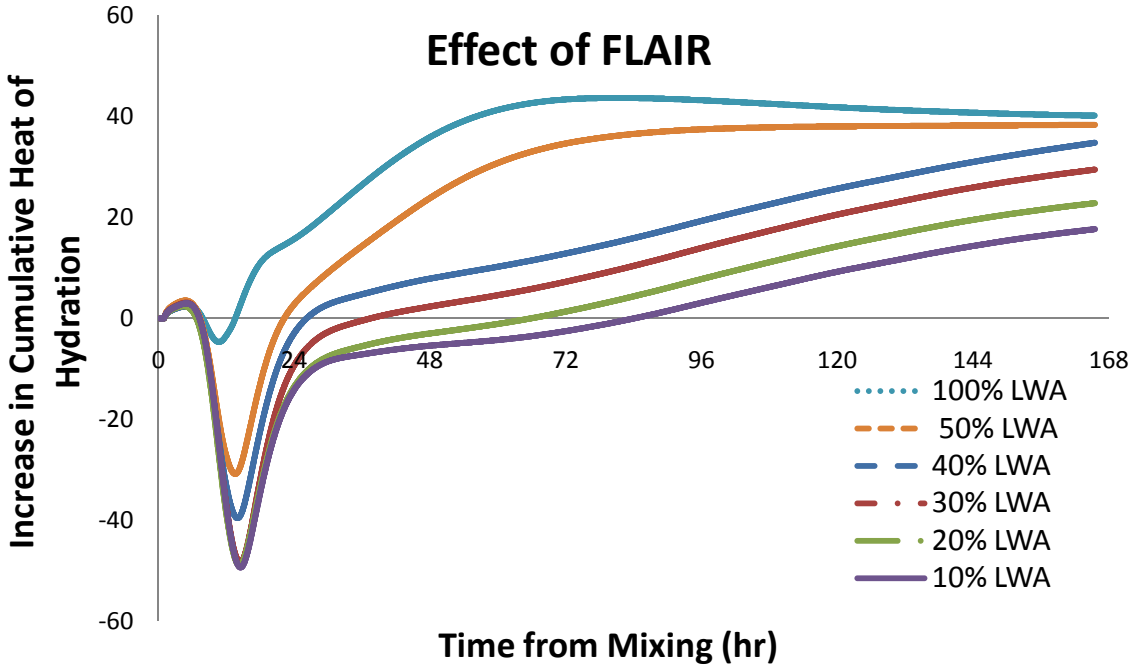
Effect of FLAIR
Increase in Cumulative Heat of Hydration
60
40
20
0
-20
-40
-60
0
24
48
72
96
120
144
168
Time from Mixing (hr)
100% LWA
50% LWA
40% LWA
30% LWA
20% LWA
10% LWA

(b)

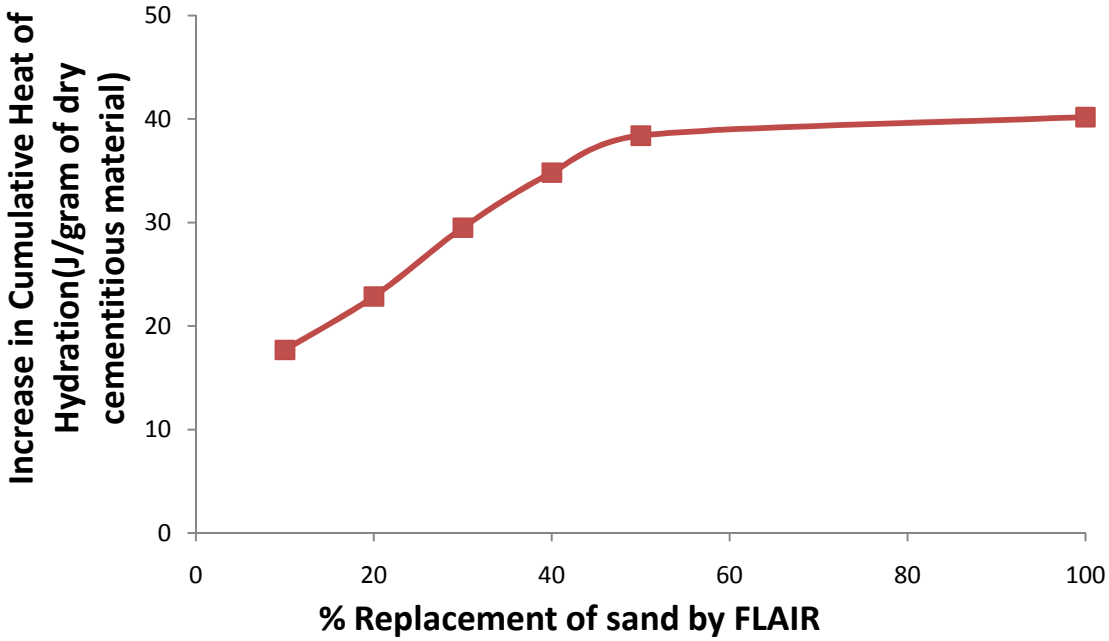

Figure 4.16: Effect of FLAIR on the DOH of Mortar at 23°C (73°F); (a) Cumulative Heat of Hydration, (b) Increase in %DOH with respect to 100% Siliceous Aggregate and (c) Increase in Cumulative heat of Hydration After 7days.

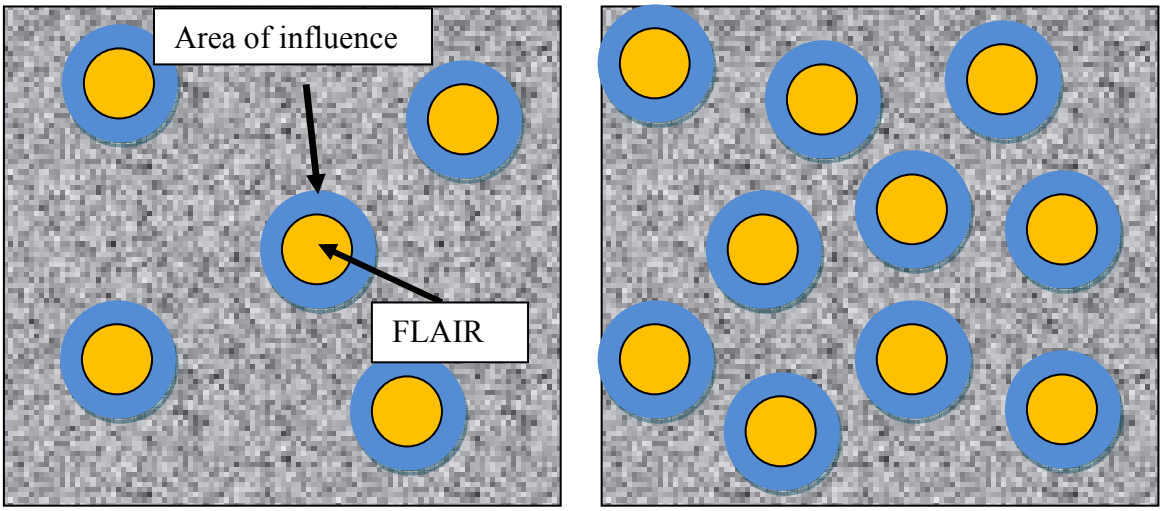

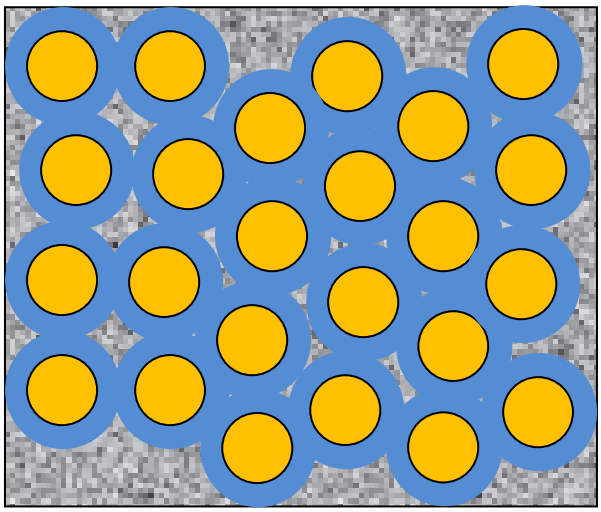

(c)

Figure 4.17: Well distributed Lightweight Fine Aggregate Improves the Coverage of Mortar; (a) Low Percentage of Lightweight Fine Aggregate Replacement, (b) High Percentage of Lightweight Fine Aggregate Improves the Coverage of Volume of Mortar, and (c) Area of Influence are Overlapping Due to the Excess Replacement of Sand by FLAIR .

Figures 4.18 and 4.19 show the effect of curing compound (CC) on the hydration of an Type I cement paste (w/cm= 0.275) at 23^{o}C (73^{o}F). Curing compound showed better result in sealed condition than cement paste with curing compound under drying conditions for different sample thickness. For the 10 mm samples, drying reduces the hydration significantly. The drierite-paste ratio is higher in thinner samples (as equal amount of drierite was used for all samples) and results in a lower relative humidity. However it is easier for the moisture to escape from the thinner samples than thicker samples. Samples cured with curing compound in a sealed environment show better hydration than sealed samples without curing compounds, probably because of the extra hydration provided by the excess water in the curing compound. Sample thickness showed significant effects on the improvement of DOH with curing compound in dry conditions but showed little increase in sealed conditions due to the presence of water in the curing comound. With the increase of thickness, curing compounds increased the hydration of

cementitous materials. Water cured samples and the curing compound samples showed almost similar response in increasing DOH, shown in Figure 4.20.

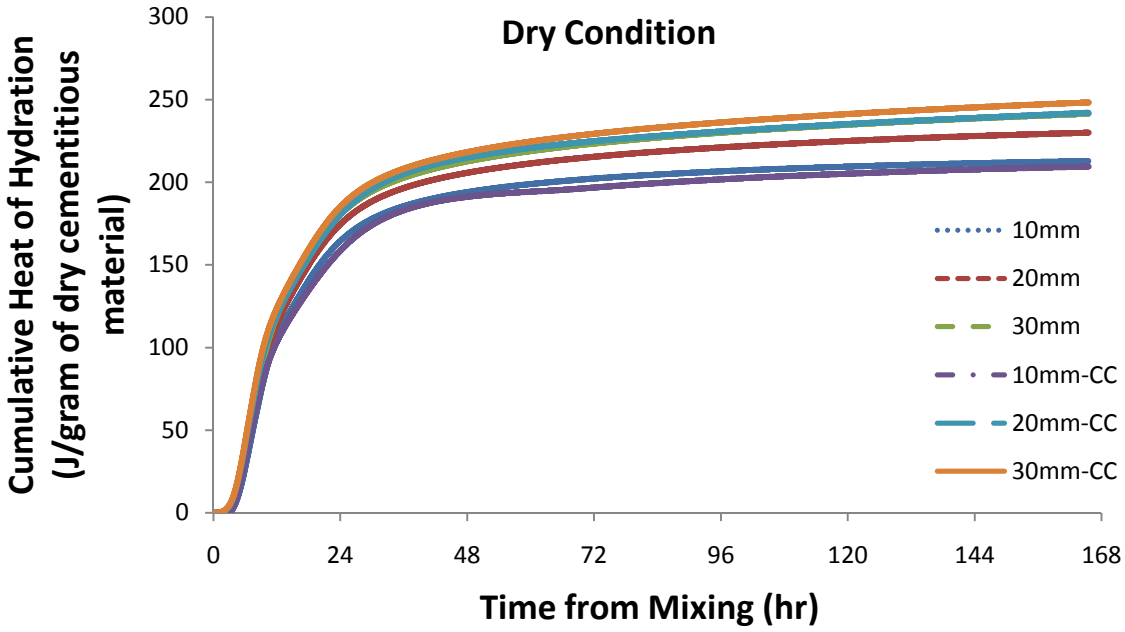

(a)

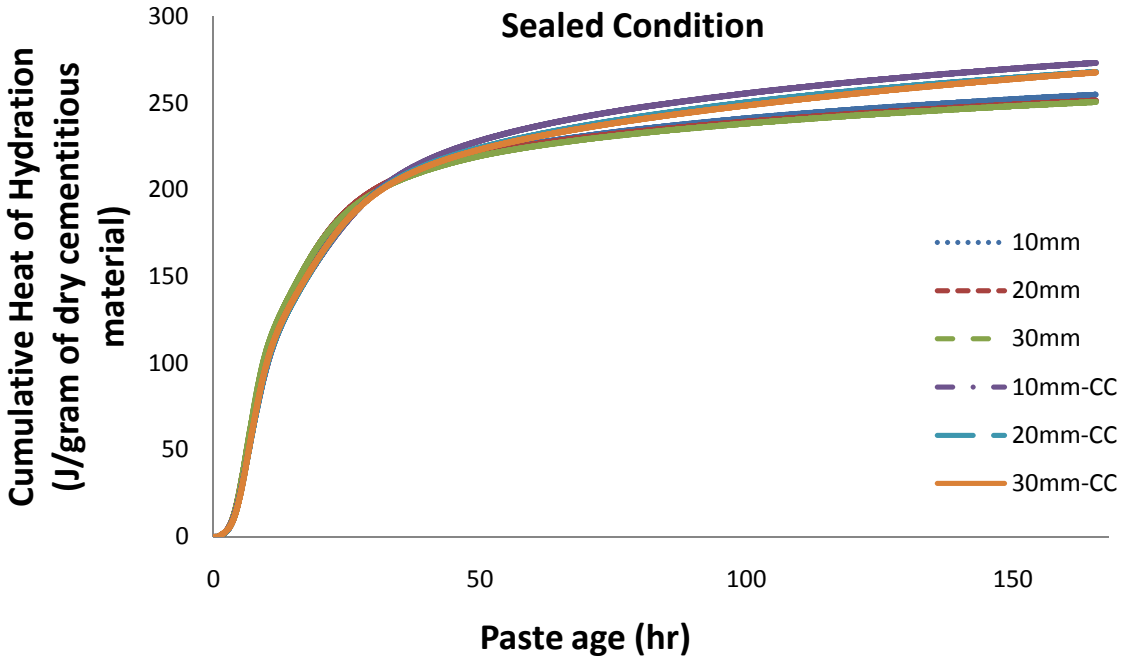

(b)

Figure 4.18: Effect of Curing Compound on the Hydration of Cementitious Materials for 100% Type I Cement w/cm of 0.275 at 23°C (73°F); (a) Dry Condition, and (b) Sealed Condition.

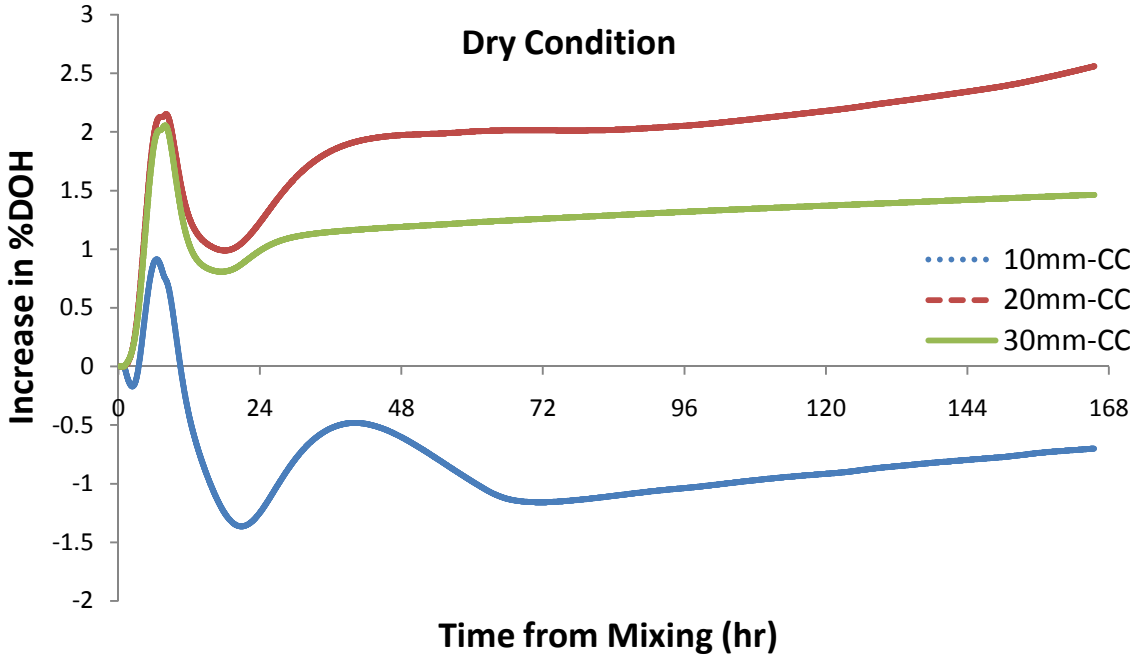

(a)

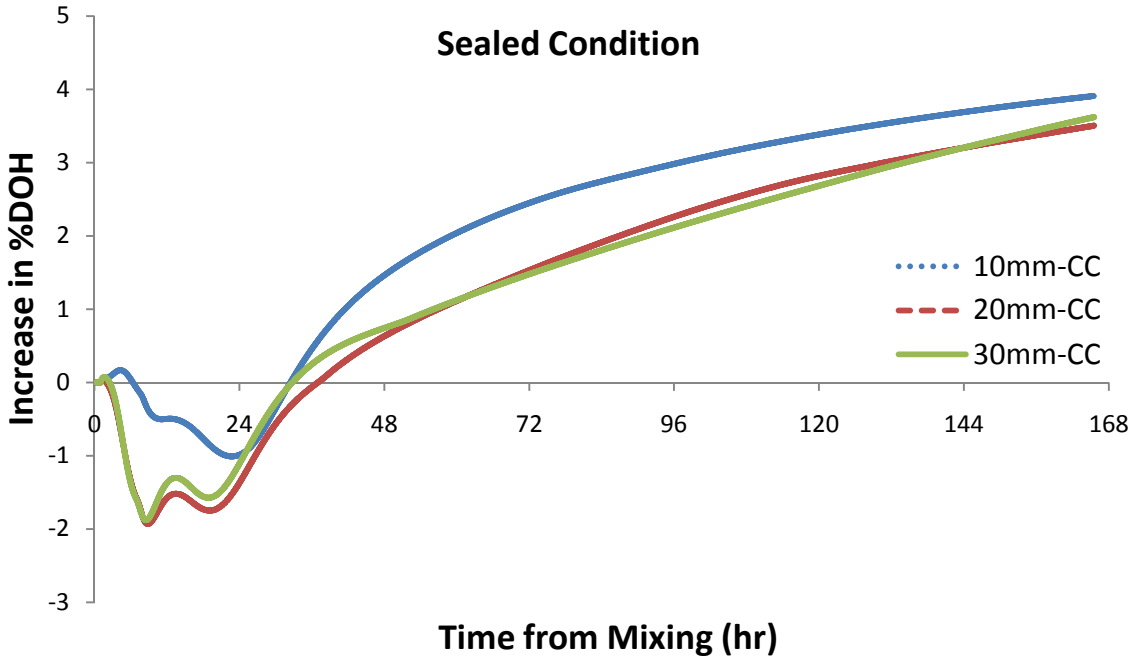

(b)

Figure 4.19: Effect of Curing Compound on the Increase in DOH of Cementitious Materials for 100% Type I Cement w/cm of 0.275 at 23°C (73°F); (a) Dry Condition, and (b) Sealed Condition.

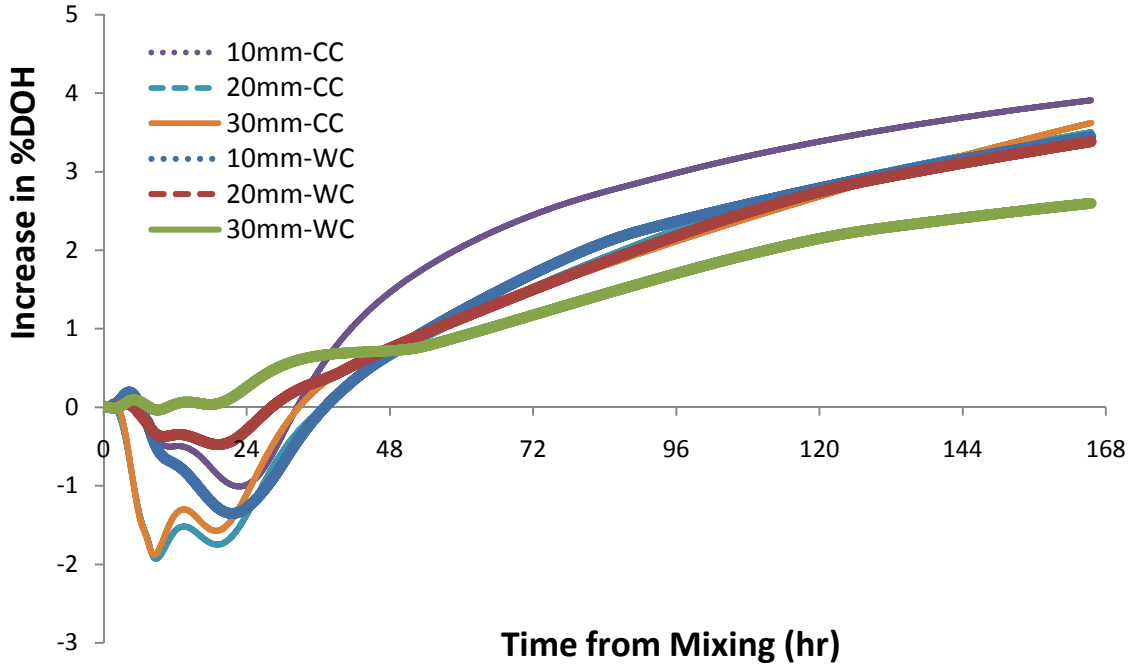

Figure 4.20: Comparison between Water Curing and the Curing Compound at Sealed Environment for 100% Type I Cement w/cm of 0.275 at 23°C (73°F).

4.5 Conclusions

The effects of different curing techniques were studied using isothermal calorimetry. From these experiments, the following conclusions can be made:

- Water curing, curing compound and FLAIR improves the hydration of cementitious materials.
- Water curing is more effective in low water-cementitious material ratio. The ionic concentration of curing water greatly affects the rate of hydration, with saturated lime water strongly accelerating the hydration. The sample curing height also showed an effect on the hydration of cement paste samples, showing that the benefits of curing water, even when applied immediately after mixing, are limited to the top 10 to 20 mm. Water curing

showed greater improvement in hydration for samples with silica fume or slag than Type I cement.

- FLAIR improves the hydration of cementitious materials significantly, although possibly through by making the water more accessible than when ponded at the top
- Curing compounds provide a similar hydration response to sample without curing in dry condition but improves the hydration significantly in a sealed environment.
- Use of drierite in isothermal calorimetry has shown promise to simulate hydration in low relative humidity conditions.
- Water curing and curing compound showed a similar response in improving the hydration of cementitious materials.

References

1. Price, W. H., "Factors influencing concrete strength," Journal of American Concrete Institute, V. 47, No. 2, 1951, pp. 417-432.
2. Neville, A. M., “Properties of Concrete,” Fourth and Final Edition, New York, USA, John Wiley and Sons Inc., 1996.
3. Meeks, K. W., and Carino, N. J., “Curing of High-Performance Concrete: Report of the State-of-the-Art,” NISTIR6295, U.S. Department of Commerce, 1999.
4. Kovler, K., and Jensen, M., "Novel Technique for Concret Curing," Concrete International, V. 27, 2005, pp. 39-42.
5. Kovler, K., Souslikov, A., and Bentur, A., “Pre-Soaked Lightweight Aggregates as Additives for Internal Curing of High-Strength Concretes,” Cement, Concrete & Aggregates,V. 26, No. 2, 2004, pp. 131-138.
6. Bentz, D., Lura, P., and Roberto, J. W., "Mixture Proportioning for Internal Curing," Concrete International, V. 27, N0. 2, 2005, pp. 35-40.
7. Klieger, P., "Early High-Strength Concrete for Prestressing," Proceedings,World Conference on Prestressed Concrete, July 1957, pp. A5(1)-A5(14).
8. Mather, B., "Self-Curing Concrete, Why Not?," Concrete International, V. 223, 2001, pp. 46-47.
9. Weber, S., and Reinhardt, H. W., "A New Generation of High-Performance Concrete: Concrete with Autogenous Curing," Advanced Cement-Based Materials, V. 6, No. 2, 1997, pp. 59-98.

10. Hoff, G., and Elimov, R. "Concrete Production for the Hibernia Platform," Second CANMET/ACI International Symposium on Advances in Concrete Technology, supplementary papers, Las Vegas, 1995, pp. 717-739.
11. Kovler, K., Bentur, A., Lange, D. A., Bentz, D., Van Breugel, K., Lura, P., Zhutovsky, S., and Souslikov, A., "Autogenous Curing of High-Strength Cementitious Materials by Fine Uniformly Distributed Lightweight Aggregate." Research Report to U.S.-Israel Binational Science Foundation, Technion, Haifa, 2004.
12. Villarreal, V. H., "Building Better Pavements Through Internal Hydration—A Work in Progress," Proceedings of the R. Villarreal International Symposium on Durability of Concrete, Monterrey, México, 2005, pp. 13.
13. Jensen, O. M., and Hansen, P. F., "Water-Entrained Cement-Based Materials: Principles and Theoretical Background," Cement and Concrete Research, V. 31, 2001, pp. 647-654.
14. Jensen, O. M., and Hansen, P. F., "Water-Entrained Cement-Based Materials: II-Experimental Obsurvations," Cement and Concrete Research, V. 32, 2002, pp. 973-978.
15. Lura, P., "Autogenous Deformation and Internal Curing of Concrete," Doctoral Dissertation, Technical University of Delft, Netherland, 2003.
16. Bentz, D. P. and Hansen, K. K.," Preliminary Observations of Water Movement in Cement Pastes During Curing Using X-ray Absorption," Cement and Concrete Research, V. 30, No. 7, 2000, pp. 1157-1168.
17. ASTM C 33, "Standard Specification for Concrete Aggregates," American Society for Testing and Materials, Pennsylvania, 2009.

18. ASTM C 305, “Standard Practice for Mechanical Mixing of Hydraulic Cement Pastes and Mortars of Plastic Consistency,” American Society for Testing and Materials, Pennsylvania, 2009.
19. Broda, M., Wirquin, E., and Duthoit. B., "Conception of an isothermal calorimeter for concrete-Determination of the apparent activation energy." Materials and Structures, V. 35, No. 251, 2002, pp. 389-394.
20. Wadsö, L., "Operational Issues in Isothermal Calorimetry," Cement and Concrete Research, V. 40, No. 7, 2010, pp. 1129-1137.
21. D’Aloia, L., and Chanvillard G., “Determining the ‘Apparent’ Activation Energy of Concrete; E_a — Numerical simulations of the Heat of Hydration of Cement,” Cement and Concrete Research, V. 32, 2002, pp. 1277-1289.
22. Kada-Benameur, H., Wirquin, E., and Duthoit, B., “Determination of Apparent Activation Energy of Concrete by Isothermal Calorimetry,” Cement and Concrete Research, V. 30, 2000, pp. 301-305.
23. Van Breugel, K., “Prediction of Temperature Development in Hardening Concrete,” Prevention of Thermal Cracking in Concrete at Early Ages, RILEM Report 15, E&FN Spon, London, 1998, pp. 51-75.
24. Copeland, L. E., Kantro, D. L., Verbeck, G., “Part IV-3 Chemistry of Hydration of Portland Cement,” 4th International Symposium of the Chemistry of Cement, Washington, D.C., 1960, pp. 429-465.
25. De Schutter, G., and Taerwe, L., “Degree of Hydration-Based Description of Mechanical Properties of Early-Age Concrete,” Materials and Structures, V. 29, No. 6, 1996, pp. 335-344.

26. Schindler, A. K., and Folliard, K. J., "Heat of Hydration Models for Cementitious Materials," ACI Materials Journal, V. 102, No. 1, 2005, pp. 24-33.
27. Lura, P., Winnefeld, F., and Klemm, S., "Simultaneous Measurements of Heat of Hydration and Chemical Shrinkage on Hardening Cement Pastes," Journal of Thermal Analysis and Calorimetry, 2009.

CHAPTER 5 - CONCLUSIONS AND FUTURE RESEARCH

5.1 Conclusions

Temperature affects the rate of strength gain of cementitious materials. In hot summer days concrete gains strength very rapidly, whereas in cold winter hydration virtually stops. Since temperatures vary greatly in the U.S. from place to place it is very important to know the temperature sensitivity of concrete. The term apparent activation energy (E_a) is used to represent the influence of temperature on the hydration of cementitious material. Apparent activation energy is also an important parameter in maturity function. Apparent activation energy also required to model the heat generation of concrete which is very important for mass concrete to avoid thermal cracking. There are various methods and calculation techniques to calculate E_a. Different methods use different physical properties to calculate the E_a values. Calculation techniques also vary the way of estimating the rate constant k.

This chapter provides a summary of the conclusions made based on the research performed and presents a few ideas for future research.

This study focused on two major areas. First, quantifying the effects of temperature on the early hydration of cementitious materials and second, evaluating the effects of different curing techniques on the early hydration of cementitious materials.

5.1.1 Effect of Temperature on the Early Hydration of Cementitious Materials

Apparent activation energy of cementitious materials is significantly affected by the methods and calculation techniques. However, some calculation techniques showed good correlation due to the similarity between the techniques. Initial and final setting time showed very close response indicating that these methods can be used interchangeably. There is no

significant effect of aggregates as both cement paste and mortar results show very close apparent activation energy values. This supports the common practice of using cement paste and mortar E_a values for concrete. Chemical shrinkage shows good promise for E_a calculation apart from the water reducing admixture. Water reducing admixtures have some air entrainment properties, which may affect the measured chemical shrinkage.

5.1.2 Effect of Curing on the Early Hydration of Cementitious Materials

Types of ion and concentration in curing water affect the hydration of cementitious materials. Curing water thickness also have significant effect on the hydration of cementitious materials. Water curing seems to be more effective in low water-cementitious material ratio. Water curing is also effective for thinner samples than thicker samples as it takes more time for the curing water to reach the bottom of the thicker sample. For slag and silica fume, water-curing showed greater improvement than ordinary portland cement (OPC). Curing compound showed similar improvement in hydration like OPC in sealed environment. Under drying conditions the curing compound was not very effective. Lightweight fine aggregate improves the hydration of cementitious materials significantly. Isothermal calorimetry results showed that it is not necessary to replace sand by lightweight aggregate to obtain better curing and improved hydration.

5.2 Suggestions for Future Research

Potential future research includes:

- Apparent activation energy can be calculated using concrete to find out the possible effect of larger aggregate.

- Extensive study needs to be done on the chemical admixture to identify the possible limitations of chemical shrinkage based apparent activation energy calculation.
- Research can be done to identify the limiting partial replacement of lightweight aggregates.
- Effect of curing methods on other supplementary cementitious materials can be studied.

Appendix A - HEAT OF HYDRATION

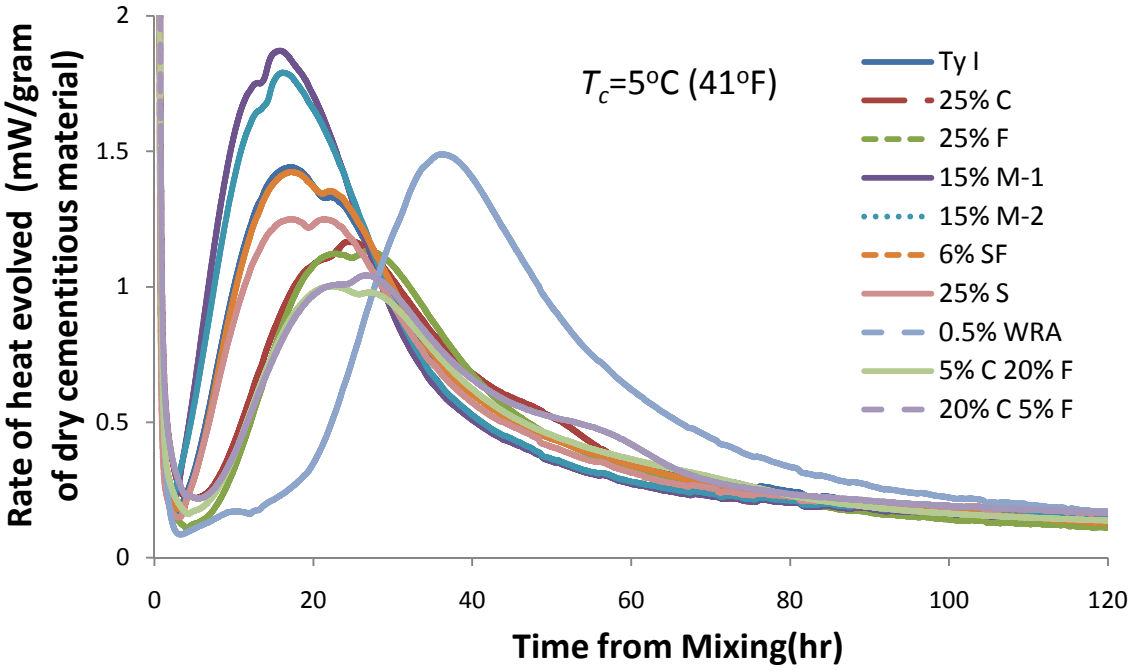
T_c=5°C (41°F)
Rate of heat evolved (mW/gram of dry cementitious material)
Time from Mixing(hr)
Ty I
25% C
25% F
15% M-1
15% M-2
6% SF
25% S
0.5% WRA
5% C 20% F
20% C 5% F
0
0.5
1
1.5
2
0
20
40
60
80
100
120

(a)

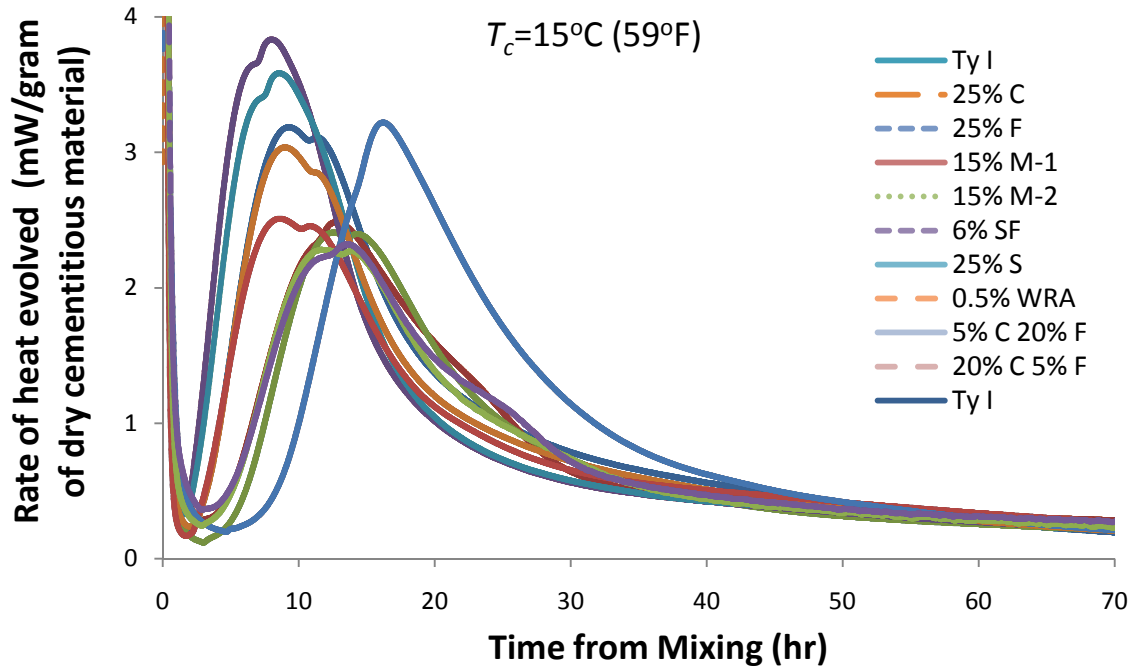
T_c=15°C (59°F)
Rate of heat evolved (mW/gram of dry cementitious material)
Time from Mixing (hr)
Ty I
25% C
25% F
15% M-1
15% M-2
6% SF
25% S
0.5% WRA
5% C 20% F
20% C 5% F
Ty I
0
1
2
3
4
0
10
20
30
40
50
60
70

(b)

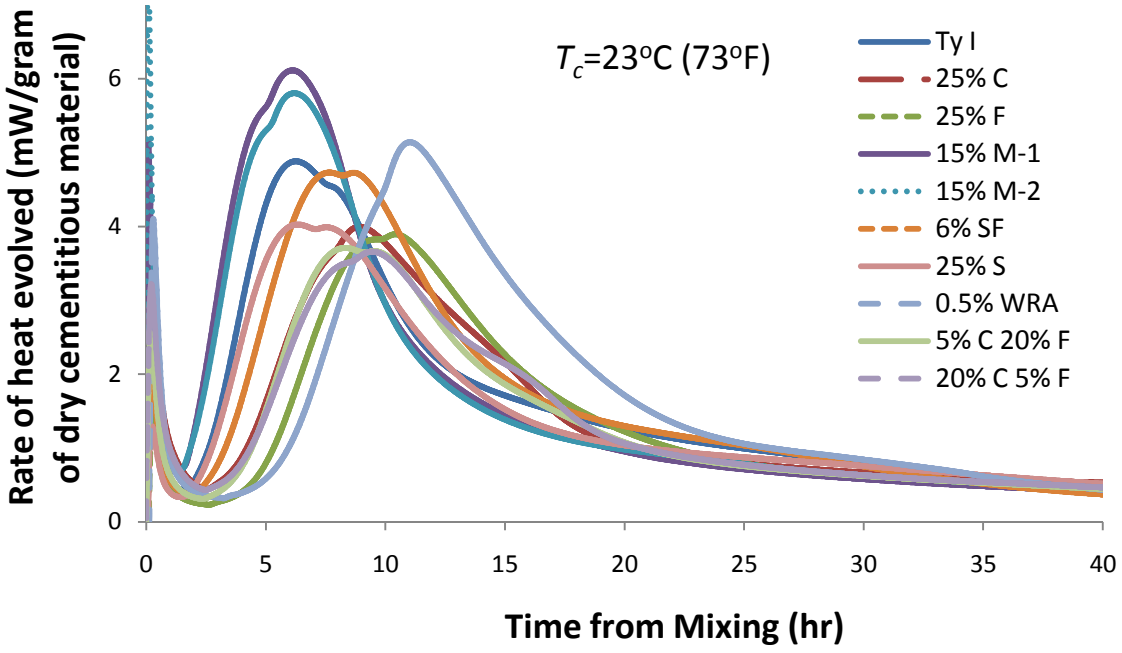
T_c=23°C (73°F)
Rate of heat evolved (mW/gram of dry cementitious material)
Time from Mixing (hr)
Ty I
25% C
25% F
15% M-1
15% M-2
6% SF
25% S
0.5% WRA
5% C 20% F
20% C 5% F
0
2
4
6
0
5
10
15
20
25
30
35
40

(c)

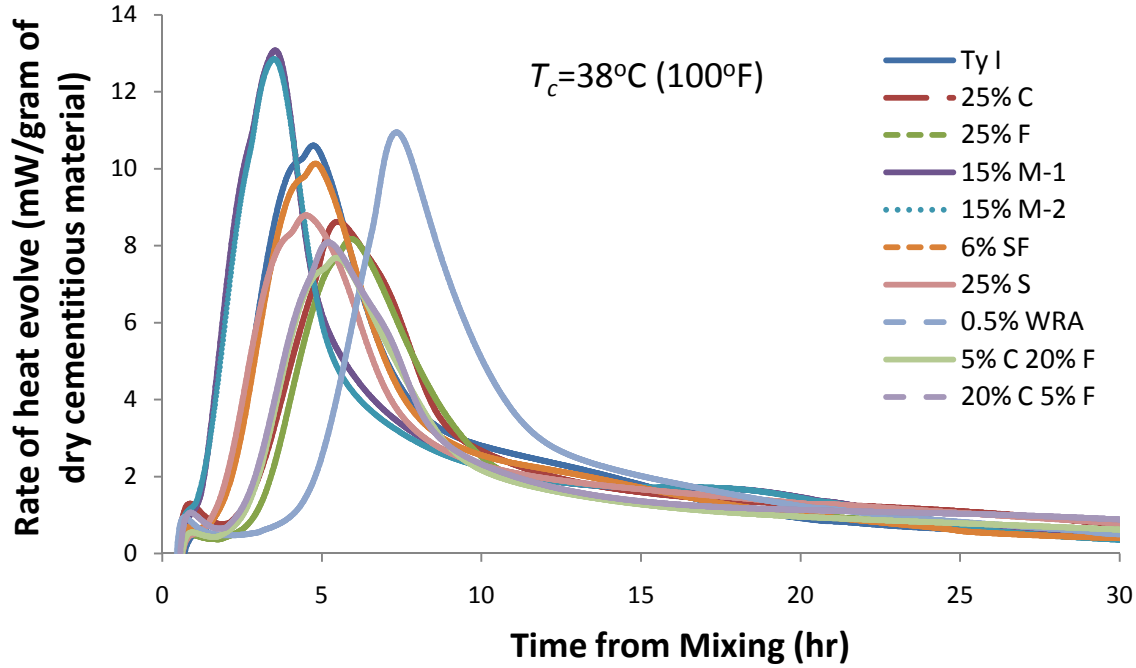
T_c=38°C (100°F)
Rate of heat evolve (mW/gram of dry cementitious material)
Time from Mixing (hr)
Ty I
25% C
25% F
15% M-1
15% M-2
6% SF
25% S
0.5% WRA
5% C 20% F
20% C 5% F
0
2
4
6
8
10
12
14
0
5
10
15
20
25
30

(d)

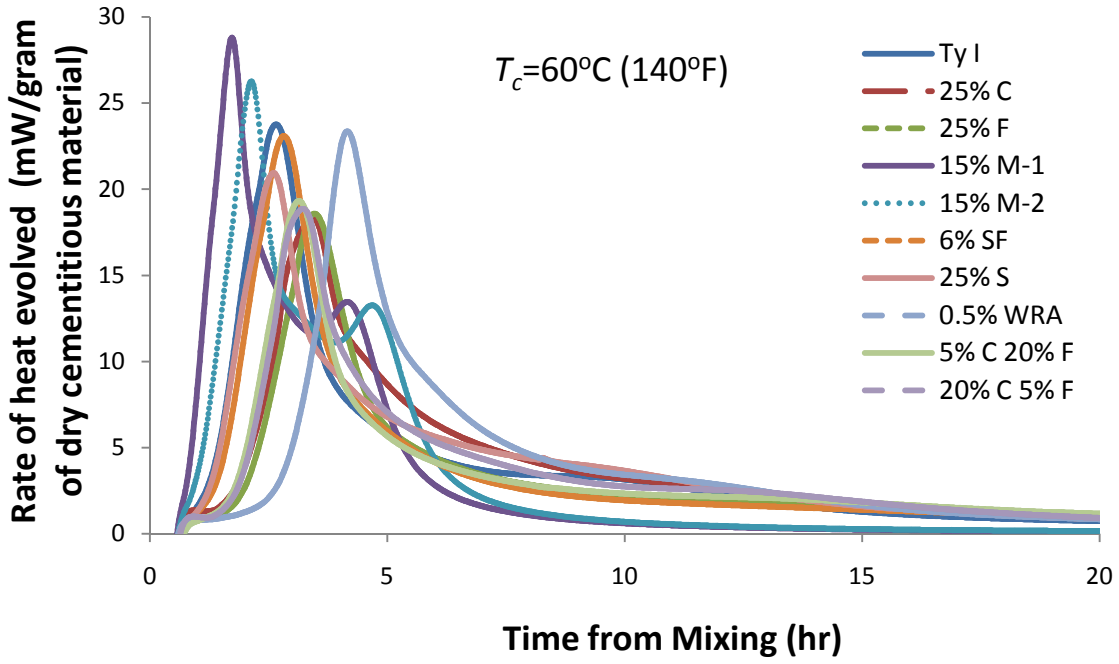

(e)

Figure A.1: Rate of Heat Evolved for Cement Paste (w/cm=0.35); (a) 5 °C (41 °F); (b) 15 °C (59 °F); (c) 23 °C (73 °F); (d) 38 °C (100 °F); and (e) 60 °C (140 °F).

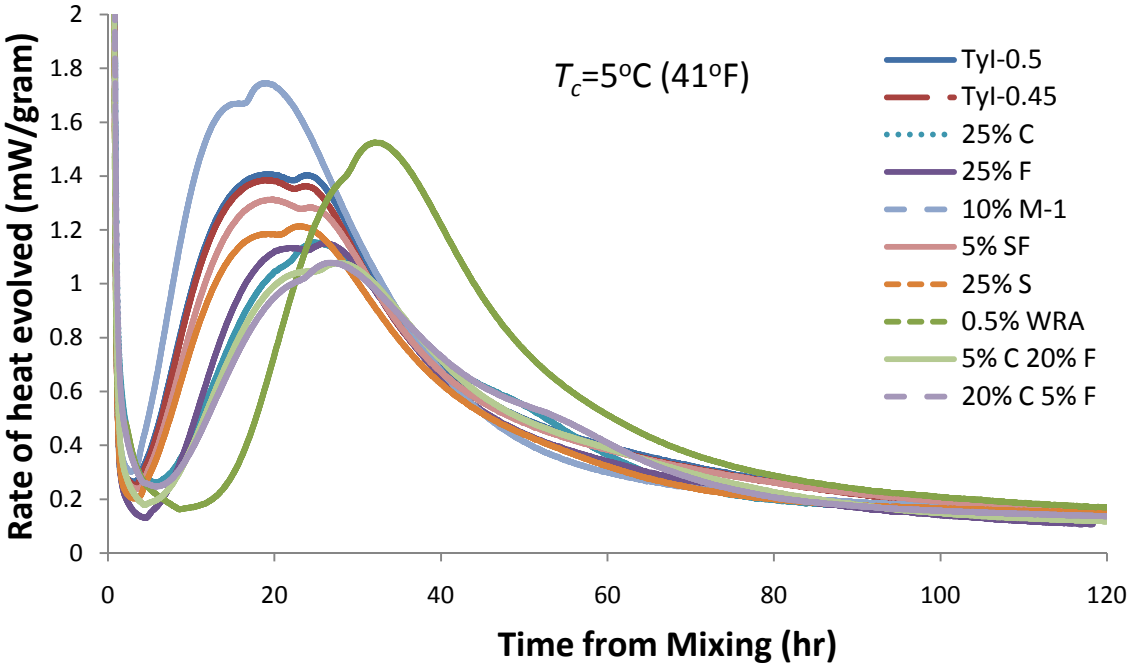

(a)

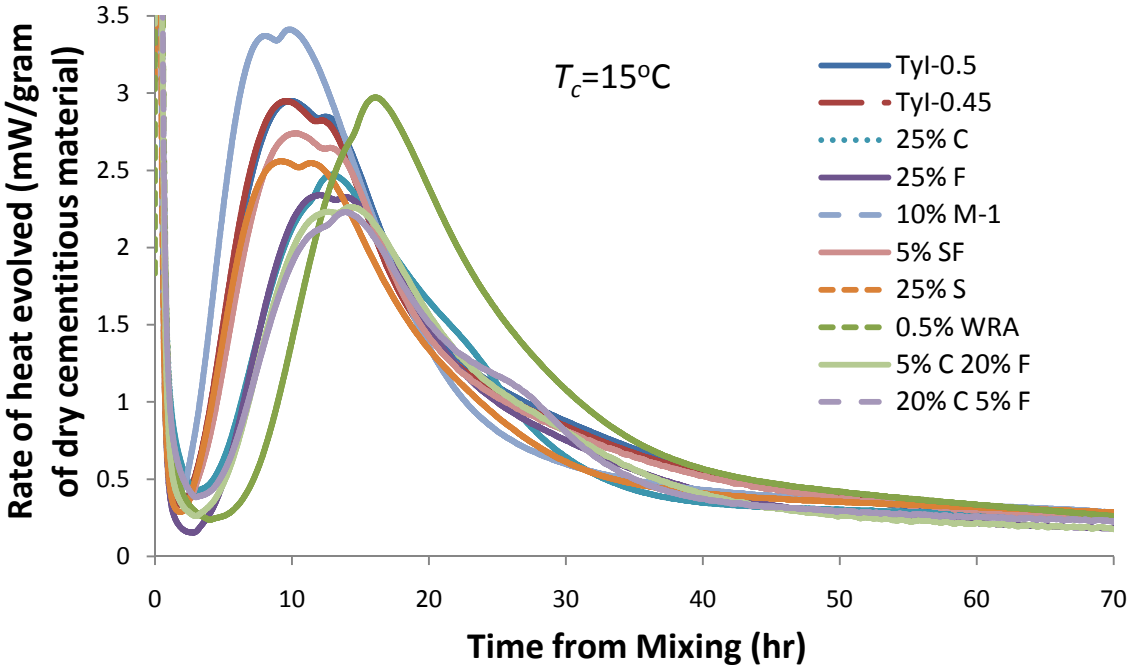
Rate of heat evolved (mW/gram of dry cementitious material)
T_c=15°C
Tyl-0.5
Tyl-0.45
25% C
25% F
10% M-1
5% SF
25% S
0.5% WRA
5% C 20% F
20% C 5% F
Time from Mixing (hr)

(b)

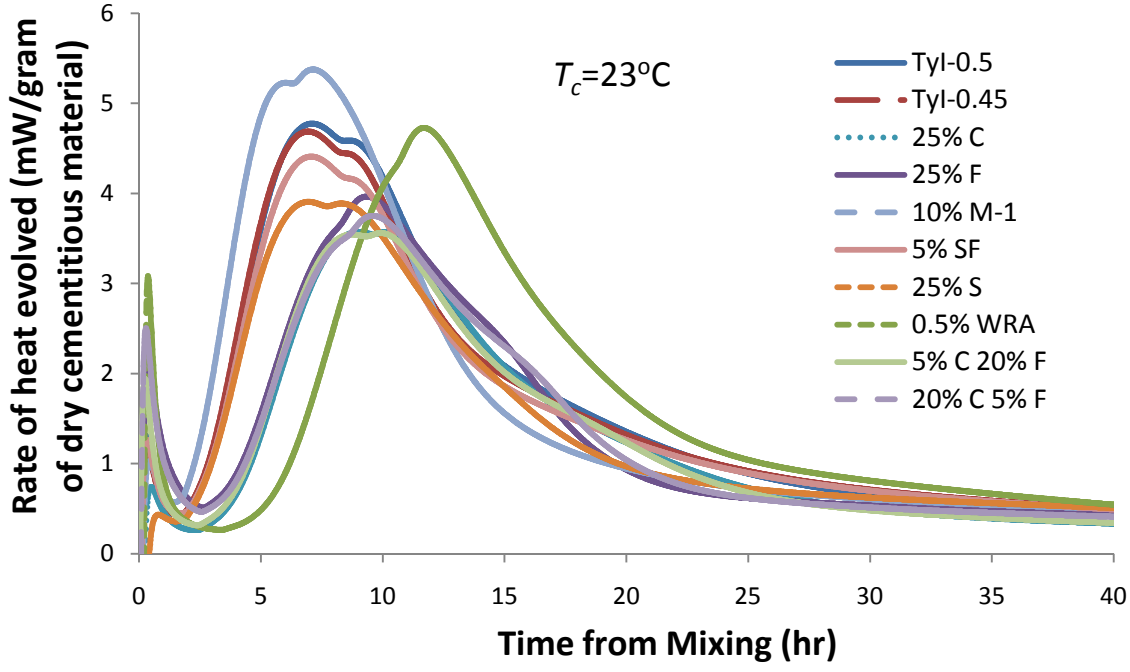
Rate of heat evolved (mW/gram of dry cementitious material)
T_c=23°C
Tyl-0.5
Tyl-0.45
25% C
25% F
10% M-1
5% SF
25% S
0.5% WRA
5% C 20% F
20% C 5% F
Time from Mixing (hr)

(c)

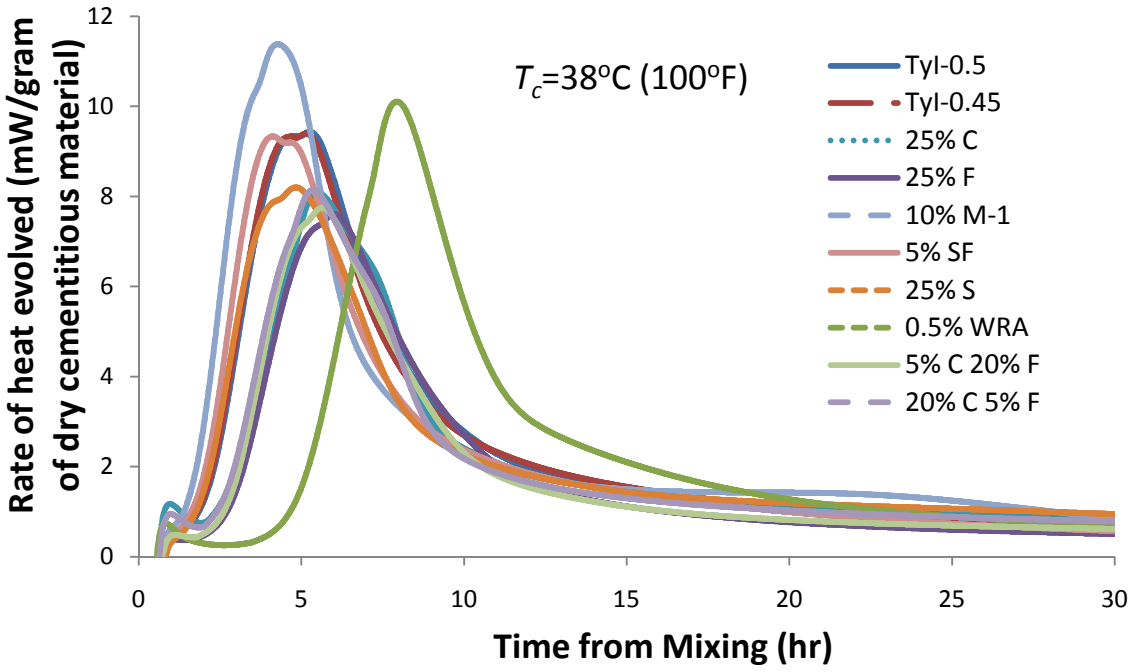

(d)

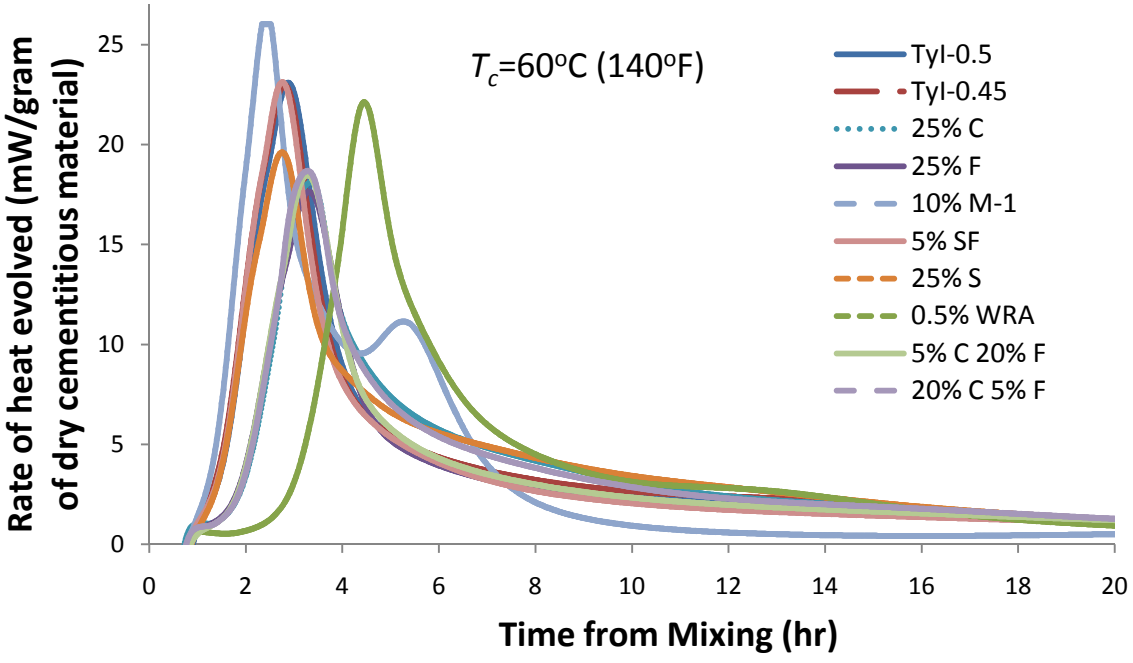

(e)

Figure A.2: Rate of Heat Evolved for Cement Paste with Same w/cm as Used in Mortar; (a) 5 °C (41 °F); (b) 15 °C (59 °F); (c) 23 °C (73 °F); (d) 38 °C (100 °F); and (e) 60 °C (140 °F).

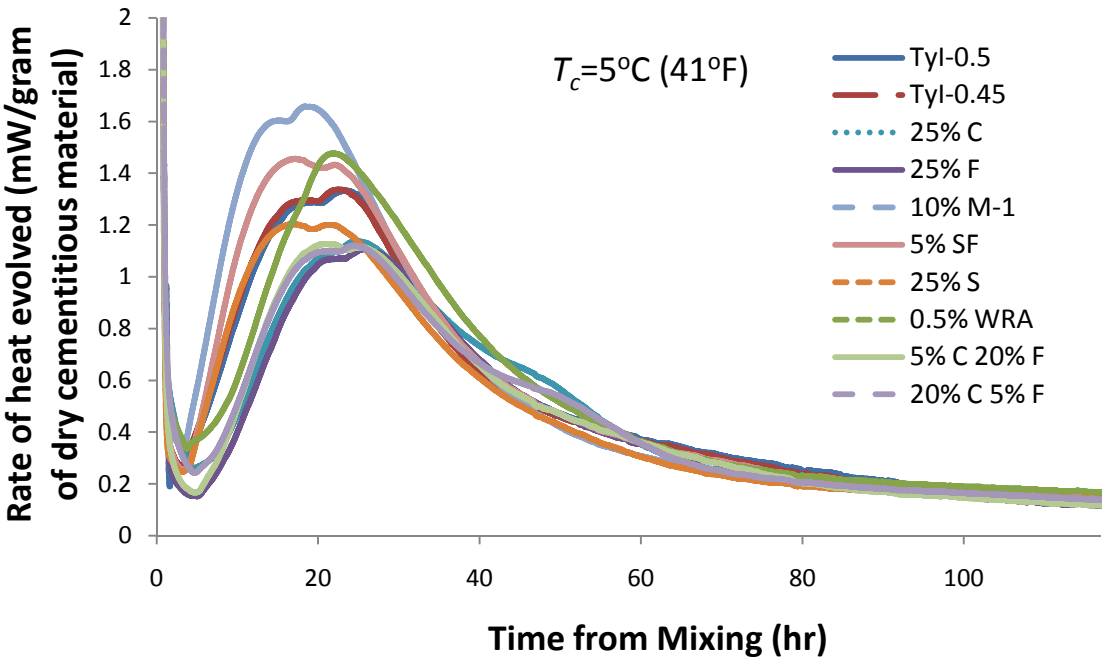
T_c=5°C (41°F)
Rate of heat evolved (mW/gram of dry cementitious material)
Time from Mixing (hr)
Tyl-0.5
Tyl-0.45
25% C
25% F
10% M-1
5% SF
25% S
0.5% WRA
5% C 20% F
20% C 5% F
0
0.2
0.4
0.6
0.8
1
1.2
1.4
1.6
1.8
2
0
20
40
60
80
100

(a)

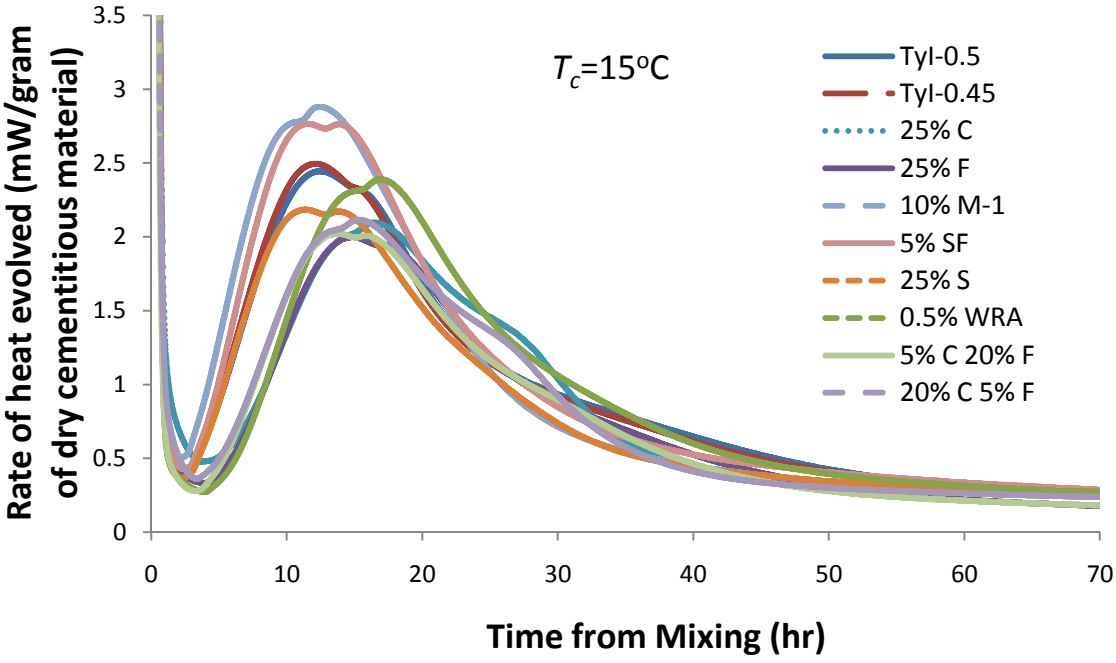
T_c=15°C
Rate of heat evolved (mW/gram of dry cementitious material)
Time from Mixing (hr)
Tyl-0.5
Tyl-0.45
25% C
25% F
10% M-1
5% SF
25% S
0.5% WRA
5% C 20% F
20% C 5% F
0
0.5
1
1.5
2
2.5
3
3.5
0
10
20
30
40
50
60
70

(b)

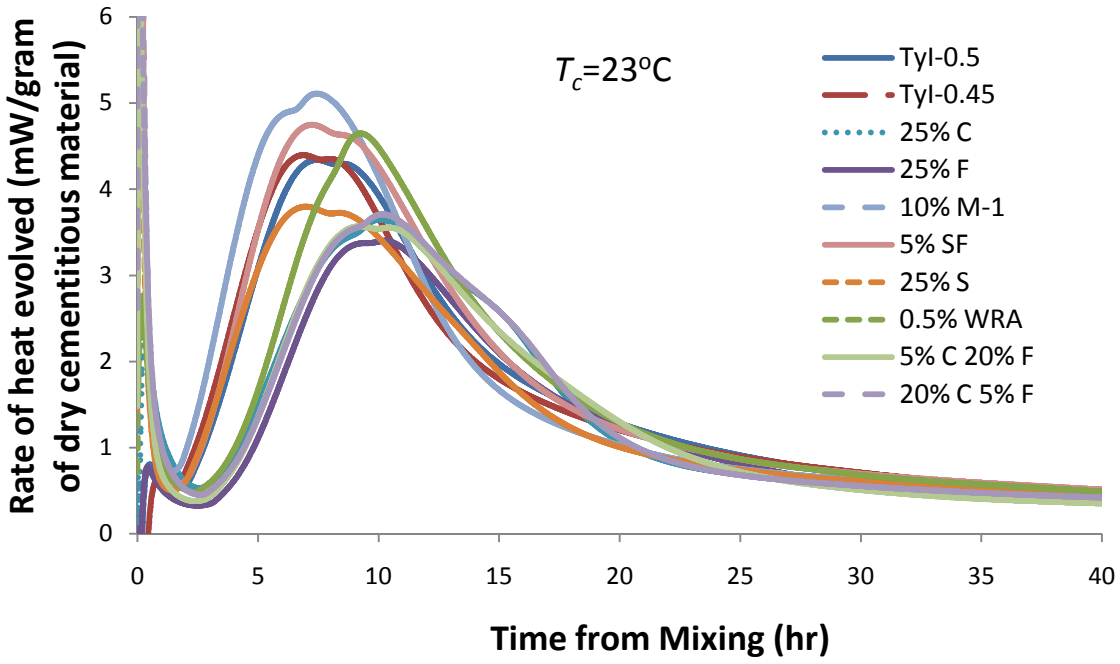
T_c=23°C
Rate of heat evolved (mW/gram of dry cementitious material)
Time from Mixing (hr)
Tyl-0.5
Tyl-0.45
25% C
25% F
10% M-1
5% SF
25% S
0.5% WRA
5% C 20% F
20% C 5% F

(c)

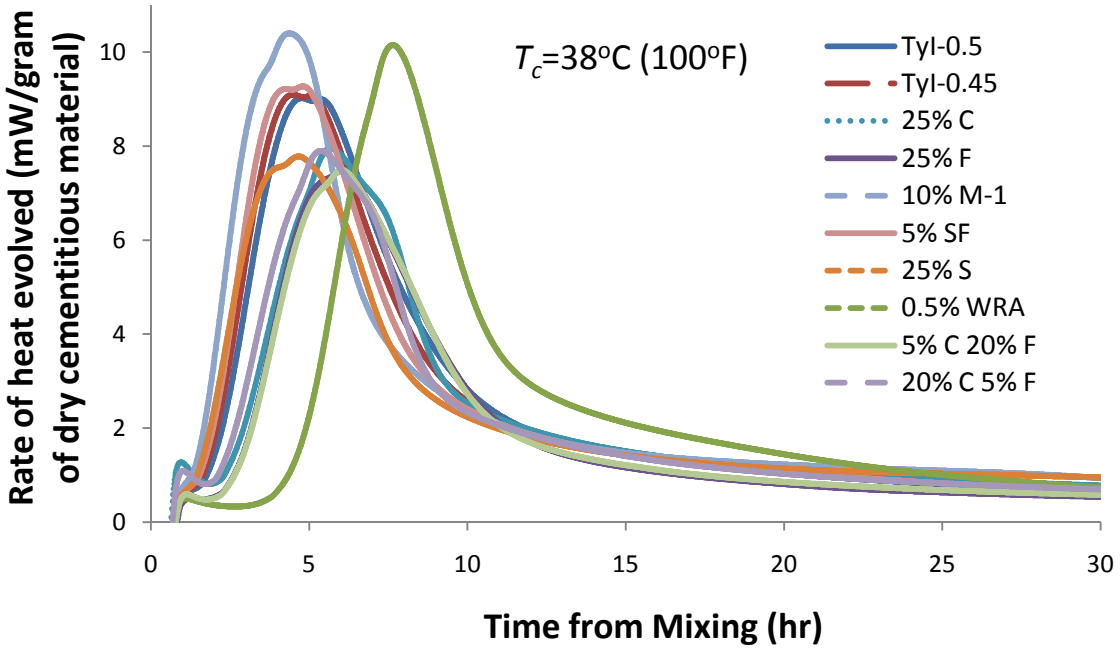
T_c=38°C (100°F)
Rate of heat evolved (mW/gram of dry cementitious material)
Time from Mixing (hr)
Tyl-0.5
Tyl-0.45
25% C
25% F
10% M-1
5% SF
25% S
0.5% WRA
5% C 20% F
20% C 5% F

(d)

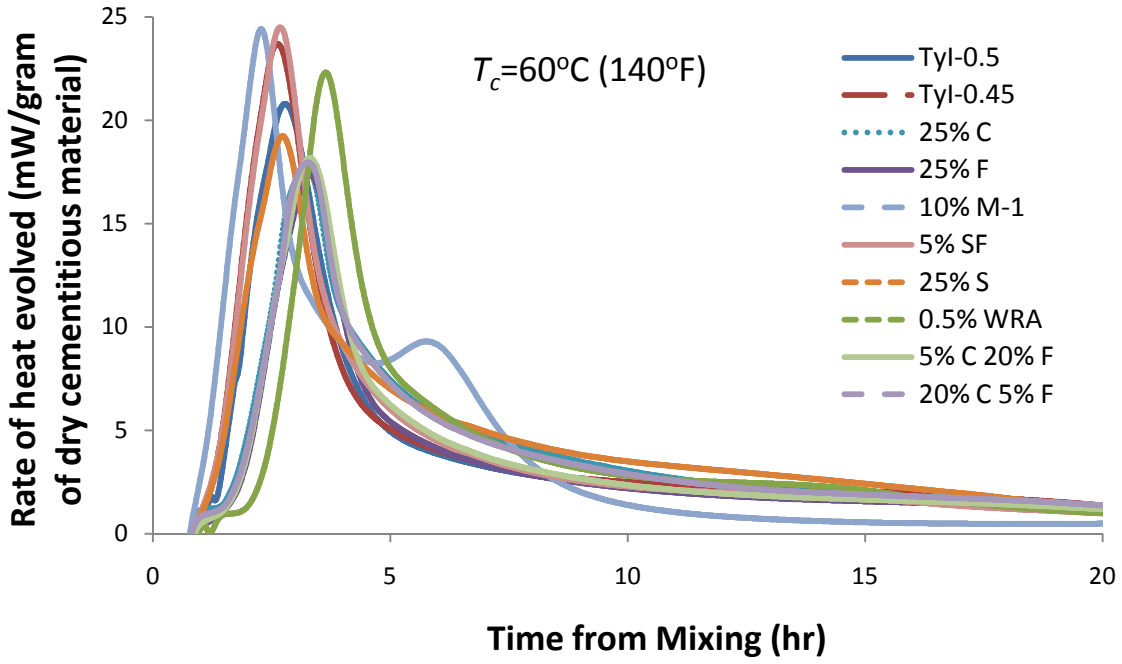

(e)

Figure A.3: Rate of Heat Evolved for Mortar; (a) 5 °C (41 °F); (b) 15 °C (59 °F); (c) 23 °C (73 °F); (d) 38 °C (100 °F); and (e) 60 °C (140 °F).

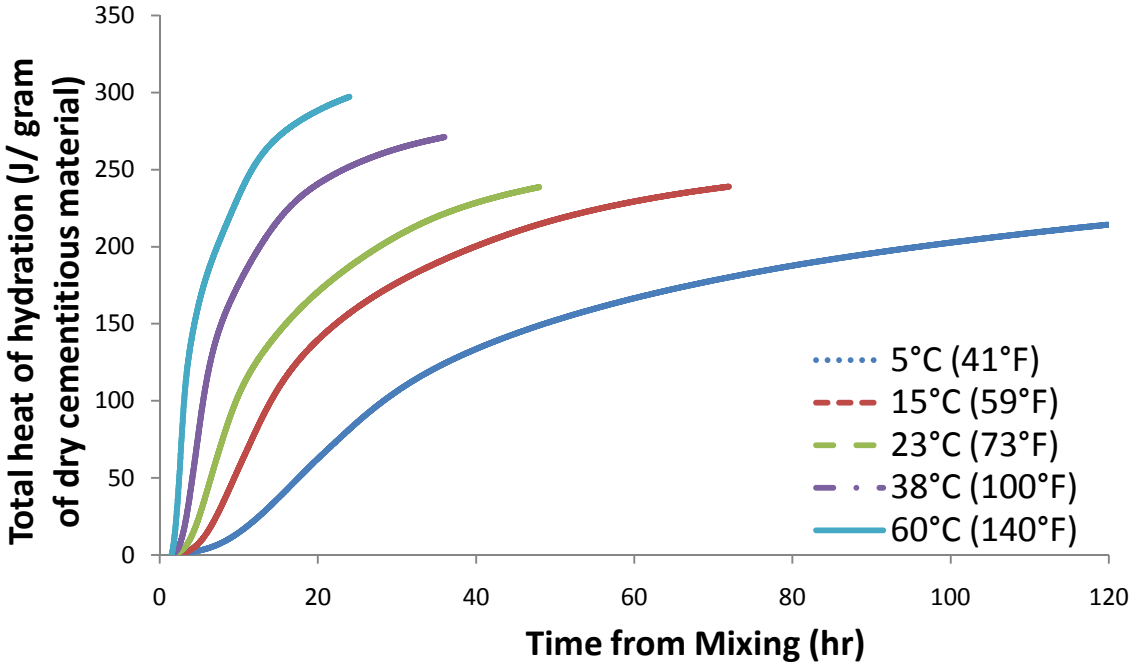

(a)

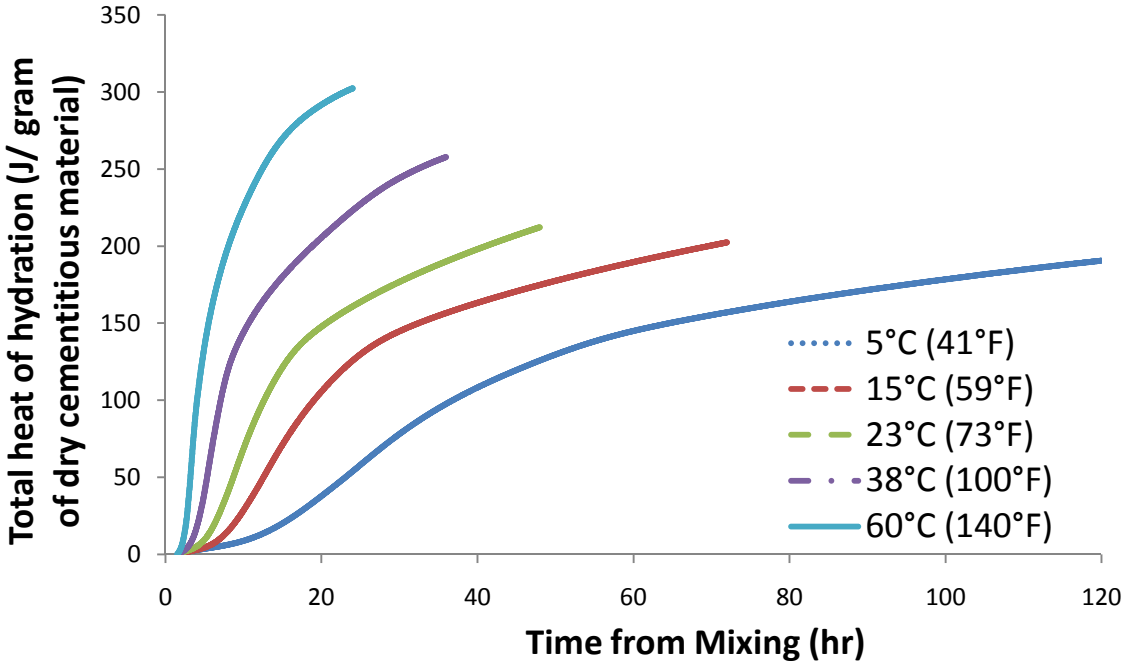
Total heat of hydration (J/ gram of dry cementitious material)
350
300
250
200
150
100
50
0
0
20
40
60
80
100
120
Time from Mixing (hr)
5°C (41°F)
15°C (59°F)
23°C (73°F)
38°C (100°F)
60°C (140°F)

(b)

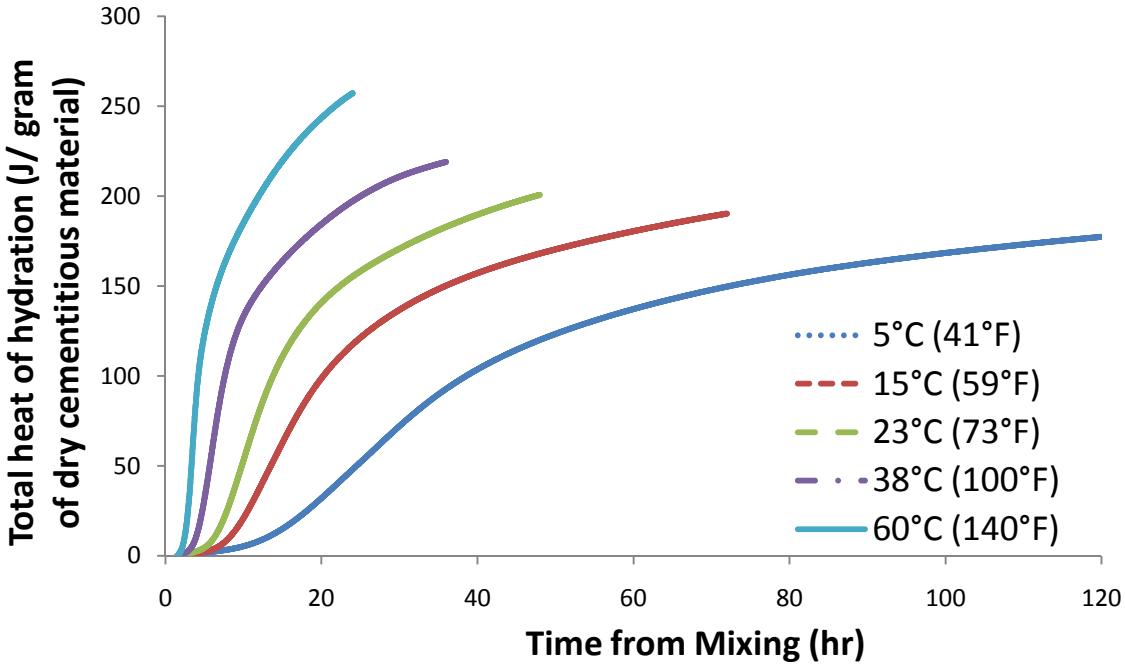
Total heat of hydration (J/ gram of dry cementitious material)
300
250
200
150
100
50
0
0
20
40
60
80
100
120
Time from Mixing (hr)
5°C (41°F)
15°C (59°F)
23°C (73°F)
38°C (100°F)
60°C (140°F)

(c)

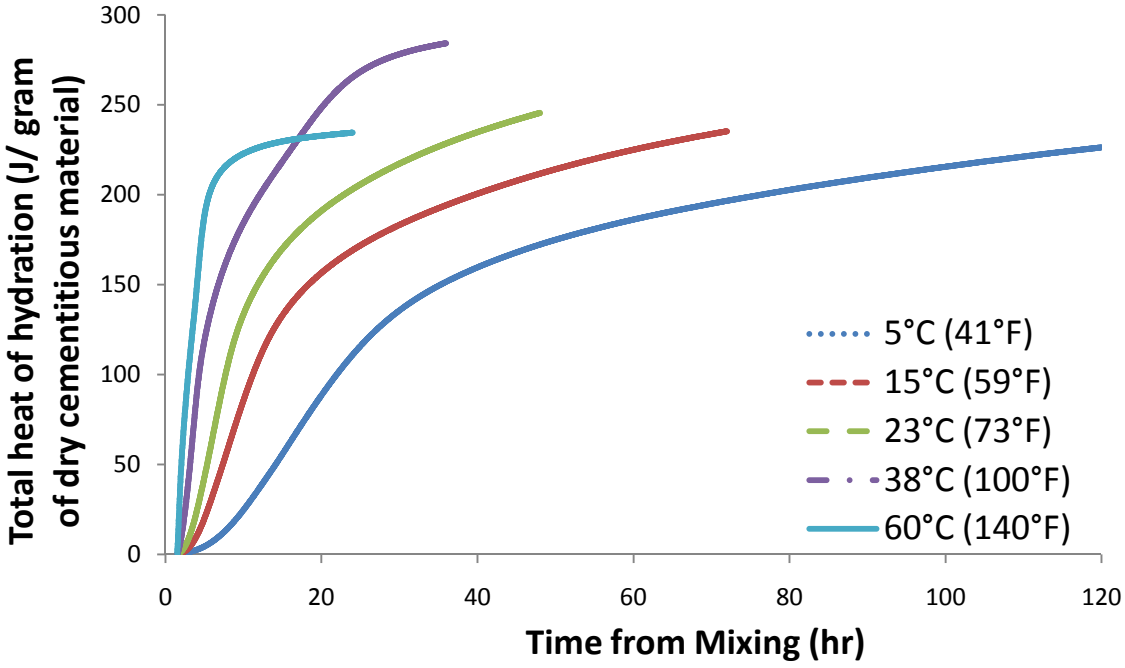
Total heat of hydration (J/ gram of dry cementitious material)
300
250
200
150
100
50
0
0
20
40
60
80
100
120
Time from Mixing (hr)
5°C (41°F)
15°C (59°F)
23°C (73°F)
38°C (100°F)
60°C (140°F)

(d)

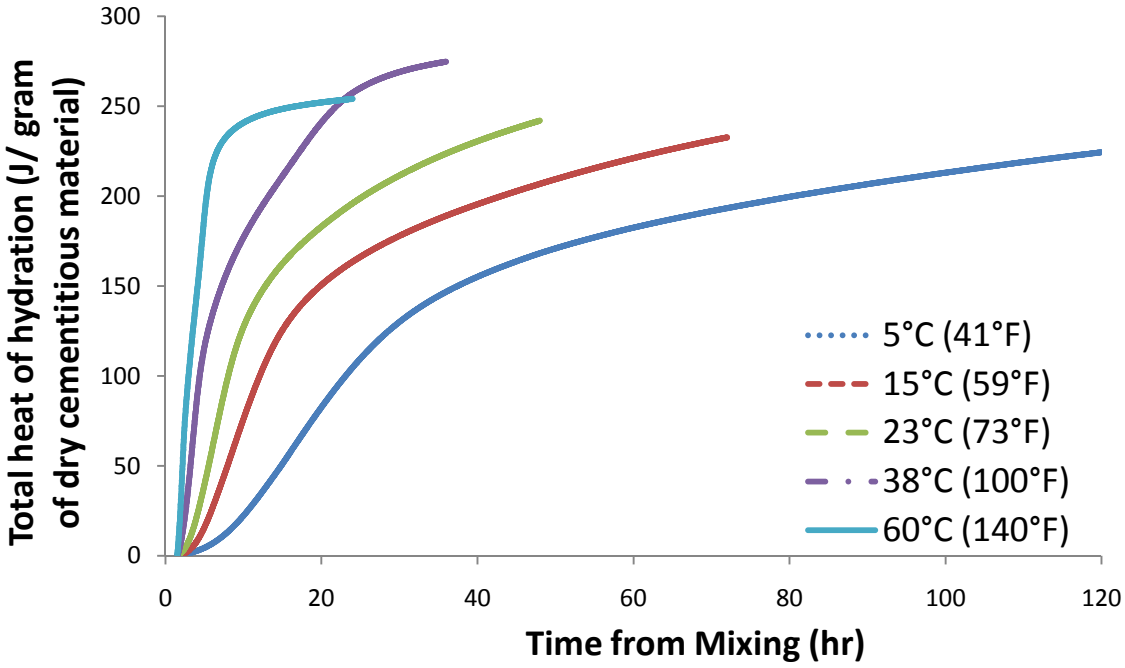
Total heat of hydration (J/ gram of dry cementitious material)
300
250
200
150
100
50
0
0
20
40
60
80
100
120
Time from Mixing (hr)
5°C (41°F)
15°C (59°F)
23°C (73°F)
38°C (100°F)
60°C (140°F)

(e)

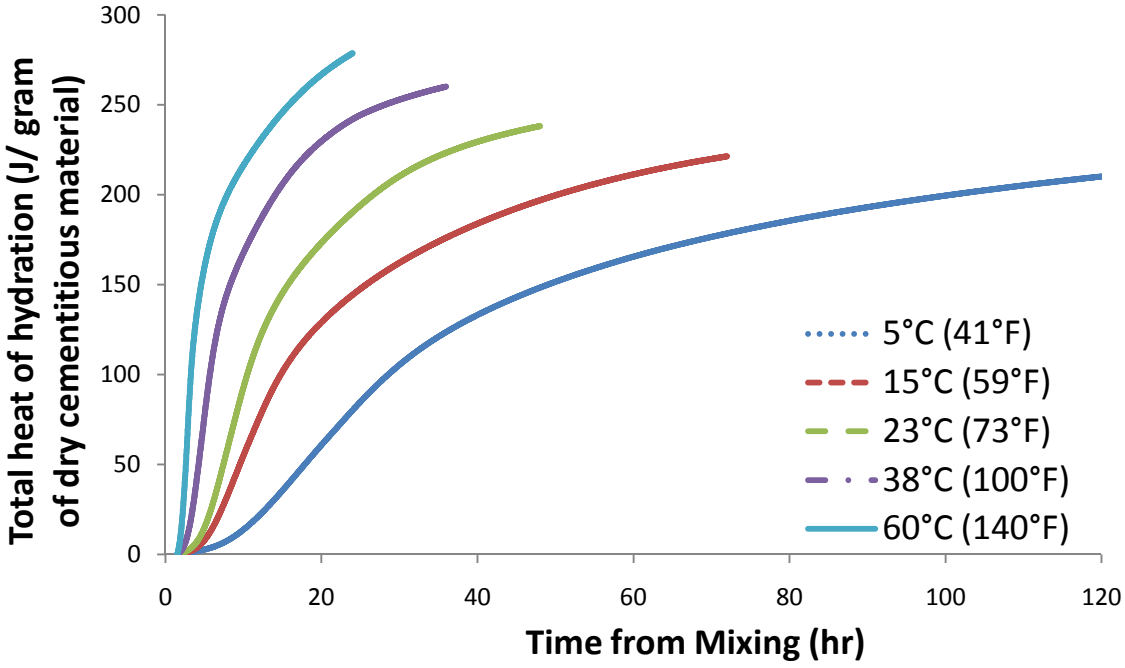
Total heat of hydration (J/ gram of dry cementitious material)
300
250
200
150
100
50
0
0
20
40
60
80
100
120
Time from Mixing (hr)
5°C (41°F)
15°C (59°F)
23°C (73°F)
38°C (100°F)
60°C (140°F)

(f)

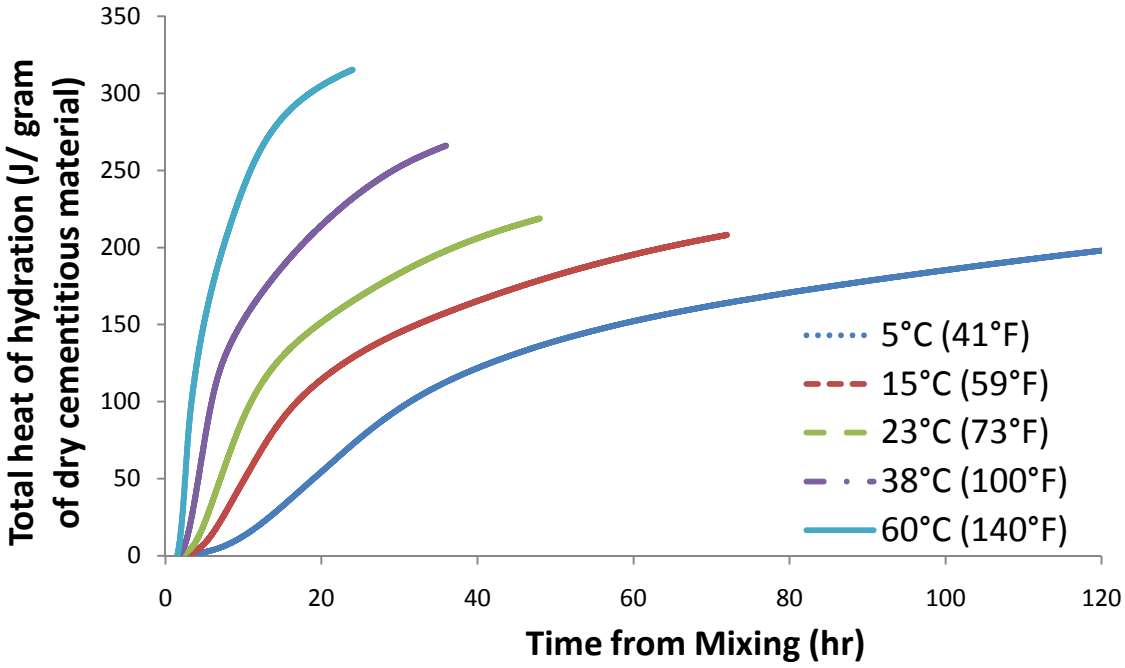
Total heat of hydration (J/ gram of dry cementitious material)
350
300
250
200
150
100
50
0
0
20
40
60
80
100
120
Time from Mixing (hr)
5°C (41°F)
15°C (59°F)
23°C (73°F)
38°C (100°F)
60°C (140°F)

(g)

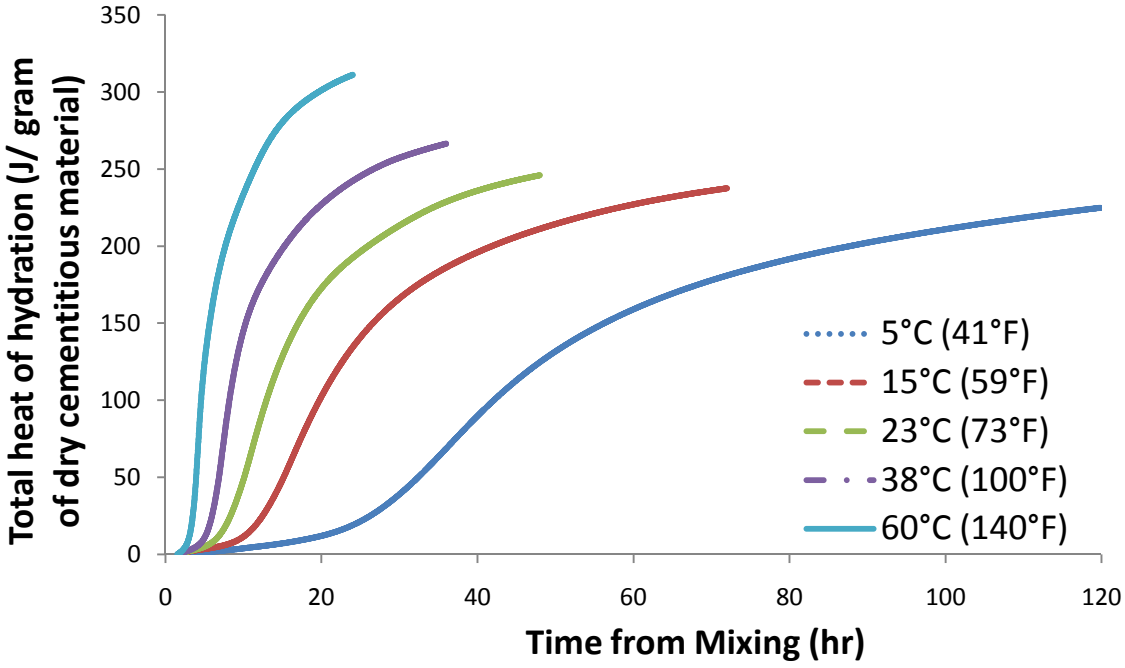
Total heat of hydration (J/ gram of dry cementitious material)
350
300
250
200
150
100
50
0
0
20
40
60
80
100
120
Time from Mixing (hr)
5°C (41°F)
15°C (59°F)
23°C (73°F)
38°C (100°F)
60°C (140°F)

(h)

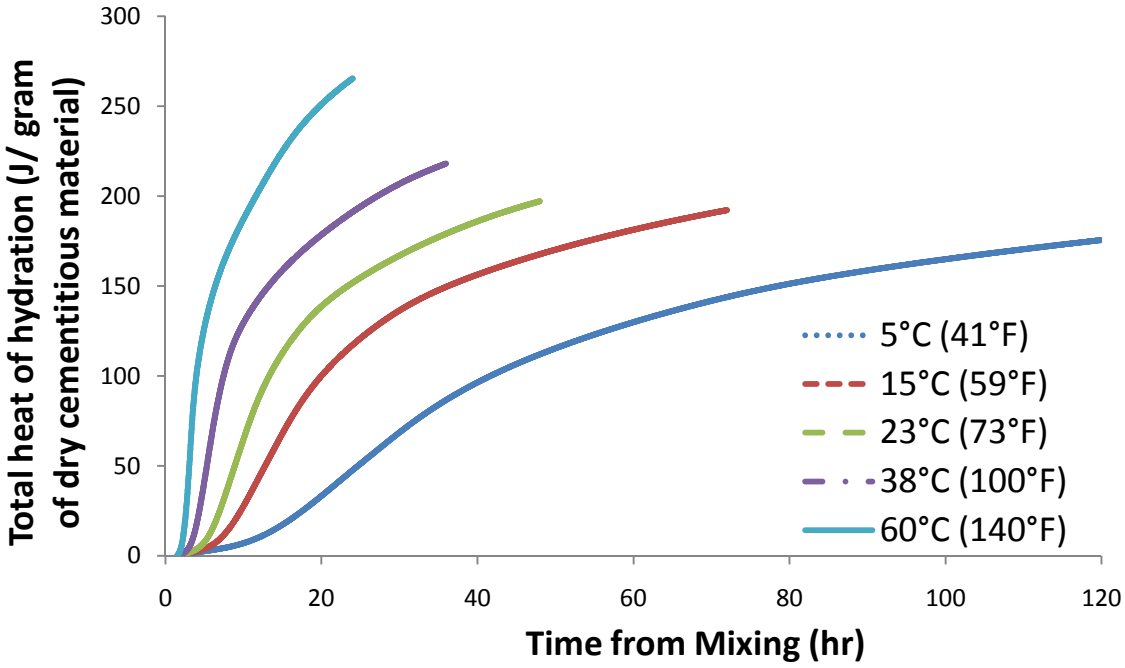
Total heat of hydration (J/ gram of dry cementitious material)
300
250
200
150
100
50
0
0
20
40
60
80
100
120
Time from Mixing (hr)
5°C (41°F)
15°C (59°F)
23°C (73°F)
38°C (100°F)
60°C (140°F)

(i)

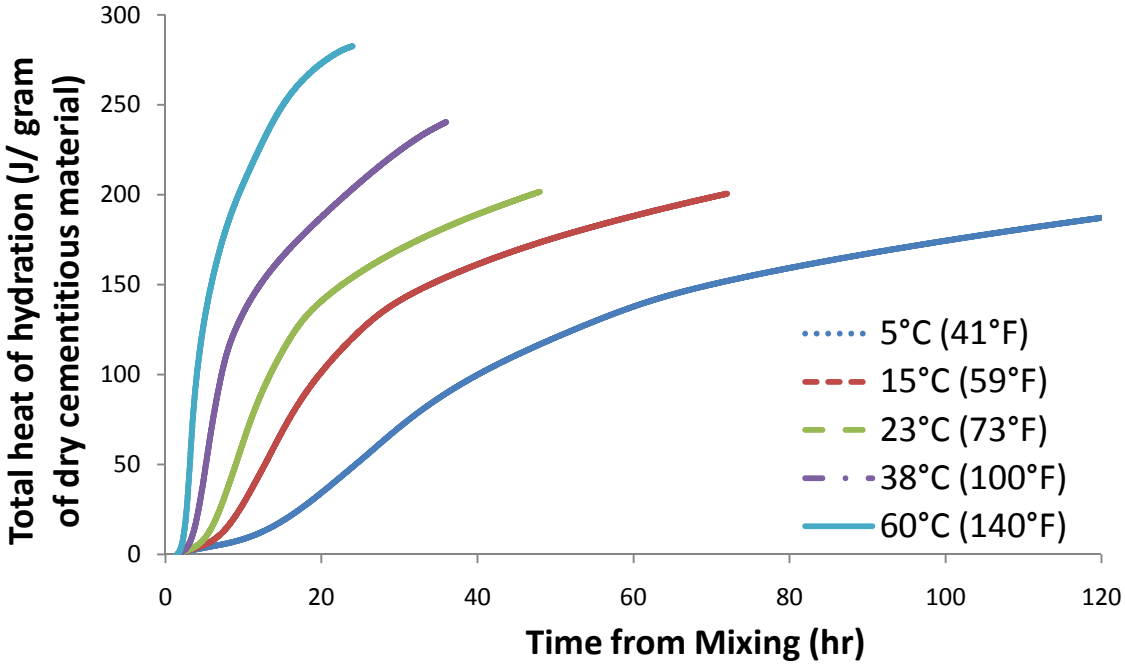

(j)

Figure A.4: Total Heat of Hydration of Cement Paste With w/cm 0.35; (a) Ty I, (b) 25% C, (c) 25% F, (d) 15% M-1, (e) 15% M-2, (f) 6% SF, (g) 25% S, (h) WRA, (i) 5% C 20% F, and (j) 20% C 5% F.

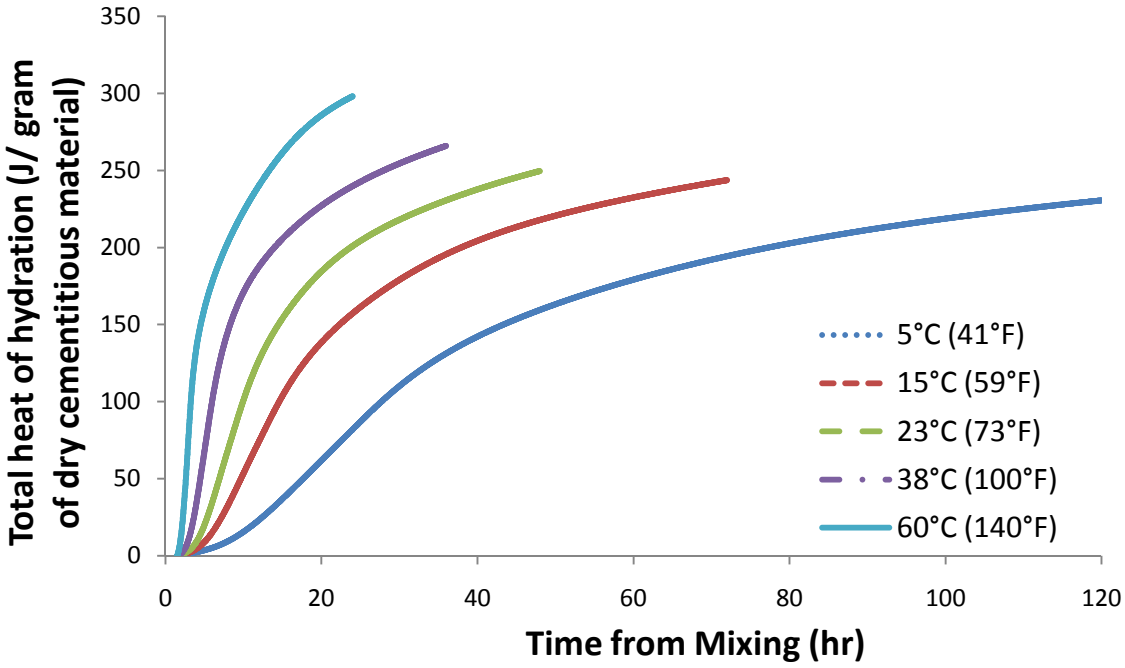

(a)

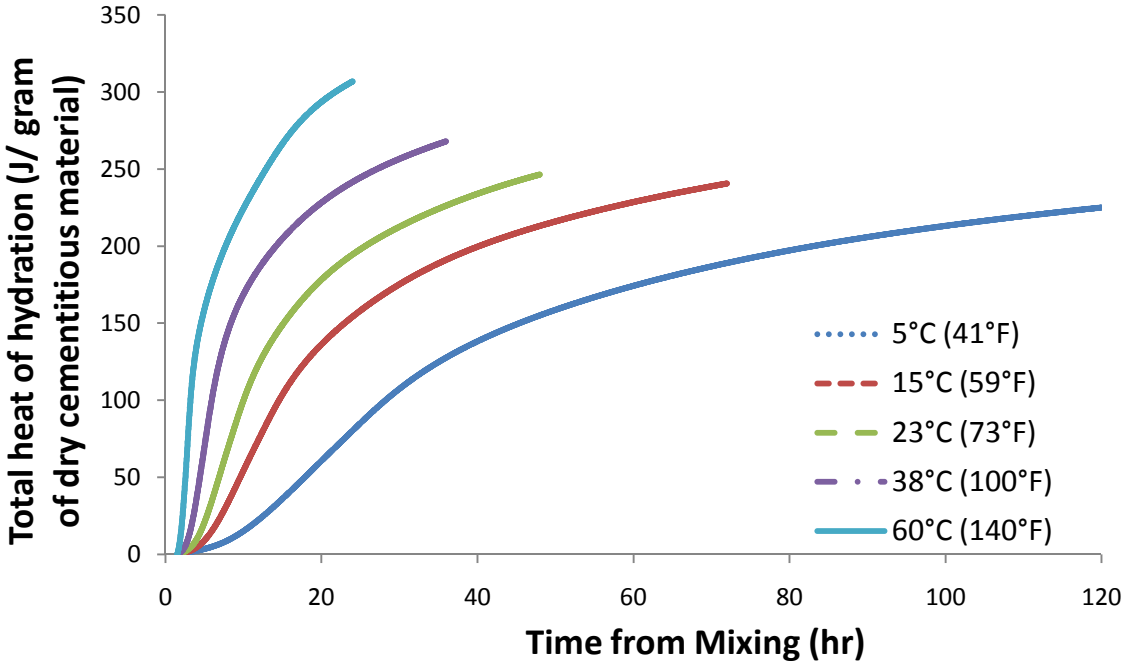
Total heat of hydration (J/ gram of dry cementitious material)
350
300
250
200
150
100
50
0
0
20
40
60
80
100
120
Time from Mixing (hr)
5°C (41°F)
15°C (59°F)
23°C (73°F)
38°C (100°F)
60°C (140°F)

(b)

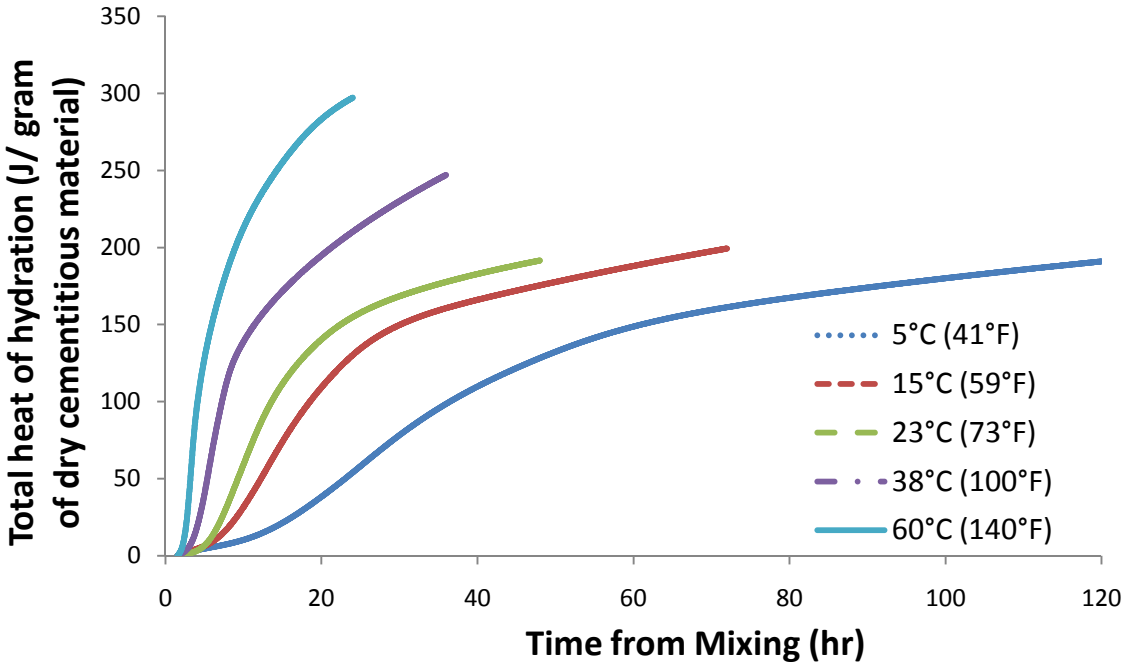
Total heat of hydration (J/ gram of dry cementitious material)
350
300
250
200
150
100
50
0
0
20
40
60
80
100
120
Time from Mixing (hr)
5°C (41°F)
15°C (59°F)
23°C (73°F)
38°C (100°F)
60°C (140°F)

(c)

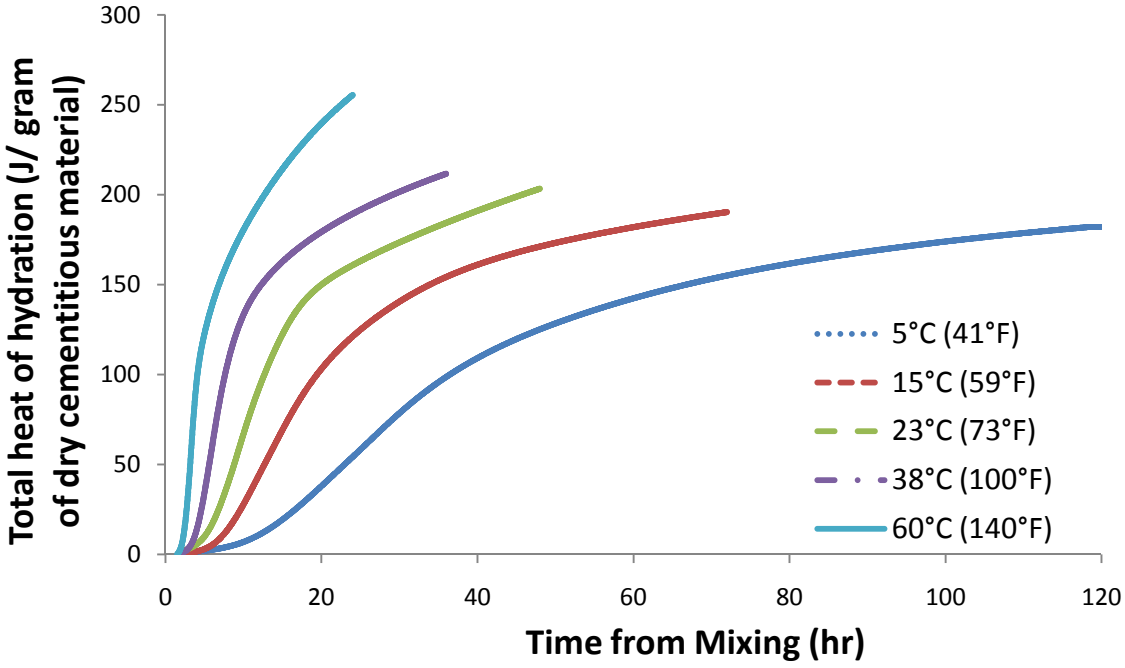
Total heat of hydration (J/ gram of dry cementitious material)
300
250
200
150
100
50
0
0
20
40
60
80
100
120
Time from Mixing (hr)
5°C (41°F)
15°C (59°F)
23°C (73°F)
38°C (100°F)
60°C (140°F)

(d)

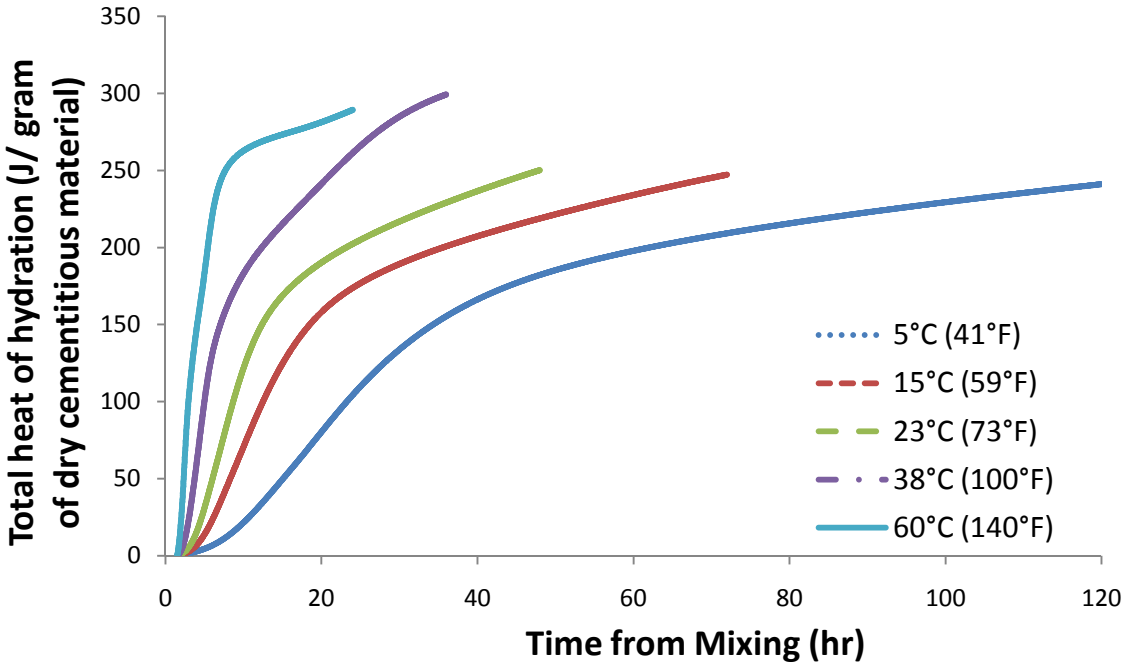
Total heat of hydration (J/ gram of dry cementitious material)
350
300
250
200
150
100
50
0
0
20
40
60
80
100
120
Time from Mixing (hr)
5°C (41°F)
15°C (59°F)
23°C (73°F)
38°C (100°F)
60°C (140°F)

(e)

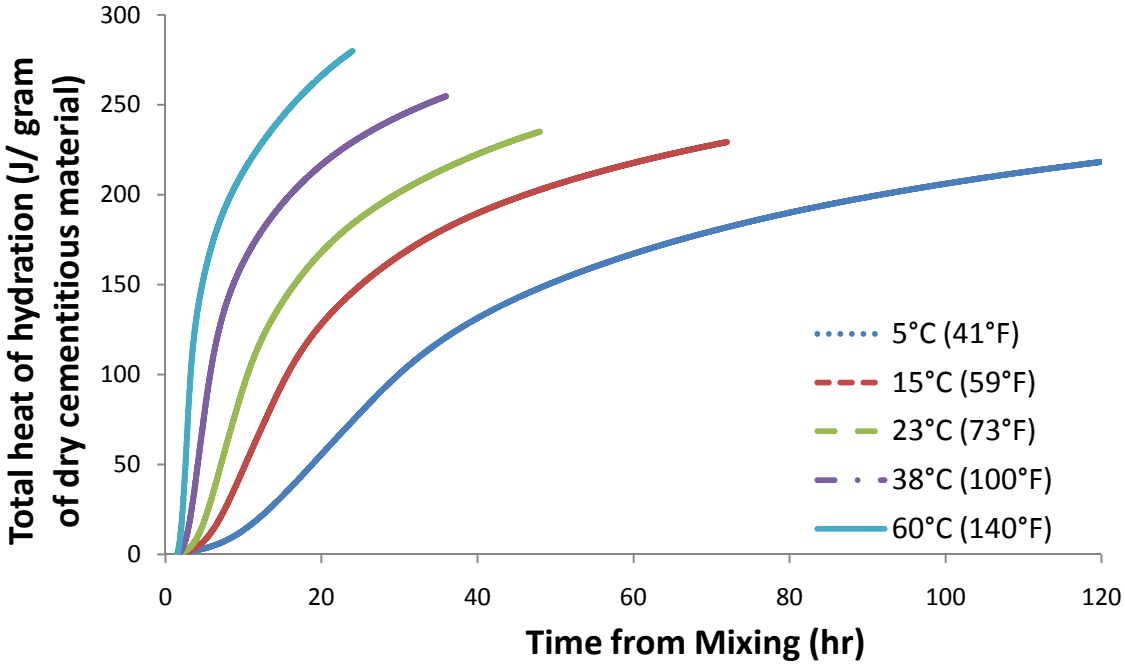
Total heat of hydration (J/ gram of dry cementitious material)
300
250
200
150
100
50
0
0
20
40
60
80
100
120
Time from Mixing (hr)
5°C (41°F)
15°C (59°F)
23°C (73°F)
38°C (100°F)
60°C (140°F)

(f)

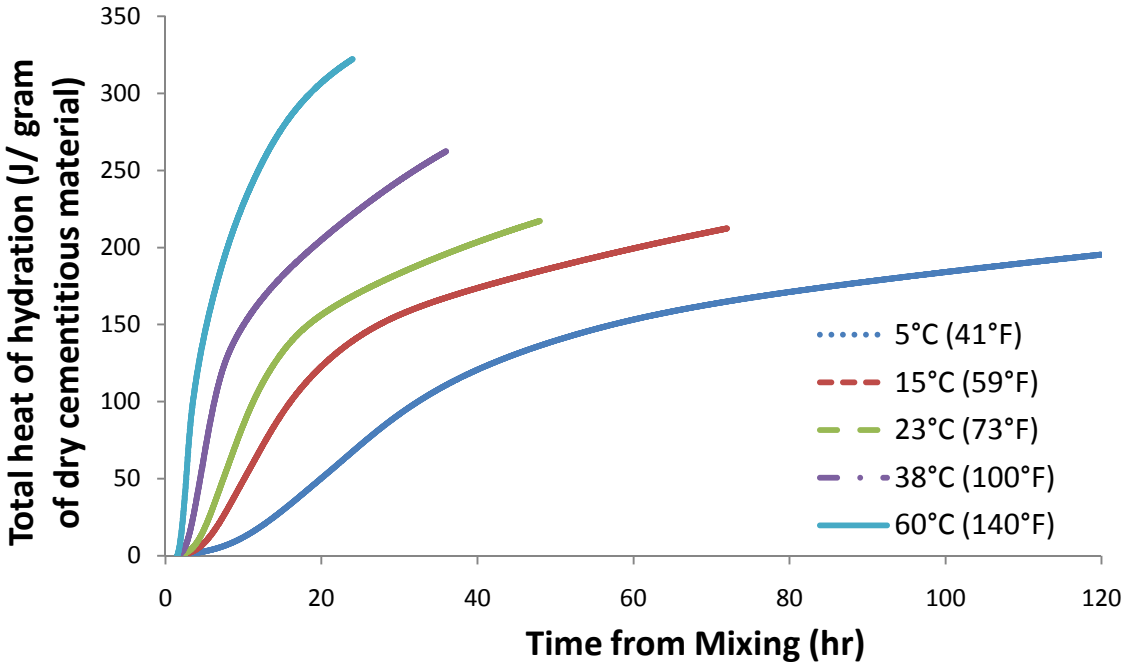
Total heat of hydration (J/ gram of dry cementitious material)
350
300
250
200
150
100
50
0
0
20
40
60
80
100
120
Time from Mixing (hr)
5°C (41°F)
15°C (59°F)
23°C (73°F)
38°C (100°F)
60°C (140°F)

(g)

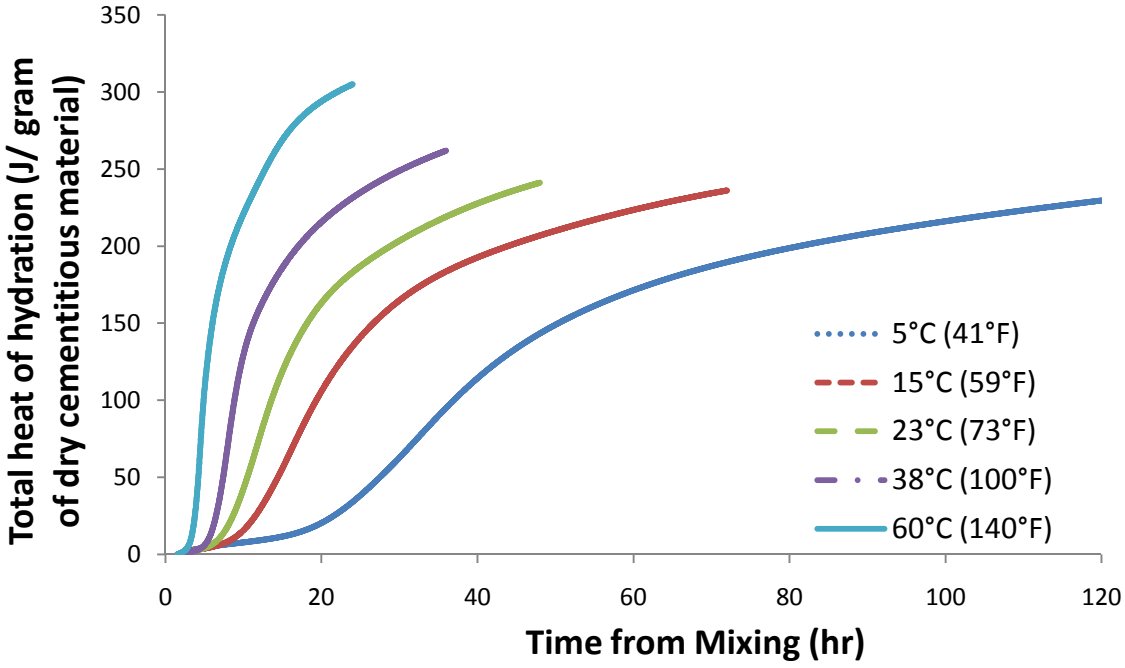
Total heat of hydration (J/ gram of dry cementitious material)
350
300
250
200
150
100
50
0
0
20
40
60
80
100
120
Time from Mixing (hr)
5°C (41°F)
15°C (59°F)
23°C (73°F)
38°C (100°F)
60°C (140°F)

(h)

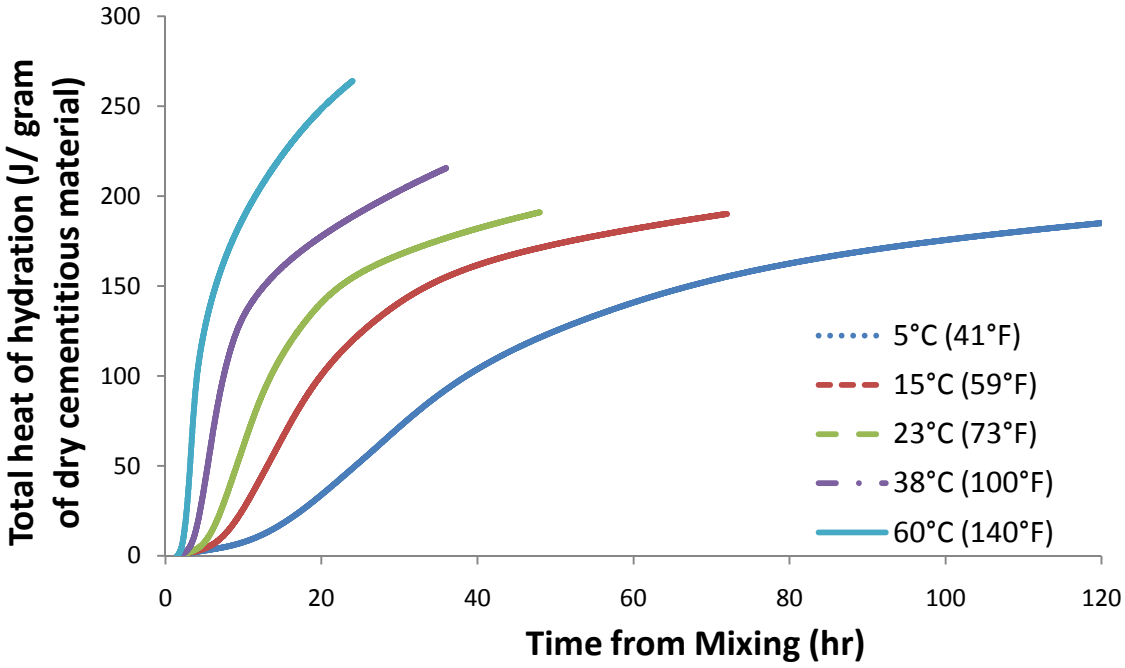
Total heat of hydration (J/ gram of dry cementitious material)
300
250
200
150
100
50
0
0
20
40
60
80
100
120
Time from Mixing (hr)
5°C (41°F)
15°C (59°F)
23°C (73°F)
38°C (100°F)
60°C (140°F)

(i)

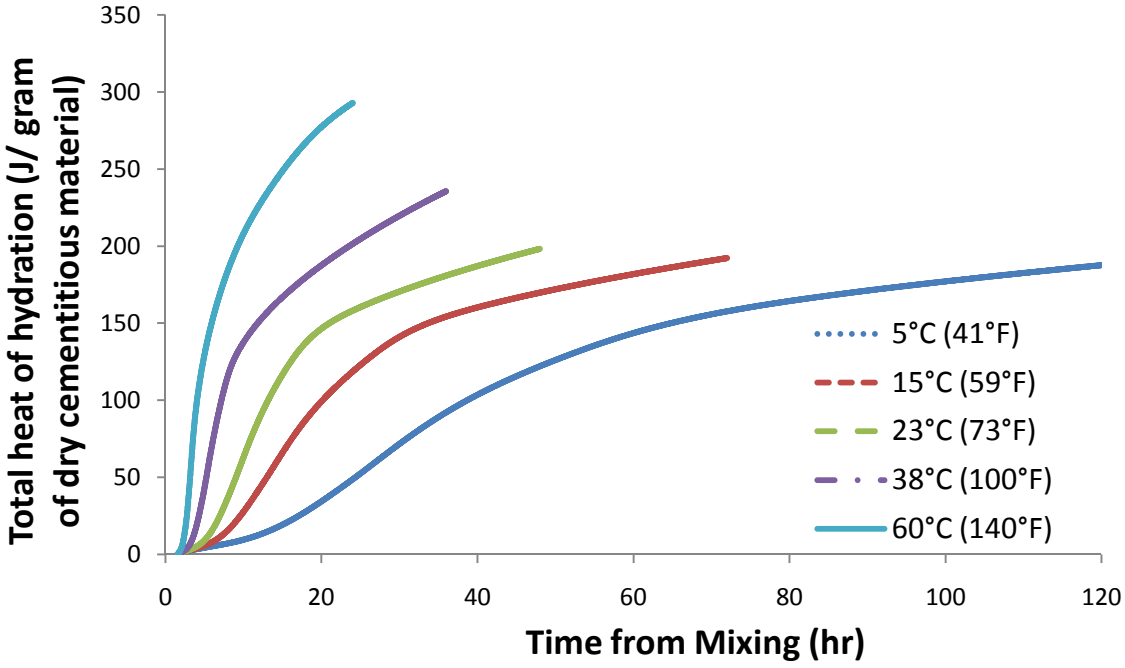

(j)

Figure A.5: Total Heat of Hydration of Cement Paste with Same w/cm as Mortar; (a) TyI-0.5, (b) TyI-0.45, (c) 25% C, (d) 25% F, (e) 10% M-1, (f) 5% SF, (g) 25% S, (h) WRA, (i) 5% C 20% F, and (j) 20% C 5% F.

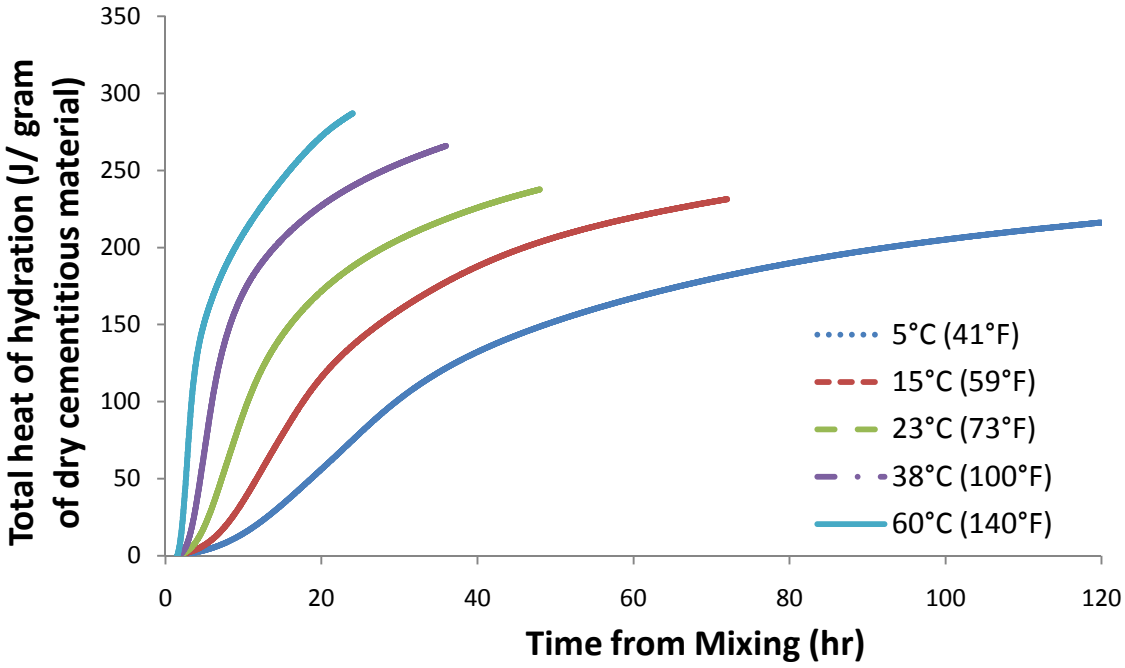

(a)

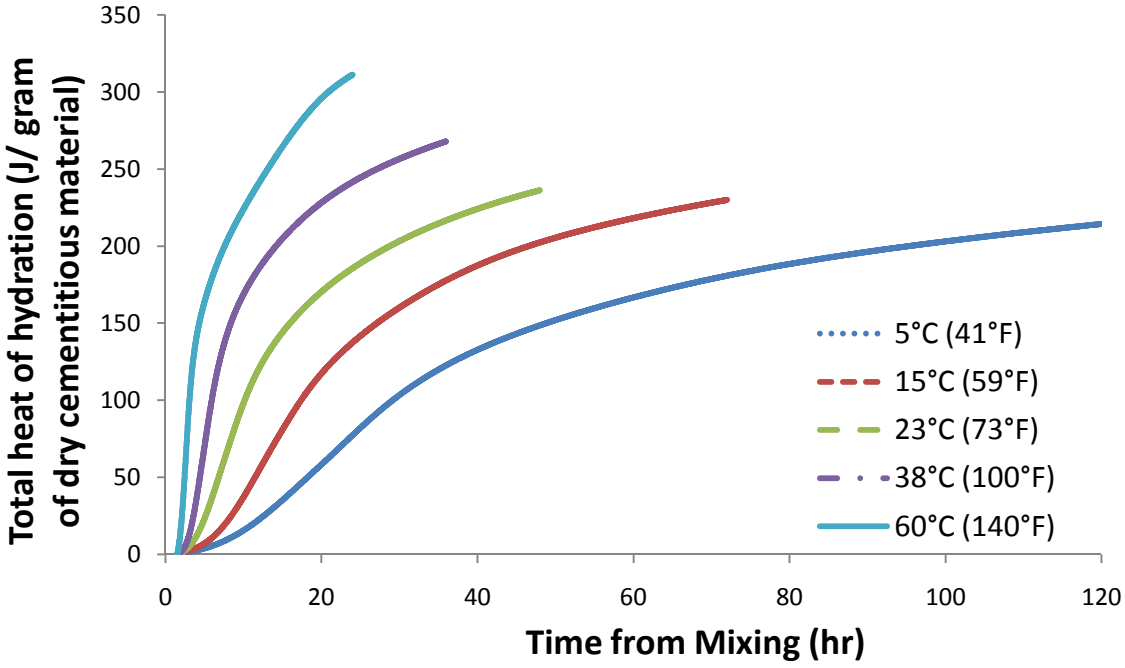
Total heat of hydration (J/ gram of dry cementitious material)
350
300
250
200
150
100
50
0
0
20
40
60
80
100
120
Time from Mixing (hr)
5°C (41°F)
15°C (59°F)
23°C (73°F)
38°C (100°F)
60°C (140°F)

(b)

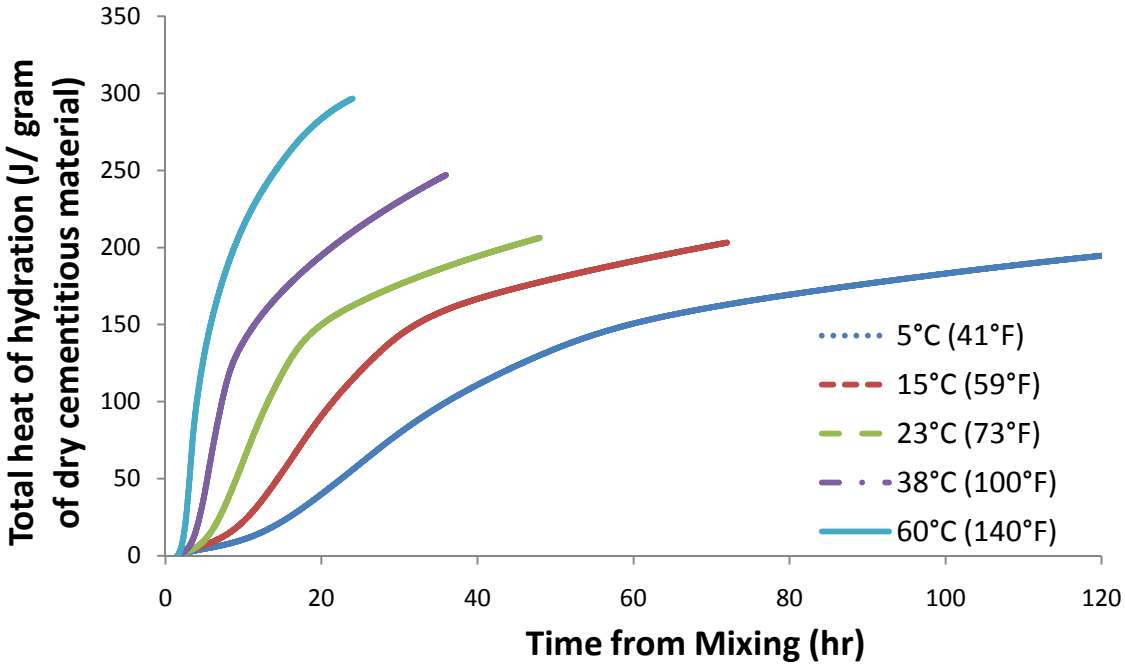
Total heat of hydration (J/ gram of dry cementitious material)
350
300
250
200
150
100
50
0
0
20
40
60
80
100
120
Time from Mixing (hr)
5°C (41°F)
15°C (59°F)
23°C (73°F)
38°C (100°F)
60°C (140°F)

(c)

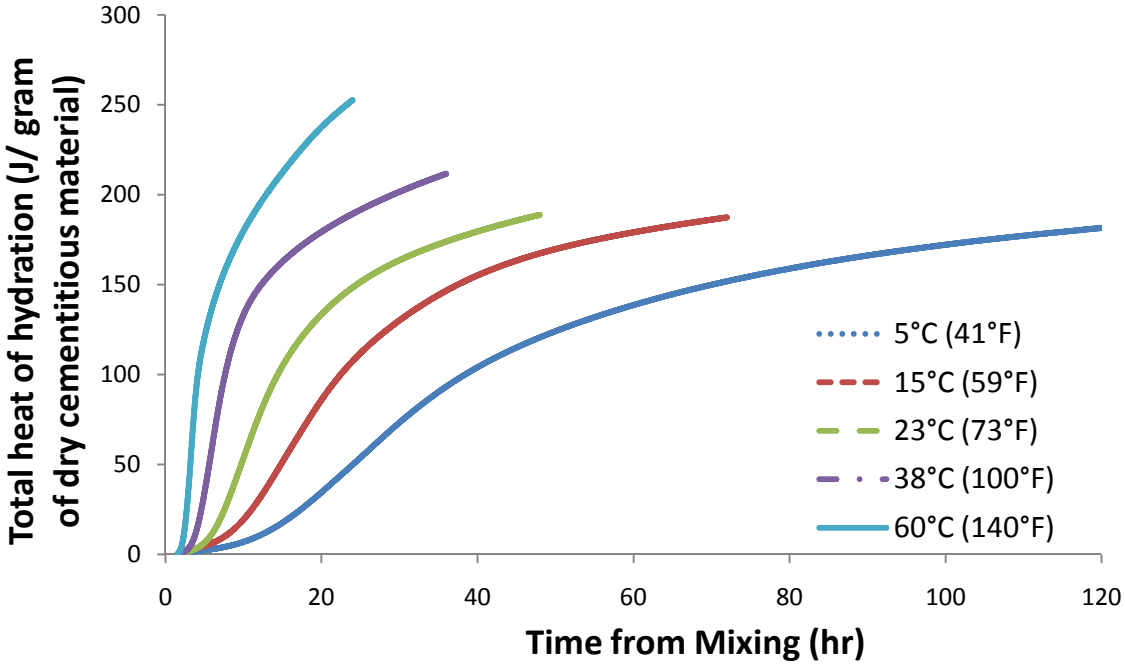
Total heat of hydration (J/ gram of dry cementitious material)
300
250
200
150
100
50
0
0
20
40
60
80
100
120
Time from Mixing (hr)
5°C (41°F)
15°C (59°F)
23°C (73°F)
38°C (100°F)
60°C (140°F)

(d)

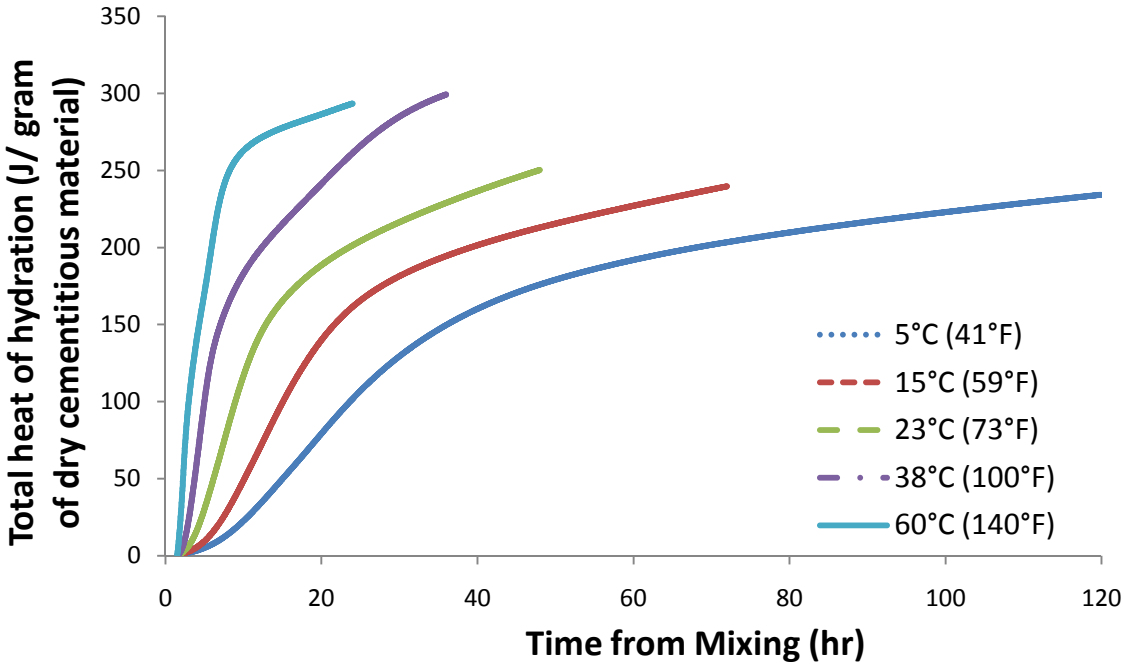
Total heat of hydration (J/ gram of dry cementitious material)
350
300
250
200
150
100
50
0
0
20
40
60
80
100
120
Time from Mixing (hr)
5°C (41°F)
15°C (59°F)
23°C (73°F)
38°C (100°F)
60°C (140°F)

(e)

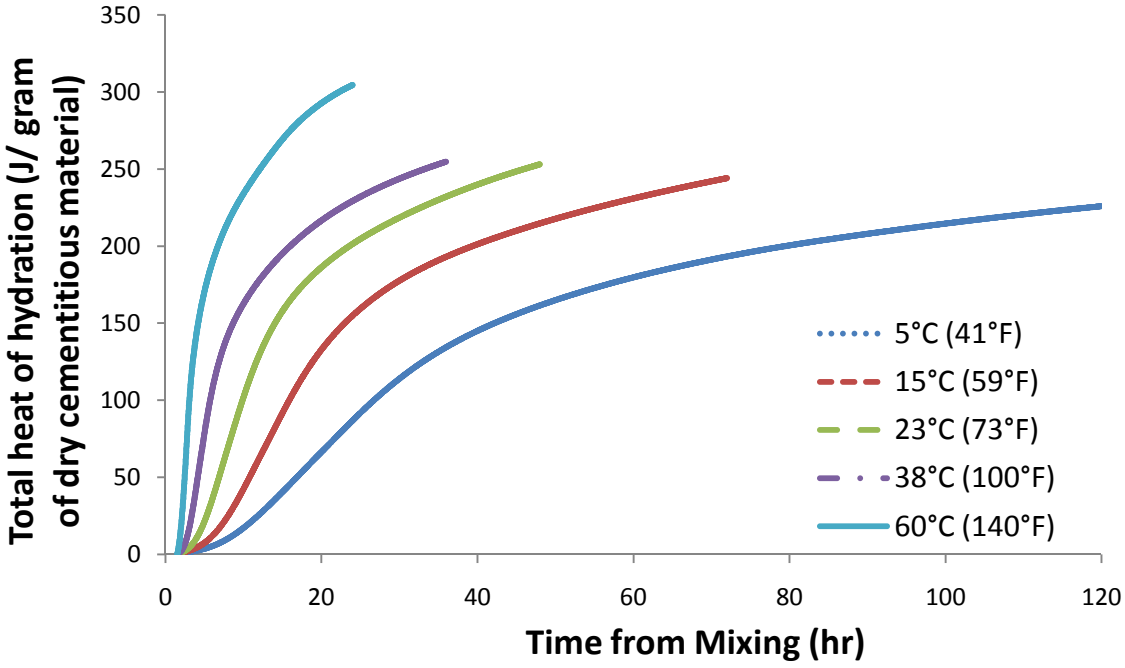
Total heat of hydration (J/ gram of dry cementitious material)
350
300
250
200
150
100
50
0
0
20
40
60
80
100
120
Time from Mixing (hr)
5°C (41°F)
15°C (59°F)
23°C (73°F)
38°C (100°F)
60°C (140°F)

(f)

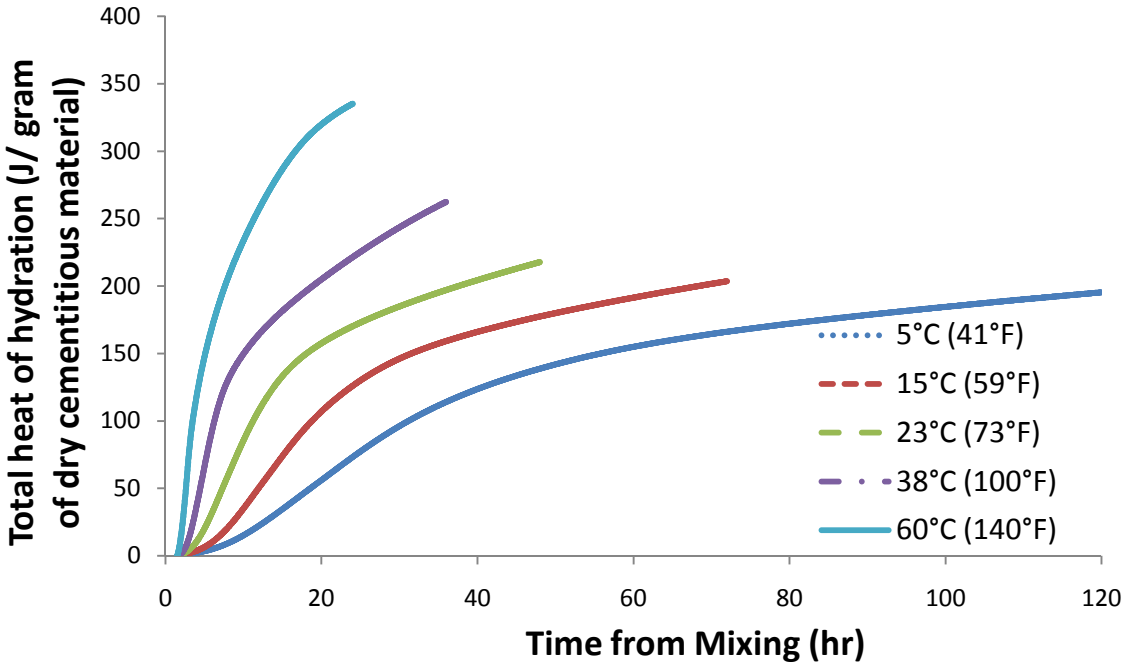
Total heat of hydration (J/ gram of dry cementitious material)
400
350
300
250
200
150
100
50
0
0
20
40
60
80
100
120
Time from Mixing (hr)
5°C (41°F)
15°C (59°F)
23°C (73°F)
38°C (100°F)
60°C (140°F)

(g)

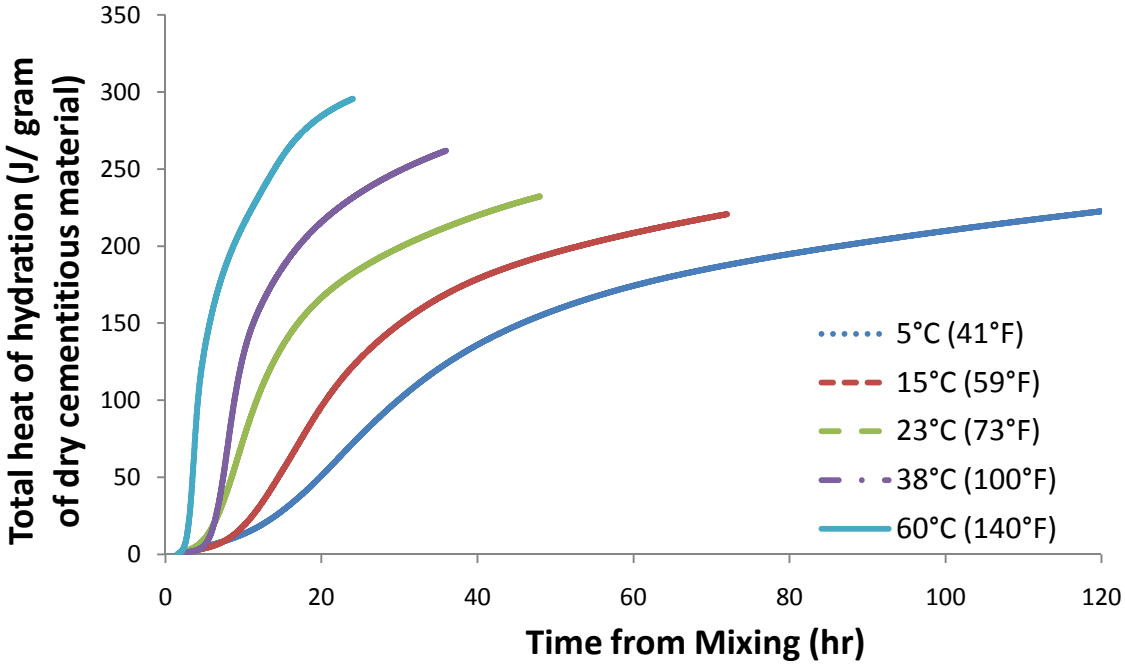
Total heat of hydration (J/ gram of dry cementitious material)
350
300
250
200
150
100
50
0
0
20
40
60
80
100
120
Time from Mixing (hr)
5°C (41°F)
15°C (59°F)
23°C (73°F)
38°C (100°F)
60°C (140°F)

(h)

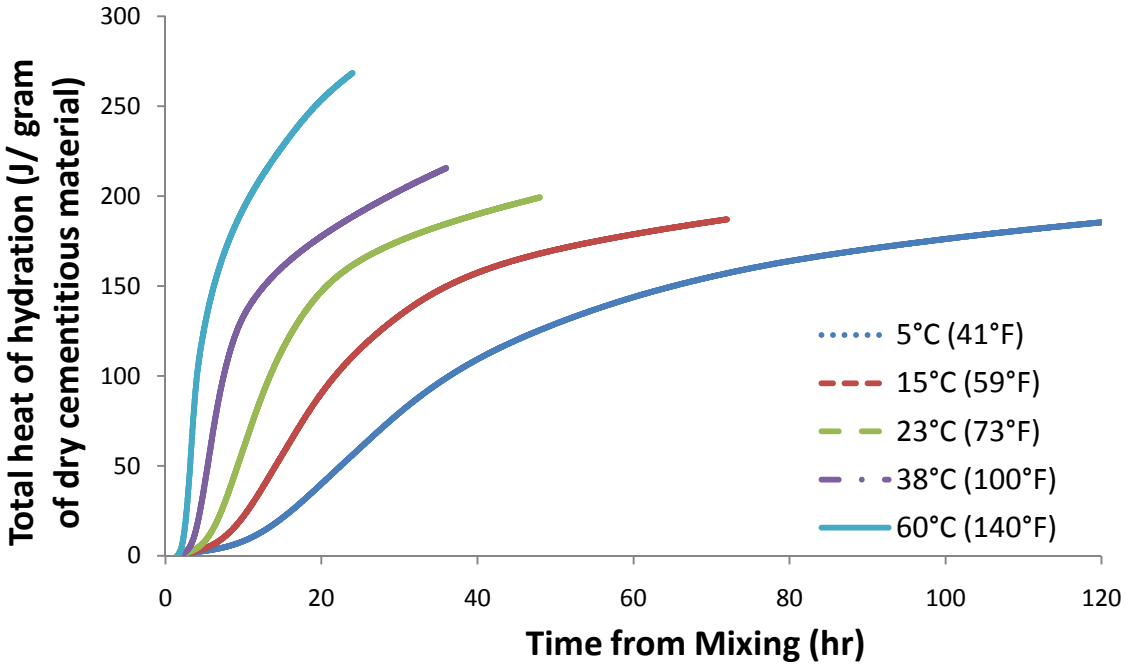
Total heat of hydration (J/ gram of dry cementitious material)
300
250
200
150
100
50
0
0
20
40
60
80
100
120
Time from Mixing (hr)
5°C (41°F)
15°C (59°F)
23°C (73°F)
38°C (100°F)
60°C (140°F)

(i)

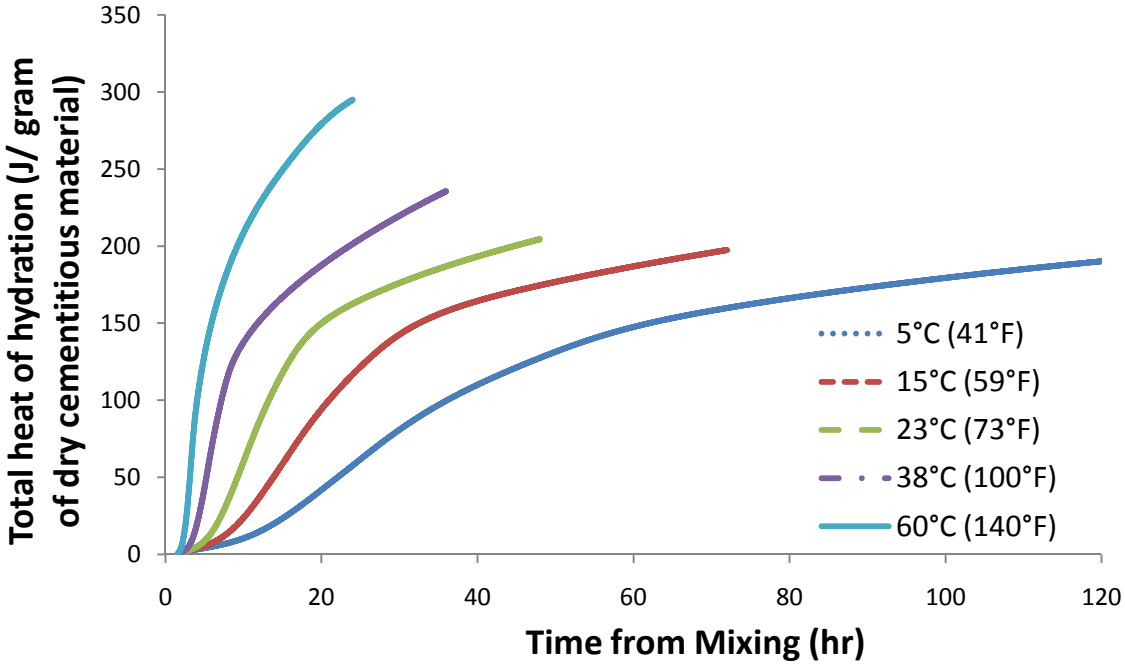

(j)

Figure A.6: Total Heat of Hydration of Mortar; (a) TyI-0.5, (b) TyI-0.45, (c) 25% C, (d) 25% F, (e) 10% M-1, (f) 5% SF, (g) 25% S, (h) WRA, (i) 5% C 20% F, and (j) 20% C 5% F.

Appendix B - E_a CALCULATED FROM CUMULATIVE HEAT OF HYDRATION

Table B.1: Summary of E_a Calculated from Cumulative Heat of Hydration for Cement Pastes with a 0.35 w/cm.

Mixes	T,°C (°F)	Single Linear Approximation			Exponential Method			ASTM C 1074 Hyperbolic function; Equal S_u			ASTM C 1074 Hyperbolic function		
		Reaction rate k	E_a, J/mole	R^{2*}	τ, hours	E_a, J/mole	$R^{2\dagger}$	Reaction rate k	E_a, J/mole	R^{2**}	Reaction rate k	E_a, J/mole	R^{2**}
Ty I	5(41)	2.58E-05	29419	0.9810	42.94	35140	0.9849	1.61E-02	39137	0.9874	1.98E-02	34766	0.9833
	15(59)	1.23E-04			19.87			3.74E-02			4.11E-02		
	23(73)	2.90E-04			13.75			5.49E-02			5.91E-02		
	38(100)	8.60E-04			6.62			1.27E-01			1.30E-01		
	60(140)	3.90E-03			3.35			2.75E-01			2.40E-01		
25% C	5(41)	1.44E-05	30045	0.9747	69.33	36564	0.9967	1.07E-02	40728	0.9990	1.46E-02	32330	0.9778
	15(59)	6.79E-05			36.54			2.06E-02			3.21E-02		
	23(73)	1.68E-04			23.18			3.40E-02			4.67E-02		
	38(100)	6.49E-04			11.61			7.35E-02			8.00E-02		
	60(140)	2.18E-03			4.99			1.98E-01			1.62E-01		
25% F	5(41)	1.67E-05	28620	0.9851	41.80	33217	0.9900	1.35E-02	36456	0.9913	1.35E-02	34808	0.9748
	15(59)	7.45E-05			21.75			2.70E-02			3.10E-02		
	23(73)	1.52E-04			14.00			4.50E-02			4.21E-02		
	38(100)	5.20E-04			7.71			8.34E-02			9.44E-02		
	60(140)	2.11E-03			3.76			1.91E-01			1.69E-01		
15% M-1	5(41)	3.34E-05	32102	0.9933	26.78	35479	0.9863	3.04E-02	40399	0.9648	3.03E-02	40222	0.9657
	15(59)	1.53E-04			14.03			6.28E-02			6.29E-02		
	23(73)	3.19E-04			8.68			9.35E-02			9.36E-02		
	38(100)	1.36E-03			4.09			1.35E-01			1.35E-01		
	60(140)	7.29E-03			2.15			6.58E-01			6.48E-01		
15% M-2	5(41)	3.08E-05	31106	0.9875	28.54	35352	0.9893	2.63E-02	39923	0.9929	2.80E-02	39177	0.9804
	15(59)	1.30E-04			15.32			5.01E-02			5.69E-02		
	23(73)	3.01E-04			9.51			8.55E-02			8.55E-02		
	38(100)	1.35E-03			4.53			2.00E-01			1.34E-01		
	60(140)	5.32E-03			2.32			4.41E-01			5.33E-01		
6% SF	5(41)	2.58E-05	28677	0.9853	37.08	33703	0.9803	1.79E-02	37414	0.9800	2.04E-02	35683	0.9928
	15(59)	1.22E-04			19.47			3.51E-02			4.16E-02		
	23(73)	2.29E-04			11.70			6.50E-02			5.58E-02		
	38(100)	7.71E-04			6.06			1.32E-01			1.26E-01		

	60(140)	3.42E-03			3.34			2.57E-01			2.67E-01		
25% S	5(41)	2.21E-05	29768	0.9862	88.39	38367	0.9990	1.14E-02	42529	0.9997	1.91E-02	30836	0.9876
	15(59)	1.01E-04			48.45			2.09E-02			3.57E-02		
	23(73)	2.27E-04			29.76			3.57E-02			5.42E-02		
	38(100)	7.37E-04			14.37			7.91E-02			9.35E-02		
	60(140)	3.44E-03			5.69			2.37E-01			1.80E-01		
0.5% WRA	5(41)	1.20E-05	29215	0.9507	46.54	32412	0.9792	1.08E-02	35290	0.9878	6.59E-03	40718	0.9404
	15(59)	7.81E-05			22.35			2.21E-02			2.30E-02		
	23(73)	1.83E-04			14.23			3.62E-02			3.62E-02		
	38(100)	5.69E-04			8.71			6.21E-02			6.97E-02		
	60(140)	1.82E-03			4.23			1.44E-01			1.45E-01		
5% C 20% F	5(41)	1.39E-05	27532	0.9639	49.93	34505	0.9897	1.41E-02	39057	0.9934	1.32E-02	34483	0.9619
	15(59)	6.72E-05			24.23			3.05E-02			3.14E-02		
	23(73)	1.55E-04			15.80			4.89E-02			4.73E-02		
	38(100)	4.95E-04			9.00			9.57E-02			9.57E-02		
	60(140)	1.47E-03			3.94			2.45E-01			1.64E-01		
20% C 5% F	5(41)	1.09E-05	27890	0.9511	59.18	35244	0.9953	1.14E-02	38892	0.9977	1.24E-02	34539	0.9679
	15(59)	5.28E-05			29.83			2.32E-02			2.99E-02		
	23(73)	1.27E-04			20.05			3.57E-02			4.53E-02		
	38(100)	4.94E-04			10.61			7.04E-02			8.34E-02		
	60(140)	1.13E-03			4.53			1.95E-01			1.61E-01		

[*] R^2 of least squares best-fit line of ln(k) versus $1/T$.

[†] R^2 of least squares best-fit line of three parameter exponential model versus measured heat of hydration.

[**] R^2 of least squares best-fit line of ASTM C 1074 hyperbolic function versus measured heat of hydration.

Table B.2: Summary of E_a Calculated from cumulative Heat of Hydration for Cement Pastes – Using the Same Mixture Proportions as Mortar Mixtures.

Mixes	T,°C (°F)	Single Linear Approximation			Exponential Method			ASTM C 1074 Hyperbolic function; Equal S_u			ASTM C 1074 Hyperbolic function		
		Reaction rate k	E_a, J/mole	R^{2*}	τ, hours	E_a, J/mole	$R^{2\dagger}$	Reaction rate k	E_a, J/mole	R^{2**}	Reaction rate k	E_a, J/mole	R^{2**}
Tyl-0.5	5(41)	2.05E-05	30311	0.9830	33.66	32250	0.9864	1.86E-02	34878	0.9886	1.84E-02	34003	0.9749
	15(59)	9.83E-05			17.32			3.75E-02			3.91E-02		
	23(73)	2.44E-04			11.08			6.09E-02			6.09E-02		
	38(100)	6.90E-04			6.49			1.07E-01			1.21E-01		
	60(140)	3.65E-03			3.19			2.39E-01			2.16E-01		
Tyl-0.45	5(41)	2.07E-05	30450	0.9808	37.83	33532	0.9897	1.68E-02	36287	0.9921	1.83E-02	32510	0.9685
	15(59)	1.02E-04			19.26			3.40E-02			3.90E-02		
	23(73)	2.48E-04			12.41			5.46E-02			5.84E-02		
	38(100)	8.23E-04			6.94			1.02E-01			1.16E-01		
	60(140)	3.60E-03			3.28			2.36E-01			1.93E-01		
25% C	5(41)	1.35E-05	31613	0.9871	53.68	35612	0.9984	1.18E-02	38927	0.9992	1.49E-02	30203	0.949001
	15(59)	6.26E-05			28.46			2.21E-02			3.67E-02		
	23(73)	1.53E-04			20.55			3.16E-02			5.02E-02		
	38(100)	5.92E-04			9.81			7.03E-02			8.33E-02		
	60(140)	2.70E-03			4.12			1.93E-01			1.46E-01		
25% F	5(41)	1.72E-05	29574	0.9915	35.87	32203	0.9863	1.44E-02	36674	0.9821	1.60E-02	32137	0.9563
	15(59)	7.20E-05			19.10			3.17E-02			3.48E-02		
	23(73)	1.53E-04			11.64			5.43E-02			5.34E-02		
	38(100)	5.15E-04			7.19			9.01E-02			1.05E-01		
	60(140)	2.54E-03			3.40			2.19E-01			1.64E-01		
10% M-1	5(41)	2.40E-05	31776	0.9855	28.22	34458	0.9967	2.50E-02	38691	0.9992	2.60E-02	36553	0.9750
	15(59)	1.39E-04			15.83			4.50E-02			5.27E-02		
	23(73)	2.56E-04			10.41			7.06E-02			7.97E-02		
	38(100)	9.91E-04			5.15			1.58E-01			1.13E-01		
	60(140)	5.52E-03			2.42			3.90E-01			4.18E-01		

	5(41)	1.87E-05			34.53			1.87E-02			1.72E-02		
	15(59)	8.77E-05			17.95			3.73E-02			3.73E-02		
5% SF	23(73)	2.23E-04	31788	0.9821	11.60	33188	0.9886	5.96E-02	35602	0.9911	5.63E-02	36894	0.9835
	38(100)	9.53E-04			6.20			1.14E-01			1.26E-01		
	60(140)	3.71E-03			3.14			2.47E-01			2.44E-01		
	5(41)	1.41E-05			76.71			1.10E-02			1.86E-02		
	15(59)	9.35E-05			38.98			2.16E-02			4.14E-02		
25% S	23(73)	1.97E-04	31178	0.9717	25.43	37495	0.9977	3.42E-02	40604	0.9986	5.80E-02	27379	0.9430
	38(100)	6.53E-04			13.14			6.89E-02			9.26E-02		
	60(140)	3.07E-03			5.01			2.10E-01			1.45E-01		
	5(41)	1.87E-05			40.18			1.18E-02			9.73E-03		
	15(59)	7.22E-05			21.59			2.17E-02			2.48E-02		
0.5% WRA	23(73)	1.70E-04	28301	0.9863	14.53	30295	0.9897	3.38E-02	33079	0.9945	3.42E-02	34276	0.9701
	38(100)	5.56E-04			9.03			5.75E-02			5.84E-02		
	60(140)	2.14E-03			4.33			1.32E-01			1.31E-01		
	5(41)	1.16E-05			38.81			1.47E-02			1.35E-02		
	15(59)	6.34E-05			20.45			2.82E-02			3.36E-02		
5% C 20% F	23(73)	1.55E-04	32211	0.9810	13.70	33509	0.9952	4.29E-02	36298	0.9972	5.15E-02	34223	0.9466
	38(100)	5.84E-04			7.65			7.83E-02			1.04E-01		
	60(140)	2.70E-03			3.37			2.09E-01			1.65E-01		
	5(41)	1.16E-05			52.14			1.19E-02			1.32E-02		
	15(59)	5.22E-05			28.48			2.17E-02			3.26E-02		
20% C 5% F	23(73)	1.41E-04	33148	0.9866	18.01	35829	0.9979	3.52E-02	38932	0.9988	5.17E-02	32757	0.9405
	38(100)	6.46E-04			9.64			6.81E-02			9.26E-02		
	60(140)	2.80E-03			3.91			1.98E-01			1.49E-01		

*R^2 of least squares best-fit line of ln(k) versus $1/T$.

†R^2 of least squares best-fit line of three parameter exponential model versus measured heat of hydration.

**R^2 of least squares best-fit line of ASTM C 1074 hyperbolic function versus measured heat of hydration.

Table B.3: Summary of E_a Calculated from Cumulative Heat of Hydration for Mortar.

Mixes	T,°C (°F)	Single Linear Approximation			Exponential Method			ASTM C 1074 Hyperbolic function equal S_u			ASTM C 1074 Hyperbolic function		
		Reaction rate k	E_a, J/mole	R^{2*}	τ, hours	E_a, J/mole	$R^{2\dagger}$	Reaction rate k	E_a, J/mole	R^{2**}	Reaction rate k	E_a, J/mole	R^{2**}
Tyl-0.5	5(41)	1.44E-05	33040	0.9834	38.200	33394	0.9789	0.016656	35685.45	0.97821	0.018232	34921.52	0.968561
	15(59)	6.00E-05			20.788			0.032586			0.029095		
	23(73)	1.98E-04			12.437			0.055143			0.057643		
	38(100)	7.71E-04			6.248			0.117051			0.121039		
	60(140)	3.40E-03			3.587			0.209596			0.201204		
Tyl-0.45	5(41)	1.91E-05	32871	0.9929	43.879	36013	0.9926	0.015166	39009.67	0.995182	0.019108	33333.79	0.960582
	15(59)	6.42E-05			23.715			0.029907			0.030469		
	23(73)	2.09E-04			14.235			0.04953			0.0605		
	38(100)	7.97E-04			7.132			0.10581			0.121195		
	60(140)	4.24E-03			3.356			0.248316			0.189351		
25% C	5(41)	1.31E-05	32528	0.9915	51.461	35882	0.9982	0.011972	39115.94	0.999603	0.015182	33133.06	0.972812
	15(59)	3.90E-05			28.897			0.02228			0.025944		
	23(73)	1.26E-04			18.197			0.035441			0.049419		
	38(100)	5.63E-04			9.194			0.074477			0.089068		
	60(140)	2.54E-03			3.953			0.198254			0.157392		
25% F	5(41)	1.34E-05	31472	0.9941	38.962	33705	0.9928	0.014773	36281.28	0.995215	0.014756	35505.01	0.970111
	15(59)	4.64E-05			21.882			0.027363			0.026018		
	23(73)	1.28E-04			14.238			0.042639			0.045556		
	38(100)	4.91E-04			6.973			0.091262			0.107095		
	60(140)	2.42E-03			3.560			0.195564			0.171607		
10% M-1	5(41)	2.33E-05	31867	0.9942	30.268	35694	0.9969	0.022177	40018.25	0.999177	0.026164	36625.06	0.990168
	15(59)	6.68E-05			17.982			0.039083			0.041873		
	23(73)	2.13E-04			10.658			0.067065			0.075856		
	38(100)	8.29E-04			5.486			0.139691			0.119936		
	60(140)	4.17E-03			2.402			0.38449			0.372339		
5% SF	5(41)	2.44E-05	31614	0.9935	34.623	34324	0.9914	0.018334	37338.04	0.991527	0.021398	35196.44	0.989114

	15(59)	7.56E-05			18.426			0.036956			0.035488		
	23(73)	2.29E-04			11.107			0.063066			0.062401		
	38(100)	8.99E-04			6.448			0.108554			0.128157		
	60(140)	4.29E-03			2.854			0.28399			0.251572		
	5(41)	1.93E-05			100.162			0.009938			0.020743		
	15(59)	6.08E-05			57.304			0.018068			0.033564		
25% S	23(73)	1.80E-04	30902	0.9946	33.296	38764	0.9982	0.031143	41838.75	0.996528	0.059644	26909.39	0.944531
	38(100)	5.96E-04			17.514			0.059814			0.098759		
	60(140)	3.20E-03			6.190			0.205481			0.137031		
	5(41)	1.85E-05			38.155			0.013713			0.017815		
	15(59)	4.95E-05			24.740			0.022573			0.023809		
0.5% WRA	23(73)	1.78E-04	30882	0.9896	14.189	31744	0.9916	0.039167	34938.23	0.991914	0.050448	30603.82	0.963623
	38(100)	5.93E-04			8.254			0.078421			0.061806		
	60(140)	2.83E-03			4.043			0.159673			0.161801		
	5(41)	1.78E-05			40.082			0.014439			0.016169		
	15(59)	5.06E-05			23.299			0.02558			0.02903		
5% C 20% F	23(73)	1.45E-04	30865	0.9966	13.741	34378	0.9950	0.045388	37499.31	0.995975	0.050546	33629.63	0.974533
	38(100)	5.34E-04			7.759			0.082086			0.102256		
	60(140)	2.77E-03			3.399			0.214975			0.172241		
	5(41)	1.60E-05			50.421			0.012112			0.015856		
	15(59)	4.45E-05			27.995			0.022721			0.029153		
20% C 5% F	23(73)	1.31E-04	32052	0.9943	17.462	35841	0.9975	0.037389	39084.15	0.998801	0.049696	31993.43	0.960527
	38(100)	6.09E-04			8.958			0.074229			0.100034		
	60(140)	2.82E-03			3.864			0.202981			0.150356		

*R^2 of least squares best-fit line of ln(k) versus 1/T.

†R^2 of least squares best-fit line of three parameter exponential model versus measured heat of hydration.

**R^2 of least squares best-fit line of ASTM C 1074 hyperbolic function versus measured heat of hydration.

APPENDIX C - STRENGTH OF MORTAR AT DIFFERENT TEMPERATURES

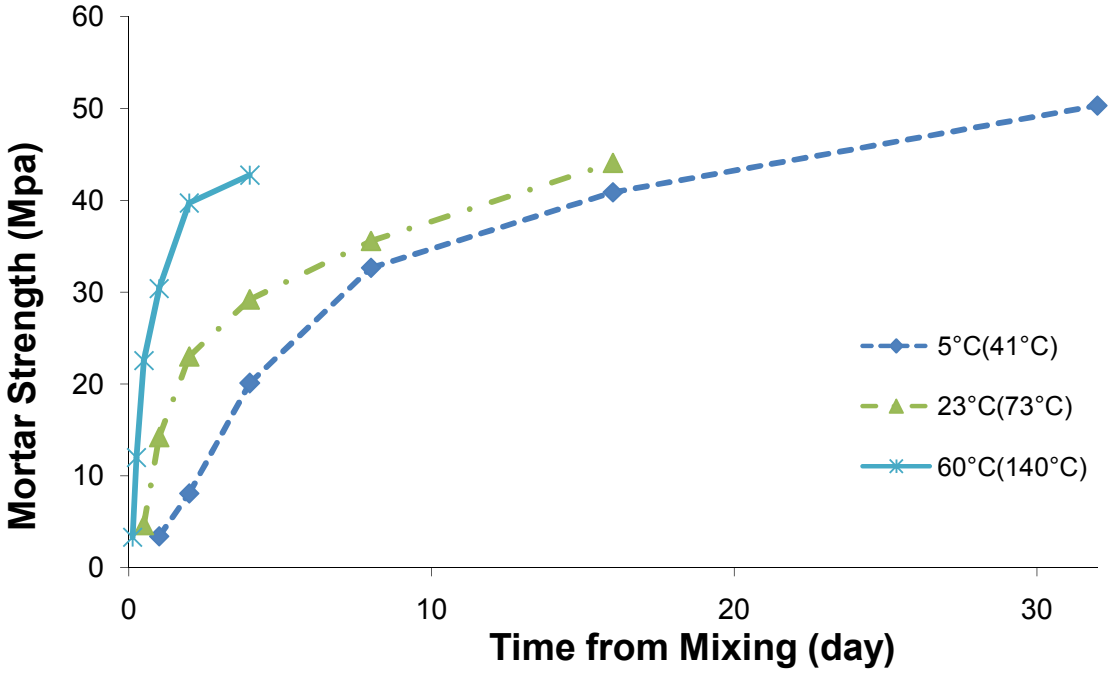
Mortar Strength (Mpa)
60
50
40
30
20
10
0
0
10
20
30
Time from Mixing (day)
5°C(41°C)
23°C(73°C)
60°C(140°C)

(a)

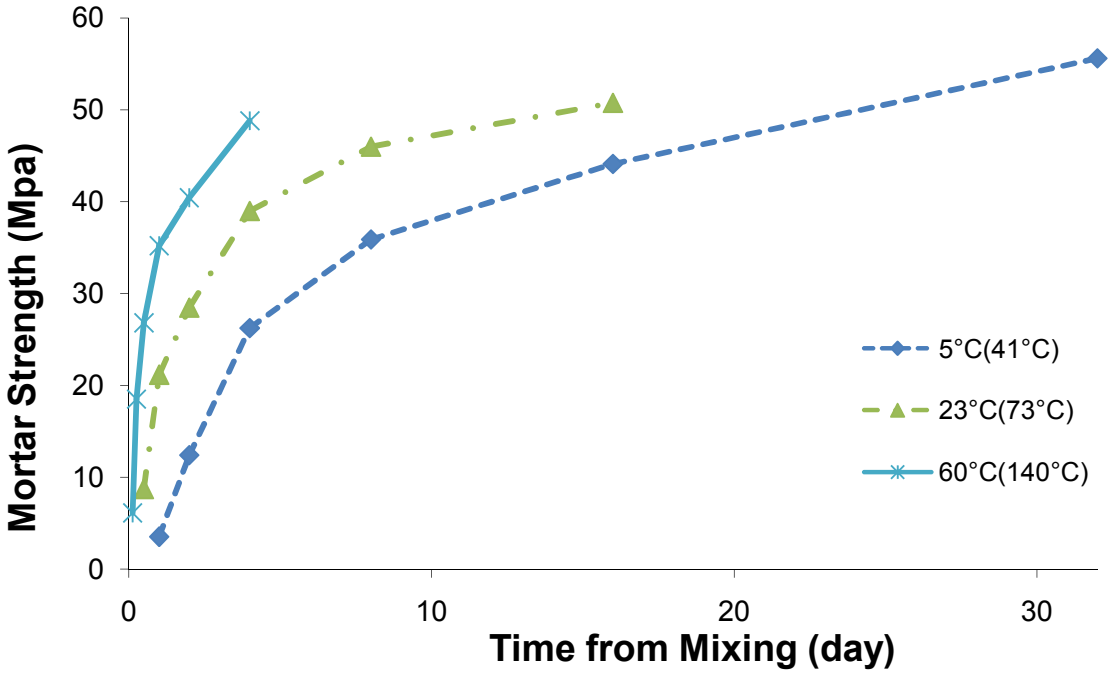
Mortar Strength (Mpa)
60
50
40
30
20
10
0
0
10
20
30
Time from Mixing (day)
5°C(41°C)
23°C(73°C)
60°C(140°C)

(b)

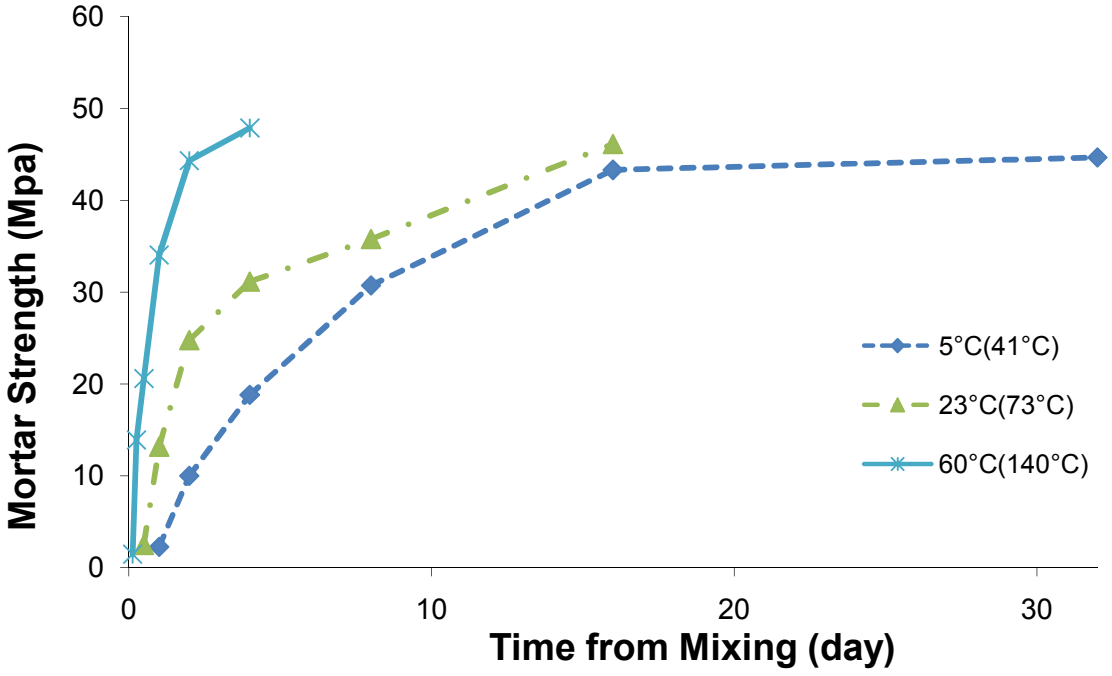
Mortar Strength (Mpa)
60
50
40
30
20
10
0
0
10
20
30
Time from Mixing (day)
5°C(41°C)
23°C(73°C)
60°C(140°C)

(c)

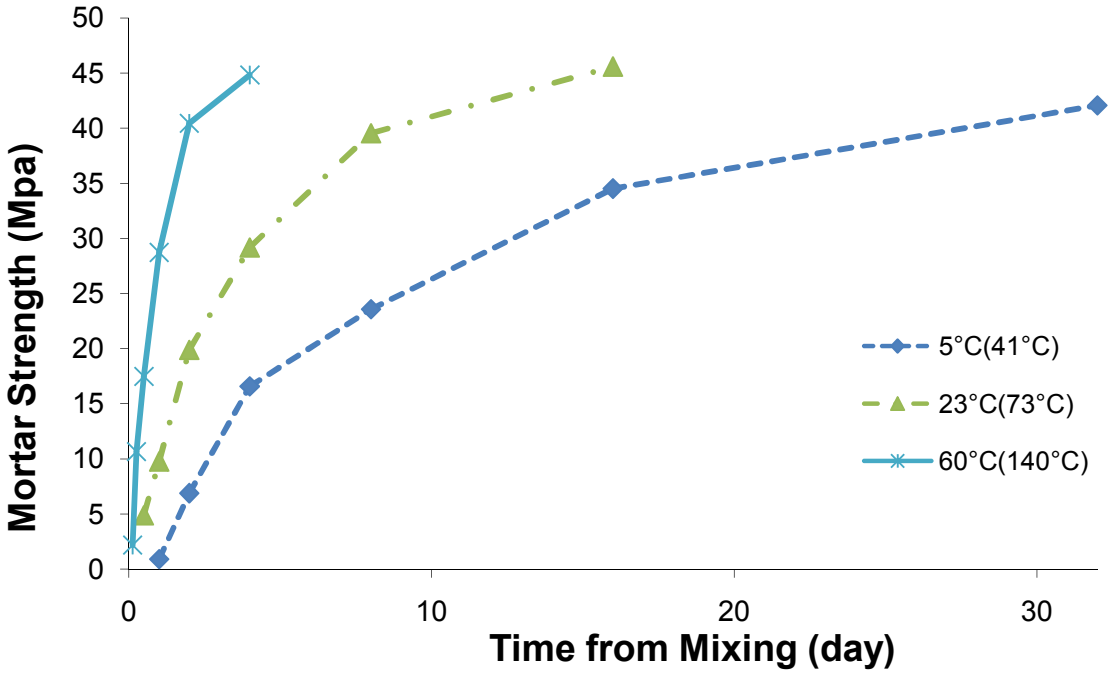
Mortar Strength (Mpa)
50
45
40
35
30
25
20
15
10
5
0
0
10
20
30
Time from Mixing (day)
5°C(41°C)
23°C(73°C)
60°C(140°C)

(d)

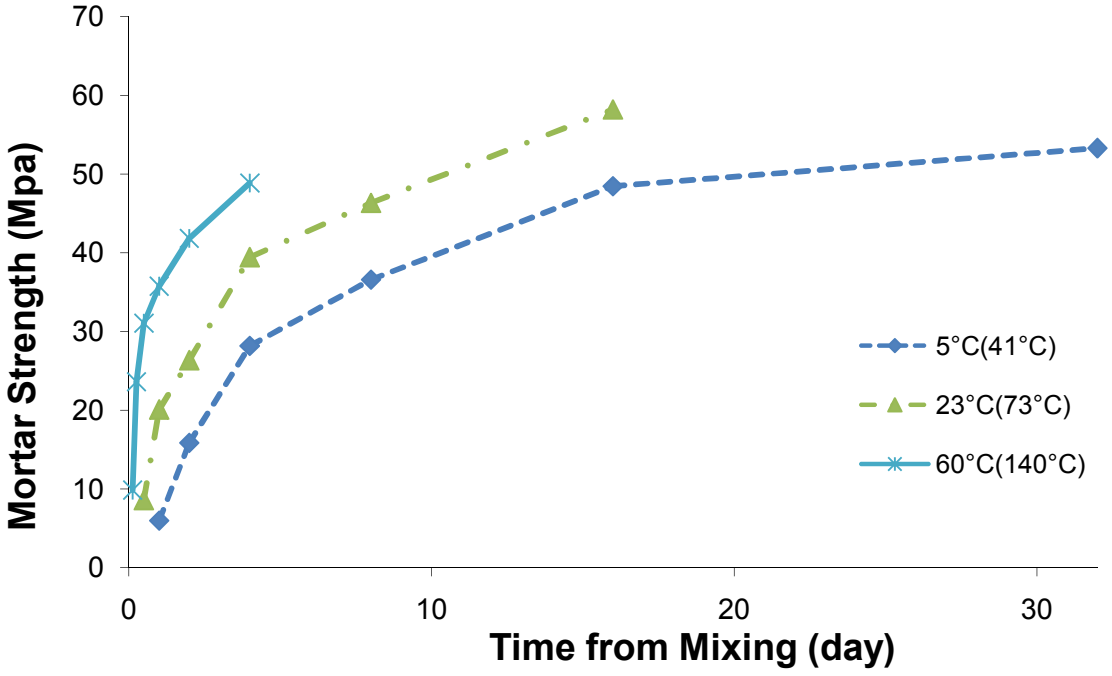
Mortar Strength (Mpa)
70
60
50
40
30
20
10
0
0
10
20
30
Time from Mixing (day)
5°C(41°C)
23°C(73°C)
60°C(140°C)

(e)

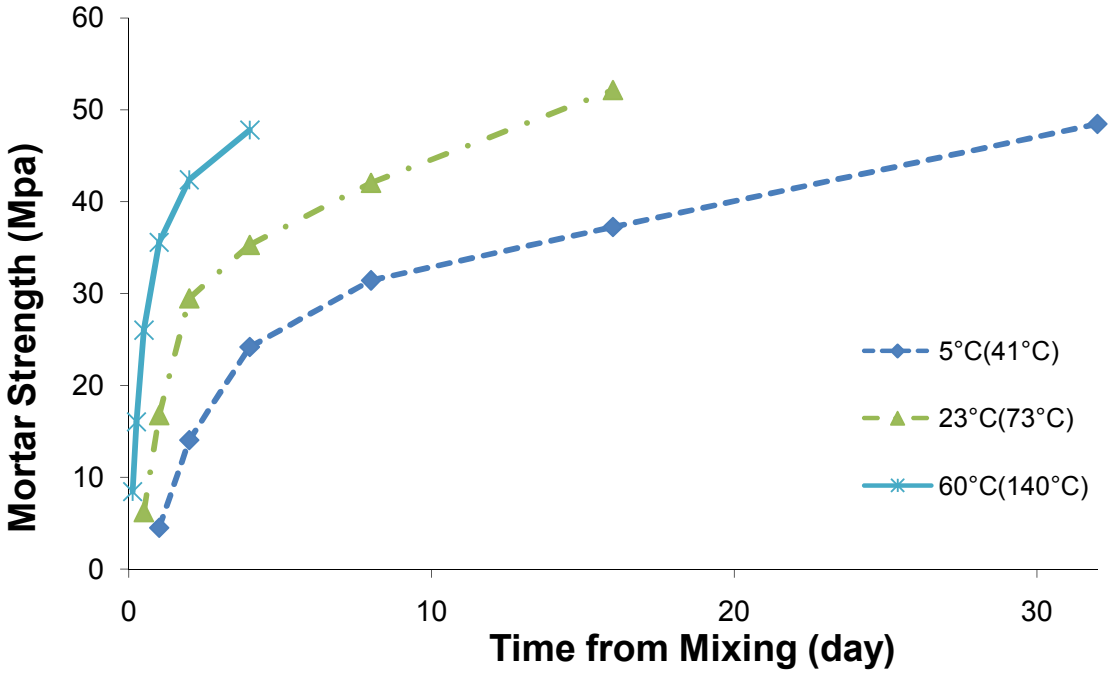
Mortar Strength (Mpa)
60
50
40
30
20
10
0
0
10
20
30
Time from Mixing (day)
5°C(41°C)
23°C(73°C)
60°C(140°C)

(f)

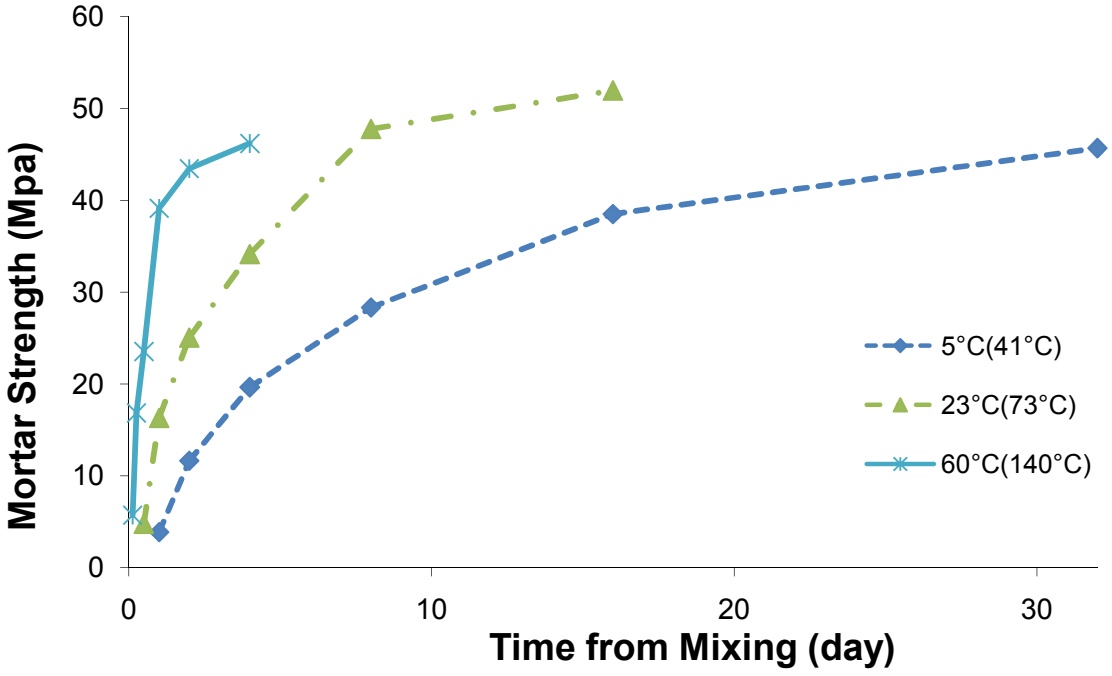
Mortar Strength (Mpa)
60
50
40
30
20
10
0
0
10
20
30
Time from Mixing (day)
5°C(41°C)
23°C(73°C)
60°C(140°C)

(g)

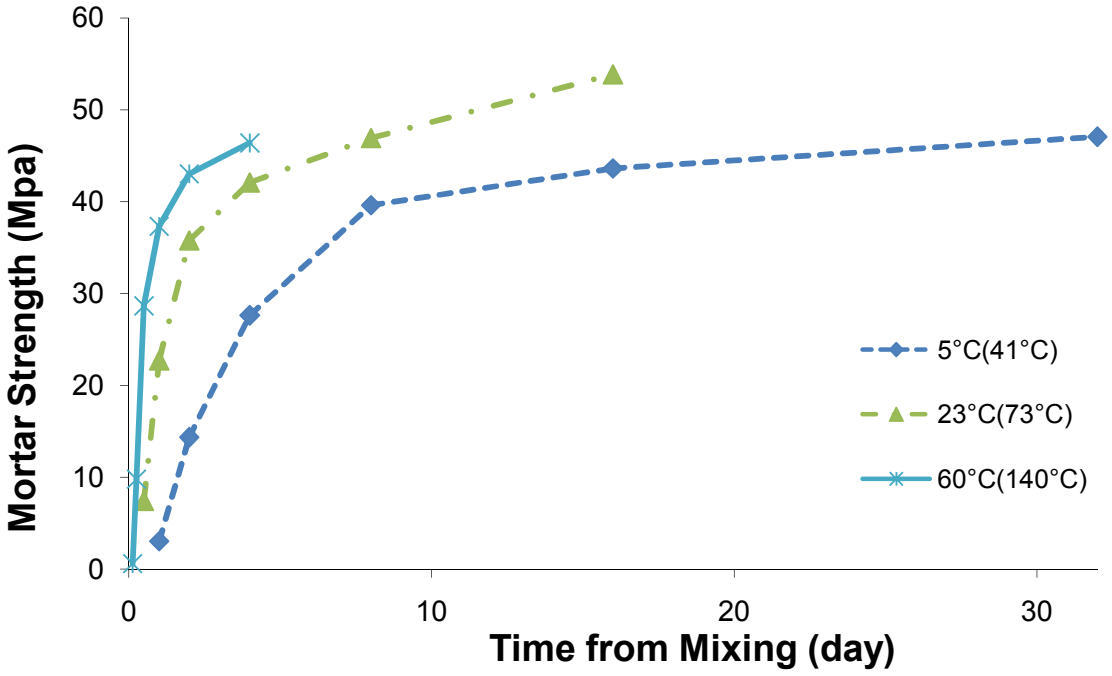
Mortar Strength (Mpa)
60
50
40
30
20
10
0
0
10
20
30
Time from Mixing (day)
5°C(41°C)
23°C(73°C)
60°C(140°C)

(h)

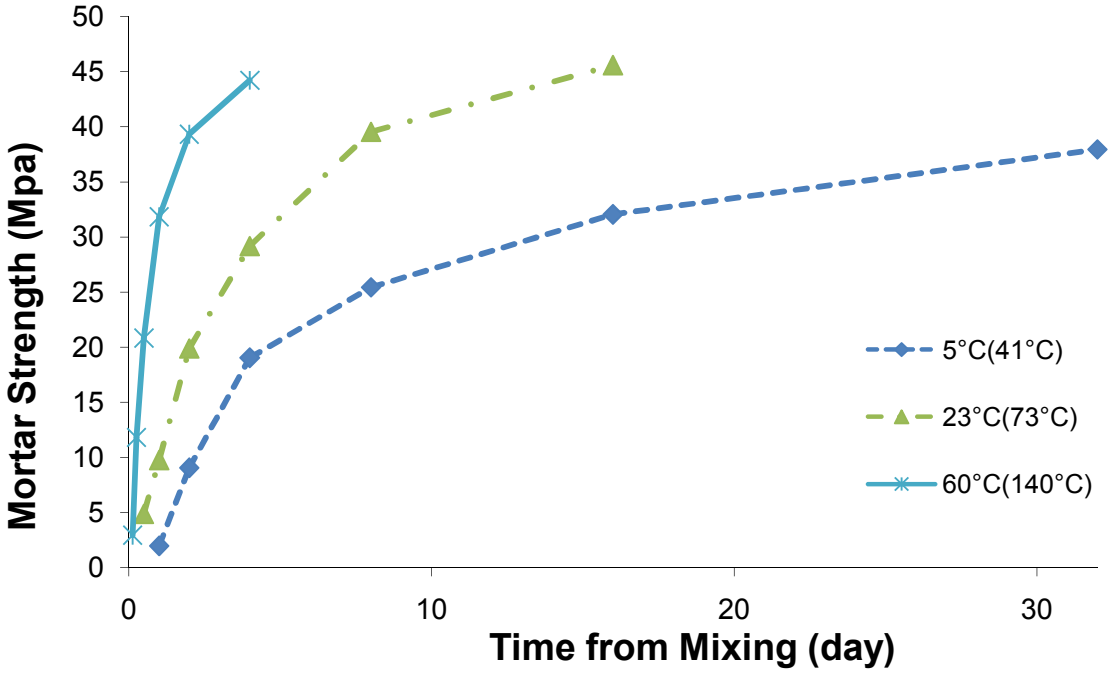

(i)

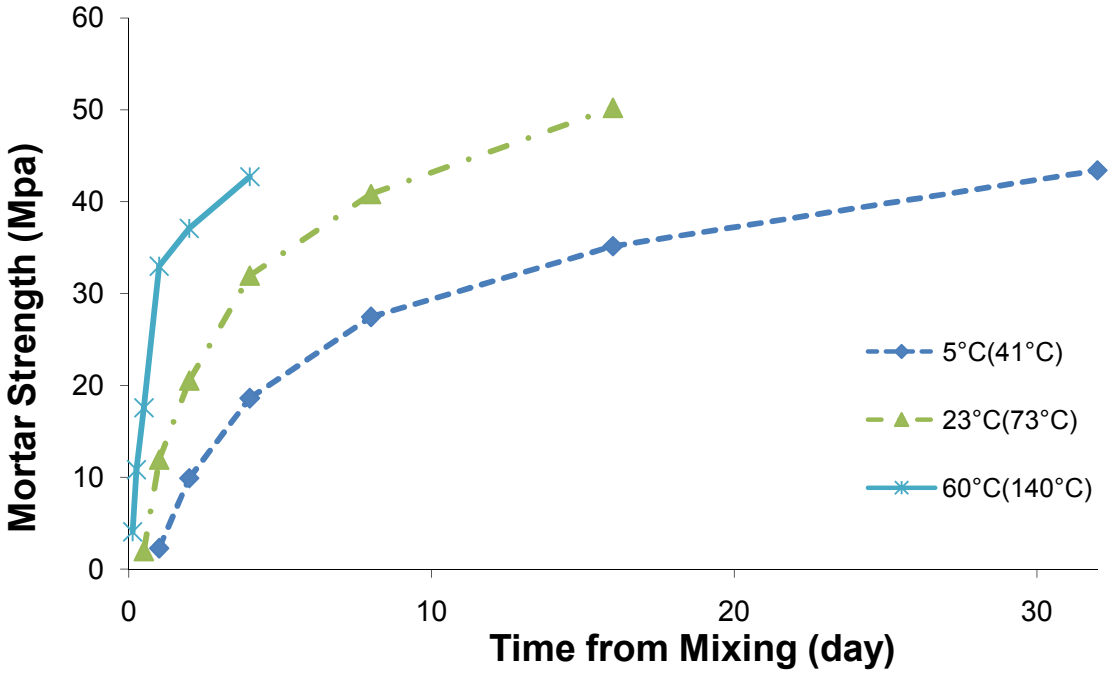

(j)

Figure C.1: Compressive Strength of Mortar; (a) TyI-0.5, (b) TyI-0.45, (c) 25% C, (d) 25% F, (e) 10% M-1, (f) 5% SF, (g) 25% S, (h) WRA, (i) 5% C 20% F, and (j) 20% C 5% F.

Appendix D - E_a FROM MORTAR STRENGTH

Table D.1: Summary of E_a for Mortar Strength

Mixes	T,°C (°F)	ASTM C 1074, Linear Fit			ASTM C 1074, Hyperbolic Function			ASTM C 1074, Two Step Method		
		Reaction rate k	E_a, J/mole	R^{2*}	Reaction rate k	E_a, J/mole	$R^{2\dagger}$	Reaction rate k	E_a, J/mole	R^{2*}
Tyl-0.5	5(41)	0.0639	47631	0.9186	0.1457	36337	0.9935	0.1376	34325	0.9879
	23(73)	0.5819			0.4622			0.4387		
	60(140)	2.2468			2.0208			1.6691		
Tyl-0.45	5(41)	0.1381	45449	0.9641	0.1867	35392	0.9854	0.1922	33445	0.9971
	23(73)	0.8249			0.6333			0.5233		
	60(140)	3.9168			2.4570			2.1416		
25% C	5(41)	0.1749	42006	0.9999	0.1820	30707	0.9765	0.1247	29343	0.8897
	23(73)	0.5125			0.5630			0.5412		
	60(140)	3.5070			1.7221			1.1369		
25% F	5(41)	0.1036	45114	0.9932	0.1266	31788	0.9999	0.1153	27736	0.9935
	23(73)	0.2641			0.2995			0.2784		
	60(140)	2.5033			1.2336			0.8586		
10% M-1	5(41)	0.2060	46666	0.9994	0.2307	40044	0.9462	0.1986	36626	0.9715
	23(73)	0.6517			0.3479			0.3415		
	60(140)	5.7213			3.6406			2.5449		
5% SF	5(41)	0.2422	35174	0.9986	0.2039	31581	0.9949	0.2165	30672	0.9981
	23(73)	0.5603			0.5456			0.5306		
	60(140)	2.9526			1.9989			1.9679		
25% S	5(41)	0.1879	39479	0.9998	0.1485	39417	0.9996	0.1340	38554	0.9948
	23(73)	0.5122			0.3973			0.3065		
	60(140)	3.1415			2.4656			2.0465		
0.5% WRA	5(41)	0.2896	32092	0.9485	0.3735	27664	0.9752	0.3763	29273	0.9986
	23(73)	1.1154			1.0411			0.8732		
	60(140)	3.1155			2.8317			3.0863		
5% C 20% F	5(41)	0.1932	38521	0.9355	0.2243	30230	0.9417	0.2063	28617	0.9475
	23(73)	0.2694			0.2995			0.2784		
	60(140)	2.5911			1.7942			1.4830		
20% C 5% F	5(41)	0.2030	37236	0.9762	0.1626	32302	0.9946	0.1505	30189	0.9916
	23(73)	0.3656			0.3240			0.2764		

	60(140)	2.7300			1.5954			1.2639		

*R^2 of least squares best-fit line of ln(k) versus 1/T.

**R^2 of least squares best-fit line of ASTM C 1074 hyperbolic function versus measured heat of hydration.

APPENDIX E - E_a FROM TIME OF SET

Table E.1: Summary of E_a for Setting Time of Cement Paste (w/cm=0.35).

Mixes	T,°C (°F)	Initial setting time			Final setting time		
		Setting time t, hour	E_a, J/mole	R^{2*}	Setting time t, hour	E_a, J/mole	R^{2*}
Ty I	5(41)	9.58	24323	0.9970	12.82	23137	0.9999
	23(73)	4.62			6.95		
	60(140)	1.66			2.45		
25% C	5(41)	10.95	23220	0.9974	17.93	25786	0.9977
	23(73)	5.48			8.37		
	60(140)	2.06			2.80		
25% F	5(41)	11.57	22950	0.9950	16.80	24266	0.9997
	23(73)	5.67			8.62		
	60(140)	2.20			2.95		
15% M-1	5(41)	8.73	22343	0.9613	13.58	25213	0.9784
	23(73)	3.58			5.43		
	60(140)	1.68			2.15		
15% M-2	5(41)	8.08	22345	0.9831	14.07	22341	0.9541
	23(73)	3.68			5.62		
	60(140)	1.58			2.70		
6% SF	5(41)	9.29	24272	0.9847	17.42	27554	0.9680
	23(73)	4.00			6.02		
	60(140)	1.59			2.30		
25% S	5(41)	11.48	24991	0.9563	17.53	26904	0.9701
	23(73)	4.15			6.28		
	60(140)	1.81			2.43		
0.5% WRA	5(41)	14.73	20789	0.9977	22.42	23001	0.9966
	23(73)	9.12			11.18		
	60(140)	3.37			4.27		
5% C 20% F	5(41)	11.93	21805	0.9949	17.68	23034	0.9841
	23(73)	6.05			7.92		
	60(140)	2.47			3.30		
20% C 5% F	5(41)	11.73	22116	0.9907	17.55	22827	0.9941
	23(73)	5.67			8.55		
	60(140)	2.36			3.37		

*R^2 of least squares best-fit line of ln(1/setting time) versus $1/T$.

Table E.2: Summary of E_a for Setting Time of Mortar.

Mixes	T,°C (°F)	Initial setting time			Final setting time		
		Setting time t, hour	E_a, J/mole	R^{2*}	Setting time t, hour	E_a, J/mole	R^{2*}
Tyl-0.5	5(41)	8.32	20105	0.9766	11.42	21304	0.9623
	23(73)	3.97			4.91		
	60(140)	1.91			2.38		
Tyl-0.45	5(41)	7.69	20820	0.9837	10.13	21877	0.9814
	23(73)	3.71			4.65		
	60(140)	1.69			2.05		
25% C	5(41)	11.64	23901	0.9875	17.41	23399	0.9487
	23(73)	5.18			6.52		
	60(140)	2.05			3.08		
25% F	5(41)	11.33	21649	0.9689	16.45	23159	0.9374
	23(73)	4.93			5.98		
	60(140)	2.31			2.94		
10% M-1	5(41)	5.36	20450	0.9999	7.93	21635	0.9984
	23(73)	3.10			4.23		
	60(140)	1.24			1.67		
5% SF	5(41)	6.77	20170	0.9911	9.44	20365	0.9897
	23(73)	3.50			4.80		
	60(140)	1.57			2.15		
25% S	5(41)	7.70	21402	0.9852	9.96	21408	0.9868
	23(73)	3.67			4.80		
	60(140)	1.62			2.10		
0.5% WRA	5(41)	12.40	21058	0.9999	18.79	20252	0.9627
	23(73)	7.02			8.43		
	60(140)	2.74			4.23		
5% C 20% F	5(41)	11.23	22531	0.9778	16.10	23650	0.9579
	23(73)	4.94			6.19		
	60(140)	2.16			2.81		
20% C 5% F	5(41)	11.62	23616	0.9856	16.62	22709	0.9385
	23(73)	5.15			6.18		
	60(140)	2.08			3.08		

*R^2 of least squares best-fit line of ln(1/setting time) versus $1/T$.

APPENDIX F - CHEMICAL SHRINKAGE OF CEMENTITIOUS MATERIALS AT DIFFERENT TEMPERATURES

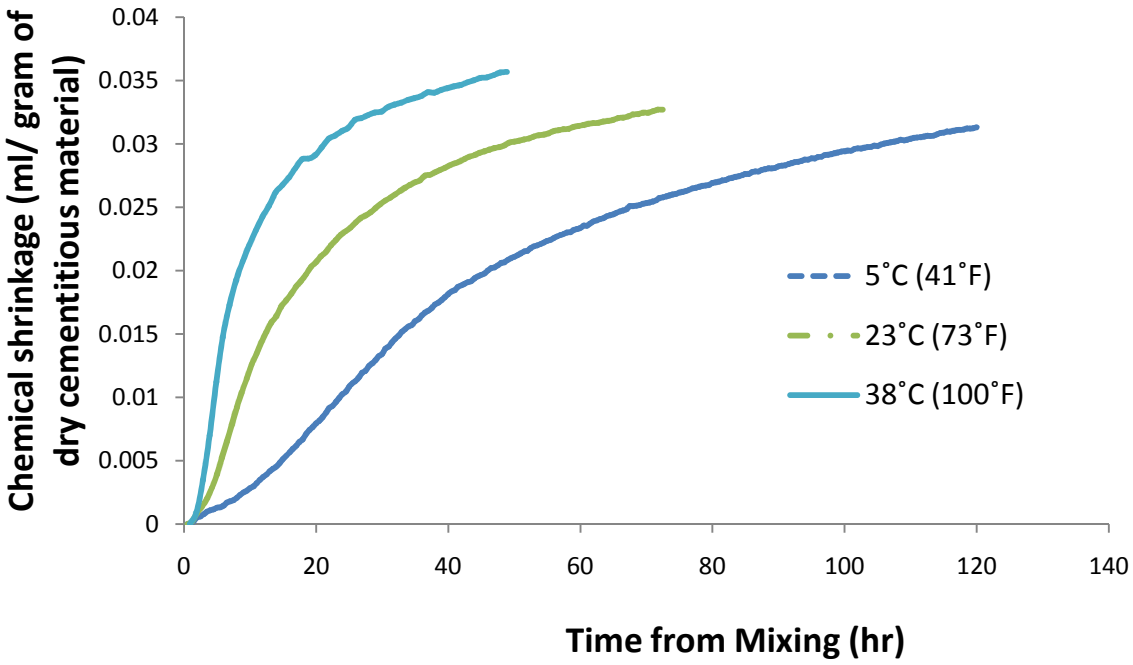
Chemical shrinkage (ml/ gram of dry cementitious material)
0.04
0.035
0.03
0.025
0.02
0.015
0.01
0.005
0
0
20
40
60
80
100
120
140
Time from Mixing (hr)
5˚C (41˚F)
23˚C (73˚F)
38˚C (100˚F)

(a)

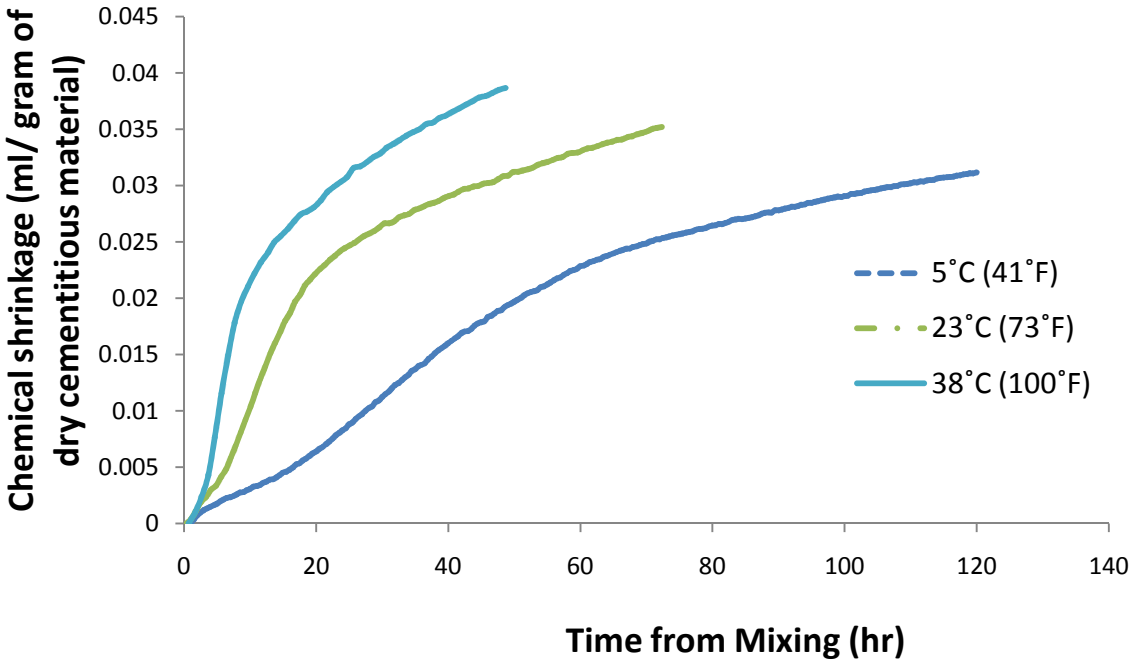
Chemical shrinkage (ml/ gram of dry cementitious material)
0.045
0.04
0.035
0.03
0.025
0.02
0.015
0.01
0.005
0
0
20
40
60
80
100
120
140
Time from Mixing (hr)
5˚C (41˚F)
23˚C (73˚F)
38˚C (100˚F)

(b)

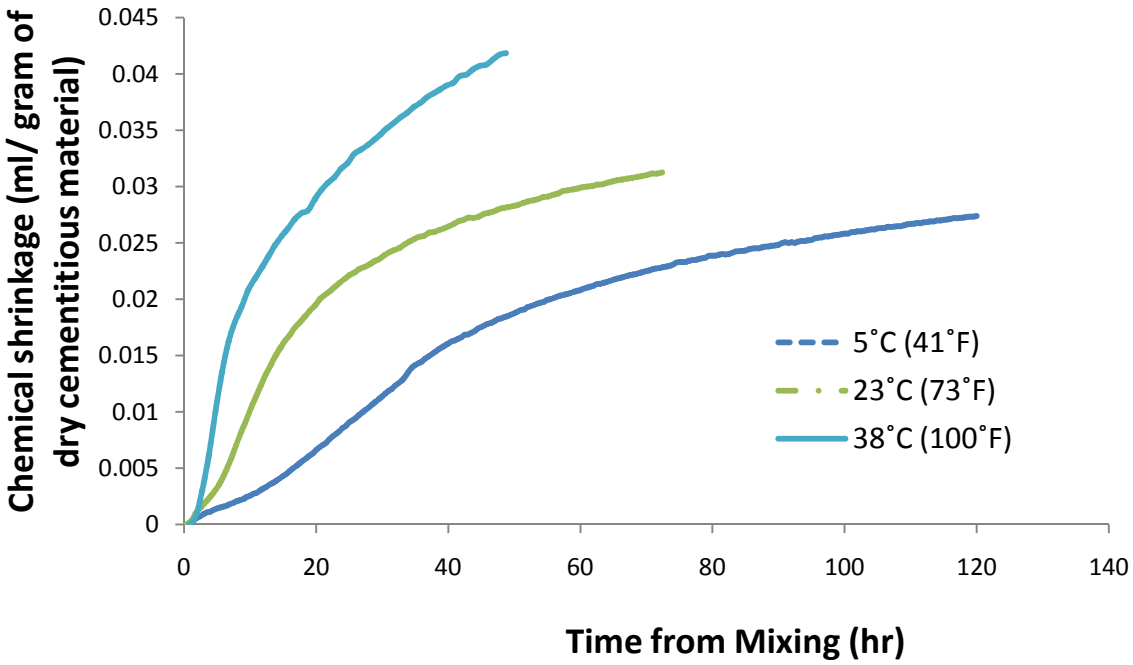
Chemical shrinkage (ml/ gram of dry cementitious material)
0.045
0.04
0.035
0.03
0.025
0.02
0.015
0.01
0.005
0
0
20
40
60
80
100
120
140
Time from Mixing (hr)
5˚C (41˚F)
23˚C (73˚F)
38˚C (100˚F)

(c)

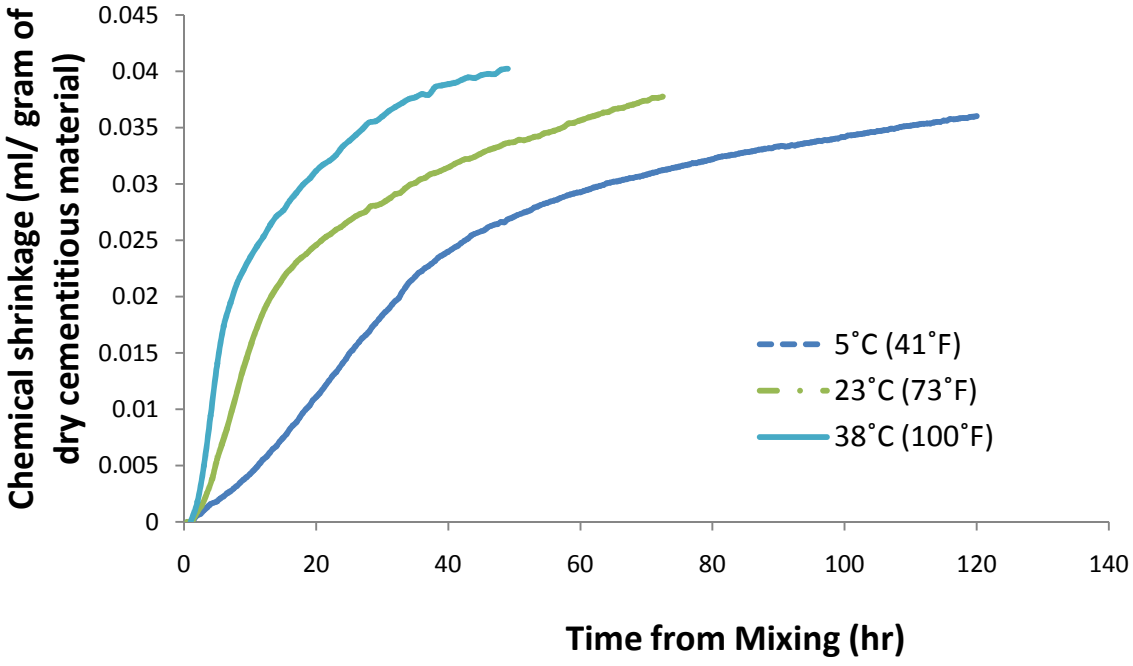
Chemical shrinkage (ml/ gram of dry cementitious material)
0.045
0.04
0.035
0.03
0.025
0.02
0.015
0.01
0.005
0
0
20
40
60
80
100
120
140
Time from Mixing (hr)
5˚C (41˚F)
23˚C (73˚F)
38˚C (100˚F)

(d)

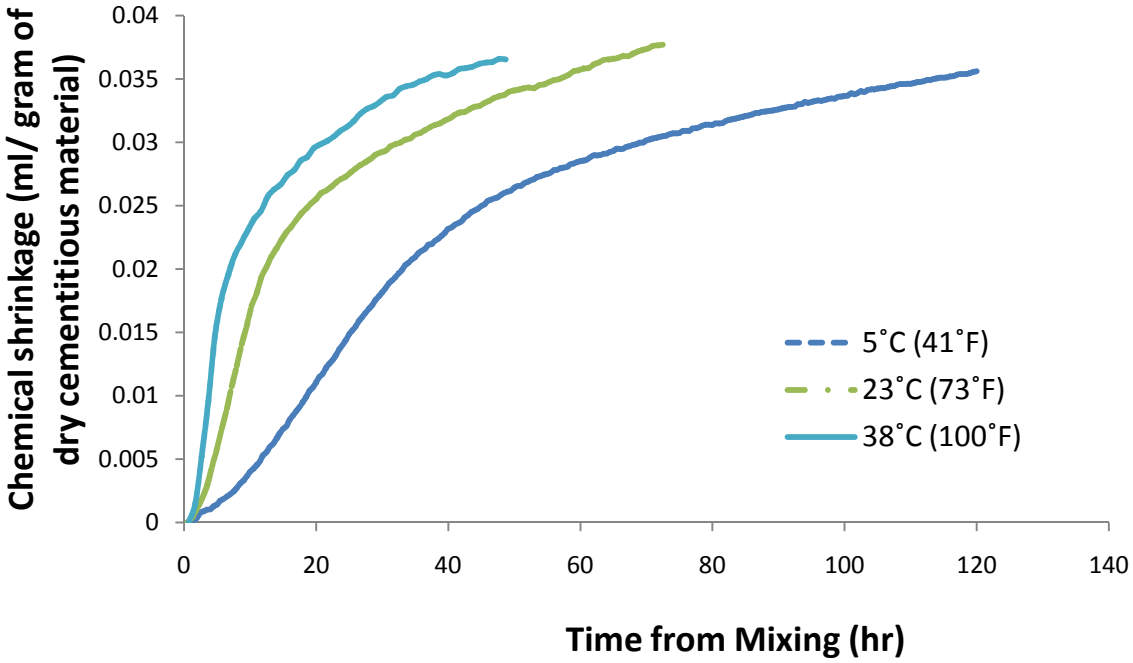
Chemical shrinkage (ml/ gram of dry cementitious material)
0.04
0.035
0.03
0.025
0.02
0.015
0.01
0.005
0
0
20
40
60
80
100
120
140
Time from Mixing (hr)
5˚C (41˚F)
23˚C (73˚F)
38˚C (100˚F)

(e)

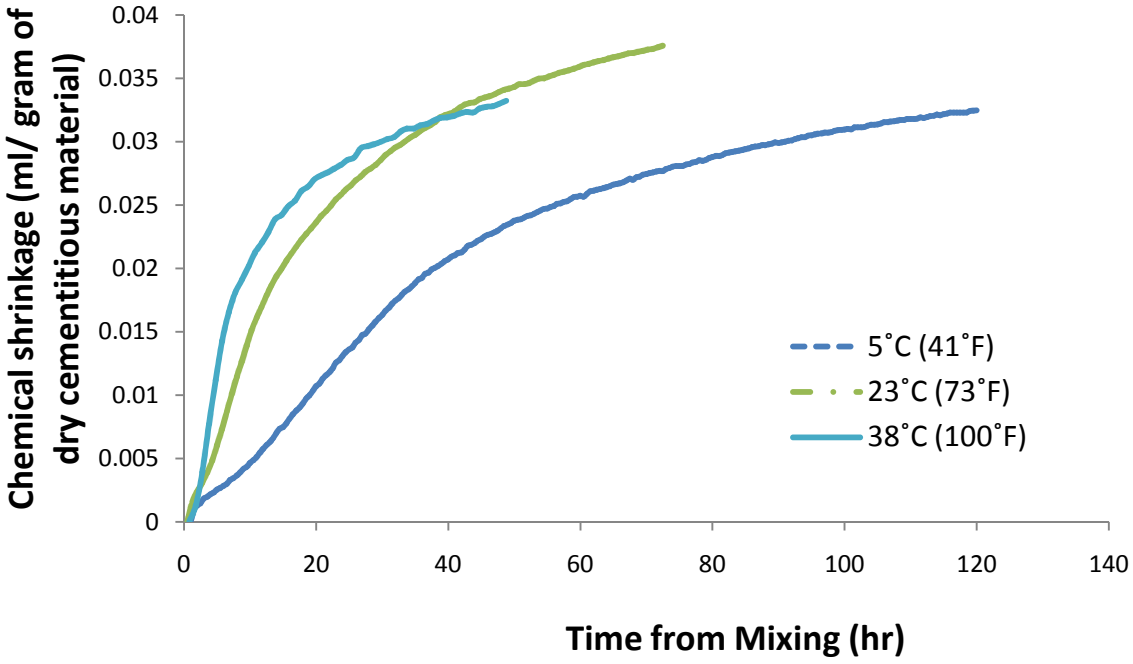
Chemical shrinkage (ml/ gram of dry cementitious material)
0.04
0.035
0.03
0.025
0.02
0.015
0.01
0.005
0
0
20
40
60
80
100
120
140
Time from Mixing (hr)
5˚C (41˚F)
23˚C (73˚F)
38˚C (100˚F)

(f)

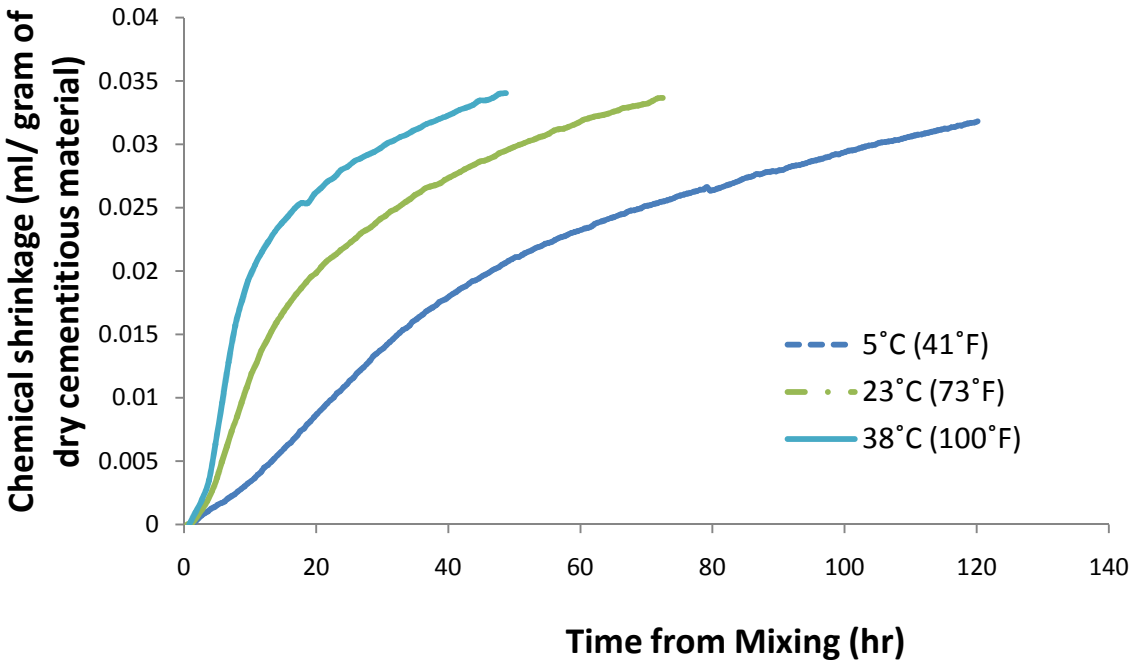
Chemical shrinkage (ml/ gram of dry cementitious material)
0.04
0.035
0.03
0.025
0.02
0.015
0.01
0.005
0
0
20
40
60
80
100
120
140
Time from Mixing (hr)
5˚C (41˚F)
23˚C (73˚F)
38˚C (100˚F)

(g)

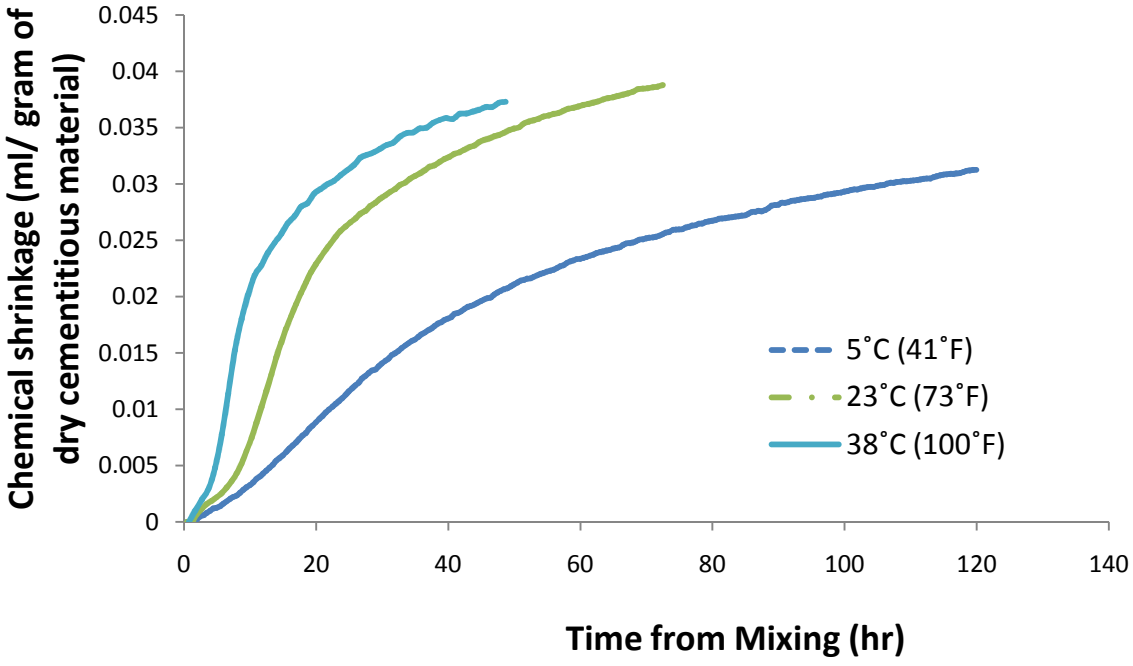
Chemical shrinkage (ml/ gram of dry cementitious material)
0.045
0.04
0.035
0.03
0.025
0.02
0.015
0.01
0.005
0
0
20
40
60
80
100
120
140
Time from Mixing (hr)
5˚C (41˚F)
23˚C (73˚F)
38˚C (100˚F)

(h)

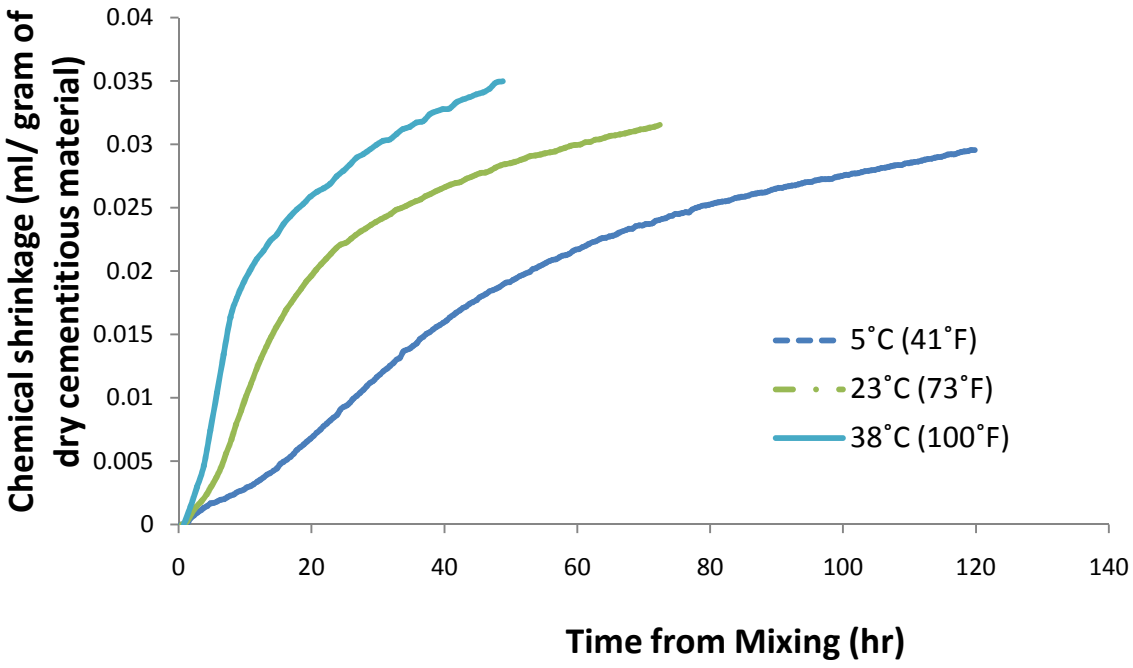

(i)

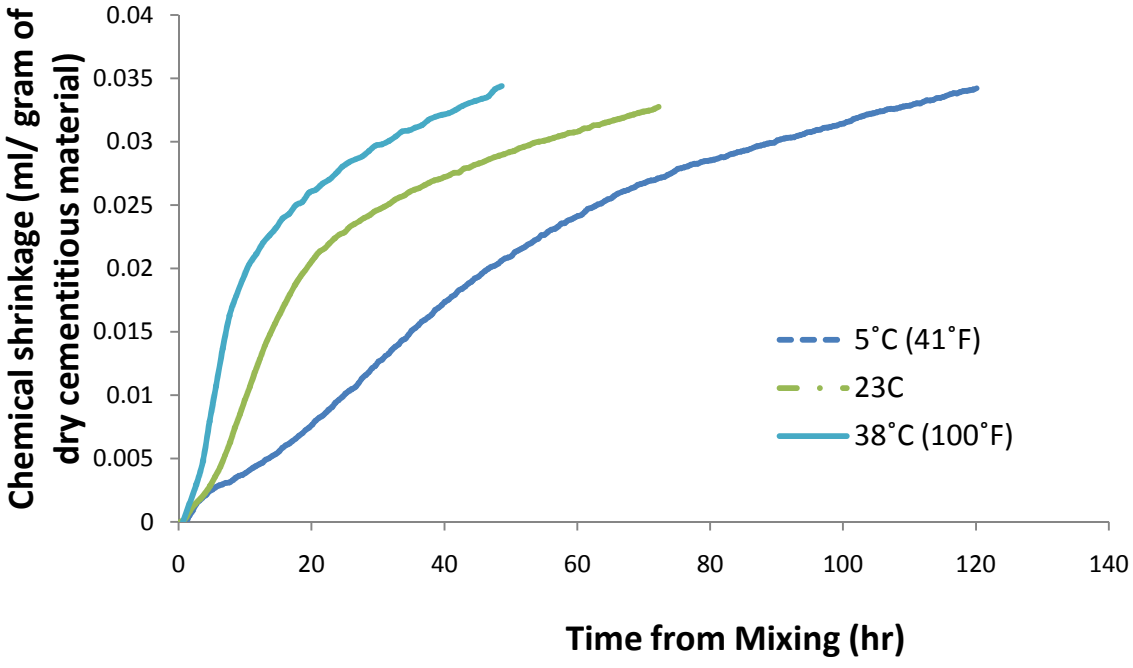

(j)

Figure F.1: Chemical Shrinkage of Cement Paste (w/cm=0.35); (a) Ty I, (b) 25% C, (c) 25% F, (d) 15% M-1, (e) 15% M-2, (f) 6% SF, (g) 25% S, (h) WRA, (i) 5% C 20% F, and (j) 20% C 5% F.

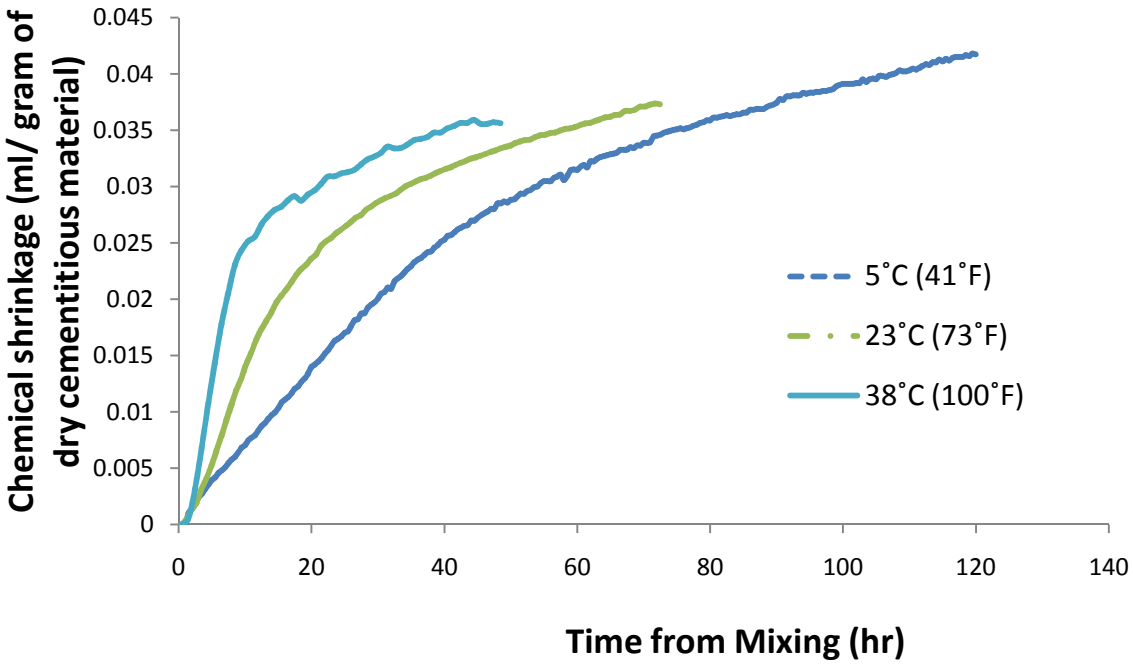
Chemical shrinkage (ml/ gram of dry cementitious material)
0.045
0.04
0.035
0.03
0.025
0.02
0.015
0.01
0.005
0
0
20
40
60
80
100
120
140
Time from Mixing (hr)
5˚C (41˚F)
23˚C (73˚F)
38˚C (100˚F)

(a)

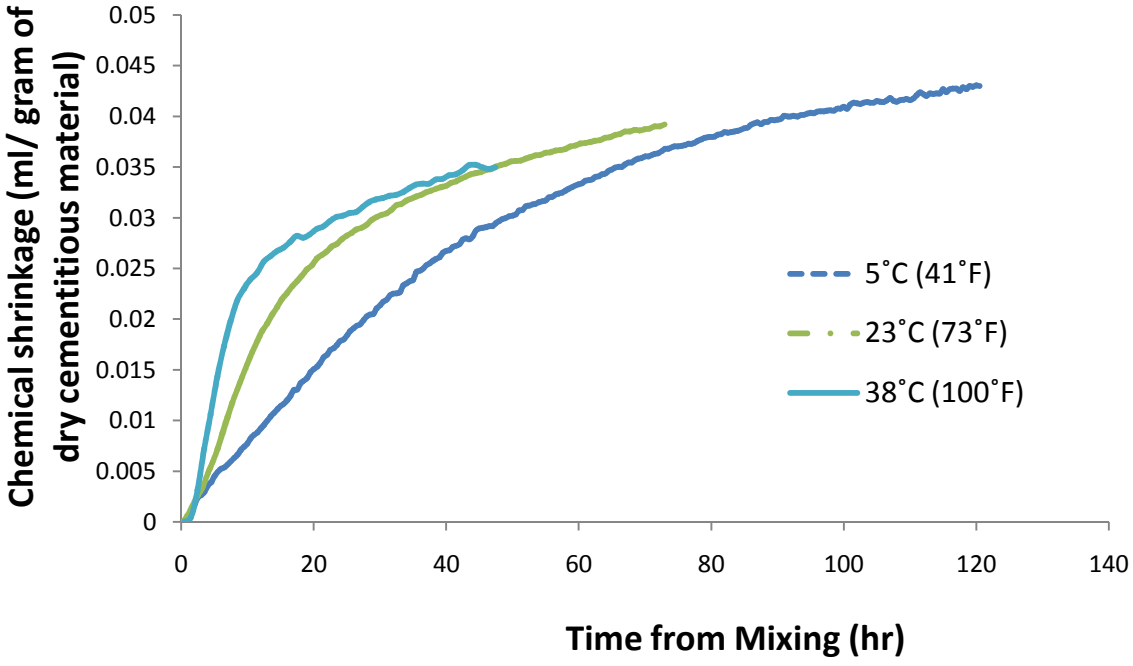
Chemical shrinkage (ml/ gram of dry cementitious material)
0.05
0.045
0.04
0.035
0.03
0.025
0.02
0.015
0.01
0.005
0
0
20
40
60
80
100
120
140
Time from Mixing (hr)
5˚C (41˚F)
23˚C (73˚F)
38˚C (100˚F)

(b)

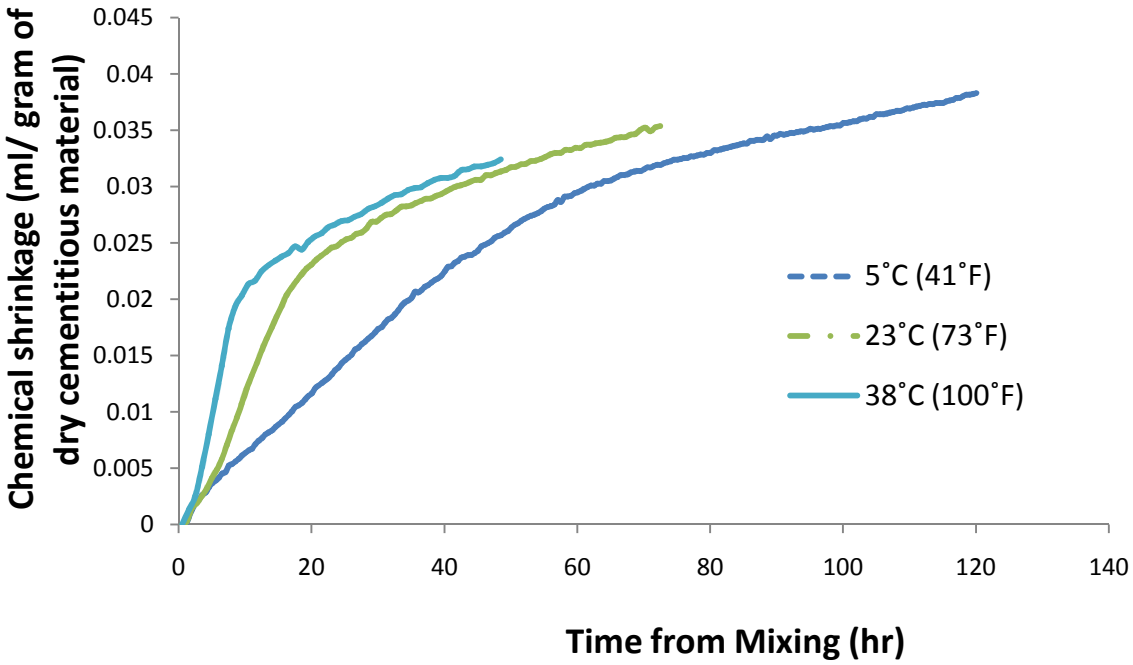
Chemical shrinkage (ml/ gram of dry cementitious material)
0.045
0.04
0.035
0.03
0.025
0.02
0.015
0.01
0.005
0
0
20
40
60
80
100
120
140
Time from Mixing (hr)
5˚C (41˚F)
23˚C (73˚F)
38˚C (100˚F)

(c)

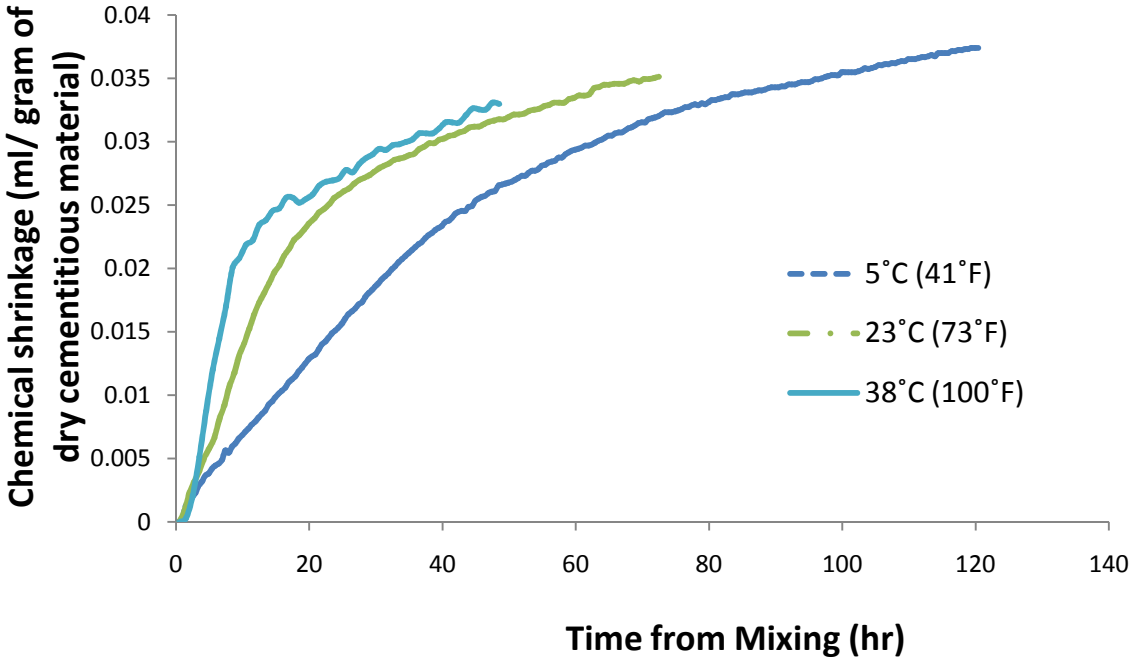
Chemical shrinkage (ml/ gram of dry cementitious material)
0.04
0.035
0.03
0.025
0.02
0.015
0.01
0.005
0
0
20
40
60
80
100
120
140
Time from Mixing (hr)
5˚C (41˚F)
23˚C (73˚F)
38˚C (100˚F)

(d)

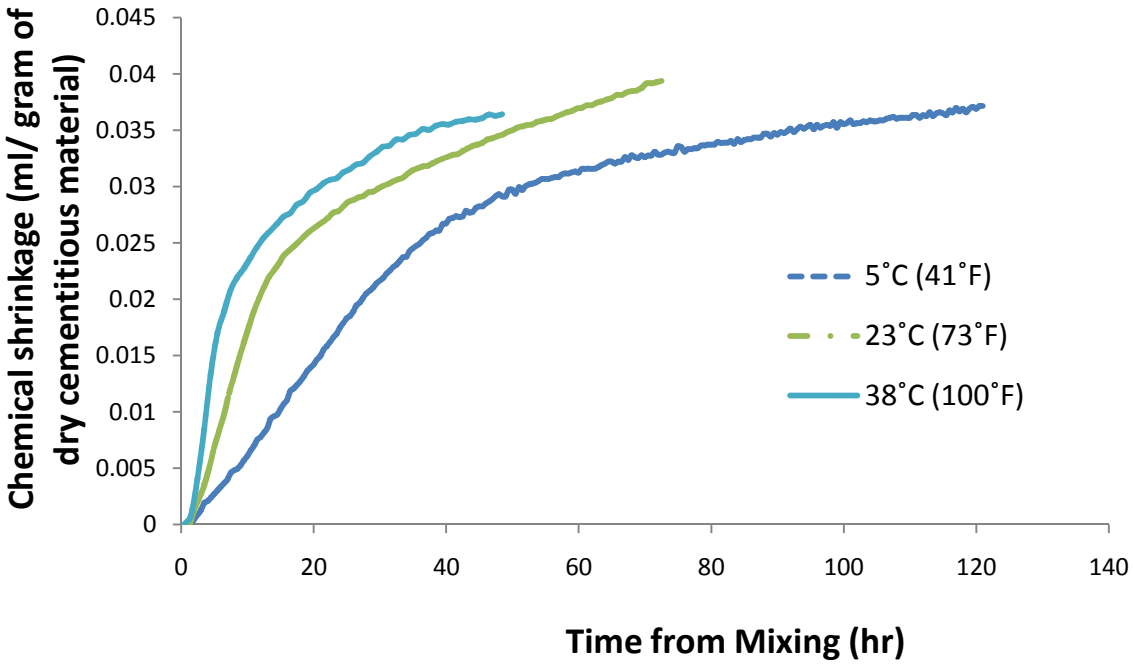
Chemical shrinkage (ml/ gram of dry cementitious material)
0.045
0.04
0.035
0.03
0.025
0.02
0.015
0.01
0.005
0
0
20
40
60
80
100
120
140
Time from Mixing (hr)
5˚C (41˚F)
23˚C (73˚F)
38˚C (100˚F)

(e)

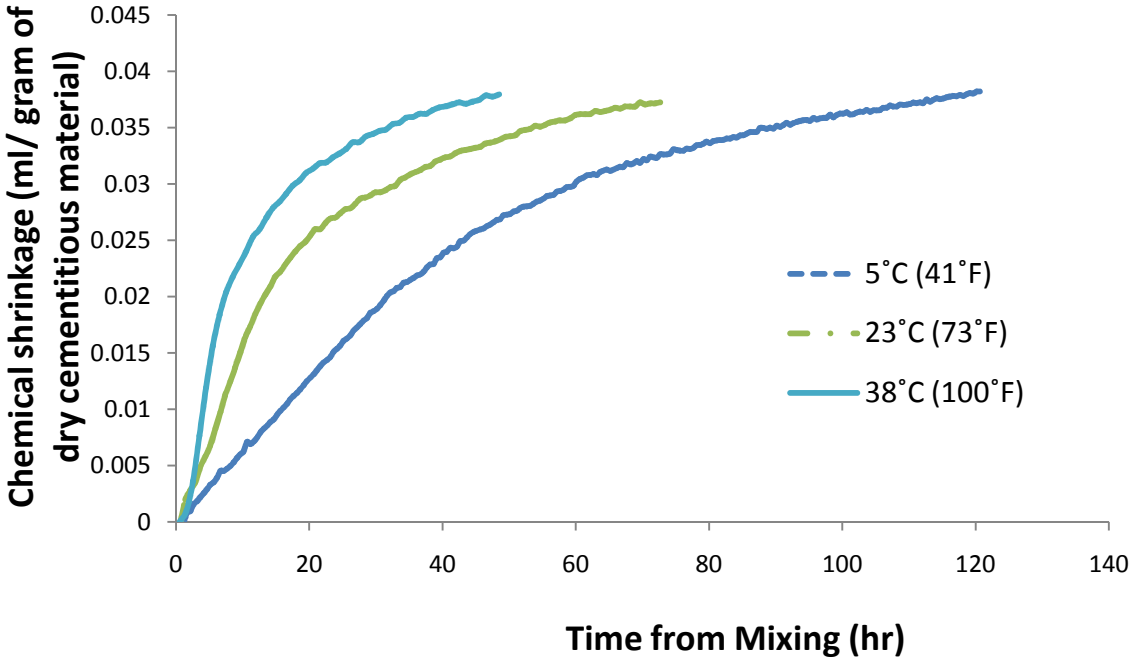
Chemical shrinkage (ml/ gram of dry cementitious material)
0.045
0.04
0.035
0.03
0.025
0.02
0.015
0.01
0.005
0
0
20
40
60
80
100
120
140
Time from Mixing (hr)
5˚C (41˚F)
23˚C (73˚F)
38˚C (100˚F)

(f)

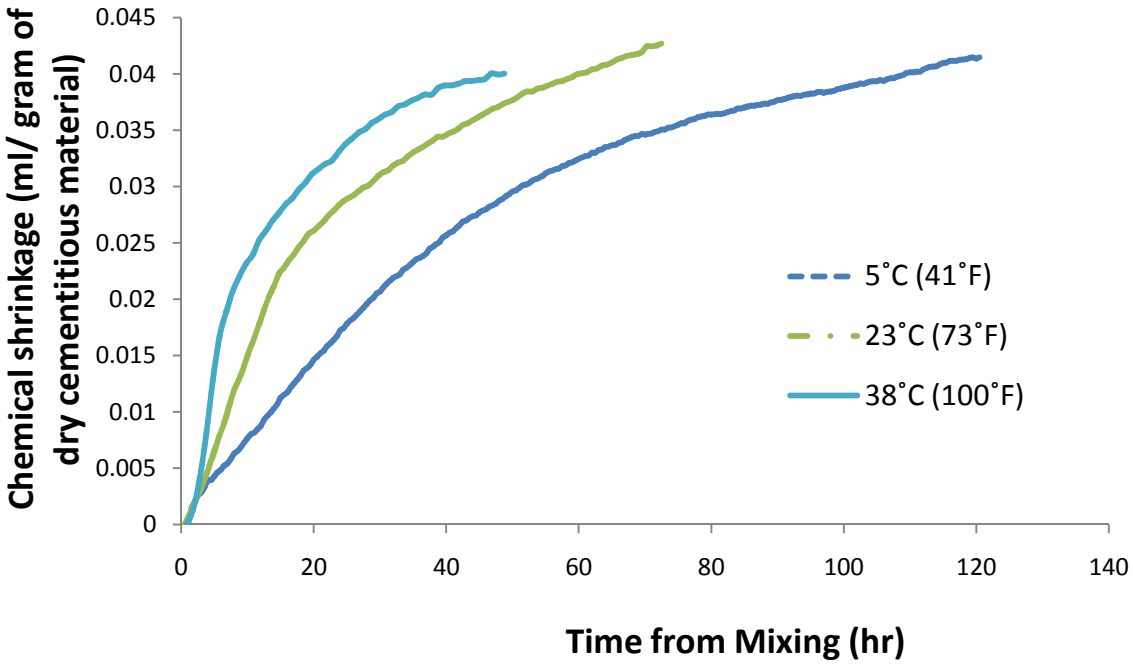
Chemical shrinkage (ml/ gram of dry cementitious material)
0.045
0.04
0.035
0.03
0.025
0.02
0.015
0.01
0.005
0
0
20
40
60
80
100
120
140
Time from Mixing (hr)
5˚C (41˚F)
23˚C (73˚F)
38˚C (100˚F)

(g)

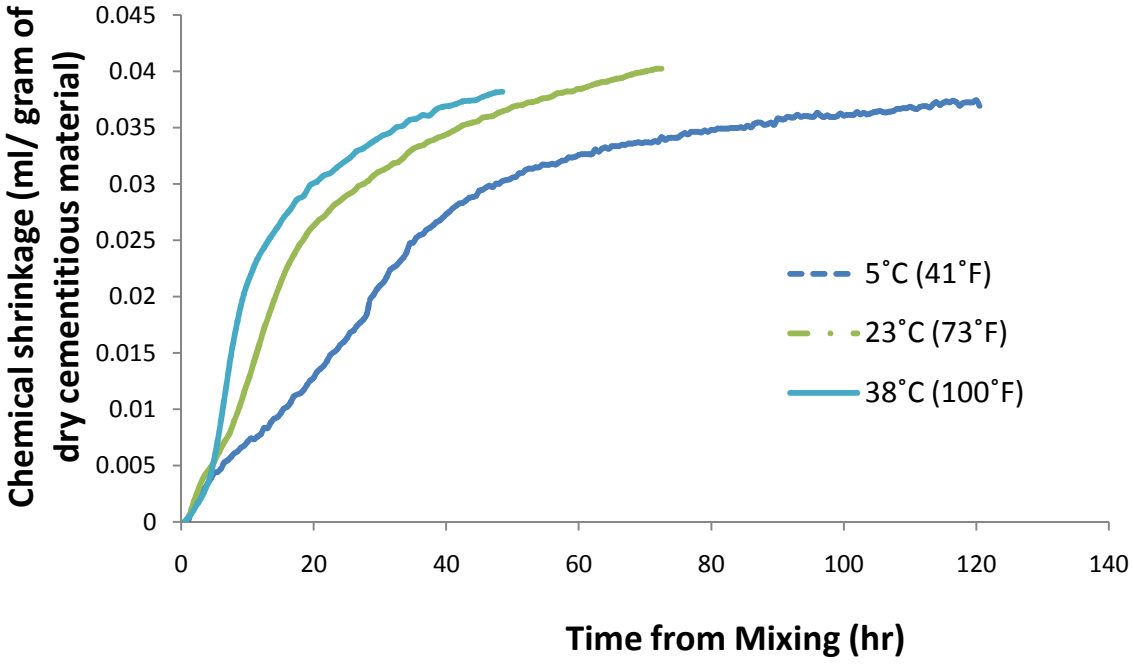
Chemical shrinkage (ml/ gram of dry cementitious material)
0.045
0.04
0.035
0.03
0.025
0.02
0.015
0.01
0.005
0
0
20
40
60
80
100
120
140
Time from Mixing (hr)
5˚C (41˚F)
23˚C (73˚F)
38˚C (100˚F)

(h)

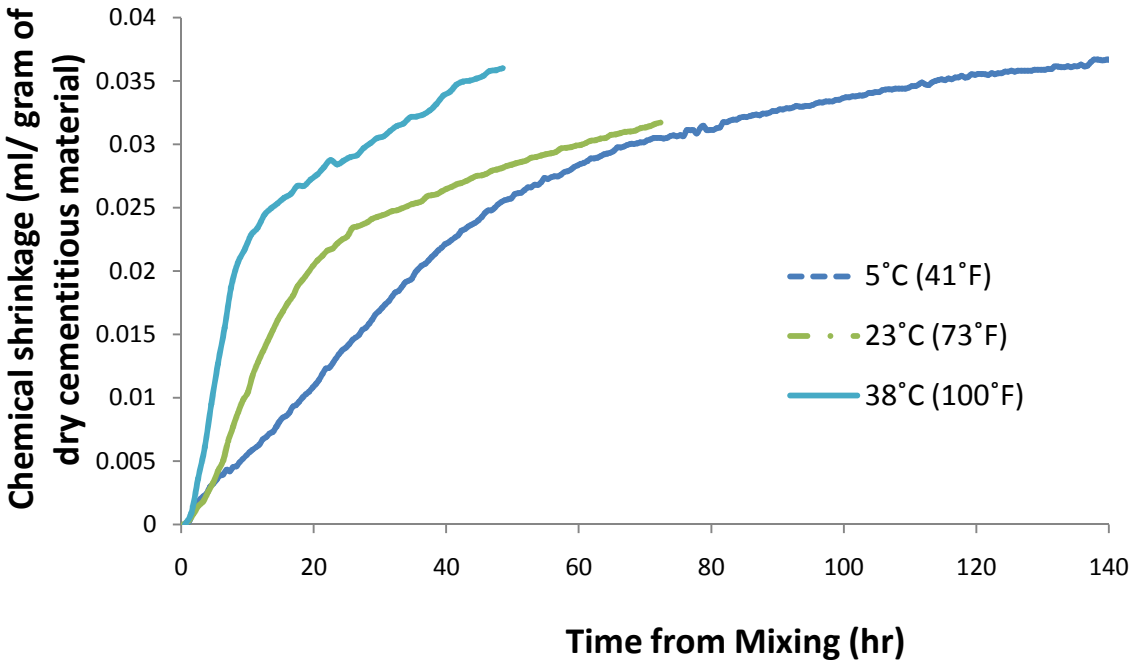

(i)

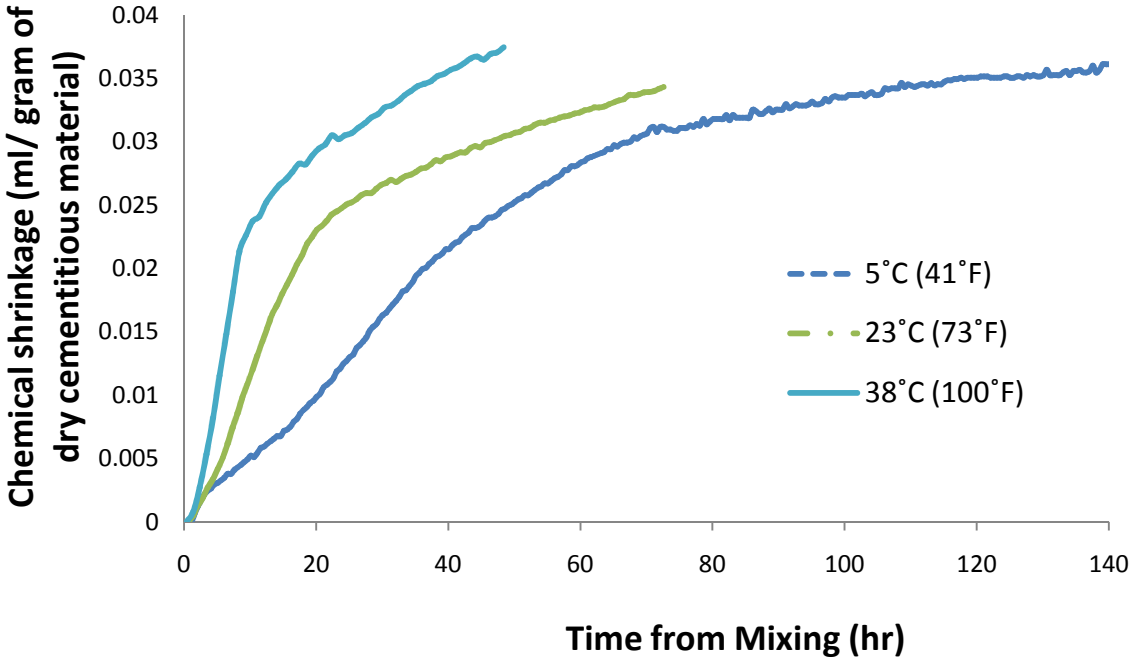

(j)

Figure F.2: Chemical Shrinkage of Cement Mortar; (a) TyI-0.5, (b) TyI-0.45, (c) 25% C, (d) 25% F, (e) 10% M-1, (f) 5% SF, (g) 25% S, (h) WRA, (i) 5% C 20% F, and (j) 20% C 5% F.

Appendix G - E_a FROM CHEMICAL SHRINKAGE

Table G.1: Summary of E_a for Chemical Shrinkage of Cement Paste (w/cm=0.35).

Mixes	T,°C (°F)	Exponential Function			Exponential Function; Unequal H_{ult}			ASTM C 1074 Hyperbolic; Equal S_u			ASTM C 1074 Hyperbolic		
		τ, hours	E_a, J/mol	$R^{2\dagger}$	τ, hours	E_a, J/mol	$R^{2\dagger}$	Reaction rate k	E_a, J/mol	R^{2**}	Reaction rate k	E_a, J/mol	R^{2**}
Ty I	5(41)	31.33	36078	0.9965	6.268	37398	0.9989	2.48E-02	35624	0.9857	1.96E-02	45296	0.9998
	23(73)	13.14			12.39			5.38E-02			6.29E-02		
	60(140)	5.93			34.72			1.29E-01			1.57E-01		
25% C	5(41)	40.73	35914	0.9991	8.361	36938	0.9918	1.89E-02	41530	0.9881	1.43E-02	52338	0.9987
	23(73)	15.19			14.98			4.74E-02			6.09E-02		
	60(140)	7.87			44.97			9.74E-02			9.96E-02		
25% F	5(41)	60.02	41826	0.9843	9.50	31383	0.9786	1.46E-02	45056	0.9700	2.12E-02	25748	0.8661
	23(73)	24.39			14.48			3.54E-02			6.13E-02		
	60(140)	8.62			39.42			1.19E-01			6.66E-02		
15% M-1	5(41)	26.91	30134	0.9984	7.04	30973	0.9972	3.19E-02	29130	0.9838	3.11E-02	27535	0.9959
	23(73)	12.76			12.07			5.96E-02			6.87E-02		
	60(140)	6.72			29.01			1.23E-01			1.09E-01		
15% M-2	5(41)	25.28	29327	0.9917	5.51	36260	0.9994	3.43E-02	25450	0.9923	2.94E-02	35468	0.9984
	23(73)	10.56			10.80			7.30E-02			7.90E-02		
	60(140)	6.65			29.04			1.09E-01			1.49E-01		
6% SF	5(41)	32.85	27183	0.9269	6.40	33990	0.9999	2.42E-02	33230	0.9853	2.36E-02	39811	0.9881
	23(73)	12.04			12.60			6.76E-02			5.70E-02		
	60(140)	9.71			30.51			7.41E-02			1.46E-01		
25% S	5(41)	35.83	29354	0.9989	8.91	33256	0.9992	2.14E-02	28987	0.9999	1.72E-02	43933	0.9930
	23(73)	15.96			16.43			4.55E-02			4.76E-02		
	60(140)	9.35			40.89			8.13E-02			1.31E-01		
0.5% WRA	5(41)	45.36	32634	0.9804	8.24	27949	0.9915	1.87E-02	37412	0.9341	1.88E-02	41006	0.9872
	23(73)	16.15			15.87			7.29E-02			6.58E-02		
	60(140)	10.32			30.03			1.00E-01			1.21E-01		
5% C 20% F	5(41)	35.42	33445	0.9999	8.17	34755	0.9923	2.02E-02	31946	0.9981	1.69E-02	38752	0.9672
	23(73)	14.70			14.21			4.44E-02			6.16E-02		
	60(140)	7.63			39.82			8.80E-02			9.77E-02		
20% C 5% F	5(41)	32.62	27790	0.9985	7.97	38856	0.9980	1.81E-02	21559	0.9884	1.25E-02	48042	0.9666
	23(73)	16.36			15.874			2.93E-02			6.21E-02		
	60(140)	9.07			47.157			4.93E-02			1.10E-01		

$^{\dagger}R^2$ of least squares best-fit line of three parameter exponential model versus measured heat of hydration.

$^{**}R^2$ of least squares best-fit line of ASTM C 1074 hyperbolic function versus measured heat of hydration.

Table G.2: Summary of E_a for Chemical Shrinkage of Mortar.

Mixes	T,°C (°F)	Exponential Function			Exponential Function; Unequal H_{ult}			ASTM C 1074 Hyperbolic; Equal S_u			ASTM C 1074 Hyperbolic		
		τ, hours	E_a, J/mol	$R^{2\dagger}$	τ, hours	E_a, J/mol	$R^{2\dagger}$	Reaction rate k	E_a, J/mol	R^{2**}	Reaction rate k	E_a, J/mol	R^{2**}
Tyl-0.5	5(41)	47.15	24,831	0.9763	36.58	34682	0.9993	2.36E-02	17960	0.9733	1.71E-02	45000	0.9981
	23(73)	28.40			15.22			3.38E-02			5.18E-02		
	60(140)	14.85			7.42			5.45E-02			1.36E-01		
Tyl-0.45	5(41)	51.60	21,435	0.9975	36.31	33909	0.9992	2.45E-02	17232	0.9808	1.81E-02	43772	0.9995
	23(73)	30.58			14.33			3.52E-02			5.54E-02		
	60(140)	19.21			7.68			4.68E-02			1.31E-01		
25% C	5(41)	44.94	22,561	0.9994	35.21	34318	0.9997	2.16E-02	15345	0.9944	1.57E-02	43060	0.9968
	23(73)	25.37			14.62			3.37E-02			5.36E-02		
	60(140)	15.92			7.27			4.34E-02			1.13E-01		
25% F	5(41)	37.55	22,540	0.9998	32.29	31297	0.9935	2.46E-02	16220	0.9936	1.87E-02	40445	0.9970
	23(73)	20.51			12.88			3.96E-02			5.89E-02		
	60(140)	13.36			7.75			5.16E-02			1.19E-01		
10% M-1	5(41)	20.42	25,295	0.9990	20.77	32819	0.9995	3.21E-02	21480	0.9867	2.94E-02	31677	0.9997
	23(73)	10.18			8.52			6.21E-02			6.62E-02		
	60(140)	6.41			4.62			8.53E-02			1.26E-01		
5% SF	5(41)	32.71	28,099	0.9995	31.88	33346	0.9836	2.43E-02	24612	0.9965	1.91E-02	39694	0.9932
	23(73)	15.99			11.27			4.40E-02			6.15E-02		
	60(140)	8.98			7.01			7.57E-02			1.17E-01		
25% S	5(41)	37.77	24,742	1.0000	34.65	30839	1.0000	2.20E-02	15289	0.8648	1.89E-02	38527	0.9919
	23(73)	19.67			15.40			4.14E-02			4.58E-02		
	60(140)	12.13			8.41			5.96E-02			9.94E-02		
0.5% WRA	5(41)	21.91	21,484	0.9902	21.85	20906	0.9926	2.64E-02	21559	0.9812	2.65E-02	23425	0.9999
	23(73)	11.48			11.77			5.21E-02			4.93E-02		

	60(140)	8.24			8.43			7.02E-02			7.75E-02		
5% C 20% F	5(41)	33.54	26,518	0.9440	29.34	33952	0.9983	2.31E-02	21959	0.8916	2.03E-02	36093	0.9992
	23(73)	21.31			12.67			3.08E-02			5.05E-02		
	60(140)	9.68			6.14			6.52E-02			1.07E-01		
20% C 5% F	5(41)	29.69	29,183	0.9884	29.31	33972	0.9989	2.28E-02	26472	0.9745	2.03E-02	35274	0.9977
	23(73)	15.53			11.50			3.89E-02			5.47E-02		
	60(140)	7.68			6.19			7.81E-02			1.02E-01		

[†] R^2 of least squares best-fit line of three parameter exponential model versus measured heat of hydration.

[**] R^2 of least squares best-fit line of ASTM C 1074 hyperbolic function versus measured heat of hydration.